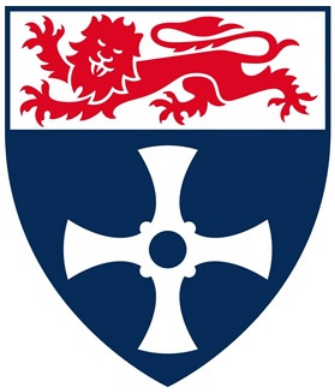

Development of the PDF kinetic approach for modelling inertial particle dispersion in turbulent boundary layers

by

Andrew Bragg

Thesis submitted for the degree of

Doctor of Philosophy

October 2011

School of Mechanical & Systems Engineering

University of Newcastle Upon Tyne

The work presented in this thesis is my own original work and where contributions have been made, they have been clearly acknowledged and referenced.

Andrew Bragg

Abstract

This thesis presents developments in the use of probability density function (PDF) kinetic equations to model the dispersion of inertial particles in turbulent boundary layers. The PDF kinetic equation is used as a master equation from which to construct continuum equations for the particle-phase, and these continuum equations form an infinite set of coupled equations which require closure in the particle velocity statistics. Furthermore, the continuum equations contain dispersion tensors which describe the effect of the underlying fluid turbulence on the dispersion of the particles throughout the flow field. These dispersion tensors themselves require closure and in this thesis new closure models are developed which are non-local and attempt to take into account the effects of turbulence inhomogeneity, anisotropy and particle-wall collisions on the dispersion tensors.

The first closure model developed is for particles dispersing under Stokes drag forcing only; appropriate for particles whose material density is much greater than that of the fluid in which they are dispersed. This closure model is tested against equivalent particle tracking simulation data over a range of particle sizes and the closure model predictions are found to be in excellent agreement. In contrast to the new closure model predictions, the traditional 'local' approximations to the dispersion tensors are found to be in significant error when compared to the particle tracking data.

The closure model is then developed to account for particles dispersing under Stokes drag, added mass and gravitational forcing; added mass forcing being important for particles whose material density is comparable to or less than that of the fluid in which they are dispersed. The modelling is presented and a discussion is given regarding the various complex terms that require approximation in this closure model. The closure model predictions are then compared against the alternative local approximations. It is seen that with added mass forcing the local approximations can be qualitatively and quantitatively different to the non-local predictions, whereas under only a drag force, errors in the local approximations are mainly quantitative.

Finally, consideration is given to the forms of the dispersion tensors appearing in the PDF and continuum equations. It is shown theoretically that the dispersion tensors (and therefore the PDF and continuum equations themselves) are free from the so called 'spurious drift' phenomena associated with certain types of models for predicting the dispersion of fluid particles in incompressible, inhomogeneous turbulent flows. However, it is also shown that closure approximations applied to the dispersion tensors may result in the introduction of a spurious drift. Nevertheless, it is demonstrated that the artificial drift introduced by closure approximations does not have any appreciable affect on the dispersion tensors when they are describing the dispersion of inertial particles.

This thesis is dedicated to my wife and my best friend,
Rachel Louise Bragg. Thank you for your love and patience
towards me, especially during all those times when I tried,
but failed, to convince you of just how fascinating the
study of particle dispersion in turbulence really is!

Acknowledgements

Firstly, I would like to express my sincerest gratitude to my primary supervisor, Dr David Swailes. His tutoring has been simply perfect; I could not have asked for more from him and I am so thankful that he took me on as a PhD student in the first place. His mathematical prowess and sharp mind has been a continual source of inspiration for me, and I hope that some of this has rubbed off onto me during my time researching under his supervision.

I would also like to thank my secondary supervisor, Prof Mike Reeks, for his enthusiasm and continual encouragement throughout the course of my PhD. Our many discussions on the fascinating subject of particle dispersion in turbulence have been both enjoyable and helpful, and his vast knowledge of the subject area has constantly inspired me to want to learn more, and to deepen my understanding.

I would then like to thank Dr Roar Skartlien for his encouragement and input to the project, and to Dr Peter Van Dijk for all his helpful suggestions and tips during the first few months of my PhD when I was trying to get to grips with running numerical simulations using MATLAB. My acknowledgments also extend to the 'FACE' project through which my PhD was sponsored, and to my fellow colleagues in room T4, working alongside whom has been a great pleasure.

Finally to my family and friends; thank you for your love and patience through these last few years, and for your understanding through those times when I perhaps neglected you because I was so busy with my PhD work! I am very thankful for your love and support.

Contents

List of Figures

Nomenclature

Abbreviations

DNS	Direct Numerical Simulation
ESM	Eulerian Statistical Models
FN	Furutsu-Novikov
FRS	Fully Resolved Simulation
GTA	Green Tensor Approximation
GT	Green Tensor
KS	Kinematic Simulation
LES	Large Eddy Simulation
LHA	Local Homogeneous Approximation
LHDI	Lagrangian History Direct Interaction
LHS	Left Hand Side
LPT	Lagrangian Particle Tracking
NS	Navier-Stokes
PDF	Probability Density Function
PT	Particle Tracking
RHS	Right Hand Side
RT	Response Tensor

VK	Van Kampen

Greek characters

$\beta = 1/\tau_p$	Inverse particle momentum response time
$\gamma(\mathbf{x})$	Gradient of mean fluid velocity at $\mathbf{x}$
$\boldsymbol{\kappa}(\mathbf{x}, \mathbf{v}, t)$	Particle phase-space dispersion tensor
$\overline{\boldsymbol{\kappa}}(\mathbf{x}, t)$	Velocity averaged form of $\boldsymbol{\kappa}(\mathbf{x}, \mathbf{v}, t)$
$\boldsymbol{\lambda}(\mathbf{x}, \mathbf{v}, t)$	Particle phase-space dispersion tensor
$\overline{\boldsymbol{\lambda}}(\mathbf{x}, t)$	Velocity averaged form of $\boldsymbol{\lambda}(\mathbf{x}, \mathbf{v}, t)$
$\boldsymbol{\mu}(\mathbf{x}, \mathbf{v}, t)$	Particle phase-space dispersion tensor
$\overline{\boldsymbol{\mu}}(\mathbf{x}, t)$	Velocity averaged form of $\boldsymbol{\mu}(\mathbf{x}, \mathbf{v}, t)$
μ^f	Fluid dynamic viscosity
ν^f	Fluid kinematic viscosity
ρ^f	Fluid material density
$\rho(\mathbf{x}, t)$	Particle concentration/number density
ρ^p	Particle material density
σ_k	R.M.S value of the distribution of wave numbers in the inhomogeneous, anisotropic KS flow field
$\sigma_{Lp} = \sqrt{\frac{\pi}{2}} \frac{1}{\tau^{Lp}}$	Rate scale of the fluid velocity correlations seen by particles in the inhomogeneous, anisotropic KS flow field
σ_w	R.M.S value of the distribution of frequencies in the inhomogeneous, anisotropic KS flow field
τ_L	Fluid Lagrangian integral timescale
τ^{Lp}	Timescale of $\boldsymbol{f}$ seen by particles
τ_p	Particle momentum response time

Roman characters

$A(\mathrm{x}_2)$	Profiling function in the inhomogeneous, anisotropic KS flow field
$\overline{\mathbf{cc}}(\mathbf{x},t)$	Particle Reynolds stress tensor
$\overline{\mathbf{ccc}}(\mathbf{x},t)$	Particle Reynolds stress flux tensor
$\frac{D}{Dt}\boldsymbol{u}^p = \frac{D}{Dt}\boldsymbol{u}(\boldsymbol{x}^p(t),t)$	Fluid acceleration evaluated at the particle position
$\left\langle \frac{D}{Dt}u_i \right\rangle^p = \left\langle \frac{D}{Dt}u_i \right\rangle (\boldsymbol{x}^p(t),t)$	Mean fluid acceleration evaluated at particle position
$\left(\frac{D}{Dt}\boldsymbol{u}^p\right)' = \langle \frac{D}{Dt}\boldsymbol{u}\rangle^p - \frac{D}{Dt}\boldsymbol{u}^p$	Fluctuating fluid acceleration evaluated at the particle position
$\boldsymbol{f}\left(\boldsymbol{x}^p(t),t\right)$	Fluctuating aerodynamic force acting on particle
$\boldsymbol{F}\left(\boldsymbol{x}^p(t),\boldsymbol{v}^p(t),t\right)$	Mean aerodynamic force acting on particle
$\overline{\boldsymbol{F}}(\mathbf{x},t)$	Velocity averaged form of $\boldsymbol{F}(\mathbf{x},\mathbf{v},t)$
$\boldsymbol{g}$	Gravitational acceleration
$\boldsymbol{G}(t;t')$	Green tensor for particle equation of motion
$\boldsymbol{\mathcal{G}}(t;t')$	Particle response tensor
m^p	Particle mass
$\mathcal{P}(\mathbf{x},\mathbf{v},t)$	Probability Density Function (PDF) corresponding to a single realisation of the turbulent flow field and a single realisation of $\boldsymbol{x}^p(0)$, $\boldsymbol{v}^p(0)$
$p(\mathbf{x},\mathbf{v},t) = \langle\mathcal{P}\rangle$	Probability Density Function (PDF)
$p^f(\mathbf{x},t)$	Pressure acting in fluid
Re_p	Particle Reynolds number
$\boldsymbol{R}(\mathbf{x}',t';\mathbf{x},t)$	Two-point, two-time correlation tensor for $\boldsymbol{f}$
S_f	Scaling parameter in the inhomogeneous, anisotropic KS flow field
$St = \tau_p/\tau^{Lp}$	Stokes number scaled on fluid timescale seen by particles
$St_E = \tau_p/\tau_E$	Stokes number scaled on fluid Eulerian integral timescale
$\boldsymbol{u}(\mathbf{x},t)$	Fluid velocity

$\langle \boldsymbol{u} \rangle(\mathbf{x}, t)$	Mean fluid velocity
$\boldsymbol{u}'(\mathbf{x}, t)$	Fluctuating fluid velocity
$\boldsymbol{u}^p = \boldsymbol{u}(\boldsymbol{x}^p(t), t)$	Fluid velocity at particle position
$\langle \boldsymbol{u} \rangle^p = \langle \boldsymbol{u} \rangle(\boldsymbol{x}^p(t), t)$	Mean fluid velocity evaluated at particle position
u_τ	Fluid wall friction velocity
$\boldsymbol{v}^p(t)$	Particle velocity
$\overline{\mathbf{v}}(\mathbf{x}, t)$	Particle mean velocity
x_2^{min}	Particle radius; co-ordinate at which particle makes contact with wall
$\boldsymbol{x}^p(t)$	Particle position
$\mathbf{x}, \mathbf{v}$	Position and velocity Eulerian phase-space variables

Symbols

$\langle ... \rangle$	Ensemble average
$\Big\langle ... \Big\rangle_{\mathbf{x}}$	Conditional ensemble average; conditioned on $\boldsymbol{x}^p(t) = \mathbf{x}$ (or sometimes $\boldsymbol{x}^p(s = 0) = \mathbf{x}$)
$\langle ... \rangle^p$	Ensemble average evaluated at the particle position
$\overline{\Big(... \Big)}$	Particle density weighted mean average

Chapter 1

Background to Research

The research presented in this thesis has been funded through the 'FACE' (The Mulitiphase Flow Assurance Centre) project which is a long term collaboration between Institutt for Energiteknikk (IFE), the Foundation for Industrial Research (SINTEF) and the Norwegian Technical and Natural Science University (NTNU). The research carried out in FACE is supported by StatoilHydro, GE Oil & Gas, FMC Technologies, SPTGroup, CD-adapco and Shell. FACE began in August 2007 with the intention of combining surface and colloid chemistry with fluid mechanics to develop models and tools which can be used to help understand, predict and prevent a broad range of flow assurance problems encountered in the oil industry. Flow assurance refers to ensuring that the oil, gas and water mixture taken from oil wells reaches the delivery location in a successful and economical manner. There are numerous flow assurance problems encountered in the oil industry, such as

- Pipeline rupture due to corrosion, and/or erosion.
- Pipeline blockage due to deposition of particles on pipe wall, the formation of dense particle beds at the bottom of the pipe or plugs which have formed.
- Large pressure losses in pipelines which cause flow rates to be reduced.

FACE is divided into three working groups; (i) suspensions, (ii) separation and (iii) multiphase transport, each of which addresses different aspects of flow assurance problems. The research presented in this thesis has been conducted within the suspension group. This group is concerned with improving the predictions of particle transport in pipelines and the understanding of the effect of the presence of the particles on the fluid flow in the pipe. One of the types of particle found in oil pipelines are hydrates. These are ice-like structures which can form when methane gas and water react under high pressure and low temperature environments.

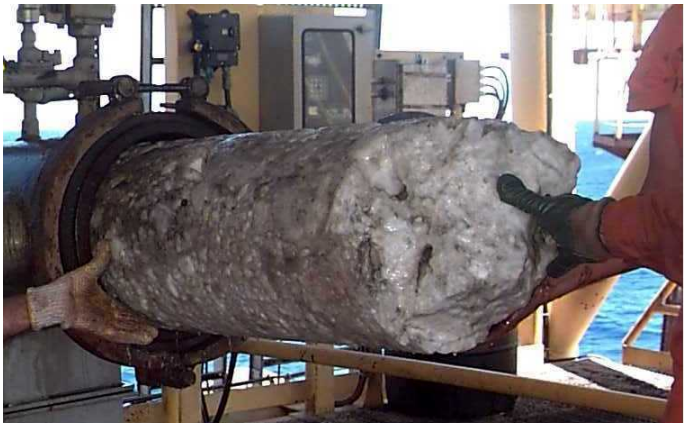

Figure 1.1: Hydrate Plug being removed from an oil pipeline (image taken from http://supercheminc.com).

As hydrate particles are transported along a pipeline within the oil they may begin to agglomerate, and can form structures so large that they block the entire pipeline (as shown in figure 1.1). Clearly this is a problem since in the event of a hydrate plug formation, the oil flow in the pipeline can be either severely restricted or prevented altogether.

Another type of particle found in oil pipelines is sand. The presence of sand particles in oil pipelines is highly problematic since it causes pipeline erosion (as shown in figure 1.2) and the sand particles may form 'beds' on the bottom of the pipes which restrict the flow of oil.

Figure 1.2: Effect of sand erosion on the pipe wall (image taken from http://ceresist.com).

In addition wax particles are also found in oil pipelines. Wax particles have a tendency to deposit on the walls of the pipes (as shown in figure 1.3) and this restricts the effective cross sectional area of the pipe and hence also restricts the oil flow.

Figure 1.3: Build up of wax deposits on the walls of a pipe (image taken from http://balmsenergy.com).

In order to address and develop solutions to such problems as these, it is important to understand how the problems arise in the first place and what physical processes govern their development. One must have an understanding of how hydrate and wax particles form from the mixture extracted from the oil wells (which includes oil, gas, water and other substances) and the physiochemical behavior of the particles which governs the way they interact with the surrounding fluid, the ability of the particles to agglomerate and break up as well as deposit on the walls of the pipe. In addition to this, one must also have an understanding of how the fluid flowing in the pipe dynamically interacts with the particles and causes them to either disperse or segregate into certain regions of the pipe.

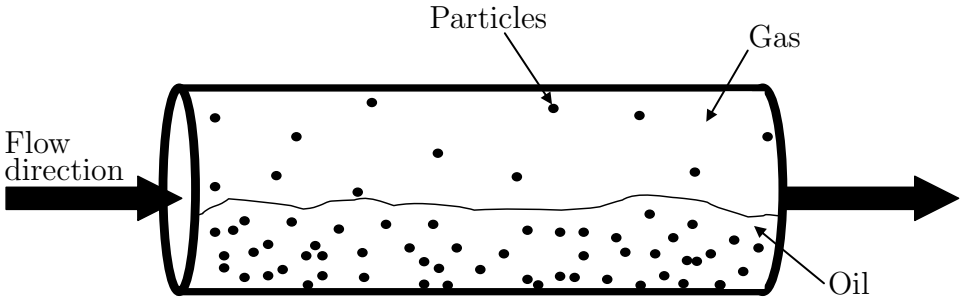

Figure 1.4: Diagram showing a possible flow regime in an oil pipeline. Oil flowing at the bottom of the pipe with gas flowing above it, with an unsteady wavy interface between the two fluids. Particles are dispersed throughout the phases with a dense regime near the pipe floor and a dilute regime above it.

Figure 1.4 shows a possible flow scenario in a pipeline; stratified flow with oil at the bottom and gas at the top flowing through the pipe, with particles dispersed throughout both fluids; typically oil droplets entrained and dispersed throughout the gas and solid particles dispersed throughout the oil. The flow of the gas and oil may be either laminar, transitional or fully turbulent, and there may be unsteady waves propagating along the surface of the oil. Often there is also water present with the oil and gas, in which case the flow is stratified into three layers, with water flowing along the bottom of the pipe (although the 3 phase mixture may be in the form of water or oil droplets dispersed throughout the gas phase). A dense regime of particles (in terms of the number of particles) near the bottom of the pipe (which occurs in part due to gravitational settling) will affect the nature of the fluid flow, and increases the possibility of inter-particle collisions and hence agglomeration or break up of particle clusters. The presence of liquid and gas phases means that slug flow may also occur as well as entrainment processes, both of which significantly increase the complexity of the dynamical interaction between the fluid and particle phases. Flows such as these, where there are different fluids and phases present are commonly referred to as ‘multiphase flows’.

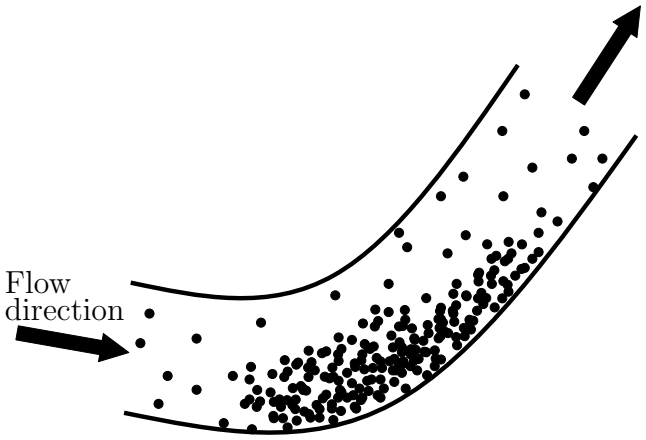

Figure 1.5: Diagram showing the accumulation of particles in a pipe bend.

Figure 1.5 shows another possible flow scenario in a pipeline. As the particles are transported by the fluid (which may contain a mixture of oil, gas and water) along the pipe towards the bend, by reason of their inertia they do not follow the streamlines of the fluid and tend to collide with the pipe wall at the bend. In this region the particles (especially wax particles) may deposit on the wall of the pipe and over time a dense bed of particles can form which can severely restrict the flow of the fluid. It is particularly in pipe bends that the problem of erosion due to sand particles arises, as is illustrated in figure 1.2.

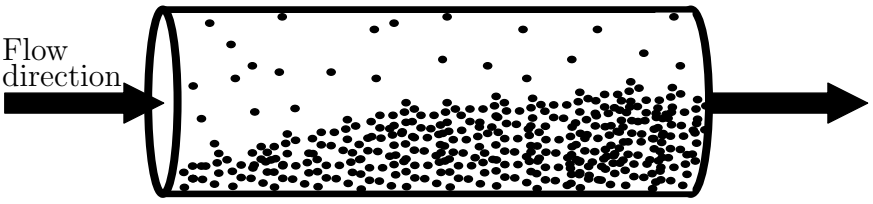

Figure 1.6: Diagram showing a dense bed of particles developing along the pipe length.

Figure 1.6 shows yet another possible flow scenario in a pipeline. As the particles are transported along the pipe by the fluid mixture a bed of particles at the bottom of the pipe develops, with a dilute regime of particles dispersing above it. The size of the particle bed increases along the length of the pipe and this significantly affects the flow dynamics of the fluid and may eventually cause blockage or severe restriction to the flow.

The formation and development of dense particle beds, particle accumulation in pipe bends and particle deposition on pipe walls all contribute to the flow assurance

problems found in the oil industry, and the dynamical interaction between the fluid and particulate phases is highly complex. Therefore, in order to address such flow assurance problems the aim of the suspension group within FACE is to begin by conducting experiments and building mathematical models which consider systems somewhat simpler to that found in real oil pipelines. The experimental work serves to provide insight for the modelling work in addition to providing data against which the models can be validated.

The research presented in this thesis is aimed at developing mathematical models to describe how particles disperse in the presence of a single fluid phase which is assumed to be fully turbulent, Newtonian, isothermal and incompressible. The particles will be assumed to be of constant mass, spherical, non-deformable, mono-disperse (i.e. all particles in the system are physically identical) and only mechanical forces acting on the particle will be considered.

Though these are considerably simplified systems, even they are as of yet not completely understood, and models which describe such systems accurately are still incomplete. Nevertheless, by developing the understanding and improving the modelling of such simplified systems, a route will be provided towards studying more realistic, complex systems in the future.

Chapter 2

Fundamentals in Modelling Disperse Particle Transport in Turbulent Flows

As discussed in chapter 1, the objective of the research presented in this thesis is to be able to improve the predictive capabilities of mathematical models for particles transport in pipelines. In this chapter the fundamentals for modelling particle dispersion in turbulent flows will be introduced. To begin, a brief discussion is given of the various types of fluid-particle flow regimes that may be encountered in disperse particle transport in turbulent flows. This is followed by a general description and comparison of two fundamentally different approaches to modelling/simulating particle dispersion in turbulent flows; Lagrangian particle tracking and Eulerian statistical models. Then models and equations describing fluid and particle motion are given, along with a description of various approximations they contain and solution methodologies. Finally, models and approximations for describing particle-boundary collisions will be considered and discussed.

2.1 Particle transport in turbulent flows: different flow regimes

Particle transport in turbulent flows can be divided into several 'regimes', and these are summarised in figure 2.1

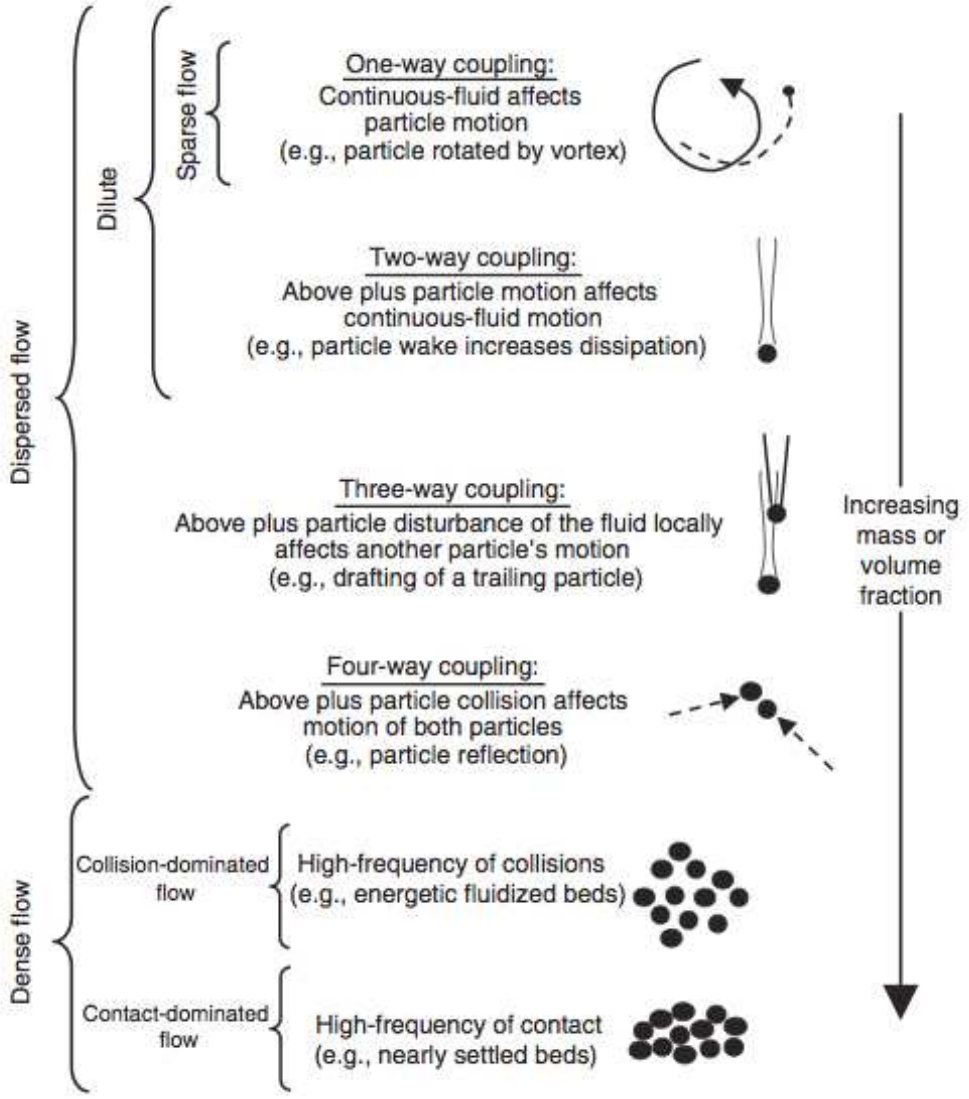

Figure 2.1: Diagram showing the various types of fluid-particle flow regimes, taken from [1].

The simplest flow regime is the dilute, one-way coupled flow regime ('sparse flow' in figure 2.1). In this regime the mass loading of particles in the fluid is considered to be sufficiently low such that the energy expended by the fluid in moving the particles is negligible. In other words, the system is 'one-way coupled', with the fluid affecting the dynamics of the particles but not vice versa. In addition, the average inter-particle distance is considered to be large such that inter-particle collisions can be assumed negligible. The applicability of the one-way coupled assumption may be, to an extent, determined by the particle Reynolds number Re_p , based on the slip velocity between the local fluid and particle velocities. For particle translation in a quiescent fluid, with $Re_p > 300$ particles shed vortices [5], and in this case it is probably unreasonable to

assume that the fluid-particle system is one-way coupled. However, even though a single particle may modify the local turbulence through vortex shedding, in order to cause significant modulation to the entire turbulent flow field the mass fraction of the particles dispersed throughout the fluid must be sufficiently large (e.g. [6]). With regard to particle transport in turbulent pipe flow, the dilute one-way coupled assumption is perhaps reasonable for particle dispersion in the upper half of the pipe (for a horizontal pipe), whereas it may be completely inapplicable to particle dispersion at the floor of the pipe if the particle bed is very dense (see figure 1.6 for example). In such cases the flow regime encountered at the floor of a pipe is very different. This scenario would be best described by the second but last regime in figure 2.1; densely packed particles with high frequency collisions, both inter-particle and particle-wall collisions. As the particles are so close together, the dynamics of the fluid flow will be severely affected, and the system can no longer be treated as being only one-way coupled. In fact, for such a scenario, it would probably be more feasible to model the fluid-particle system as being one 'fluid' with a modified viscosity, due to the presence of the particles (e.g. [7]).

In this thesis attention will be given to the development of models which describe the transport of a dilute, one-way coupled system of particles dispersing in turbulence, such as might be applicable in the upper regions of a pipe cross section. Such dilute disperse flows are also found in other environmental and industrial applications such as the dispersion of water droplets in atmospheric turbulence leading to the formation of rain (i.e. cloud physics), the dispersion of ash particles emitted during volcanic eruptions, the dispersion and deposition of radioactive aerosols in nuclear reactors, the dispersion of fuel droplets in combustion engines etc. Therefore it is clear that given such a diverse range of important applications, it is of great importance to study such systems.

2.2 Modelling and Simulation of Particle Dispersion in a Turbulent Fluid

Regardless of which type of flow regime is being considered, there are essentially two approaches to modelling and simulating the particle dispersion process in a turbulent fluid: Lagrangian particle tracking (LPT) and Eulerian statistical modelling (ESM). Both have their own advantages and disadvantages, and a brief discussion of each is now given.

2.2.1 Lagrangian Particle Tracking

In a LPT simulation the fluid flow field is prescribed by either solving the Navier-Stokes equation numerically or by using some statistical model (these issues are discussed in section 2.3). In its simplest 'one-way coupled' form (i.e. with the assumption that the particles do not affect the turbulent flow field) the fluid flow field solutions are used as input into the particle equation of motion, which is then solved (usually numerically). By solving the particle equation of motion in this way, particles may be 'tracked' through the flow field, from which information regarding the trajectory and velocity of the particle are obtained. In addition to providing information on individual particle trajectories, by tracking many particles one may also obtain statistical information regarding the particle dispersion process (i.e. the mean particle velocities, the mean particle concentrations etc). The advantages of LPT are

1. Relatively simple to include complicated forces on the particle
2. Relatively simple to simulate 'two-way' coupled systems, where the particle forcing on the turbulence needs to be taken into account
3. Simple to include complex particle-boundary interactions (inelastic collisions, rough boundary surfaces etc)
4. Enables the instantaneous features of the particle dispersion process to be observed and analysed (i.e. particle clustering in certain regions of the flow field, which is important for modelling the agglomeration of particles, for example)

The disadvantages of LPT are

1. If the turbulent flow field is described by either DNS or LES (see section 2.3) then obtaining statistically steady state results for particle dispersion in a pipe or channel flow often requires extremely large simulation times [8, 9].
2. LPT can generate much information that is not required; for example often only statistical information of the dispersion process is required in which case LPT may be considered an inefficient way to obtain such information.

2.2.2 Eulerian Statistical Models

Whereas in LPT many particles are tracked in order to obtain the statistical information of the particle dispersion process, in ESM the statistics of the dispersion process are modelled directly. There are different ESM available, such as PDF (probability density function) equations and particle continuum equations (also called 'two-fluid' models).

In this thesis attention will be given to a PDF model which provides a theoretically sound model for the particle statistics in a turbulent flow. Nevertheless, regardless of which type of ESM is used, its advantages compared to LPT are

1. Solutions can be obtained relatively quickly compared with LPT, giving steady state, or transient solutions
2. Gives insight into the physics of the statistical processes governing the particle dispersion
3. ESM can often be solved using the same computational method as is used for the flow field (i.e. for the case of continuum equations coupled with RANS equations, see section 2.3), making them efficient to implement numerically

The disadvantages of ESM compared to LPT are

1. Difficult to incorporate complicated aerodynamic forces acting on the particles
2. Difficult to include complicated particle-boundary interactions in the continuum equation (although possible to specify more complex boundary conditions in PDF equations)
3. Some information of the dispersion process is lost via a statistical description

Although ESM are often difficult to construct and close, their advantages over LTP make them worthy of study (particularly for industrial applications, where the computational expense of LPT can be unacceptable, if not impossible with current computational power). Indeed, none of their difficulties are necessarily insurmountable.

There is much value in both LPT and ESM, and as discussed, both have their own advantages and disadvantages. Results obtained from LPT studies are particularly useful for providing the necessary insight and information needed to correctly construct and close ESM as well as providing data against which to validate the models. The study of both LPT and ESM is therefore of great benefit for the multiphase flow research community.

2.3 Models for the dynamics of a turbulent fluid

Both LPT and ESM require a description of the turbulent flow field in which the particles are dispersing. LPT requires information concerning the instantaneous values of the flow field, whilst ESM only require solutions for the statistics of the turbulent flow

field. Nevertheless, as already mentioned, LPT studies are useful in order to provide data against which to validate ESM and will be used in this thesis to that end. In this section a description of models and equations describing the dynamics of a turbulent fluid will be considered.

2.3.1 Navier-Stokes and DNS

Even though turbulence appears to be a random process, it is not *intrinsically* random (in contrast to systems described by quantum mechanics) and is therefore described using deterministic mechanics. Under the continuum hypothesis, Newtons 2^{nd} law of motion may be used in conjunction with the continuity equation to derive a set of equations governing the dynamics of an incompressible, Newtonian and isothermal fluid

$$\frac{\partial}{\partial \mathrm{x}_i} u_i = 0 \tag{2.1}$$

$$\rho^f \left(\frac{\partial}{\partial t} u_i + \frac{\partial}{\partial \mathrm{x}_j} u_j u_i \right) = - \frac{\partial}{\partial \mathrm{x}_i} p^f + \mu^f \frac{\partial}{\partial \mathrm{x}_j} \frac{\partial}{\partial \mathrm{x}_j} u_i + \rho^f F_i^b \tag{2.2}$$

where $\boldsymbol{u}(\mathbf{x}, t)$ is the fluid velocity, ρ^f is the fluid material density, $p^f(\mathbf{x}, t)$ is the pressure acting in the fluid, μ^f is the fluid dynamic viscosity and $\boldsymbol{F}^b$ are the body forces acting on the fluid (e.g. gravity). Equation (2.1) specifies that the flow field is incompressible and is a degenerate form of the fluid-mass continuity equation for constant density flows. Equation (2.2) is the Navier-Stokes (NS) equation for an incompressible, Newtonian, isothermal fluid. The solutions to equations (2.1) and (2.2) form the basis of the description of the dynamics of the flow field through which particles disperse in a multiphase flow. If there is a momentum coupling between the fluid and particle phases, an additional forcing term is added to equation (2.2) (although for very dense particle loadings it is perhaps necessary to modify the viscosity of the fluid μ^f since the effective viscosity of the fluid-particle mixture will differ from the pure fluid viscosity). Whilst it is generally believed that the NS equation exactly describes turbulence (when the continuum hypothesis is applicable), unfortunately it is yet to be proved that solutions to the NS equation always exist in three dimensions, or that the solutions do not contain singularity. Generic, analytic three dimensional solutions to the NS equation are at the present time unavailable, and therefore alternative numerical solution procedures must be adopted.

To attempt to solve the NS equation numerically direct numerical simulations (DNS) are used. In DNS, the NS equation is solved numerically (by finite difference, finite volume or spectral methods) on a grid sufficiently fine so that the Kolmogorov length

scales are resolved, and with a sufficiently small time step so that the Kolmogorov temporal scales are also resolved. DNS was first used by Orszag and Patterson [10] for a simulation of homogeneous isotropic turbulence. The first DNS of a wall bounded flow was by Kim *et.al.* [11] in which a DNS of a fully developed turbulent channel flow was performed, from which important statistics were obtained and compared with experimental data. Since these pioneering works DNS has been used extensively and has proved to be a very powerful tool for fundamental turbulence research. DNS, along with experiments, has been successfully used to discover certain coherent structures in turbulent wall-bounded flows, such as turbulent streaks, tubes, sheets, horseshoe and various other types of turbulent structures [12–19]. Recently Wu *et.al.* [20] used DNS to study a developing turbulent boundary layer and found for the first time using DNS that solutions to the NS equation predict a dominance of hairpin vortices for such a turbulent flow, something only before seen in experiments. However, DNS is computationally very expensive both in terms of computational memory and computational time (see [21] for a discussion on the computational costs of DNS), and simulations of the type of flows that are found in industry and the environment, where the Reynolds number is very high and the geometry is often complex, are still far from possible.

2.3.2 Models

While equations (2.1) and (2.2) describe the true deterministic physics of classical (incompressible, Newtonian and isothermal) fluids in motion, the difficulty in solving them (using DNS) for turbulent flows has prompted studies into the use of models to generate turbulent-like flow fields.

One such model is large eddy simulation (LES), which was first proposed by Smagorinsky [22]. In LES a filtered version of the NS equation is solved numerically. The turbulence energy spectrum is 'cut off' at a particular wave number and flow scales up to this wave number are resolved in the simulation, whilst flow scales with wave number larger than the cut off wave number are modelled by some form of subgrid scale model (e.g. dynamic Smagorinsky model [23]). The idea behind LES is that in some cases only the largest scales of the turbulence are of importantance, and that the small scale dynamics may be suitably represented using a model. Depending on the type of flow, LES can be significantly less expensive than DNS. For wall bounded flows, in which the turbulence is much more complicated than unbounded flows, the minimum wave cut off number required in order for the LES to be sufficiently accurate is such that LES is almost as expensive as DNS (e.g. [24]). There are also several fundamental issues with LES concerning its fundamental conceptualisation, and the effect of the filtering on the turbulent fields produced by LES that are yet to be resolved and quantified [25].

In addition, in [26] it was shown that LES can produce inaccurate results for particle dispersion in wall-bounded flows, and in [27] it was shown that LES cannot properly capture the clustering of inertial particles in homogeneous, isotropic turbulence.

In some instances only averaged properties of the turbulent field are required. To obtain equations describing the mean properties of a turbulent velocity field, the NS equation is 'Reynolds averaged' by splitting up the fluid velocity into a mean component $\langle \boldsymbol{u} \rangle$ and a fluctuating component $\boldsymbol{u}'$ (with $\boldsymbol{u} = \langle \boldsymbol{u} \rangle + \boldsymbol{u}'$). The equation that results from this averaging procedure is known as the Reynolds averaged Navier-Stokes (RANS) equation, and it contains an additional unknown term, the Reynolds stress tensor (essentially $\langle \boldsymbol{u}'\boldsymbol{u}' \rangle$). Different models are available for the Reynolds stress tensor, from more basic $k - \epsilon$ models [28] to the more advanced Reynolds stress models [29]. With a model for the Reynolds stress tensor, solutions for the mean fluid velocity field may be obtained by solving the RANS equations.

Whilst LES and RANS are explicitly based on the NS equation itself, alternative 'stochastic models' (i.e. not based on the deterministic NS equation) have also been presented in the literature as models which generate turbulent-like flows. One such stochastic model, often referred to as a 'synthetic turbulence model', is kinematic simulation (KS). KS was first introduced by Kraichnan [30] and has since been developed and used in numerous papers for a variety of different types of turbulent flows (e.g. [31–38]). In KS an Eulerian flow field is generated by the linear superposition of many random Fourier modes, producing a Gaussian (though not necessarily restricted to Gaussian) flow field correlated in space and time. One of the great advantages of KS is that it can be used to generate turbulent-like flow fields with energy spectrum's containing large scale separations (i.e. large Reynolds number flows, which at present would be unfeasible to generate with DNS). This makes KS very useful for studying particle pair dispersion, for example. Certainly KS does not truly capture the complex physics of a turbulent flow. In particular, the sweeping effect of the small scales by the largest scales which occurs in real turbulence is not captured in KS since, in KS, the Fourier modes which are superimposed are independent of one another. However KS does contain sufficient qualitative features of a turbulent flow to make it a useful research tool, particularly for studying particle dispersion in turbulent flows.

Another stochastic modelling approach that has been developed to simulate turbulent-like flows is through the use of Langevin equations. Rather than providing a model for the turbulent field, Langevin equations are used to define the turbulent fluid velocity along a particle trajectory in a stochastic Lagrangian manner. Langevin based models have been developed in many studies (e.g. [21,39–49]) and have been shown to reproduce DNS statistics well, making them a useful research tool.

Langevin models, along with KS, have the great advantage of being computationally

'cheap' compared to DNS (or LES), and therefore they provide a very efficient means of testing models for particle dispersion in turbulent flows, models which can later be validated against DNS and/or experimental data.

2.4 Models for Inertial Particle Dynamics

In order to simulate or model how an inertial particle moves within a turbulent flow field, the particle equation of motion must be specified. Applying Newtons 2^{nd} law for translational motion due to gravity and the aerodynamic fluid force acting on a particle of constant mass yields the following equation of motion

$$m^p \frac{d}{dt} v_i^p(t) = m^p g_i + \int_S \sigma_{ij} \mathrm{n}_j dS \tag{2.3}$$

where m^p is the particle mass, $\boldsymbol{v}^p(t)$ is the particle velocity, $\boldsymbol{g}$ is the gravitational acceleration, $\boldsymbol{\sigma}$ is the fluid stress tensor, $\mathbf{n}$ is the unit normal vector and the integral in equation (2.3) is over the entire surface of the particle. The fluid stress tensor for a Newtonian fluid is

$$\sigma_{ij} = -p^f \delta_{ij} + \mu^f \left[\frac{\partial u_i}{\partial \mathrm{x}_j} + \frac{\partial u_j}{\partial \mathrm{x}_i} \right] \tag{2.4}$$

where δ_{ij} is the Kronecker delta. In principle, equation (2.3) may be solved numerically for a turbulent flow in a LPT simulation, with the fluid velocity required in $\boldsymbol{\sigma}$ prescribed by the NS equation. Such numerical simulations are referred to as Fully Resolved Simulations (FRS) since they fully resolve the fluid stresses acting on the particle surface. In several studies various numerical strategies have been implemented in order to perform FRS for finite size inertial particles dispersing in a laminar flow field (e.g. [50–55]). However, due to the very high computational cost, use of FRS for particle dispersion in turbulent flows is somewhat limited at present, usually with no more than 1000 particles being tracked in a low Reynolds number turbulent flow (e.g. [56–58]). In general, it would be desirable to use FRS since the finite size of the particle can be important, and may cause modification to the local turbulent flow structure which may either augment or attenuate the local turbulence (experimental investigations show that small particles tend to attenuate the fluid turbulence whilst large particles tend to augment it [59, 60]). However, the computational expense of FRS, even for relatively simple turbulent flows, is so high that it is unfeasible for studying anything of any real industrial or environmental relevance.

An alternative procedure is to approximate the particle as being a 'point particle', that is, rather than taking into account the finite size of the particle and integrating the fluid stress acting on it over its entire surface, the assumption is made that the particle is small compared to the smallest scales over which the fluid velocity field varies (i.e. the local Kolmogorov spatial scales). Then only the fluid force acting at a point is required, rather than needing to integrate the fluid stress over the entire particle surface. With the additional assumptions that the particle is rigid, spherical and that the slip velocity between the particle and the local fluid is small (i.e. small particle Reynolds number, $Re_p \ll 1$, such that the flow 'around' the particle may be considered as unsteady Stokes flow) a formal equation of motion may be derived. Under these assumptions, the equation of motion for an inertial particle moving in a fluid is (e.g. [61–65])

$$\begin{aligned} m^p \frac{d}{dt} v_i^p =& \frac{1}{2}\rho^f C_D \mathrm{A}^p |u_i^p - v_i^p| \left(u_i^p - v_i^p\right) + \left(m^p - \rho^f \mathrm{V}^p\right) g_i + \rho^f \mathrm{V}^p \frac{D}{Dt} u_i^p \\ &+ \frac{\rho^f \mathrm{V}^p}{2}\left(\frac{D}{Dt}u_i^p - \frac{d}{dt}v_i^p\right) + \frac{3}{2}\mathrm{d}^2\sqrt{\pi\rho^f\mu^f}\left[\int_0^t \frac{\frac{D}{Dt}u_i^p - \frac{d}{dt}v_i^p}{\sqrt{t-t'}}dt' + \frac{u_i^p(0) - v_i^p(0)}{\sqrt{t}}\right] \end{aligned} \tag{2.5}$$

where $\boldsymbol{x}^p(t)$ is the particle position, C_D is the particle drag coefficient, A^p is the particle cross sectional area, $\boldsymbol{u}^p = \boldsymbol{u}(\boldsymbol{x}^p(t), t)$ is the fluid velocity at the particle position, V^p is the particle volume and d is the particle diameter. The material derivative in equation (2.5) is the fluid acceleration at the instantaneous particle position (not along the particle trajectory), that is

$$\frac{D}{Dt}u_i^p = \frac{\partial}{\partial t}u_i^p + u_j^p \frac{\partial}{\partial \mathrm{x}_j}u_i^p \tag{2.6}$$

The first term on the RHS of equation (2.5) is the aerodynamic drag force. The nature of the drag coefficient C_D, and therefore the drag force, is in general a complicated function of many different parameters, such as the particle shape, the particle orientation with respect to the flow, the flow Reynolds number and Mach number. In the regime $Re_p \ll 1$ the Stokes drag coefficient may be used

$$C_D = \frac{24}{Re_p} \tag{2.7}$$

Various empirical forms of C_D have been obtained (see [61]) which are valid for $Re_p > 1$, among these is the widely used formula [66]

$$C_D = \frac{24}{Re_p}\left(1 + 0.15 Re_p^{0.687}\right) \tag{2.8}$$

which is considered to be valid up to $Re_p \approx 800$. C_D is also affected when the particle is moving near a boundary, such as a wall. Recent research has shown that the drag force on a particle is significantly higher when the particle is very close to a wall boundary as compared to when it is far from any boundaries [67].

The second term on the RHS of equation (2.5) is the 'effective buoyancy' force, which is the buoyancy force acting on the particle subtracted from the weight of the particle. The third term on the RHS of equation (2.5) is the force on the particle arising from viscous stresses and pressure gradients in the fluid. The fourth term on the RHS of equation (2.5) is the added mass force. The added mass force relates to the force required to accelerate the surrounding fluid. The fifth term on the RHS of equation (2.5) is the Basset history force. This term describes the effect of the delay in boundary layer development surrounding the particle as the relative velocity between the local fluid and the particle changes with time. For detailed derivation and discussion on the particle equation of motion see [61–65]. In the cited papers additional terms appear in the particle equation of motion which include lift forces and terms due to the non-uniformity of the fluid velocity field (Faxen forces etc).

In this thesis a Stokes drag coefficient will be adopted, and the Basset history term in equation (2.5) will be ignored. This is a sufficient approximation when $\rho^p \gg \rho^f$ [68]. However it is noted that for $\rho^p \to \rho^f$, in which limit the added mass force becomes important, the Basset history force may be also important. Equation (2.5) may then be re-arranged to give

$$\frac{d}{dt}v_i^p = \frac{1}{\tau_p\left(1 + \frac{1}{2}\frac{\rho^f}{\rho^p}\right)}\left(u_i^p - v_i^p\right) + \frac{2(\rho^p - \rho^f)}{2\rho^p + \rho^f}g_i + \frac{3\rho^f}{2\rho^p + \rho^f}\frac{D}{Dt}u_i^p \tag{2.9}$$

where ρ^p is the particle material density, and

$$\tau_p = \frac{\rho^p \mathrm{d}^2}{18\mu^f} \tag{2.10}$$

is the particle momentum response time which is the time required for a particle released from rest to obtain 63% of the fluid free stream velocity [61]. The inverse particle response time $\beta = 1/\tau_p$ shall also be used in this thesis. For later use in the PDF kinetic

equation (see section 4.1), equation (2.9) shall be re-written as

$$\frac{d}{dt}v_i^p = \underbrace{F_i\left(\boldsymbol{x}^p(t), \boldsymbol{v}^p(t), t\right)}_{\text{Mean Force}} + \underbrace{f_i\left(\boldsymbol{x}^p(t), t\right)}_{\text{Fluctuating Force}} \tag{2.11}$$

where the mean aerodynamic force is

$$F_i\left(\boldsymbol{x}^p(t), \boldsymbol{v}^p(t), t\right) = \frac{1}{\tau_p\left(1+\frac{1}{2}\frac{\rho^f}{\rho^p}\right)}\left(\langle u_i\rangle^p - v_i^p\right) + \frac{2(\rho^p-\rho^f)}{2\rho^p+\rho^f}g_i + \frac{3\rho^f}{2\rho^p+\rho^f}\left\langle\frac{D}{Dt}u_i\right\rangle^p \tag{2.12}$$

where $\langle\boldsymbol{u}\rangle^p = \langle\boldsymbol{u}\rangle(\boldsymbol{x}^p(t),t)$,$\left\langle\frac{D}{Dt}u_i\right\rangle^p = \left\langle\frac{D}{Dt}u_i\right\rangle(\boldsymbol{x}^p(t),t)$, and the fluctuating aerodynamic force is

$$f_i\left(\boldsymbol{x}^p(t), t\right) = \frac{1}{\tau_p\left(1+\frac{1}{2}\frac{\rho^f}{\rho^p}\right)}u_i^{p\prime} + \frac{3\rho^f}{2\rho^p+\rho^f}\left(\frac{D}{Dt}u_i^p\right)' \tag{2.13}$$

where by definition

$$\left(\frac{D}{Dt}u_i^p\right)' = \frac{D}{Dt}u_i^p - \left\langle\frac{D}{Dt}u_i\right\rangle^p \tag{2.14}$$

2.5 Particle-Boundary Interactions

For particle dispersion in pipe and channel flows, it is important to be able to quantify the effect of particle-boundary interactions (which includes both particle-wall and particle-particle collisions) on the motion of the particles. For rigid particles, there are essentially three types of interaction; elastic collisions, inelastic collisions and deposition (or agglomeration in the case of particle-particle collisions). Another crucial factor is whether or not the particles slide or rotate upon contact with a boundary. Factors which influence the nature of the particle-boundary interactions include the malleability of the particle and boundary materials, electrostatic forces and wall roughness.

There are essentially two different approaches to model the effect of the particle-boundary interactions. The simplest approach is the 'hard sphere' approach (e.g. [61, 69]), in which the dynamics of the particle deformation upon impact with the boundary is not explicitly accounted for. Rather, the particle dynamics pre and post collision are related by an appropriate coefficient of restitution, in addition to coefficients of friction if rough boundaries are being considered. A recent hard-sphere model has also been

developed which takes into account cohesive and adhesive forces for particle interaction with a boundary [70].

The second approach is the 'soft sphere' approach (e.g. [61,71]), in which the particle deformation during the particle-boundary interaction is modelled and its effect upon the instantaneous dynamics of the particle is accounted for. The soft sphere approach is more physically meaningful than the hard sphere approach when the particles of interest are deformable, however its computational expense is significantly greater. There are additional, more complex models for accounting for particle-boundary interactions, some of which consider the effect of hydrodynamic interactions (e.g. [72–76]).

If the wall (or boundary surface) is rough this also affects the particle-wall collision, and indeed affects the overall characteristics of the particle dispersion (e.g. [77]). Some models have attempted to account for this effect by modelling the particle-wall collision as a stochastic process, where the rough wall is treated as randomly affecting the particle motion upon collision with the wall (e.g. [78, 79]).

The models for particle-boundary collisions discussed thus far are strictly speaking only of use in LPT simulations. However these models can be applied to formulate boundary conditions for ESM which account for the particle-boundary interactions in a statistical manner, and these are discussed in chapter 4.

Chapter 3

Characteristics of Particle Dispersion in Turbulent Channel Flows

Although the aim of the work presented in this thesis is to describe particle dispersion in turbulent pipe flows, particle dispersion in turbulent channel flows is qualitatively very similar. Further, mathematical models are easier to derive and implement for channel flows than they are for pipe flows. Therefore particle dispersion in turbulent channel flows will be the focus of attention in this thesis. In this chapter some of the particularities of this type of multiphase flow will be discussed, and a summary will be given of the current understanding of particle dispersion in turbulent channel flows.

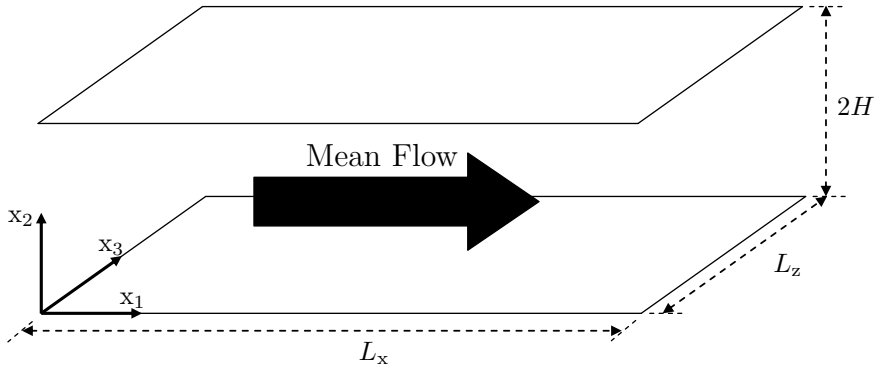

Figure 3.1: Diagram of Channel Flow. The flow is between two flat parallel plates separated in the wall-normal direction by a distance $2H$. x_1 is the 'stream-wise' direction, x_2 is the 'wall-normal' direction, and x_3 is the 'span-wise' direction (with $(x_1,x_2,x_3)\equiv(x,y,z)$). The mean fluid velocity is in the x_1 direction.

Figure 3.1 shows the typical geometry used for numerical studies of turbulent channel flows. Unlike a 'true' enclosed channel flow, the channel flow in numerical simulations is a flow between two flat parallel plates separated in the wall-normal direction, where

the mean flow rate is in the stream-wise direction and the flow is made periodic in the stream-wise and span-wise directions with periodic lengths L_{x} and L_{z} respectively. Channel flow simulation results are usually expressed in 'wall units', where the respective variables are scaled using appropriate combinations of the fluid kinematic viscosity ν^f and the wall friction velocity u_τ (also in some cases the half channel height H). The superscript '+' shall be used to indicate that a variable is being expressed in wall units. Of particular importance are

$$\mathrm{x}_i^+ = \mathrm{x}_i \frac{u_\tau}{\nu^f} \tag{3.1}$$

$$\tau_p^+ = \tau_p \frac{u_\tau^2}{\nu^f} \tag{3.2}$$

$$u_i^+ = \frac{u_i}{u_\tau} \tag{3.3}$$

However, *for notational convenience and simplicity the superscript '+' will be omitted henceforth in this thesis and unless otherwise stated, all results presented in this thesis will be expressed in terms of wall units.*

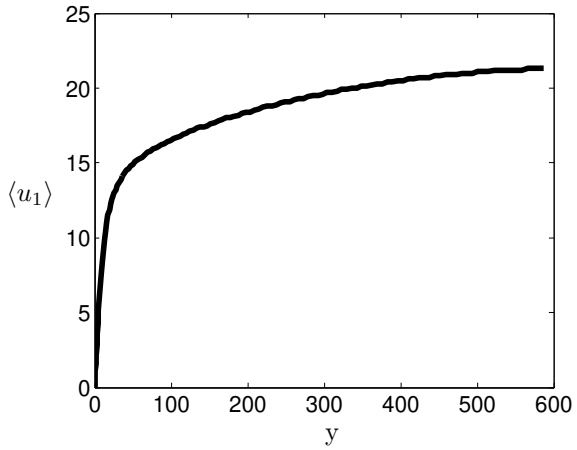

Figure 3.2: Diagram showing the mean stream-wise fluid velocity as a function of distance from the wall.

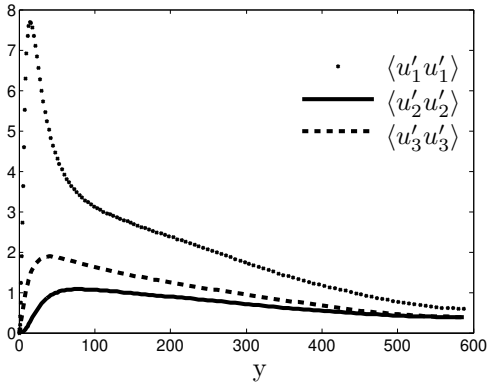

Figure 3.3: Plot showing the diagonal components of the fluid velocity Reynolds stress tensor.

Figures 3.2 and 3.3 show solutions for the mean stream-wise fluid velocity and the diagonal components of the fluid velocity Reynolds stress tensor, plotted against distance from the wall, and are taken from [4] in which a DNS of turbulent channel flow was performed. The mean velocity profile in a turbulent channel flow can be considered to be linear in the viscous sublayer ($y < 5$) and nonlinear everywhere else. The diagonal components of the fluid velocity Reynolds stress tensor in a turbulent channel flow are strongly inhomogeneous and anisotropic. To leading order, $\langle u_1' u_1' \rangle$ and $\langle u_3' u_3' \rangle$ are proportional to y^2 whilst $\langle u_2' u_2' \rangle$ is proportional to y^4 (e.g. [21]).

The results in figures 3.2 and 3.3 highlight three characteristic features of a turbulent channel flow which are particularly important for particle dispersion; there is a strong mean shearing of the fluid velocity field (revealed in the large wall-normal gradients of the mean stream-wise fluid velocity), the statistics are strongly anisotropic and very strongly inhomogeneous in the wall-normal direction. Other statistics, not shown here, reveal the same features; strong anisotropy and very strong inhomogeneity in the wall-normal direction. However, the turbulence statistics are homogeneous in the stream-wise and span-wise directions. It can be seen from figures 3.2 and 3.3 that the region of very strong inhomogeneity and anisotropy is concentrated within the region $0 \leq \mathrm{y} \leq 100$; this region may be considered to be the turbulent boundary layer of the channel flow (this is of course not a strict definition of the domain of the turbulent boundary layer which would properly be defined by a parameter such as the momentum thickness. However, in this context this rather loose definition of the turbulent boundary layer is sufficient).

In a turbulent channel flow there are essentially three causes of particle dispersion (neglecting molecular diffusion); the mean shearing of the fluid, body forces acting on the particles and the fluid turbulence. Inertial particles initially uniformly distributed across the channel will disperse because of the mean shear; particles near the center of

the channel will move with greater mean velocities than those near the wall and so the particles will disperse non-uniformly across the channel.

Body forces, such as gravity, will cause an initially uniform distribution of particles to migrate in the direction of the body force. For example, particles dispersed in a horizontal channel will tend to settle to the bottom of the channel due to gravitational settling. However the particles will not all simply settle and remain at the bottom of the channel under gravity; the fluid turbulence suspends particles within the flow field, and particles which have settled to the bottom of the channel may be resuspended by the turbulence.

Unlike the effect of the mean shearing of the fluid and body forces, the effect of the fluid turbulence on the particle dispersion process is complex, and at present, only partially understood. One characteristic feature of a turbulent flow field is that, whether homogeneous or inhomogeneous, it will demix a suspension of initially uniformly distributed inertial particles; a feature resulting from the interaction between particles and turbulent structures in the flow field, with particles tending to accumulate in regions of high strain and low vorticity (e.g. [80]). Nevertheless, for particle dispersion in a statistically steady state homogeneous isotropic turbulent flow field the average particle concentration is necessarily spatially uniform (when there are no body forces acting on the particles). However, in a turbulent channel flow, even when there are no body forces acting on the particles, the average particle concentration in the wall-normal direction may be strongly non-uniform. In particular, it is found that inertial particles accumulate in the near-wall regions of the channel [9,81] (the same effect is found in pipe flows, see [8] for example), and the effect is commonly referred to as 'turbophoresis' [82, 83].

From a statistical perspective, turbophoresis describes a particle drift down gradients in the wall-normal particle kinetic stresses, and its strength depends upon the particle inertia (this strength being zero in the limits $\tau_p \to 0$ and $\tau_p \to \infty$). The kinetic energy that inertial particles receive in regions of intense turbulence is 'carried' by the particles into regions of lower turbulence intensity, which gives rise to a skewness in the particle velocities. The particle velocity skewness is directly related to the turbophoretical drift [82,84]. From a dynamic perspective, turbophoresis is understood in the following way; strongly correlated 'sweep' events (fluid downwash towards the wall) bring particles into the near-wall region, where they accumulate in or below low speed streaks in the turbulent velocity field [85]. 'Ejection' events (fluid upwash away from the wall) are responsible for transferring particles away from the wall, but they are less efficient in particle transport than sweep events, and hence the particles accumulate and remain for a long time in the near-wall region of the flow. For a detailed discussion on the interaction between turbulent near-wall structures and inertial particle dispersion, along with its relation to turbophoresis see [85].

The nature of the particle-wall interaction can strongly affect the near-wall accumulation of inertial particles in a channel flow. Most research has focused on either depositing particles (e.g. [86, 87]) or perfectly elastic particle-wall collisions (e.g. [2, 9, 81, 84]). The results show that the near-wall particle accumulation is much greater for elastic collisions than for depositing particles, since particles which elastically rebound from the wall tend to (depending on the particle inertia) remain 'trapped' near the wall for long periods of time.

Another feature of particle dispersion in a turbulent channel flow is that the particles preferentially sample the fluid velocity field (e.g. [2,81,88]). This feature is intrinsically related to the non-uniform particle concentration, and may be understood to be the result of the preferential motion of inertial particles in sweep and ejection events (as argued in [85]) .

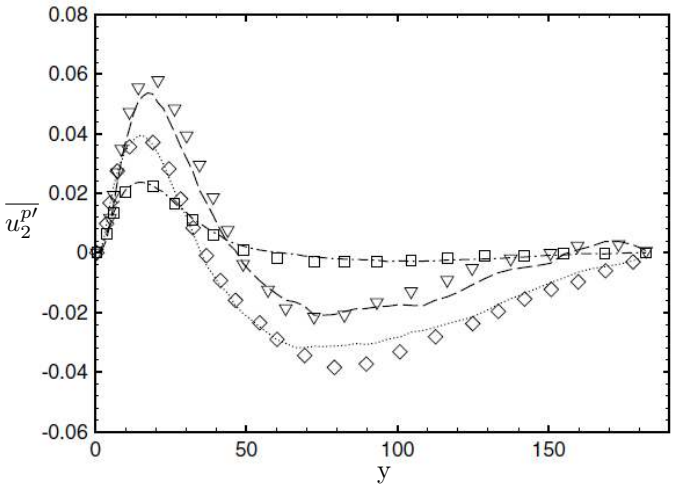

Figure 3.4: Average wall-normal fluctuating fluid velocity at the particle position for different τ_p values. Symbols: ($\square$) $\tau_p = 1.2$; ($\diamondsuit$) $\tau_p = 6.8$; (∇) $\tau_p = 27.1$. Figure taken from [2] (the additional data in the figure indicated by the broken lines is not relevant to the present discussion).

Figures 3.4 and 3.5 show results of the average fluctuating wall-normal and stream-wise fluid velocity at the particle position , respectively, for different particle response times. The figures are taken from [2] in which a DNS of particle dispersion in a turbulent channel flow was performed (with dilute particle mass loading, no gravity and elastic particle-wall collisions). It can be seen from figure 3.4 that $\overline{u_2^{p\prime}}$ depends strongly upon both the wall-normal position and τ_p, taking on values greater than and less than 0 in different parts of the domain. In the region where $\overline{u_2^{p\prime}} > 0$ the particles preferentially

sample ejection events in the turbulence cycle by which they are transported away from the wall, whereas in the region where $\overline{u_2^{p\prime}} < 0$ the particles preferentially sample sweep events by which they are transported towards the wall. In the limits $\tau_p \to 0$ and $\tau_p \to \infty$, $\overline{u_2^{p\prime}} \to 0$ everywhere (i.e. no preferential sampling). In general, the turbophoretical drift and the drift arising from the preferential sampling of the fluid velocity field are in opposition to each other.

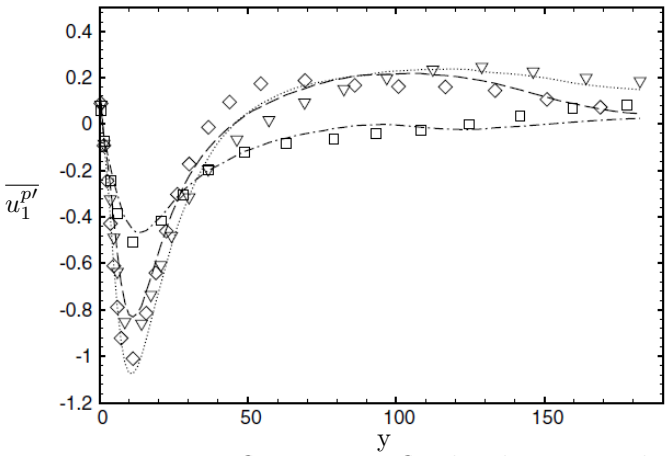

Figure 3.5: Average stream-wise fluctuating fluid velocity at the particle position for different τ_p values. Symbols: ($\square$) $\tau_p = 1.2$; ($\diamondsuit$) $\tau_p = 6.8$; (∇) $\tau_p = 27.1$. Figure taken from [2] (the additional data in the figure indicated by the broken lines is not relevant to the present discussion).

It can be seen from figure 3.5 that $\overline{u_1^{p\prime}}$ also depends strongly upon both the wall-normal position and τ_p, taking on values greater than and less than 0 in different parts of the domain. The negative near-wall values of $\overline{u_1^{p\prime}}$ confirm that inertial particles tend to cluster in near-wall stream-wise streaks, structures which have stream-wise velocities less than the local mean stream-wise velocity. The tendency of inertial particles to segregate into stream-wise streak structures has been found in other studies also (see, for example, [89–92]).

Such characteristic features as these (inhomogeneous particle concentrations, preferential sampling of the turbulent flow field etc) which have been discovered through LPT and experimental studies must be captured in a statistical manner through whichever ESM is pursued to model particle dispersion in a turbulent channel flow. In the next chapter a PDF kinetic equation will be considered which provides a fundamentally sound way to model particle dispersion in a turbulent channel flow. From this PDF equation, continuum equations can be derived and it is shown that they capture the effect of the preferential sampling of the turbulent flow field and predict inhomogeneous particle concentrations.

Chapter 4

The PDF Kinetic equation and its associated Continuum Equations

In the previous chapter consideration was given to the motion of inertial particles in turbulent channel flows and boundary layers. The objective of the work presented in this thesis is to develop mathematical models to describe the motion of inertial particles in such flows.

The motion of macroscopic inertial particles in a classical fluid which is turbulent is entirely deterministic, and is not intrinsically random. Nevertheless, just as with many thermodynamic and chaotic systems, turbulence *appears* to be random, due to the intractability of the precise nature of the initial conditions and the large number of degrees of freedom. Therefore, just as statistical physics has been successfully used to describe thermodynamical systems (Boltzmann equation etc), it may also be used to describe the motion of inertial particles in a turbulent flow.

When developing a PDF (probability density function) equation the first and most important choice is what variables to retain in the phase-space vector, that is, what variables should be described by the PDF? For example, in the case of particles dispersing in turbulence the particle position, particle velocity, the fluid velocity at the particle position, the fluid acceleration at the particle position, the rate of change of the fluid acceleration at the particle position etc may be all included in the phase-space vector of the PDF. Any variables which are not retained in the phase-space vector will require closure in the transport equation for the PDF. The important decision is then to decide which variables are really of interest, and furthermore, which variables, if not included in the phase-space vector, can be reliably modelled and closed in the PDF transport equation. In the case of particle dispersion in turbulent flows two approaches have been used. The first is to retain only the particle position and velocity in the phase-space vector in the tradition of the Boltzmann equation. This PDF equation, known as the

kinetic equation, has been developed in several works [83, 93–96]. The other approach has been to retain, in addition to the particle position and velocity, the fluid velocity at the particle position. This approach has been developed extensively in [42, 97].

The pre-defined scope of the research undertaken in this thesis was to consider developments to the kinetic approach, and so only this form will be considered in this thesis. However, it is recognised that the higher dimensional PDF equation in [42, 97] has its own advantages over the kinetic approach and these, along with a discussion on the issue of which variables to retain in the phase-space vector are considered in detail in [42].

In this chapter a summary will be given of a PDF (probability density function) kinetic equation for particle position and velocity in phase-space which has previously been derived by Reeks [83], Swailes [93], Hyland [94], Zaichik [95] and Pozorski & Minier [96]. The PDF kinetic equation is similar to the Boltzmann equation, only that instead of inter-particle collisions causing the dispersion of the particles it is the turbulence, treat as a stochastic process correlated in space and time which causes the particles to be dispersed throughout the phase-space.

The derivation of the PDF kinetic equation for particle position and velocity in a turbulent flow field will be presented in order to highlight subtle but important differences between the PDF equations presented in the cited works. Then the continuum equations which are obtained from the PDF kinetic equation are introduced, and a discussion is given regarding the various terms in them that require closure.

4.1 Derivation of PDF kinetic equation

Begin by defining a Lagrangian PDF for particle position and velocity at time t corresponding to a single realisation of the turbulent flow field and initial conditions $\boldsymbol{x}^p(0)$, $\boldsymbol{v}^p(0)$

$$\mathcal{P}(\mathbf{x}, \mathbf{v}, t) = \delta(\boldsymbol{x}^p(t) - \mathbf{x})\delta(\boldsymbol{v}^p(t) - \mathbf{v}) \tag{4.1}$$

where $\delta(...)$ is the Dirac delta function, $\mathbf{x}$ and $\mathbf{v}$ are the fixed phase-space position and velocity variables (Eulerian), $\boldsymbol{x}^p(t)$ and $\boldsymbol{v}^p(t)$ are the particle position and velocity at time t (Lagrangian). Formal differentiation of equation (4.1) with respect to t yields

$$\frac{\partial \mathcal{P}}{\partial t} = -\frac{\partial}{\partial \mathrm{x}_i}\left[v_i^p \mathcal{P}\right] - \frac{\partial}{\partial \mathrm{v}_i}\left[(F_i(\boldsymbol{x}^p(t), \boldsymbol{v}^p(t), t) + f_i(\boldsymbol{x}^p(t), t))\mathcal{P}\right] \tag{4.2}$$

where $\boldsymbol{F}(\boldsymbol{x}^p(t), \boldsymbol{v}^p(t), t)$ and $\boldsymbol{f}(\boldsymbol{x}^p(t), t)$ are the mean and fluctuating aerodynamic forces acting upon the particle (see equation (2.11)). By ensemble averaging equation (4.2) over all realisations of $\boldsymbol{f}$ and over all initial conditions $\boldsymbol{x}^p(0)$, $\boldsymbol{v}^p(0)$ a transport equation for the PDF, p , is obtained for the particle phase-space density at time t

$$\frac{\partial p}{\partial t} = -\frac{\partial}{\partial \mathrm{x}_i}\left[\mathrm{v}_i p\right] - \frac{\partial}{\partial \mathrm{v}_i}\left[F_i(\mathbf{x}, \mathbf{v}, t) p\right] - \frac{\partial}{\partial \mathrm{v}_i}\langle f_i(\boldsymbol{x}^p(t), t)\mathcal{P}\rangle \tag{4.3}$$

where

$$p(\mathbf{x}, \mathbf{v}, t) = \langle \mathcal{P}(\mathbf{x}, \mathbf{v}, t)\rangle \tag{4.4}$$

Equation (4.3) is unclosed since $\langle \boldsymbol{f}(\boldsymbol{x}^p(t), t)\mathcal{P}\rangle$ is unknown. This unknown term, referred to as the phase-space diffusion current, describes the average effect that the fluid turbulence has on dispersing the particles throughout the flow field. It is therefore necessary that this term is closed correctly if the PDF equation is to accurately describe particle dispersion in a turbulent fluid. Three methods have been used to close this unknown term; Reeks [83] used the Lagrangian History Direct Interaction (LHDI) approximation, Swailes [93], Hyland [94] and Zaichik [95] used the Furutsu-Novikov (FN) correlation splitting technique and Pozorski & Minier used Van Kampen's (VK) method [96]. Whilst it is claimed in the literature that each method produces *exactly* the same result (e.g. [98]) they do not, and this will be discussed in section 4.2.

The FN technique for closing the phase-space diffusion current is as follows. If $\boldsymbol{f}(\mathbf{x}, t)$ is modelled as a Gaussian stochastic field correlated in both space and time (although FN can also be used to deal with non Gaussian stochastic fields, see [93]), then using the FN formula gives the exact result

$$\langle f_i(\boldsymbol{x}^p(t), t)\mathcal{P}\rangle = \int_0^t \int_{\mathbf{x}'} \left\langle \frac{\delta \mathcal{P}}{\delta f_j(\mathbf{x}', t') d\mathbf{x}' dt'} R_{ji}(\mathbf{x}', t'; \mathbf{x}, t)\right\rangle d\mathbf{x}' dt', \qquad 0 \le t' \le t \tag{4.5}$$

where $\boldsymbol{R}(\mathbf{x}', t'; \mathbf{x}, t) = \langle \boldsymbol{f}(\mathbf{x}', t')\boldsymbol{f}(\mathbf{x}, t)\rangle$ is the Eulerian two-point, two-time correlation tensor for $\boldsymbol{f}$, and

$$\frac{\delta \mathcal{P}}{\delta f_j(\mathbf{x}', t') d\mathbf{x}' dt'}$$

describes how a perturbation in the flow field at $(\mathbf{x}', t')$ will affect the phase-space position of the particle at time t. Then

$$\frac{\delta\mathcal{P}}{\delta f_j(\mathbf{x}',t')d\mathbf{x}'dt'} = -\left(\frac{\partial\mathcal{P}}{\partial \mathrm{x}_k}\frac{\delta x_k^p(t)}{\delta f_j(\boldsymbol{x}^{p\prime},t')dt'} + \frac{\partial\mathcal{P}}{\partial \mathrm{v}_k}\frac{\delta v_k^p(t)}{\delta f_j(\boldsymbol{x}^{p\prime},t')dt'}\right)\delta(\boldsymbol{x}^{p\prime}-\mathbf{x}') \tag{4.6}$$

where $\boldsymbol{x}^{p\prime}$ is the particle position at time t'. Substituting (4.6) into (4.5) gives

$$\langle f_i(\boldsymbol{x}^p(t),t)\mathcal{P}\rangle = -\int_0^t\int_{\mathbf{x}'}\left\langle\left(\frac{\partial\mathcal{P}}{\partial \mathrm{x}_k}\frac{\delta x_k^p(t)}{\delta f_j(\boldsymbol{x}^{p\prime},t')dt'} + \frac{\partial\mathcal{P}}{\partial \mathrm{v}_k}\frac{\delta v_k^p(t)}{\delta f_j(\boldsymbol{x}^{p\prime},t')dt'}\right)R_{ji}(\mathbf{x}',t';\mathbf{x},t)\delta(\boldsymbol{x}^{p\prime}-\mathbf{x}')\right\rangle d\mathbf{x}'dt' \tag{4.7}$$

Since $\boldsymbol{R}$ is also a function of $\mathbf{x}$ equation (4.7) may be expressed as

$$\begin{aligned}\langle f_i(\boldsymbol{x}^p(t),t)\mathcal{P}\rangle = \int_0^t\int_{\mathbf{x}'}&\frac{\partial}{\partial \mathrm{x}_k}\left\langle\frac{\delta x_k^p(t)}{\delta f_j(\boldsymbol{x}^{p\prime},t')dt'}\mathcal{P}R_{ji}(\mathbf{x}',t';\mathbf{x},t)\delta(\boldsymbol{x}^{p\prime}-\mathbf{x}')\right\rangle\\ &-\left\langle\frac{\delta x_k^p(t)}{\delta f_j(\boldsymbol{x}^{p\prime},t')dt'}\mathcal{P}\frac{\partial}{\partial \mathrm{x}_k}R_{ji}(\mathbf{x}',t';\mathbf{x},t)\delta(\boldsymbol{x}^{p\prime}-\mathbf{x}')\right\rangle\\ &+\frac{\partial}{\partial \mathrm{v}_k}\left\langle\frac{\delta v_k^p(t)}{\delta f_j(\boldsymbol{x}^{p\prime},t')dt'}\mathcal{P}R_{ji}(\mathbf{x}',t';\mathbf{x},t)\delta(\boldsymbol{x}^{p\prime}-\mathbf{x}')\right\rangle d\mathbf{x}'dt'\end{aligned} \tag{4.8}$$

Now because averaging and integrating processes commute [99], the order of the ensemble averages and spatial integration in equation (4.8) may be reversed so that integration over all $d\mathbf{x}'$ may be performed. Also, since $\mathcal{P}(\mathbf{x},\mathbf{v},t) = \delta(\boldsymbol{x}^p(t)-\mathbf{x})\delta(\boldsymbol{v}^p(t)-\mathbf{v})$, the joint probabilities in equation (4.8) may be re-written in terms of conditional probabilities to give

$$\begin{aligned}\langle f_i(\boldsymbol{x}^p(t),t)\mathcal{P}\rangle = -\int_0^t&\frac{\partial}{\partial \mathrm{x}_k}p\left\langle\frac{\delta x_k^p(t)}{\delta f_j(\boldsymbol{x}^{p\prime},t')dt'}R_{ji}(\boldsymbol{x}^{p\prime},t';\mathbf{x},t)\right\rangle_{\mathbf{x},\mathbf{v}} - p\left\langle\frac{\delta x_k^p(t)}{\delta f_j(\boldsymbol{x}^{p\prime},t')dt'}\frac{\partial}{\partial \mathrm{x}_k}R_{ji}(\boldsymbol{x}^{p\prime},t';\mathbf{x},t)\right\rangle_{\mathbf{x},\mathbf{v}}\\ &+\frac{\partial}{\partial \mathrm{v}_k}p\left\langle\frac{\delta v_k^p(t)}{\delta f_j(\boldsymbol{x}^{p\prime},t')dt'}R_{ji}(\boldsymbol{x}^{p\prime},t';\mathbf{x},t)\right\rangle_{\mathbf{x},\mathbf{v}}dt'\end{aligned} \tag{4.9}$$

where the subscripts to the angled brackets indicate conditional ensemble averaging over all particle trajectories which satisfy $\boldsymbol{x}^p(t) = \mathbf{x}$ and $\boldsymbol{v}^p(t) = \mathbf{v}$. Equation (4.9) is generally written in terms of three dispersion tensors

$$\langle f_i(\boldsymbol{x}^p(t),t)\mathcal{P}\rangle = -\left(\frac{\partial}{\partial \mathrm{x}_k}p\lambda_{ki} + \frac{\partial}{\partial \mathrm{v}_k}p\mu_{ki} - p\kappa_i\right) \tag{4.10}$$

where the dispersion tensors are given by

$$\lambda_{ki}(\mathbf{x},\mathbf{v},t) = \int_0^t \left\langle \frac{\delta x_k^p(t)}{\delta f_j(\boldsymbol{x}^{p\prime},t')dt'} R_{ji}(\boldsymbol{x}^{p\prime},t';\mathbf{x},t) \right\rangle_{\mathbf{x},\mathbf{v}} dt' \tag{4.11}$$

$$\mu_{ki}(\mathbf{x},\mathbf{v},t) = \int_0^t \left\langle \frac{\delta v_k^p(t)}{\delta f_j(\boldsymbol{x}^{p\prime},t')dt'} R_{ji}(\boldsymbol{x}^{p\prime},t';\mathbf{x},t) \right\rangle_{\mathbf{x},\mathbf{v}} dt' \tag{4.12}$$

$$\kappa_i(\mathbf{x},\mathbf{v},t) = \int_0^t \left\langle \frac{\delta x_k^p(t)}{\delta f_j(\boldsymbol{x}^{p\prime},t')dt'} \frac{\partial}{\partial \mathrm{x}_k} R_{ji}(\boldsymbol{x}^{p\prime},t';\mathbf{x},t) \right\rangle_{\mathbf{x},\mathbf{v}} dt' \tag{4.13}$$

Therefore the final form of the PDF kinetic equation is

$$\frac{\partial p}{\partial t} = -\frac{\partial}{\partial \mathrm{x}_i}(\mathrm{v}_i p) - \frac{\partial}{\partial \mathrm{v}_i}(F_i p) + \frac{\partial}{\partial \mathrm{v}_i}\left(\frac{\partial}{\partial \mathrm{x}_k}(\lambda_{ki} p) + \frac{\partial}{\partial \mathrm{v}_k}(\mu_{ki} p) - \kappa_i p\right) \tag{4.14}$$

It is important to note that the expression for $\langle \boldsymbol{f}(\boldsymbol{x}^p(t),t)\mathcal{P}\rangle$ in equation (4.10) is not closed in the proper sense. Rather, equation (4.10) provides a way to relate the unknown diffusion current to statistics defined in the dispersion tensors which are in principle easier to close since these statistics are better understood. The dispersion tensors themselves require closure since they depend upon the statistics of the flow field evaluated along stochastic particle trajectories (i.e. they contain $\boldsymbol{x}^p(t')$, $\boldsymbol{x}^p(t)$ which are unknown).

In equations (4.11) to (4.13) an expression for the response tensor

$$\mathcal{G}_{kj} = \frac{\delta x_k^p(t)}{\delta f_j(\boldsymbol{x}^{p\prime},t')dt'}$$

is needed. The response tensor describes the effect of a perturbation in $\boldsymbol{f}$ at the particle position at time t' upon the position of the particle at time t ($t' \leq t$). An evolution equation for the response tensor is constructed by taking the functional derivative of the particle equation of motion

$$\frac{d^2}{dt^2}\frac{\delta x_k^p(t)}{\delta f_j(\boldsymbol{x}^{p\prime},t')dt'} = \frac{\delta}{\delta f_j(\boldsymbol{x}^{p\prime},t')dt'}[F_k(\boldsymbol{x}^p(t),\boldsymbol{v}^p(t),t) + f_k(\boldsymbol{x}^p(t),t)] \tag{4.15}$$

Then

$$\frac{d^2}{dt^2}\mathcal{G}_{kj} = \frac{\partial F_k}{\partial \mathrm{v}_i}\frac{d}{dt}\mathcal{G}_{ij} + \left(\frac{\partial F_k}{\partial \mathrm{x}_i} + \frac{\partial f_k}{\partial \mathrm{x}_i}\right)\mathcal{G}_{ij} \tag{4.16}$$

In [93] and [94] it was assumed that

$$\frac{\delta f_k(\boldsymbol{x}^p, t)}{\delta f_j(\boldsymbol{x}^{p\prime}, t')dt'} = \delta(t - t')\delta_{kj} \tag{4.17}$$

however in general this assumption is incorrect; if a particle experiences a perturbation at time t' then since its trajectory has been modified, the fluctuating force $\boldsymbol{f}$ it will experience at a later time will differ compared to that which it would have experienced had its trajectory not been perturbed. The correct form of the response tensor evolution equation is therefore given in equation (4.16). Nevertheless, in previous work (4.17) was invoked, along with the assumption that F can be approximated as being linear in $\mathbf{x}$ and $\mathbf{v}$. With these assumptions equation (4.16) reduces to a deterministic ordinary differential equation, whose solution is the Green tensor for the particle equation of motion. For example, with Stokes drag acting on the particles with a linear mean shear in the fluid turbulence (γ is the gradient of the mean fluid velocity)

$$F_k(\boldsymbol{x}^p(t), \boldsymbol{v}^p(t), t) = \beta\gamma\delta_{k1}\delta_{j2}x_j^p(t) - \beta v_k^p(t) \tag{4.18}$$

equation (4.16) reduces to (under the aforementioned approximations)

$$\frac{d^2}{dt^2}G_{kj} + \beta\frac{d}{dt}G_{kj} - \beta\gamma\delta_{k1}\delta_{i2}G_{ij} = \delta(t - t')\delta_{kj} \tag{4.19}$$

where $\boldsymbol{G}$ is the Green tensor for the particle equation of motion (and $\boldsymbol{G}$ is now the approximation to $\boldsymbol{\mathcal{G}}$). Strictly speaking, equation (4.17) is only true if $\boldsymbol{f}(t)$ or if $\boldsymbol{x}^{p\prime} = \boldsymbol{x}^p$. Since the response tensors will not in general tend to zero for $t' \ll t$, the integrand in the dispersion tensors (see equations (4.11) to (4.13)) tends to zero for times greater than the characteristic correlation times in $\boldsymbol{R}(\boldsymbol{x}^{p\prime}, t'; \mathbf{x}, t)$. For large particles (large compared to the timescale on which the local turbulence fluctuates), it is a reasonable approximation to say that $\boldsymbol{x}^{p\prime} \approx \boldsymbol{x}^p$ for $|t' - t| \leq$ the local fluid turbulence correlation time scale, in which case $\boldsymbol{\mathcal{G}} \approx \boldsymbol{G}$. However for smaller particles this approximation will be less applicable and in chapter 9 the effect of the approximation $\boldsymbol{\mathcal{G}} \approx \boldsymbol{G}$ upon the dispersion tensors is examined over a range of particle sizes.

4.2 Alternative PDF equation derivations

In section 4.1, a PDF kinetic equation was derived using the FN technique, consistent with the derivation presented in [93]. However, there are alternative derivations of

the PDF kinetic equation in the literature, some using alternative closure methods for the phase-space diffusion current. Reeks [83] used the Lagrangian History Direct Interaction (LHDI) approximation, Hyland [94] and Zaichik [95] used the Furutsu-Novikov (FN) correlation splitting technique and Pozorski & Minier used Van Kampen's (VK) method [96]. In this chapter the PDF equations in the cited works are analysed in order to highlight the fact that they are not the same, even though in the literature they are claimed to be (e.g. [98]).

4.2.1 Reeks result using LHDI

An important observation is that the dispersion tensors defined in (4.11) to (4.13) which have been obtained using the FN closure method are not exactly the same as those obtained by Reeks using LHDI [83]. The difference lies in the form of $\boldsymbol{R}(\mathbf{x}', t'; \mathbf{x}, t)$. In equations (4.11) to (4.13), $\boldsymbol{R}(\mathbf{x}', t'; \mathbf{x}, t)$ is given by

$$R_{ji}(\mathbf{x}', t'; \mathbf{x}, t) = \langle f_j(\mathbf{x}', t') f_i(\mathbf{x}, t) \rangle \tag{4.20}$$

which is the predefined Eulerian two-point, two-time correlation tensor for $\boldsymbol{f}$ and depends upon *all* realisations of the flow field $\boldsymbol{f}$. Reeks, using LHDI, has $\boldsymbol{R}(\mathbf{x}', t'; \mathbf{x}, t)$ given by

$$R_{ji}(\mathbf{x}', t'; \mathbf{x}, t) = f_j(\mathbf{x}', t') f_i(\mathbf{x}, t) \tag{4.21}$$

These forms of $\boldsymbol{R}$ are intrinsically different, since equation (4.20) is deterministic and equation (4.21) is stochastic. The difference this makes is that the FN defined dispersion tensors depend upon the full Eulerian statistics of $\boldsymbol{f}$ whereas the LHDI dispersion tensors depend upon the statistics of $\boldsymbol{f}$ sampled by the inertial particles. Since inertial particles preferentially sample turbulent flow fields in turbulent boundary layers the FN and LHDI defined dispersion tensors, and hence their PDF equations, are therefore not equivalent.

A fundamental reason why the resulting PDF equations from LHDI and FN are different (in terms of the way their dispersion tensors are defined) is that in LHDI the flow field *seen by the particles* is assumed Gaussian whereas in FN it is the Eulerian flow field which is assumed to be Gaussian. Inertial particles preferentially sample the statistics of turbulent flow fields such that even if the Eulerian flow field is Gaussian, the flow field seen by the particles may be non-Gaussian. Therefore the nature of the Gaussian assumption in the FN and LHDI formulations is fundamentally different.

Nevertheless, in the limit $\tau_p \to \infty$ LHDI and FN PDF equations are equivalent, in which limit both PDF equations reduce to the Fokker-Planck equation.

4.2.2 Zaichik and Hyland result using FN

Hyland [94] and Zaichik [95] use the FN technique to derive the PDF kinetic equation and yet also obtain a final expression with $\boldsymbol{R}(\mathbf{x}', t'; \mathbf{x}, t) = \boldsymbol{f}(\mathbf{x}', t')\boldsymbol{f}(\mathbf{x}, t)$ in the dispersion tensors, just as Reeks obtained using LHDI. However the analysis in equations (4.5) to (4.9) in section 4.1 shows quite clearly that using the FN formula, the form of $\boldsymbol{R}$ in the dispersion tensors must be that given in equation (4.20).

In [95] (and in later papers such as [100,101], etc) the closure Zaichik (& co-workers) obtains for the phase-space diffusion current using FN is

$$\langle f_i(\boldsymbol{x}^p(t), t)\mathcal{P}\rangle = -\tau_p \left(\Lambda_{ij}(\mathbf{x}, t)\frac{\partial p}{\partial \mathrm{v}_j} + M_{ij}(\mathbf{x}, t)\frac{\partial p}{\partial \mathrm{x}_j} \right) \tag{4.22}$$

where $\tau_p\Lambda$ is claimed to be equivalent to equation (4.12) and $\tau_p M$ equivalent to equation (4.11). However equation (4.22) is not equivalent to equation (4.10) for two reasons.

First of all, the closed expression for the phase-space diffusion current given in equation (4.22) does not contain the $\boldsymbol{\kappa}$ dispersion tensor. The argument given is that the $\boldsymbol{\kappa}$ dispersion tensor 'cancels out' via

$$\begin{aligned} \frac{\partial}{\partial \mathrm{x}_k} p\lambda_{ki} - p\kappa_i &= p\frac{\partial}{\partial \mathrm{x}_k}\lambda_{ki} - p\kappa_i + \lambda_{ki}\frac{\partial}{\partial \mathrm{x}_k}p \\ &= \lambda_{ki}\frac{\partial}{\partial \mathrm{x}_k}p, \qquad \text{with} \qquad \kappa_i = \frac{\partial}{\partial \mathrm{x}_k}\lambda_{ki} \end{aligned} \tag{4.23}$$

However

$$\begin{aligned} \frac{\partial}{\partial \mathrm{x}_k}\lambda_{ki} - \kappa_i = \int_0^t \int_{\mathbf{x}'} R_{ji}(\mathbf{x}', t'; \mathbf{x}, t) \left[\frac{\partial}{\partial \mathrm{x}_k} \left\langle \frac{\delta x_k^p(t)}{\delta f_j(\boldsymbol{x}^{p\prime}, t')dt'} \delta\left(\boldsymbol{x}^{p\prime} - \mathbf{x}'\right) \right\rangle_{\mathbf{x},\mathbf{v}} \right] d\mathbf{x}' dt' \\ \neq 0 \quad \text{except in the limits} \quad \tau_p \to 0, \tau_p \to \infty \end{aligned} \tag{4.24}$$

Of particular importance is the fact that by assuming $\kappa_i = \partial_k \lambda_{ki}$ a term in the particle momentum equation is removed, a term which is not zero for inertial particles (see section 4.3.3).

Secondly, in [95] a PDF equation for particle position, velocity and temperature is derived. Therefore the PDF at time t corresponding to a single realisation of the turbulent field and a single realisation of $\boldsymbol{x}^p(0)$, $\boldsymbol{v}^p(0)$, $\boldsymbol{\theta}^p(0)$ is defined in [95] to be

$$\mathcal{P} = \delta(\boldsymbol{x}^p(t) - \mathbf{x})\delta(\boldsymbol{v}^p(t) - \mathbf{v})\delta(\boldsymbol{\theta}^p(t) - \boldsymbol{\theta}) \tag{4.25}$$

where $\boldsymbol{\theta}^p(t)$ is the particle temperature at time t, $\boldsymbol{\theta}$ is a temperature phase-space variable, and the PDF obtained by averaging over all realisations of the turbulent field and over all initial conditions is $p = \langle \mathcal{P} \rangle$. In view of the form of equation (4.25), the dispersion tensors in equation (4.22) ought to be functions of $\mathbf{x}, \mathbf{v}, \boldsymbol{\theta}, t$, yet they are not. The reason for this is believed to be as follows; in [95] the form of the FN formula quoted is (see equation (5) in the paper quoted)

$$\langle f_i(\boldsymbol{x}^p(t), t)\mathcal{P} \rangle = \int_0^t \int_{\mathbf{x}'} \left\langle \frac{\delta \mathcal{P}(\mathbf{x}, t)}{\delta f_j(\mathbf{x}', t') d\mathbf{x}' dt'} R_{ji}(\mathbf{x}', t'; \mathbf{x}, t) \right\rangle d\mathbf{x}' dt', \qquad t' \leq t \tag{4.26}$$

which is incorrect in view of the form of equation (4.25). The correct form of the FN formula would have been

$$\langle f_i(\boldsymbol{x}^p(t), t)\mathcal{P} \rangle = \int_0^t \int_{\mathbf{x}'} \left\langle \frac{\delta \mathcal{P}(\mathbf{x}, \mathbf{v}, \boldsymbol{\theta}, t)}{\delta f_j(\mathbf{x}', t') d\mathbf{x}' dt'} R_{ji}(\mathbf{x}', t'; \mathbf{x}, t) \right\rangle d\mathbf{x}' dt', \qquad t' \leq t \tag{4.27}$$

However because Zaichik uses equation (4.26) the dispersion tensors become functions of $\mathbf{x}, t$ only.

Finally, in [94] Hyland makes an approximation which results in the trajectories $\boldsymbol{x}^p(t)$ in the dispersion tensors becoming deterministic (i.e. not depending upon $\boldsymbol{f}$; see page 6182 in [94]). This approximation is said to be invoked in order to be able to evaluate the spatial integral in the FN expression (i.e. the step going from equation (4.8) to (4.9)). This is unnecessary since the spatial integration may be performed by the process described in section 4.1. The trajectories in the dispersion tensors defined by FN (equations (4.11) to (4.13)) are stochastic, *not* deterministic, and are defined by the full flow field, i.e. by

$$\frac{d^2}{dt^2} x_i^p(t) = \frac{d}{dt} v_i^p(t) = F_i + f_i$$

Furthermore, it is claimed in [94] that the trajectories in the LHDI dispersion tensors are also deterministic, being based on the particle equation of motion in the absence of $\boldsymbol{f}$. This is not the case; the trajectories in the dispersion tensors defined by Reeks using LHDI are also stochastic.

4.2.3 Pozorski & Minier result using VK

In Pozorski & Minier [96] a PDF kinetic equation was derived using the Van Kampen (VK) method (e.g. [102,103]). It was recognised in [98] that the original result obtained by Pozorski & Minier in [96] was incorrect and in [98] the correct solution using VK to derive the PDF equation was given (the authors of [98] affirm that their corrected result was verified as being so by correspondence with Pozorski). Therefore it is the result given in [98] which will be considered.

Once again, in [96] and [98] it is claimed that the result obtained using VK is identical to that obtained by Reeks using LHDI, however this is not the case. First of all, in [98] the PDF equation is written as (some of the notation used in [98] is changed in what follows to make it consistent with the notation used in this thesis)

$$\frac{\partial}{\partial t}p = A_0 p + \alpha\Big\langle A_1\mathcal{P}\Big\rangle \tag{4.28}$$

where $\mathcal{P} = \delta(\boldsymbol{x}^p(t) - \mathbf{x})\delta(\boldsymbol{v}^p(t) - \mathbf{v})$, $p = \langle\mathcal{P}\rangle$, α represents the level of fluctuations and $A_0(\mathbf{x},\mathbf{v},t)$ and $A_1(\mathbf{x},\mathbf{v},t)$ are operators defined as

$$A_0(\mathbf{x},\mathbf{v},t) = -\frac{\partial}{\partial \mathrm{x}_i}\left[\mathrm{v}_i\cdot\right] - \frac{\partial}{\partial \mathrm{v}_i}\left[\mathrm{F}_i\cdot\right] \tag{4.29}$$

$$\alpha A_1(\mathbf{x},\mathbf{v},t) = -\frac{\partial}{\partial \mathrm{v}_i}\left[f_i\cdot\right] \tag{4.30}$$

such that

$$A_0(\mathbf{x},\mathbf{v},t)p = -\frac{\partial}{\partial \mathrm{x}_i}\left[\mathrm{v}_i p\right] - \frac{\partial}{\partial \mathrm{v}_i}\left[F_i p\right] \tag{4.31}$$

$$\alpha\Big\langle A_1(\mathbf{x},\mathbf{v},t)\mathcal{P}\Big\rangle = -\frac{\partial}{\partial \mathrm{v}_i}\Big\langle f_i\mathcal{P}\Big\rangle \tag{4.32}$$

The VK method can then be used to close the term $\alpha\Big\langle A_1(\mathbf{x},\mathbf{v},t)\mathcal{P}\Big\rangle$. The VK closure given in [98] is said to be appropriate for $\alpha\tau_c \ll 1$, where τ_c is the correlation time for A_1, and it would therefore appear that the VK result is not exact, but is only an approximation valid for $\alpha\tau_c \ll 1$ (and it is not clear that such a condition is satisfied for a turbulent boundary layer). Secondly it is stated that the VK result used to close $\alpha\Big\langle A_1(\mathbf{x},\mathbf{v},t)\mathcal{P}\Big\rangle$ is exact when A_1 is Gaussian [98] (although it would seem to be only exact in the limit $\alpha\tau_c \ll 1$).

Here then are two fundamental differences between the VK result and either the FN or LHDI result. First of all, the FN and LHDI results are exact when $\boldsymbol{f}$ is Gaussian (or

more precisely, FN is exact when the field $\boldsymbol{f}$ is Gaussian, and LHDI is exact when $\boldsymbol{f}$ seen by the particles is Gaussian) whereas the VK result appears to be an approximation, valid only if $\alpha\tau_c \ll 1$.

Secondly a Gaussian assumption for the operator A_1 is incompatible with the the nature of the Gaussian assumption in either FN or LHDI. In FN it is the Eulerian flow field $\boldsymbol{f}$ which is assumed Gaussian, whereas in LHDI it is $\boldsymbol{f}$ seen by the particles which is assumed Gaussian. The VK assumption that the operator A_1 is Gaussian is incompatible with either the FN or LHDI Gaussian assumptions.

Now in equation (4.121) in [98], the integrand (from which their dispersion tensors eventually arise) contains correlations of $\boldsymbol{f}$ evaluated along trajectories defined by

$$\frac{d^2}{dt^2}\mathcal{X}_i^p(t) = \frac{d}{dt}\mathcal{V}_i^p(t) = F_i(\boldsymbol{\mathcal{X}}^p(t), \boldsymbol{\mathcal{V}}^p(t), t) \tag{4.33}$$

so that the integrand in equation (4.121) in [98] contains $\boldsymbol{f}(\boldsymbol{\mathcal{X}}^p(t'), t'|\mathbf{x}, \mathbf{v}, t)$, that is, $\boldsymbol{f}$ evaluated at time t' along deterministic particle trajectories (defined by equation (4.33)) which arrive at phase-space position $\mathbf{x}, \mathbf{v}$ at time t. At the end of their VK closure analysis the dispersion tensors they obtain (see equation (4.125) in [98]) contain $\boldsymbol{f}(\boldsymbol{\mathcal{X}}^p(t'), t'|\mathbf{x}, \mathbf{v}, t)$[1]. Therefore the VK result cannot be consistent with the LHDI result since the LHDI result contains $\boldsymbol{f}(\boldsymbol{x}^p(t'), t'|\mathbf{x}, \mathbf{v}, t)$, that is, $\boldsymbol{f}$ evaluated along stochastic trajectories defined by

$$\frac{d^2}{dt^2}x_i^p(t) = \frac{d}{dt}v_i^p(t) = F_i(\boldsymbol{x}^p(t), \boldsymbol{v}^p(t), t) + f_i(\boldsymbol{x}^p(t), t) \tag{4.34}$$

which arrive at phase-space position $\mathbf{x}, \mathbf{v}$ at time t. The VK result expressed in equation (4.125) in [98] can be manipulated (using simple product rule) to yield three dispersion tensors which are superficially similar to the LHDI forms for $\boldsymbol{\lambda}$,$\boldsymbol{\mu}$ and $\boldsymbol{\kappa}$, however they are not the same for the reasons just presented.

Therefore, a striking difference between the VK and LHDI (and also FN) closures is that the VK dispersion tensors are closed, whereas the LHDI and FN dispersion tensors involve non-local correlations of $\boldsymbol{f}$ evaluated along stochastic particle trajectories and therefore require closure.

It has therefore been demonstrated that the FN, LHDI and VK closures offered for the

[1]Note that due to a lack of notational clarity it is not quite clear whether the dispersion tensors they obtain (see equation (4.125) in [98]) actually contain $\boldsymbol{f}(\boldsymbol{x}^p(t'), t'|\mathbf{x}, \mathbf{v}, t)$ or $\boldsymbol{f}(\boldsymbol{\mathcal{X}}^p(t'), t'|\mathbf{x}, \mathbf{v}, t)$. However, if one follows through their analysis starting from equation (4.121) in [98] to their final answer in equation (4.125), it is clear that their dispersion tensors ought to contain $\boldsymbol{f}(\boldsymbol{\mathcal{X}}^p(t'), t'|\mathbf{x}, \mathbf{v}, t)$ *not* $\boldsymbol{f}(\boldsymbol{x}^p(t'), t'|\mathbf{x}, \mathbf{v}, t)$.

PDF kinetic equation in the literature are not equivalent, but differ in some fundamental aspects. The PDF equation given in section 4.1, consistent with the derivation in [93] will be used in this thesis since it is known to be exact for Gaussian flow fields, and in addition, since, as demonstrated in appendix C this PDF kinetic equation can be proven to be free from any spurious drifts, whereas such proofs for the LHDI and VK results have not been offered and it is unclear whether or not they contain spurious drift.

4.3 Continuum Equations

The continuum equations for particles dispersed in a turbulent flow are given by the velocity moments of the PDF kinetic equation [104]. The advantage of constructing the continuum equations in this manner is that since the PDF equation has been derived directly from the particle equation of motion, all of the physics consistent with the underlying particle equation of motion will be incorporated into the continuum equations, rather than having to intuitively 'guess' what terms should be present in the continuum equations.

Integrating the PDF equation (equation (4.14)) over $\mathbf{v}$ yields the particle continuity equation

$$\frac{\partial}{\partial t}\rho + \frac{\partial}{\partial \mathrm{x}_i}(\rho \overline{\mathrm{v}}_i) = 0 \tag{4.35}$$

where the particle concentration (or number density) is defined as the integral of the Lagrangian PDF $p\left(\mathbf{x}, \mathbf{v}, t\right)$

$$\rho(\mathbf{x}, t) = \int_{\mathbf{v}} p\left(\mathbf{x}, \mathbf{v}, t\right) d\mathbf{v} \tag{4.36}$$

and

$$\overline{\mathrm{v}}_i(\mathbf{x}, t) = \frac{1}{\rho\left(\mathbf{x}, t\right)} \int_{\mathbf{v}} \mathrm{v}_i p\left(\mathbf{x}, \mathbf{v}, t\right) d\mathbf{v} \tag{4.37}$$

is the i^{th} component of the density weighted mean particle velocity. Multiplying the PDF equation by $\mathbf{v}$ and integrating over $\mathbf{v}$ yields the particle momentum equation

$$\rho\left(\frac{\partial}{\partial t}\overline{\mathrm{v}}_i+\overline{\mathrm{v}}_k\frac{\partial}{\partial \mathrm{x}_k}\overline{\mathrm{v}}_i\right)=-\frac{\partial}{\partial \mathrm{x}_k}\left[\rho(\overline{\mathrm{c}_k\mathrm{c}_i}+\overline{\lambda}_{ki})\right]+\rho(\overline{F}_i+\overline{\kappa}_i) \tag{4.38}$$

where $\mathrm{c}_i=\mathrm{v}_i-\overline{\mathrm{v}}_i$ is the fluctuating component of the particle velocity and

$$\overline{\mathrm{c}_k\mathrm{c}_i}(\mathbf{x},t)=\frac{1}{\rho\left(\mathbf{x},t\right)}\int\limits_{\mathbf{v}}\mathrm{c}_k\mathrm{c}_i p\left(\mathbf{x},\mathbf{v},t\right)d\mathbf{v} \tag{4.39}$$

is the ki component of the density weighted particle Reynolds stress tensor. Similarly

$$\overline{\lambda}_{ki}(\mathbf{x},t)=\frac{1}{\rho\left(\mathbf{x},t\right)}\int\limits_{\mathbf{v}}\lambda_{ki} p\left(\mathbf{x},\mathbf{v},t\right)d\mathbf{v} \tag{4.40}$$

$$\overline{\mu}_{ki}(\mathbf{x},t)=\frac{1}{\rho\left(\mathbf{x},t\right)}\int\limits_{\mathbf{v}}\mu_{ki} p\left(\mathbf{x},\mathbf{v},t\right)d\mathbf{v} \tag{4.41}$$

$$\overline{\kappa}_i(\mathbf{x},t)=\frac{1}{\rho\left(\mathbf{x},t\right)}\int\limits_{\mathbf{v}}\kappa_i p\left(\mathbf{x},\mathbf{v},t\right)d\mathbf{v} \tag{4.42}$$

are the velocity averaged forms of the particle dispersion tensors, and

$$\overline{F}_i(\mathbf{x},t)=\frac{1}{\rho\left(\mathbf{x},t\right)}\int\limits_{\mathbf{v}}F_i p\left(\mathbf{x},\mathbf{v},t\right)d\mathbf{v} \tag{4.43}$$

is the i^{th} component of the density weighted mean force acting on the particle. Multiplying the PDF equation by $\mathbf{vv}$ and integrating over $\mathbf{v}$ yields the particle Reynolds stress equation

$$\begin{aligned}\rho\left(\frac{\partial}{\partial t}\overline{\mathrm{c}_i\mathrm{c}_j}+\overline{\mathrm{v}}_k\frac{\partial}{\partial \mathrm{x}_k}\overline{\mathrm{c}_i\mathrm{c}_j}\right)&=-\frac{\partial}{\partial \mathrm{x}_k}(\rho\overline{\mathrm{c}_i\mathrm{c}_j\mathrm{c}_k})+\rho(\mathrm{S}_{ij}+\mathrm{S}_{ji})\\ \mathrm{S}_{ij}&=-(\overline{\mathrm{c}_i\mathrm{c}_k}+\overline{\lambda}_{ik})\frac{\partial}{\partial \mathrm{x}_k}\overline{\mathrm{v}}_j+\overline{\mathrm{c}_i(F_j+\kappa_j)}+\overline{\mu}_{ij}-\frac{1}{\rho}\frac{\partial}{\partial \mathrm{x}_k}(\rho\overline{\lambda_{ki}\mathrm{c}_j})\end{aligned} \tag{4.44}$$

where

$$\overline{\mathrm{c}_i\mathrm{c}_j\mathrm{c}_k}(\mathbf{x},t)=\frac{1}{\rho\left(\mathbf{x},t\right)}\int\limits_{\mathbf{v}}\mathrm{c}_i\mathrm{c}_j\mathrm{c}_k p\left(\mathbf{x},\mathbf{v},t\right)d\mathbf{v} \tag{4.45}$$

is the ijk component of the density weighted particle Reynolds stress flux tensor.

4.3.1 Closure Approximations in the Continuum Equations

Chapman-Enskog approximation

The PDF equation yields an infinite set of coupled moment equations and therefore at some level the system must be closed in order to obtain a finite, tractable set of continuum equations which can be used to model particle dispersion in a turbulent flow field. The set of continuum equations is usually closed at the second order level by applying the Chapman-Enskog closure approximation [101, 104]

$$\overline{\mathrm{c}_i\mathrm{c}_j\mathrm{c}_k} = -\frac{\tau_p}{3}\left(\left(\overline{\mathrm{c}_i\mathrm{c}_n} + \overline{\lambda}_{in}\right)\frac{\partial}{\partial \mathrm{x}_n}\overline{\mathrm{c}_j\mathrm{c}_k} + \left(\overline{\mathrm{c}_j\mathrm{c}_n} + \overline{\lambda}_{jn}\right)\frac{\partial}{\partial \mathrm{x}_n}\overline{\mathrm{c}_i\mathrm{c}_k} + \left(\overline{\mathrm{c}_k\mathrm{c}_n} + \overline{\lambda}_{kn}\right)\frac{\partial}{\partial \mathrm{x}_n}\overline{\mathrm{c}_j\mathrm{c}_i}\right) \tag{4.46}$$

The Chapman-Enskog approximation assumes that the fourth order correlations of the fluctuating particle velocity may be approximated as quasi-Gaussian, such that

$$\overline{\mathrm{c}_n\mathrm{c}_i\mathrm{c}_j\mathrm{c}_k} \approx \overline{\mathrm{c}_n\mathrm{c}_i}\;\overline{\mathrm{c}_j\mathrm{c}_k} + \overline{\mathrm{c}_n\mathrm{c}_j}\;\overline{\mathrm{c}_i\mathrm{c}_k} + \overline{\mathrm{c}_n\mathrm{c}_k}\;\overline{\mathrm{c}_i\mathrm{c}_j} \tag{4.47}$$

For particle dispersion in a turbulent boundary layer it is known that the particle velocity PDF's are far from Gaussian, and as such the use of a Chapman-Enskog approximation is perhaps questionable. Wang *et.al.* [105] tested a Chapman-Enskog type approximation against large eddy simulation (LES) of particle dispersion in a turbulent channel flow. They found that the Chapman-Enskog approximation agreed in a qualitative sense with the LES data, but there was some quantitative disagreement.

Velocity Independence of the Particle Dispersion Tensors

In the particle Reynolds stress equation (equation (4.44)) a closure is required for $\overline{\mathbf{c}\boldsymbol{\kappa}}$ and $\overline{\boldsymbol{\lambda}\mathbf{c}}$. By definition, $\boldsymbol{\kappa}$ and $\boldsymbol{\lambda}$ are velocity dependent (see equations (4.11) and (4.13)) and therefore $\overline{\mathbf{c}\boldsymbol{\kappa}}$ and $\overline{\boldsymbol{\lambda}\mathbf{c}}$ are not zero in general. Consider the form of $\boldsymbol{\lambda}$ given in equation (4.48) in which the unknown correlation tensor is $\langle \boldsymbol{R}(\boldsymbol{x}^{p\prime}, t'; \mathbf{x}, t)\rangle_{\mathbf{x},\mathbf{v}}$. This is the correlation tensor of the fluctuating flow field seen by inertial particles which arrive at phase-space position $\mathbf{x}, \mathbf{v}$ at time t in the flow field. Particles which move toward and arrive at $\mathbf{x}$ at t with high velocities will have seen a faster rate of decorrelation in the flow field than particles which move toward and arrive at $\mathbf{x}$ at t with small velocities. Since the correlations of the flow field seen by particles are highly dependent upon the particle velocities, $\overline{\mathbf{c}\boldsymbol{\kappa}}$ and $\overline{\boldsymbol{\lambda}\mathbf{c}}$ are never zero except in the limit $\tau_p \to \infty$. However, for want of a better approximation/model, $\overline{\mathbf{c}\boldsymbol{\kappa}}$ and $\overline{\boldsymbol{\lambda}\mathbf{c}}$ are usually set to zero.

The local homogeneous approximation for the dispersion tensors

With the Green tensor approximation for the response tensor, the dispersion tensors (equations (4.11) to (4.13)) become

$$\lambda_{ki}(\mathbf{x},\mathbf{v},t) = \int_0^t G_{kj}(t;t')\Big\langle R_{ji}(\boldsymbol{x}^{p'},t';\mathbf{x},t)\Big\rangle_{\mathbf{x},\mathbf{v}} dt' \tag{4.48}$$

$$\mu_{ki}(\mathbf{x},\mathbf{v},t) = \int_0^t \dot{G}_{kj}(t;t')\Big\langle R_{ji}(\boldsymbol{x}^{p'},t';\mathbf{x},t)\Big\rangle_{\mathbf{x},\mathbf{v}} dt' \tag{4.49}$$

$$\kappa_i(\mathbf{x},\mathbf{v},t) = \int_0^t G_{kj}(t;t')\Big\langle \frac{\partial}{\partial \mathrm{x}_k} R_{ji}(\boldsymbol{x}^{p'},t';\mathbf{x},t)\Big\rangle_{\mathbf{x},\mathbf{v}} dt' \tag{4.50}$$

For the continuum equations the velocity averaged forms of the dispersion tensors are required (see section 4.3)

$$\overline{\lambda}_{ki}(\mathbf{x},t) = \int_0^t G_{kj}(t;t')\Big\langle R_{ji}(\boldsymbol{x}^{p'},t';\mathbf{x},t)\Big\rangle_{\mathbf{x}} dt' \tag{4.51}$$

$$\overline{\mu}_{ki}(\mathbf{x},t) = \int_0^t \dot{G}_{kj}(t;t')\Big\langle R_{ji}(\boldsymbol{x}^{p'},t';\mathbf{x},t)\Big\rangle_{\mathbf{x}} dt' \tag{4.52}$$

$$\overline{\kappa}_i(\mathbf{x},t) = \int_0^t G_{kj}(t;t')\Big\langle \frac{\partial}{\partial \mathrm{x}_k} R_{ji}(\boldsymbol{x}^{p'},t';\mathbf{x},t)\Big\rangle_{\mathbf{x}} dt' \tag{4.53}$$

In order to close the conditional averages in equations (4.51) and (4.52) a locally homogeneous approximation (LHA) is generally used, in addition to the assumption that the averages are statistically stationary (e.g. [49, 100, 106]). Then the conditional averages in equations (4.51) and (4.52) take the form

$$\Big\langle R_{ji}(\boldsymbol{x}^p(s),s;\mathbf{x},0)\Big\rangle_{\mathbf{x}} \approx \langle f_j(\mathbf{x}) f_i(\mathbf{x})\rangle \exp\left(\frac{s}{\tau_{ji}^{Lp}(\mathbf{x},\tau_p)}\right) \tag{4.54}$$

where no summation of indices is intended and $s = t' - t \leq 0$. The timescale $\tau_{ji}^{Lp}(\mathbf{x},\tau_p)$ is the Lagrangian timescale of $\boldsymbol{f}$ seen by particles with response time τ_p whose trajectories *converge* (backward in time dispersion) to $\mathbf{x}$ at time $s = 0$. A model for this timescale is then required, and this is usually done by either approximating it by the fluid Lagrangian timescale or by a local homogeneous model (such as given in [107,108]).

Inserting (4.54) into (4.51) and (4.52) gives

$$\overline{\lambda}_{ki}(\mathbf{x},s) = \int_s^0 G_{kj}(s_1)\langle f_j(\mathbf{x})f_i(\mathbf{x})\rangle \exp\left(\frac{s_1}{\tau_{ji}^{Lp}(\mathbf{x},\tau_p)}\right) ds_1 \tag{4.55}$$

$$\overline{\mu}_{ki}(\mathbf{x},s) = \int_s^0 \dot{G}_{kj}(s_1)\langle f_j(\mathbf{x})f_i(\mathbf{x})\rangle \exp\left(\frac{s_1}{\tau_{ji}^{Lp}(\mathbf{x},\tau_p)}\right) ds_1 \tag{4.56}$$

Since the integrand in (4.55) and (4.56) tends to zero for $|s| \gg \tau_{ji}^{Lp}(\mathbf{x},\tau_p)$, the lower integral limit may be set to $-\infty$. Then the asymptotic forms of the dispersion tensors may be derived for Stokes drag forcing [109]

$$\overline{\lambda}_{ki}(\mathbf{x}) = \frac{\beta^2\left(\tau_{ki}^{Lp}\right)^2}{1+\beta\tau_{ki}^{Lp}}\left(\langle u_k'(\mathbf{x})u_i'(\mathbf{x})\rangle + \delta_{k1}\frac{\beta\gamma\left(\tau_{ki}^{Lp}\right)^2}{1+\beta\tau_{ki}^{Lp}}\langle u_2'(\mathbf{x})u_i'(\mathbf{x})\rangle\right) \tag{4.57}$$

$$\overline{\mu}_{ki}(\mathbf{x}) = \frac{\overline{\lambda}_{ki}(\mathbf{x})}{\tau_{ki}^{Lp}(\mathbf{x},\tau_p)} \tag{4.58}$$

(no summation is implied in (4.57) and (4.58)). In order to approximate $\overline{\boldsymbol{\kappa}}(\mathbf{x})$ the 'passive scalar approximation' (PSA) may be invoked

$$\overline{\kappa}_i(\mathbf{x}) = \frac{\partial}{\partial \mathrm{x}_k}\overline{\lambda}_{ki}(\mathbf{x}) \tag{4.59}$$

which is obtained by considering the necessary form of the particle momentum equation in the limit $\tau_p \to 0$ [110].

4.3.2 Boundary Conditions for the Continuum Equations

In general, in order to solve the continuum equations both initial conditions and boundary conditions are required. The initial conditions are easily specified, and depend upon the particular problem being solved for. Specifying the boundary conditions for the continuum equations is however more problematic. For the case of particle dispersion in a turbulent channel flow, Alipchenkov *et.al.* [111] and Zaichik [112] used an approximate solution to the PDF equation to derive the following boundary conditions

$$\overline{\mathrm{v}}_2\Big|_{wall} = -\frac{1-\chi}{1+\chi}\left(\frac{2}{\pi}\overline{\mathrm{c}_2\mathrm{c}_2}\right)^{\frac{1}{2}}\Big|_{wall} \tag{4.60}$$

$$\tau_p\frac{d}{\mathrm{x}_2}\overline{\mathrm{c}_1\mathrm{c}_1}\Big|_{wall} = 3\left(\frac{1-\chi e_1^2}{1+\chi e_1^2}-\frac{1-\chi}{1+\chi}\right)\left(\frac{2}{\pi\overline{\mathrm{c}_2\mathrm{c}_2}}\right)^{\frac{1}{2}}\overline{\mathrm{c}_1\mathrm{c}_1}\Big|_{wall} \tag{4.61}$$

$$\tau_p\frac{d}{\mathrm{x}_2}\overline{\mathrm{c}_2\mathrm{c}_2}\Big|_{wall} = \left(\frac{2-2\chi e_2^2}{1+\chi e_2^2}-\frac{1-\chi}{1+\chi}\right)\left(\frac{2}{\pi}\overline{\mathrm{c}_2\mathrm{c}_2}\right)^{\frac{1}{2}}\Big|_{wall} \tag{4.62}$$

$$\tau_p\frac{d}{\mathrm{x}_2}\overline{\mathrm{c}_3\mathrm{c}_3}\Big|_{wall} = 3\left(\frac{1-\chi e_3^2}{1+\chi e_3^2}-\frac{1-\chi}{1+\chi}\right)\left(\frac{2}{\pi\overline{\mathrm{c}_2\mathrm{c}_2}}\right)^{\frac{1}{2}}\overline{\mathrm{c}_3\mathrm{c}_3}\Big|_{wall} \tag{4.63}$$

$$\overline{\mathrm{c}_1\mathrm{c}_2}\Big|_{wall} = -\left(\frac{1-\chi e_1}{1+\chi e_1}-\frac{1-\chi}{1+\chi}\right)\left(\frac{2}{\pi}\overline{\mathrm{c}_2\mathrm{c}_2}\right)^{\frac{1}{2}}\overline{\mathrm{v}}_1\Big|_{wall} \tag{4.64}$$

where the subscripts $1, 2, 3$ represent the stream-wise, wall-normal and span-wise directions of the channel respectively, χ is the probability of the particle rebounding after the wall collisions ($\chi = 0$ for a perfectly absorbing wall, and $\chi = 1$ if particle deposition is absent), e_i is the particle coefficient of restitution for momentum loss in the i^{th} direction due to collision with the wall. The boundary conditions given in equations (4.60) to (4.64) were derived using perturbation techinques to solve a reduced form of the PDF equation (one in which the fluid forcing on the particle was assumed to be δ correlated) in the near wall region assuming a near-Gaussian PDF solution. It is therefore possible that these boundary value solutions will not be quantitatively accurate, and they need to be tested against particle tracking data. In other works (e.g. [113, 114]) boundary conditions for particles which collide with smooth walls have also been developed, and in [115] boundary conditions accounting for wall roughness are presented.

In each of the cited works, significant simplifications are made regarding the form of the particle velocity PDF near the wall, and in general the simplifictions made are probably quite unrealistic. However, boundary conditions for the PDF kinetic equation are much simpler to specify and therefore one way to derive boundary conditions for the continuum equations is to derive them from solutions to the PDF kinetic equation at the boundaries. That is, rather than deriving boundary conditions for the continuum equations by making approximations to the particle velocity PDF at the wall, one can solve the PDF equation directly (numerically, in the case of turbulent boundary layers) and then simply obtain the required continuum equation boundary conditions from the computed PDF itself. Work has been done on numerical solutions to PDF equations (e.g. [116, 117]) such that this method of deriving the continuum equation boundary conditions is possible.

4.3.3 Do the continuum equations describe the characteristics of particle dispersion in turbulent boundary layers?

In chapter 3 the characteristics of particle dispersion in turbulent channel flows (in particular, in the boundary layer) were considered and three important features were noted; (i) particles tend to accumulate in the near wall region, (ii) particles experience a turbophoretic drift, and (iii) inertial particle preferentially sample the turbulent flow field. The particle momentum equation (equation (4.38)) will now be examined in order to highlight that the PDF derived continuum equations do, to an extent, describe such characteristics in a statistical manner.

In steady state the particle momentum equation can be written as

$$\rho\overline{\mathrm{v}}_k\frac{\partial}{\partial \mathrm{x}_k}\overline{\mathrm{v}}_i = -(\overline{\mathrm{c}_k\mathrm{c}_i}+\overline{\lambda}_{ki})\frac{\partial}{\partial \mathrm{x}_k}\rho + \rho\left(\overline{\kappa}_i - \frac{\partial}{\partial \mathrm{x}_k}\overline{\lambda}_{ki}\right) - \rho\frac{\partial}{\partial \mathrm{x}_k}\overline{\mathrm{c}_k\mathrm{c}_i} - \rho\overline{F}_i \tag{4.65}$$

With Stokes drag forcing on the particles $\overline{\boldsymbol{F}} = \beta\left(\overline{\mathbf{u}}-\overline{\mathbf{v}}\right)$. For a turbulent boundary layer, the fluid turbulence is only inhomogeneous in the wall-normal direction. Considering only transport in the wall-normal direction, equation (4.65) then becomes

$$\tau_p\rho\overline{\mathrm{v}}_2\frac{\partial}{\partial \mathrm{x}_2}\overline{\mathrm{v}}_2 = -\tau_p(\overline{\mathrm{c}_2\mathrm{c}_2}+\overline{\lambda}_{22})\frac{\partial}{\partial \mathrm{x}_2}\rho + \tau_p\rho\left(\overline{\kappa}_2 - \frac{\partial}{\partial \mathrm{x}_2}\overline{\lambda}_{22}\right) - \tau_p\rho\frac{\partial}{\partial \mathrm{x}_2}\overline{\mathrm{c}_2\mathrm{c}_2} - \rho\overline{\mathrm{v}}_2 \tag{4.66}$$

From the particle continuity equation (equation (4.35)) it is found that for statistically steady state particle dispersion in a turbulent boundary layer with elastic particle-wall collisions, the mean wall-normal particle velocity must be zero. In this case, the wall-normal particle momentum equation is

$$0 = -\tau_p(\overline{\mathrm{c}_2\mathrm{c}_2}+\overline{\lambda}_{22})\frac{\partial}{\partial \mathrm{x}_2}\rho + \tau_p\rho\left(\overline{\kappa}_2 - \frac{\partial}{\partial \mathrm{x}_2}\overline{\lambda}_{22}\right) - \tau_p\rho\frac{\partial}{\partial \mathrm{x}_2}\overline{\mathrm{c}_2\mathrm{c}_2} \tag{4.67}$$

The first term on the RHS of equation (4.67) is the flux due to gradient diffusion, from which it can be seen that the physical interpretation of $\overline{\boldsymbol{\lambda}}$ is that of a particle diffusion tensor, and the total particle diffusion coefficient in the wall-normal direction is $\tau_p(\overline{\mathrm{c}_2\mathrm{c}_2}+\overline{\lambda}_{22})$. That the diffusion term is simply gradient diffusion results from the fact that the fluid turbulence has been assumed Gaussian in the formulation of the PDF kinetic equation. Had a non-Gaussian flow field been used in the construction of the PDF equation then the diffusive flux would contain terms with higher order derivatives of the particle concentration and additional diffusion tensors [93, 118]. It is worthwhile mentioning that this is one of the strengths of the PDF derived continuum equations

in that they offer a generalised particle diffusion coefficient in the momentum equation which is valid over the whole particle size range $0 \leq \tau_p \leq \infty$. This is in contrast to other models, constructed in a more ad-hoc manner, and in which the particle diffusion coefficient is simply approximated by the local fluid diffusivity (e.g. [119]). The local fluid diffusion coefficient is not in general a good approximation for the particle diffusion coefficient since it does not capture either the effects of particle inertia or the influence of turbulence inhomogeneity on the dispersion process, and such an approximation has been shown to lead to erroneous results (see e.g. [49]).

The second term on the RHS of equation (4.67) represents the flux due to the fluid turbulence inhomogeneity. Finally, the third term on the RHS of equation (4.67) represents the flux due to the gradients in the wall-normal particle kinetic stresses; this is the turbophoretic drift [120].

Equation (4.67) shows that the particle concentration is governed by the balance between the diffusion and drift mechanisms, and in general equation (4.67) yields inhomogeneous solutions for ρ. Clearly the continuum equations account for the turbophoretic drift via the term

$$\tau_p \rho \frac{\partial}{\partial \mathrm{x}_2} \overline{\mathrm{c}_2 \mathrm{c}_2}$$

but the PDF method also accounts for the effect of the preferential sampling of the flow field by the inertial particles. The phase-space diffusion current, derived in section 4.1 using the Furutsu-Novikov closure method provides an exact closure (when the Eulerian turbulent flow field is Gaussian) for the flux arising from the preferential sampling of the turbulent field. The diffusion current is given by

$$\langle f_i(\boldsymbol{x}^p(t),t)\mathcal{P}\rangle = p\Big\langle f_i(\boldsymbol{x}^p(t),t)\Big\rangle_{\mathbf{x},\mathbf{v}} = -\left(\frac{\partial}{\partial \mathrm{x}_k} p\lambda_{ki} + \frac{\partial}{\partial \mathrm{v}_k} p\mu_{ki} - p\kappa_i\right) \tag{4.68}$$

$$\tag{4.69}$$

The flux arising from the preferential sampling of the turbulent flow field is then given by

$$\begin{aligned} \int_{\mathbf{v}} p\Big\langle f_i(\boldsymbol{x}^p(t),t)\Big\rangle_{\mathbf{x},\mathbf{v}} d\mathbf{v} = \rho\Big\langle f_i(\boldsymbol{x}^p(t),t)\Big\rangle_{\mathbf{x}} &= -\int_{\mathbf{v}} \left(\frac{\partial}{\partial \mathrm{x}_k} p\lambda_{ki} + \frac{\partial}{\partial \mathrm{v}_k} p\mu_{ki} - p\kappa_i\right) d\mathbf{v} \\ &= \underbrace{-\overline{\lambda}_{ki}\frac{\partial}{\partial \mathrm{x}_k}\rho}_{\text{Diffusive}} + \underbrace{\rho\Big(\overline{\kappa}_i - \frac{\partial}{\partial \mathrm{x}_k}\overline{\lambda}_{ki}\Big)}_{\text{Drift}} \end{aligned} \tag{4.70}$$

terms which may be readily identified in equation (4.67). Although the dispersion tensors describe the average effect of the preferential sampling of the turbulent flow

field, they themselves depend upon the *instantaneous* preferential sampling of the flow field through the form of the response tensor $\boldsymbol{\mathcal{G}}$. As described in section 4.1, the evolution equation for the response tensor is

$$\frac{d^2}{dt^2}\mathcal{G}_{kj} = \frac{\partial F_k}{\partial \mathrm{v}_i}\frac{d}{dt}\mathcal{G}_{ij} + \left(\frac{\partial F_k}{\partial \mathrm{x}_i} + \frac{\partial f_k}{\partial \mathrm{x}_i}\right)\mathcal{G}_{ij} \tag{4.71}$$

For Stokes drag $\boldsymbol{f} = \beta \boldsymbol{u}'$ and therefore the contribution to the evolution of the response tensor from the stochastic field is given by (for Stokes drag)

$$\frac{\partial f_k}{\partial \mathrm{x}_i}\mathcal{G}_{ij} = \beta\frac{\partial u'_k}{\partial \mathrm{x}_i}\mathcal{G}_{ij} = \beta\left[\underbrace{\frac{1}{2}\left(\frac{\partial u'_k}{\partial \mathrm{x}_i} + \frac{\partial u'_i}{\partial \mathrm{x}_k}\right)}_{\text{Strain}} + \underbrace{\frac{1}{2}\left(\frac{\partial u'_k}{\partial \mathrm{x}_i} - \frac{\partial u'_i}{\partial \mathrm{x}_k}\right)}_{\text{Rotation}}\right]\mathcal{G}_{ij} \tag{4.72}$$

Given that RHS of equation (4.72) is evaluated along inertial particle trajectories in the evolution equation for the response tensor it shows that the dispersion tensors, via the response tensor $\boldsymbol{\mathcal{G}}$ depend upon the tendency of inertial particles to cluster in high strain, low rotation regions of the instantaneous turbulent flow field.

Therefore the PDF derived continuum equations are able to predict inhomogeneous particle concentrations since they capture both the effect of turbophoretic drift and preferential sampling of the turbulent flow field in a statistical manner. Of course whether or not the continuum equations are able to make quantitatively accurate predictions for particle concentrations in turbulent boundary layers, as compared to experimental or DNS data is a matter for investigation.

It is worth noting again that the PDF method (which, using FN is exact for a Gaussian flow field) predicts that the effect of the preferential sampling of the flow field is both diffusive and convective (see equation (4.70)). In many continuum models it is assumed to be simply diffusive. An investigation into the importance of the convective term in equation (4.70) is investigated later in this thesis.

4.4 Conclusions

In this chapter a summary of the PDF kinetic equation for particle position and velocity has been presented, along with its associated continuum equations which form an infinite set of coupled partial differential equations which require closure. A discussion has then been given regarding the various terms within the continuum equations that require closure.

The PDF kinetic approach provides a rigorous and fundamentally sound way to

construct continuum equations since the PDF equation itself is derived directly from the particle equation of motion, meaning that the continuum equations will contain all of the physics consistent with the underlying particle equation of motion. The only real concern with the PDF method for modelling particle dispersion in turbulent boundary layers is that it assumes that the underlying fluid turbulence is Gaussian, when yet boundary layer turbulence is certainly non-Gaussian (see for example figure 4 in [41] for plots of the skewness and flatness of the fluid velocity field in a turbulent boundary layer). For example, the turbulent velocity field in a boundary layer is quite non-Gaussian; the velocity PDF's are asymmetric and have extended tails, which is related to the intermittent nature of turbulence. The intermittent nature of turbulence, manifest in burst events, for example, must have an effect on the overall transport of the particles, and this is not captured when a Gaussian velocity field is assumed. Whilst the PDF kinetic equation could in principle be extended to describe non-Gaussian flow fields (see [93]) the resulting PDF equation would no longer be exact since the phase-space diffusion current for a non-Gaussian $\boldsymbol{f}$ cannot be closed exactly (in addition to the fact that the PDF equation for a non-Gaussian flow field would be significantly more complex than for a Gaussian field).

Chapter 5

Particle Dispersion in a 1D Inhomogeneous Flow: Testing the Continuum Equations

In the previous chapter a summary of the derivation of a PDF kinetic equation for particle dispersion in a turbulent fluid was considered, along with the continuum equations that are derived from from this equation. Various closure approximations were also considered which are used to obtain a set of closed continuum equations for modelling the statistics of inertial particle dispersion in turbulent flows. In obtaining a closed set of continuum equations the following closure approximations were made

1. The fluctuating aerodynamic force field in which the particles are dispersed is assumed to be Gaussian
2. The particle dispersion tensors are approximated as being locally homogeneous
3. The particle dispersion tensors are approximated as being velocity independent
4. The Chapman-Enskog approximation can be used to approximate $\overline{\mathbf{ccc}}$

Incorporating these closure approximations, in several papers the PDF kinetic equation and its resulting continuum equations have been tested against particle tracking data of particle dispersion in homogeneous isotropic flow fields, simple shear flows and rotating flows (e.g. [94, 106, 121]). In [122] analytic solutions to the PDF kinetic equation were obtained for particle dispersion in simple shear flows (both fully developed and transient cases) and were tested against equivalent LES data. The results showed that the PDF equation predictions were in excellent agreement with the particle tracking data. These studies show that the PDF method can be a powerful mathematical model for accurately

predicting the statistics of particle dispersion in certain turbulent flows. However, in the cited papers, the nature of the turbulent flow fields in which the particles were dispersing are such that the aforementioned closure approximations adopted in the continuum equations (and the underlying PDF equation) are probably reasonable. For particle dispersion in a turbulent boundary layer these closure approximations are more questionable.

In [100] the PDF-derived continuum equations were tested against data obtained from particle tracking in a DNS of turbulent channel flow (the DNS data was taken from [81]). The results showed reasonable agreement for the particle velocity statistics over the particle sizes considered, however the particle concentration predictions from the continuum equations were in considerable error (the logarithmic scale of the concentration plots in [100] (see Fig.1 in the cited paper) suppress the differences somewhat). The same trend can also be seen in [101].

Therefore, motivated by the apparent model deficiencies, this chapter presents a detailed investigation into the performance of the continuum equation solutions when compared to equivalent particle tracking data for particle dispersion in a turbulent boundary layer. This provides not only a test of the performance of the continuum equation solutions themselves, but also a way to identify which of the closure approximations invoked in the continuum equations are responsible for any prediction errors.

5.1 Particle Tracking

As a simple test case particles were tracked in a simplified (1D) model of a "turbulent boundary layer", the configuration illustrated in figure 5.1

Figure 5.1: Diagram of 1D domain in which particles were tracked. Upper boundary is at $\mathrm{x}_2 = 120$ and the wall is located at $\mathrm{x}_2 = 0$.

Particles were introduced into the domain at time $t = 0$ with a uniform random distribution. Particles collided elastically with the wall when $x_2^p(t) = \mathrm{x}_2^{min}$, where x_2^{min} is the particle radius (in wall units), defined by

$$\mathrm{x}_2^{min} = \sqrt{\frac{9\tau_p \rho^f}{2\rho^p}} \tag{5.1}$$

where, as in [85], ρ^f/ρ^p was chosen to be $1/770$. When the particles crossed the upper boundary they were elastically reflected back into the domain. The particle dispersion statistics were computed only in the the range $\mathrm{x}_2^{min} \leq \mathrm{x}_2 \leq \mathrm{x}_2^{max}$ (where $\mathrm{x}_2^{max} = 100$) so that the statistics were not affected by the upper boundary. With the particles prescribed as being much heavier than the carrier fluid the only relevant force acting on the particles is a drag force (gravity was also neglected so that the influence of the turbulence inhomogeneity on the continuum equations could be considered without its effect being somewhat 'masked' by an additional effect of gravity). The particle equation of motion is then given by

$$\frac{d}{dt}x_2^p(t) = v_2^p(t) \tag{5.2}$$

$$\frac{d}{dt}v_2^p(t) = \frac{1}{\tau_p}\left(u_2^p(t) - v_2^p(t)\right) \tag{5.3}$$

where x_2^p is the wall-normal particle position, v_2^p is the wall-normal particle velocity, τ_p is the particle momentum response time and u_2^p is the wall-normal component of the fluid velocity at the particle position (the mean fluid velocity in the wall-normal direction is zero so that $u_2^{p\prime} = u_2^p$). In order to simulate the fluid velocity at the particle position a modified Langevin equation was used. The use of Langevin equations to model the fluid velocity seen by an inertial particle in a turbulent channel flow/boundary layer is well established (e.g. [41–49]). Originally in this test case the Langevin equation given in [41, 43–45, 49] was used. However it was found that when tracking inertial particles using this Langevin equation $\overline{u_2^p} \not\to 0$ as $\tau_p \to \infty$. In [48] the drift term appropriate for finite inertia particles was developed which satisfies the necessary physical criteria that $\overline{u_2^p} \to 0$ as $\tau_p \to \infty$, in addition to the fully mixed fluid particle limit $\overline{u_2^p} \to 0$ as $\tau_p \to 0$, and this modified drift term was used in this test case[1]. For particle dispersion in the wall-normal direction the Langevin equation chosen is

[1]It was later discovered that the same deficiencies in standard Langevin models for particle dispersion in inhomogeneous flows were noted and considered in [123]. In particular, in [123] it was shown that the Langevin models presented in [42,97] do not correctly predict the statistics of the fluid velocity at the particle position in the limit $\tau_p \to \infty$. Furthermore, it is mentioned in [123] that the modification they make to the standard Langevin models in order to properly account for the limit $\tau_p \to \infty$ is similar to the modifications suggested in [48].

$$dU_2(t) = -\frac{U_2}{\tau^{Lp}}dt + \Big(\frac{1}{1+St}\Big)\frac{d\sigma_2}{d\mathrm{x}_2}dt + \sqrt{\frac{2}{\tau^{Lp}}}dW_2 \tag{5.4}$$

where $U_2 = u_2^p/\sigma_2$, $\sigma_2 = \sigma_2(x_2^p(t))$ is the wall-normal fluid velocity r.m.s., $\tau^{Lp} = \tau^{Lp}(x_2^p(t))$ is the timescale of the fluid velocity correlations seen by the particles, $St = \tau_p/\tau^{Lp}$ is the particle Stokes number and dW_2 is a Wiener process, with mean equal to zero and variance dt. (Note that the Langevin equation in (5.4) which is in terms of the fluid velocity scaled by the local fluid velocity r.m.s. is a particular choice of model, whilst in other works, such as in [42], the Langevin equation is written for the actual fluid velocity seen by the particle, and these models may not be exactly equivalent).

Particles were then tracked by solving equations (5.2) and (5.3) in conjunction with equation (5.4) using an explicit second order Adams-Bashforth scheme. For numerical stability the time step δt in the numerical simulations was defined so that $\tau_p/\delta t \geq 10$ (e.g. [9]). A range of particle sizes were considered and for each size $\mathcal{O}(10^4)$ particles were tracked over a long period of time and the required statistics were computed. The spatial domain was divided into bins with a Chebyshev distribution (for fine bin resolution near the wall). The results shown in section 5.4 are those recorded once the system had reached a statistically steady state.

5.2 Continuum Equations in 1D

In a statistically steady state, 1D wall-normal particle dispersion in a turbulent boundary layer the particle continuity equation becomes (see equation (4.35))

$$\frac{d}{d\mathrm{x}_2}\rho\overline{\mathrm{v}}_2 = 0 \tag{5.5}$$

With elastic particle wall collisions $\overline{\mathrm{v}}_2 = 0$ at the wall, and therefore equation (5.5) implies the solution $\overline{\mathrm{v}}_2(\mathrm{x}_2) = 0$ throughout the entire domain. Therefore from equation (4.38) the required form of the particle momentum equation is

$$0 = -\frac{d}{d\mathrm{x}_2}\left[\rho\left(\overline{\mathrm{c}_2\mathrm{c}_2} + \overline{\lambda}_{22}\right)\right] + \rho\overline{\kappa}_2 \tag{5.6}$$

and the required form of the particle Reynolds stress equation is

$$0 = -\frac{d}{d\mathrm{x}_2}\rho\overline{\mathrm{c}_2\mathrm{c}_2\mathrm{c}_2} + \rho\left(2\overline{\mu}_{22} - 2\beta\overline{\mathrm{c}_2\mathrm{c}_2}\right) \tag{5.7}$$

Using the Chapman-Enskog closure approximation (see chapter 4) for $\overline{\mathrm{c}_2\mathrm{c}_2\mathrm{c}_2}$, and combining equations (5.6) and (5.7) an ordinary differential equation for the particle kinetic stress is obtained

$$\left(\overline{\mathrm{c}_2\mathrm{c}_2} + \overline{\lambda}_{22}\right)\frac{d^2}{d\mathrm{x}_2^2}\overline{\mathrm{c}_2\mathrm{c}_2} + \overline{\kappa}_2\frac{d}{d\mathrm{x}_2}\overline{\mathrm{c}_2\mathrm{c}_2} + 2\beta\overline{\mu}_{22} - 2\beta^2\overline{\mathrm{c}_2\mathrm{c}_2} = 0 \tag{5.8}$$

and a solution for the particle concentration from the momentum equation [49]

$$\rho(\mathrm{x}_2) = \rho(\mathrm{x}_2^{min})\left(\frac{\overline{\mathrm{c}_2\mathrm{c}_2}(\mathrm{x}_2^{min}) + \overline{\lambda}_{22}(\mathrm{x}_2^{min})}{\overline{\mathrm{c}_2\mathrm{c}_2}(\mathrm{x}_2) + \overline{\lambda}_{22}(\mathrm{x}_2)}\right)\exp\left(\int_{\mathrm{x}_2^{min}}^{\mathrm{x}_2}\frac{\overline{\kappa}_2(z)}{\overline{\mathrm{c}_2\mathrm{c}_2}(z) + \overline{\lambda}_{22}(z)}dz\right) \tag{5.9}$$

The LHA (local homogeneous approximation) forms of $\overline{\lambda}_{22}$ and $\overline{\mu}_{22}$ and the PSA (passive scalar approximation) form of $\overline{\kappa}_2$ were used (see chapter 4). In 1D, for particles experiencing only a Stokes drag force the dispersion tensors are

$$\overline{\lambda}_{22}(\mathrm{x}_2) = \frac{\sigma_2^2\beta^2\left(\tau^{Lp}\right)^2}{1+\beta\tau^{Lp}} \tag{5.10}$$

$$\overline{\mu}_{22}(\mathrm{x}_2) = \frac{\overline{\lambda}_{22}(\mathrm{x}_2)}{\tau^{Lp}} \tag{5.11}$$

$$\overline{\kappa}_2(\mathrm{x}_2) = \frac{d}{d\mathrm{x}_2}\overline{\lambda}_{22}(\mathrm{x}_2) \tag{5.12}$$

Equation (5.8) is solved numerically first, and the solution obtained for $\overline{\mathrm{c}_2\mathrm{c}_2}$ is used in equation (5.9) to compute the solution for ρ. In order to solve equation (5.8) the boundary conditions $\overline{\mathrm{c}_2\mathrm{c}_2}(\mathrm{x}_2^{min})$ and $\overline{\mathrm{c}_2\mathrm{c}_2}(\mathrm{x}_2^{max})$ are required. The aim here is to assess the accuracy of the solutions to the continuum equations (with the closure approximations used). To avoid complications in this assesment introduced by further approximations associated with the specification of boundary conditions, $\overline{\mathrm{c}_2\mathrm{c}_2}(\mathrm{x}_2^{min})$ and $\overline{\mathrm{c}_2\mathrm{c}_2}(\mathrm{x}_2^{max})$ are taken from the particle tracking data (as was done in [49]). Since $\rho(\mathrm{x}_2)$ is a PDF it must satisfy

$$\int_{\mathrm{x}_2^{min}}^{\mathrm{x}_2^{max}}\rho\, d\mathrm{x}_2 = 1 \tag{5.13}$$

Therefore the boundary condition $\rho(\mathrm{x}_2^{min})$ required in equation (5.9) is given by

$$\rho(\mathrm{x}_2^{min}) = \left(\int_{\mathrm{x}_2^{min}}^{\mathrm{x}_2^{max}} \left(\frac{\overline{\mathrm{c}_2\mathrm{c}_2}(\mathrm{x}_2^{min}) + \overline{\lambda}_{22}(\mathrm{x}_2^{min})}{\overline{\mathrm{c}_2\mathrm{c}_2}(\mathrm{x}_2) + \overline{\lambda}_{22}(\mathrm{x}_2)} \right) \exp \left(\int_{\mathrm{x}_2^{min}}^{\mathrm{x}_2} \frac{\overline{\kappa}_2(z)}{\overline{\mathrm{c}_2\mathrm{c}_2}(z) + \overline{\lambda}_{22}(z)} dz \right) d\mathrm{x}_2 \right)^{-1} \tag{5.14}$$

Equation (5.8) was solved numerically using the MATLAB function bvp4c (an adaptive finite difference solver) and equation (5.9) was integrated numerically.

5.3 Fluid Turbulence Statistics

Input data for σ_2 and τ^{Lp} are required as input into both equation (5.4) and the particle dispersion tensors in equations (5.10) to (5.12). Accurate specification of these inputs is not needed since what is important is how well the continuum equations and the particle tracking data compare, given the same fluid turbulence statistics.

Strictly speaking the Lagrangian timescale in the dispersion tensors (equations (5.10) to (5.12)) and the timescale in the Langevin equation are not the same; properly defined, the timescale in the dispersion tensors is defined backwards in time, whilst the timescale in the Langevin equation is defined forwards in time, and for particle dispersion in a turbulent boundary layer these timescales are not the same. Nevertheless since there is no model available to distinguish between forward and backward in time timescales they will be approximated as being the same. Data for σ_2 and τ^{Lp} are taken from the curve fits given in [3], with τ^{Lp} specified by the fluid Lagrangian timescale τ_L.

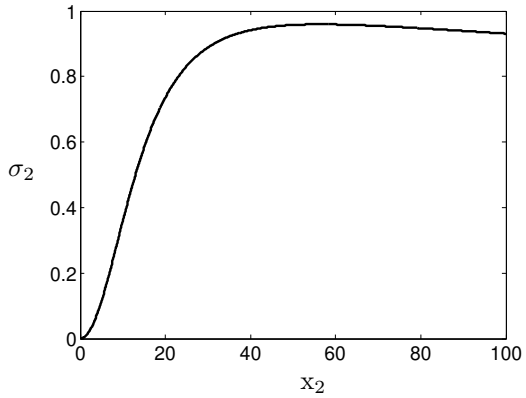

Figure 5.2: Plot of $\sigma_2(\mathrm{x}_2)$ using the function given in [3].

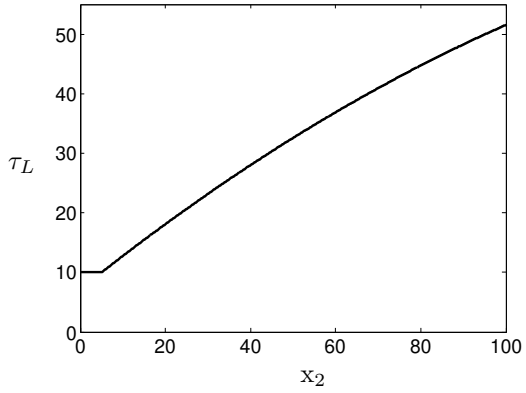

Figure 5.3: Plot of $\tau_L(x_2)$ using the function given in [3].

5.4 Results

In this section the results of the comparison between the particle tracking data and the continuum equation solutions are presented. Figure 5.4 shows the comparison between the particle tracking data ($\times$), the continuum solution (-) and the local homogeneous approximation (- -) for $\overline{c_2 c_2}$, where the local approximation for $\overline{c_2 c_2}$ is given by $\overline{c_2 c_2} \approx \overline{\mu}_{22}/\beta$. Figure 5.5 shows the comparison between the particle tracking data and the continuum solution for the particle concentration $\rho(x_2)$, which have been plotted against each other as a ratio for added clarity in their comparison.

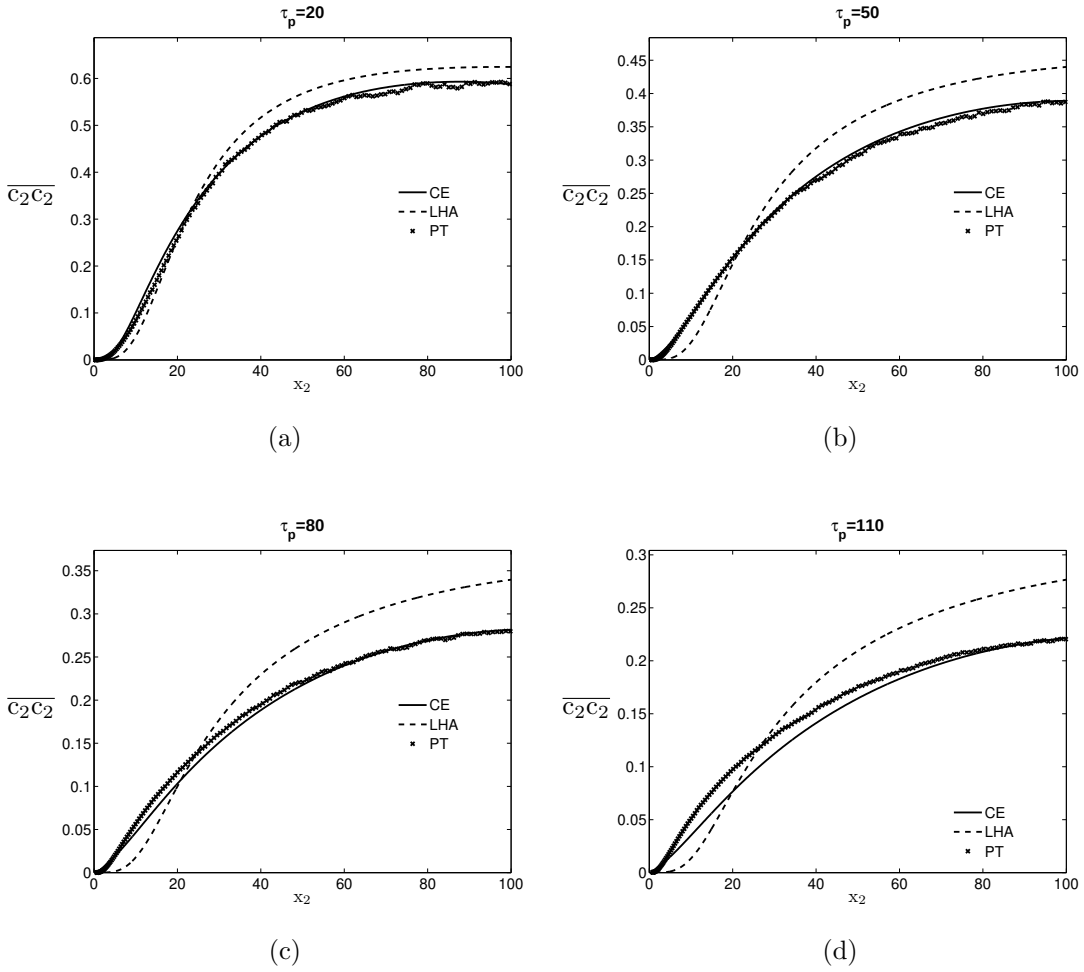

Figure 5.4: Comparison between particle tracking data (×), continuum equation solutions (-) and the local homogeneous approximation (–) for $\overline{c_2c_2}$.

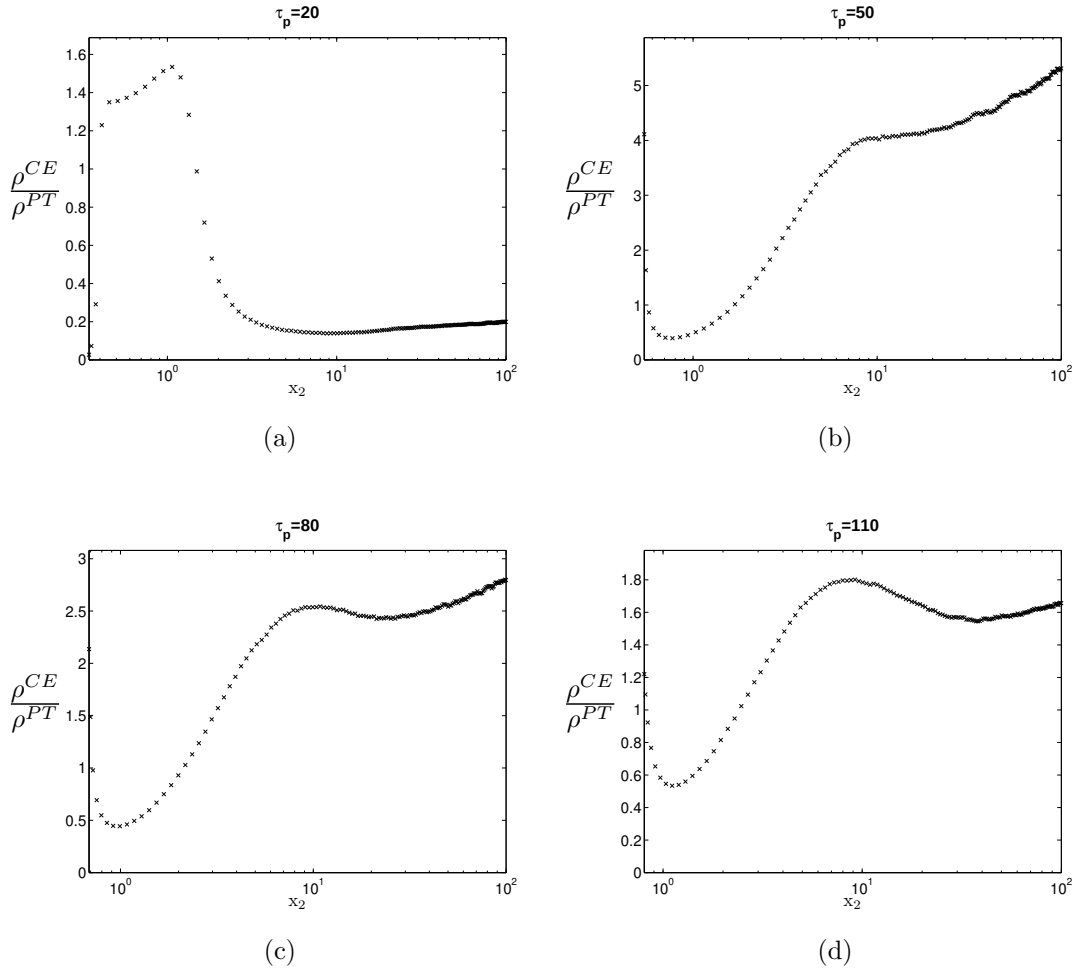

Figure 5.5: Plots of the ratio of the continuum solution for the particle concentration (ρ^{CE}) against the particle concentration data obtained in the PT simulation (ρ^{PT}).

5.5 Discussion of Results

The comparison of the results from particle tracking and the continuum equations are shown in section 5.4. All variables are expressed in wall units (usually denoted by a superscript '+' but omitted here for ease of reading). The results are for four different response times; $\tau_p = 20, 50, 80$ and 110 which cover a greater range than that investigated in [49].

In the closure of the continuum equations (using Furutsu-Novikov (FN) derived PDF equation) there are essentially four different approximations made

1. The fluctuating aerodynamic force field in which the particles are dispersed is assumed to be Gaussian
2. The particle dispersion tensors are approximated as being locally homogeneous
3. The particle dispersion tensors are approximated as being velocity independent
4. The Chapman-Enskog approximation can be used to approximate $\overline{\mathbf{ccc}}$

which shall be referred to as approximations 1,2,3 and 4 hereafter in this chapter. The validity of these approximations may now be considered in light of the results in section 5.4.

Though the random term dW_2 in the Langevin equation (see equation (5.4)) is Gaussian, this does not necessarily imply that the fluid velocity generated by the Langevin equation is Guassian for inhomogeneous flows, as noted in [42]. Furthermore, even if the Langevin equation did produce Gaussian fluid velocities, this is still not strictly consistent with the the approximation made in the FN derived PDF equation, which approximates the velocity *field* as Gaussian. However, the effects of this discrepancy is expected to be small relative to the effects of approximations 2-4 and will therefore be neglected.

The results for $\overline{c_2 c_2}$ are shown in figure 5.4. For $\tau_p = 20, 50$ and 80 it can be seen that the continuum solutions are in excellent agreement with the PT data whilst there is some discrepancy for $\tau_p = 110$, and also that the the error in the local approximation for $\overline{c_2 c_2}$ increases with τ_p within the range of particle sizes considered. Whilst the CE solutions for $\overline{c_2 c_2}$ for $\tau_p = 20, 50$ and 80 are in excellent agreement with the PT data, for the same particle sizes the results in figure 5.5 show that the continuum solution for the concentration exhibit significant errors. For these particle sizes approximations 3 and 4 cannot be invoked as the causes of the errors in the continuum solutions for the concentration. Approximations 3 and 4 refer to closure approximations made in the particle stress equation and do not affect the concentration solutions except by

their influence on $\overline{c_2 c_2}$. However it is evident from figure 5.4 these approximations have had little effect on the stress equation since the continuum predictions are in excellent agreement with the PT data for $\overline{c_2 c_2}$ for these particle sizes. Therefore the only remaining source of error in the continuum solution for ρ is approximation 2 since the momentum equation (from which the concentration solution is found) depends only upon the kinetic stresses and the dispersion tensors. It is recalled from chapter 4 that approximation 2 not only consists in making local approximations to $\overline{\lambda}_{22}$ and $\overline{\mu}_{22}$ but also in applying a passive scalar approximation to $\overline{\kappa}_2$. That is, it is assumed that in the momentum equation

$$\overline{\kappa}_2 - \frac{d}{d\mathrm{x}_2}\overline{\lambda}_{22} = 0, \qquad \text{for all } \tau_p \tag{5.15}$$

whereas this is only strictly true in the limits $\tau_p \to 0$ and $\tau_p \to \infty$. The removal of this drift in the particle momentum equation will undoubtedly have an effect on the concentration solutions. Unfortunately, since in this PT simulation the fluid velocity is supplied by a Lagrangian Langevin equation, rather than by an Eulerian flow field, there is no reliable way to measure the drift

$$\overline{\kappa}_2 - \frac{d}{d\mathrm{x}_2}\overline{\lambda}_{22}$$

from the PT data.

It is possible, however, to compute $\overline{\lambda}_{22}$ and $\overline{\mu}_{22}$ from the PT data, with two precautionary notes. Again, since fluid velocity is supplied by a Lagrangian Langevin equation, rather than by an Eulerian flow field it is not possible to compute the particle response tensor $\boldsymbol{\mathcal{G}}$ (see chapter 4) nor is it possible to measure the dispersion tensors in the manner defined by the FN formulation (i.e. measures of *the correlation of the Eulerian flow field* along particle trajectories). Nevertheless, it is possible to compute the dispersion tensors as defined by Reeks using LHDI [83], which in this 1D flow would be given by

$$\overline{\lambda}_{22}(\mathrm{x}_2) = \beta^2 \int_{-\infty}^{0} G_{22}(s)\Big\langle u_2^p(0)u_2^p(s)\Big\rangle_{\mathrm{x}_2} ds \tag{5.16}$$

$$\overline{\mu}_{22}(\mathrm{x}_2) = \beta^2 \int_{-\infty}^{0} \dot{G}_{22}(s)\Big\langle u_2^p(0)u_2^p(s)\Big\rangle_{\mathrm{x}_2} ds \tag{5.17}$$

where $s = t' - t \leq 0$ and

$$G_{22}(s) = \tau_p(1 - \exp[\beta s]) \tag{5.18}$$

$$\dot{G}_{22}(s) = \exp[\beta s] \tag{5.19}$$

and the autocovariances in equations (5.16) and (5.17) are defined backwards in time (as implied in equations (5.16) and (5.17) since $s \leq 0$), such that the fluid velocities are evaluated along trajectories which *arrive* at x_2 at $s = 0$ and which were dispersed relative to one another at a time in the past s. The dispersion tensors defined in equations (5.16) and (5.17) were computed in the PT simulation for each particle size and the results are shown in figures 5.6 and 5.7

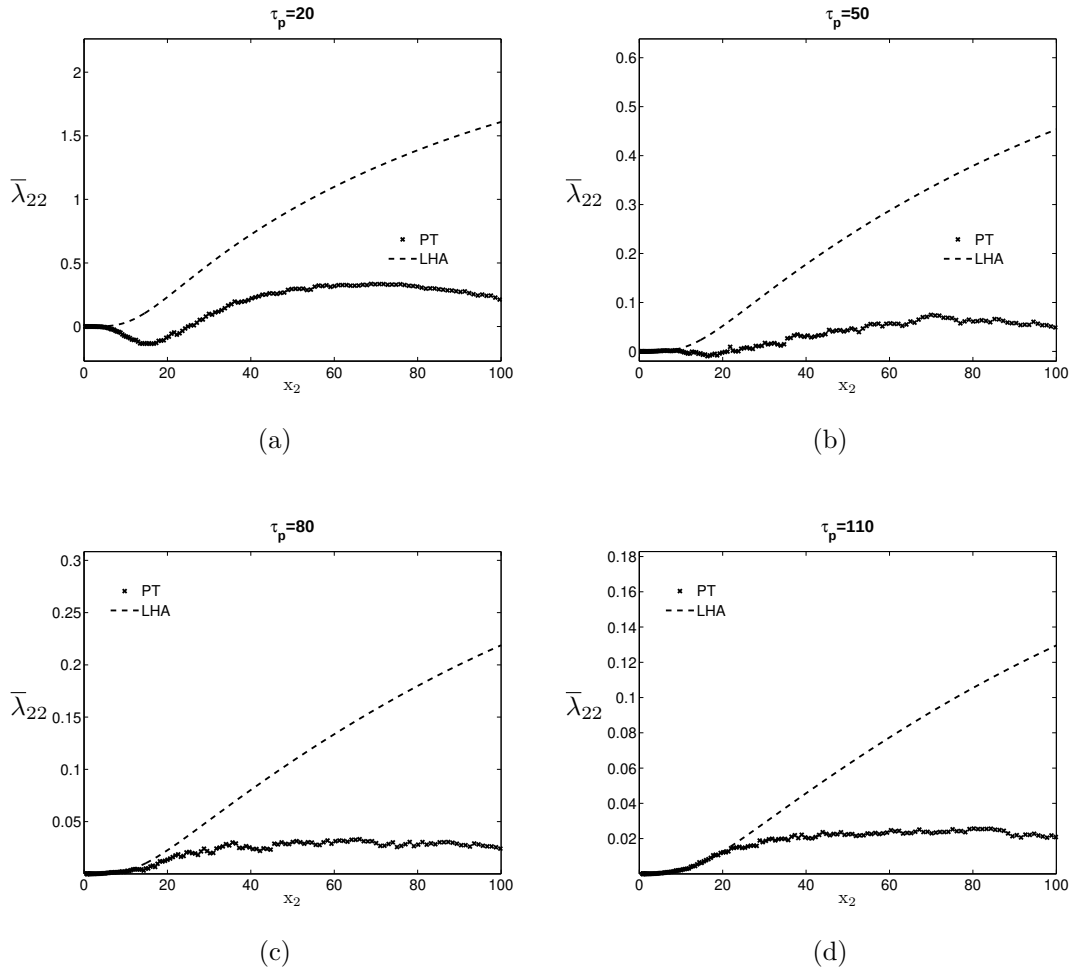

Figure 5.6: Plots of $\overline{\lambda}_{22}$ as obtained from the PT simulation using equation (5.16) and as given by LHA (equation (5.10)).

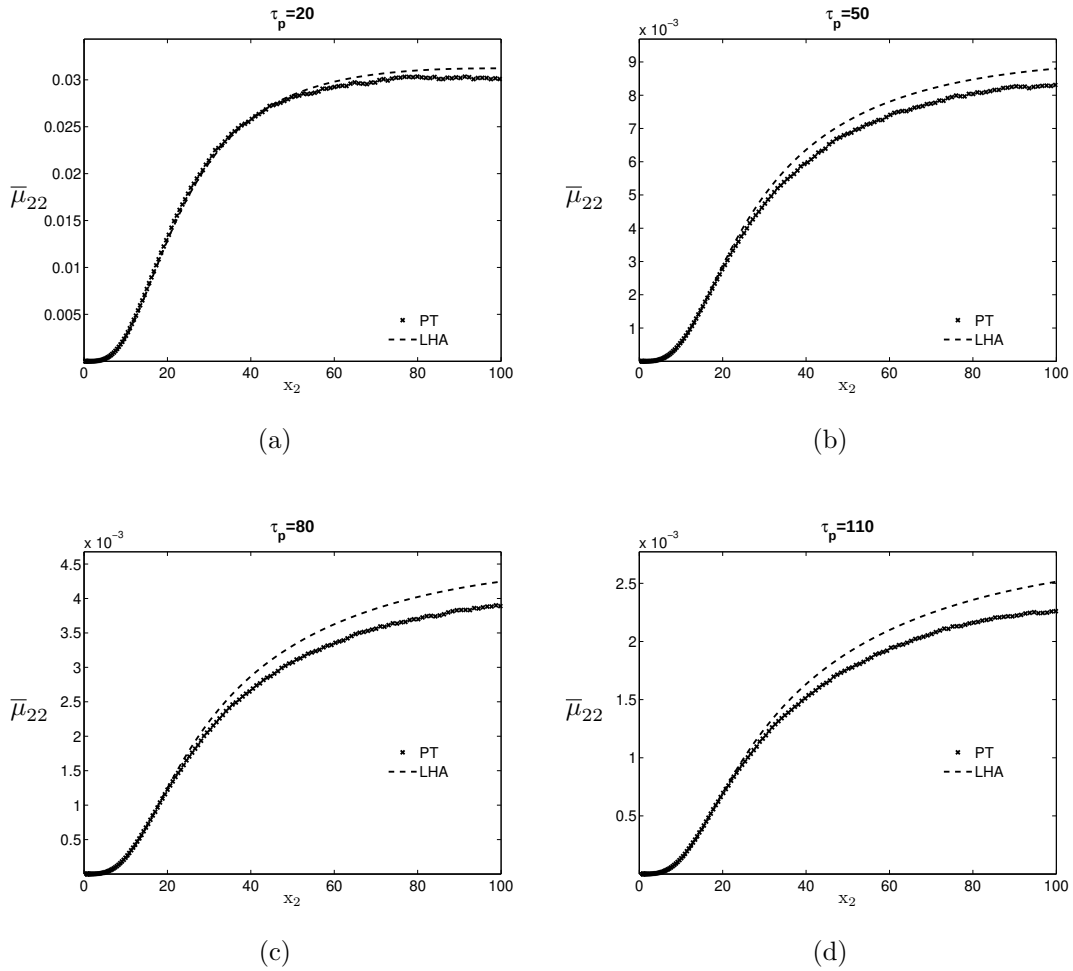

Figure 5.7: Plots of $\overline{\mu}_{22}$ as obtained from the PT simulation using equation (5.17) and as given by LHA (equation (5.11)).

The results show very clearly that $\overline{\lambda}_{22}$ is very strongly affected by the inhomogeneity in the fluid turbulence whilst $\overline{\mu}_{22}$ is not. These findings are in accord with that found in [49], and following that paper the explanation for why this is so is as follows. Consider figure 5.8

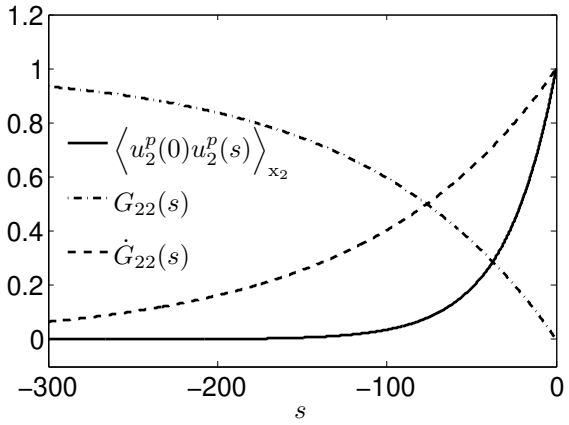

Figure 5.8: Plots to demonstrate how $G_{22}(s)$ and $\dot{G}_{22}(s)$ weight the contributions of the autocovariance of the fluid velocity differently in $\overline{\lambda}_{22}$ and $\overline{\mu}_{22}$.

The autocovariance in figure 5.8 is represented by a simple decaying exponential function, and it, $G_{22}(s)$ and $\dot{G}_{22}(s)$ have all been scaled to give a maximum value of 1 so that they can be clearly compared (since it is their form, not their value which is important in this discussion). As the figure demonstrates, whilst $G_{22}(s)$ increases backward in time, $\dot{G}_{22}(s)$ decays backwards in time. Therefore, in the dispersion tensors (equations (5.16) and (5.17)) since $\overline{\lambda}_{22}$ contains $G_{22}(s)$ and $\overline{\mu}_{22}$ contains $\dot{G}_{22}(s)$, values of the autocovariance for large s will be weighted much more heavily in $\overline{\lambda}_{22}$ than in $\overline{\mu}_{22}$. Furthermore values of the autocovariance for small s will be weighted more heavily in $\overline{\mu}_{22}$ than in $\overline{\lambda}_{22}$. Given that the particle trajectories along which the fluid velocity autocovariances are evaluated become increasingly dispersed with increasing $|s|$ (i.e. so that $\left\langle u_2^p(0)u_2^p(s)\right\rangle_{x_2}$ becomes increasingly non-local) this explains why $\overline{\lambda}_{22}$ is sensitive to the non-locality of the dispersion process whilst $\overline{\mu}_{22}$ is not.

In order to test the hypothesis that the strong inhomogeneity of the fluid turbulence is the cause of the significant difference between $\overline{\lambda}_{22}$ computed in the PT simulation, and $\overline{\lambda}_{22}$ given by the local approximation, a simulation was performed for a much larger particle. The dispersion tensors for large particles (i.e. large Stokes number) should be much less sensitive to the fluid turbulence inhomogeneity since the characteristic distances that large particles move within the time for which the fluid is correlated are sufficiently small so that they see a turbulence which is approximately homogeneous. Figure 5.9 shows the results for $\tau_p = 500$

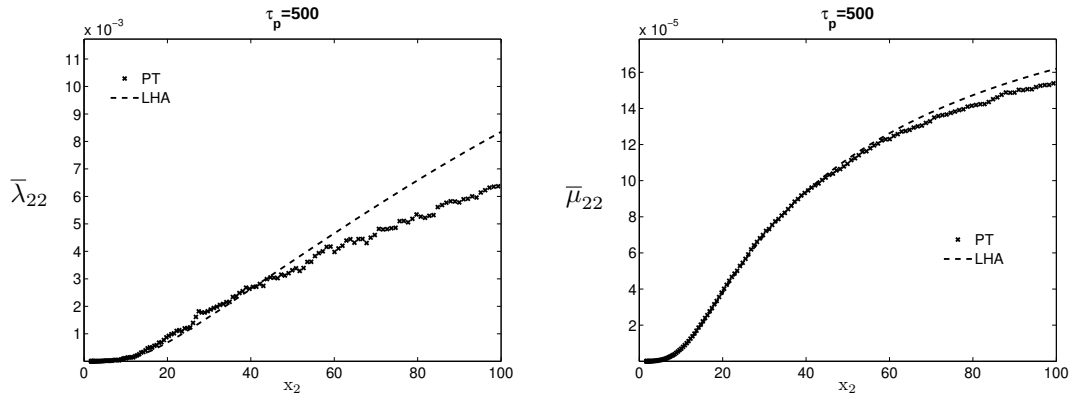

(a) (b)

Figure 5.9: Plots of $\overline{\lambda}_{22}$ and $\overline{\mu}_{22}$ as obtained from the PT simulation using equations (5.17) and as given by LHA.

The results in figure 5.9 would indicate that this hypothesis is indeed correct; even though there is still some discrepancy between the PT data and the LHA forms of the dispersion tensors, the difference, especially for $\overline{\lambda}_{22}$, has been significantly reduced and would suggest that the LHA becomes more exact as $\tau_p \to \infty$. (With $\tau_p = 500$ this gives a Stokes number $St = \tau_p/\tau_L \approx 10$ near the edge of the boundary layer, which is not too large and explains why there is still some discrepancy for the LHA form of $\overline{\lambda}_{22}$ near the edge of the boundary layer. Near the wall, for example, for $\mathrm{x}_2 \leq 40$, $St > 20$ and in this region the LHA for $\overline{\lambda}_{22}$ is in excellent agreement with the PT data).

There are two interesting features of the results in figure 5.6 that require explanation. First of all, for $\tau_p = 20$, $\overline{\lambda}_{22} < 0$ near the wall. It is not immediately clear why this should be so, as it indicates that the autocovariances of the fluid velocity seen by the particles in this near wall region contain negative 'loops'. Upon examination of the PT data, it is seen that the fluid velocity autocovariances measured in the PT simulation along particle paths, that is

$$\left\langle u_2^p(0) u_2^p(s) \right\rangle_{\mathrm{x}_2}$$

do indeed feature negative loops for x_2 in the near wall region, as shown in figure 5.10

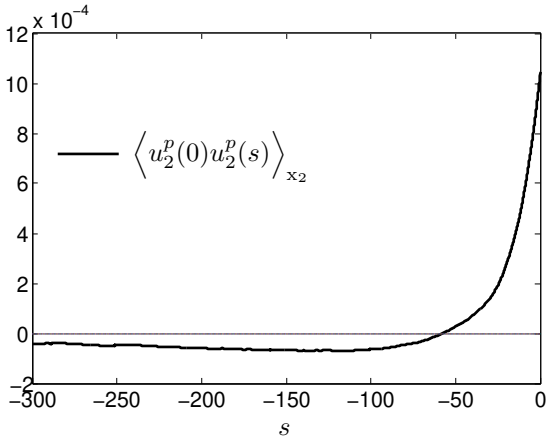

Figure 5.10: Plot of the fluid velocity autocovariance evaluated along particle trajectories for $\tau_p = 20$ at $\mathrm{x}_2 = 16$

Although the negative loops are not very large, the way that the autocovariances are weighted in $\overline{\lambda}_{22}$ by $G_{22}(s)$ mean that they can have a significant effect. The negative loops must be due to the particle-wall collisions and the effect that this has on the directionality of the fluid velocities the particles sample. For example, it is well known that inertial particles preferentially sample turbulent velocities in turbulent boundary layers. The mean of the fluid velocities sampled at the particle position when $x_2^p(t) = \mathrm{x}_2$, for $\tau_p = 20$ and $\tau_p = 50$ are shown in figure 5.11

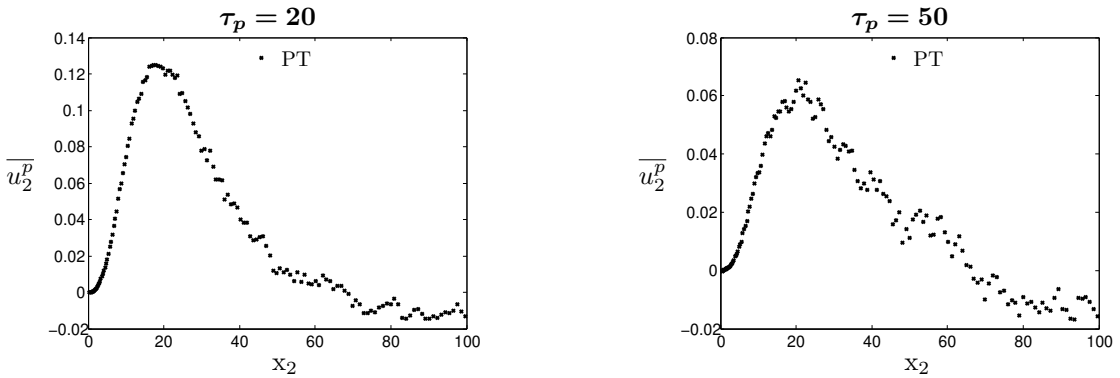

(a) (b)

Figure 5.11: Plots of $\overline{u_2^p}$, the mean of the fluid velocities sampled at the particle position when $x_2^p(t) = \mathrm{x}_2$, obtained from the PT simulation.

The location of the peak value of $\overline{u_2^p}$ for $\tau_p = 20$ corresponds very closely with the largest negative value of $\overline{\lambda}_{22}$. In addition, the peak value of $\overline{u_2^p}$ for $\tau_p = 50$ is much smaller than for $\tau_p = 20$, and correspondingly, the largest negative value of $\overline{\lambda}_{22}$ for $\tau_p = 50$ is much

smaller than that for $\tau_p = 20$. Both suggest that the the preferential sampling of the flow field in the near wall region is in some sense connected with the negative values of $\overline{\lambda}_{22}$. If this is indeed the case, then the negative values of $\overline{\lambda}_{22}$ in the near wall region are a feature of the dispersion tensors defined by Reeks using LHDI and this feature *would not* be found with the FN defined dispersion tensors. The fluid velocity correlations in the FN dispersion tensors are defined in terms of Eulerian correlations of the flow field measured along particle paths. Being Eulerian, these correlations are based upon *all* realisations of the flow field, and do not contain any information regarding preferential sampling.

The second interesting feature of the results in figure 5.6 is that the LHA forms of the dispersion tensors are always greater in value than those computed in the PT simulation. Since the dispersion process even in this simple 1D flow is complex, it is not easy to ascertain why this should be. However there are two possible explanations. First of all, the PT results indicate that the particle velocities are negatively skewed throughout the boundary layer. A negatively skewed velocity PDF means that there is a greater probability of finding a particle moving away from the wall than there is towards the wall. Recalling that in the dispersion tensors the trajectories along which the velocity correlations are evaluated are backward in time, this means that there is a greater probability of particles moving towards x_2 from $x_2^p(s) \leq \mathrm{x}_2$ than there is from $x_2^p(s) \geq \mathrm{x}_2$. Consequently the fluid statistics will be sampled asymmetrically with respect to x_2, with a bias towards values sampled at $x_2^p(s) \leq \mathrm{x}_2$. From figures 5.2 and 5.3 it can be seen that in the region $\mathrm{x}_2 \leq 40$ the fluid statistics have positive gradients. Therefore, in this region the particles will preferentially sample values of σ_2 and τ_L less than at x_2. In the region $40 \leq \mathrm{x}_2 \leq 100$, σ_2 is approximately constant, but τ_L still has large positive gradients. Therefore again, the particles will preferentially sample values of τ_L less than at x_2. This would to an extent explain why the LHA to the dispersion tensors are too large, since they do not account for the asymmetric sampling of the flow field in inhomogeneous turbulence.

The second explanation is as follows. The upper boundary of the domain imposes the constraint that $x_2^p(t) \leq 120$ (recalling that the particles collided with the upper boundary at $\mathrm{x}_2 = 120$ not at x_2^{max}). For $\mathrm{x}_2 \geq 50$ the fluid velocity r.m.s. is approximately homogeneous whereas the fluid integral timescale is strongly inhomogeneous with a positive gradient (see figures 5.2 and 5.3). Therefore, for x_2 near to the upper boundary, there is the constraint that

$$\tau_L(x_2^p(s)) \leq \tau_L(\mathrm{x}_2)$$

Consequently in this region, the correlations evaluated along the particle trajectories will have shorter correlation times than those based on a local approximation which use

$\tau_L(\mathrm{x}_2)$. This would then lead to an over prediction of the values of the dispersion tensors using a local approximation, and this is what the results indicate. Furthermore, since in this region the particle velocities are relatively large (compared to those in the region $\mathrm{x}_2 \leq 20$ for example where the inhomogeneity is strongest) the distances they move within the time for which they see a correlated fluid velocity along their trajectory may be large. Therefore in this region the amount by which $\tau_L(x_2^p(s))$ deviates from $\tau_L(\mathrm{x}_2)$ may be significant, and this again would explain the large error in the local approximations to the dispersion tensors.

In higher dimensions (i.e. 2D or 3D) it may not be the case that a local approximation leads to an over prediction of the dispersion tensors since in that case the anisotropy of the one and two point statistics (e.g. different length scales in different directions) will affect the dispersion tensors also.

In [49] Skartlien fitted curves to the PT data for the dispersion tensors and then used these in the continuum equations to see how the concentration solutions predicted would be improved with correct specification of the dispersion tensors. This improved the continuum predictions for the concentration. However the passive scalar approximation for $\overline{\kappa}_2$ was still invoked in this test. It is anticipated that with $\overline{\kappa}_2$ correctly specified, the continuum equation prediction for the concentration would be improved even further.

Finally, a comment on the use of the Langevin equation. In [85] it is argued that the effects of the preferential sampling of the turbulent flow field and the mechanism of turbophoresis are to be understood dynamically in terms of the interaction between inertial particles and coherent structures (e.g. sweeps and ejections) in the turbulent velocity field in the boundary layer. However, the results presented in this chapter make this conclusion questionable. Both turbophoresis and preferential sampling of the fluid velocities (see figure 5.11) were found in the simulations presented in this chapter where a Langevin equation was used to describe the fluid velocity at the particle position. However the Langevin equation used here contains no structure and therefore contains no information at all about sweeps and ejections (which are non-Gaussian events, characterised by different timescales and different intensities). Therefore it is clear that particle interactions with turbulent coherent structures cannot explain, or at least fully explain, the dynamical phenomena responsible for preferential sampling and turbophoresis.

A statistical-physical argument for the origin of turbophoresis and preferential sampling is as follows. Turbophoresis occurs because inertial particles are not in equilibrium with the fluid turbulence, therefore the energy they receive from the turbulence in highly energetic regions is transported by the particles into regions where the turbulence intensity is less. Turbophoresis depends both upon τ_p and the gradients in the particle kinetic stresses $\overline{\mathrm{c}_2\mathrm{c}_2}$. In the near wall region where the turbophoretical drift is towards the wall,

only strongly positive values of the fluid velocity are able to give the particles sufficient energy to overcome the wall-ward turbophoretic drift and hence move away from the wall. Therefore in the near wall region the inertial particles preferentially sample values of the fluid velocity greater than the mean value of the field (i.e. $\overline{u_2^p} > \langle u_2 \rangle = 0$). This explanation agrees with what is observed in figures (5.4) and (5.11).

5.6 Conclusions

In this chapter the PDF derived continuum equations were tested against equivalent PT data. The results showed that for $\tau_p = 20, 50$ and 80 the kinetic stress predictions were in excellent agreement with the PT data whilst the concentration solution predictions were in significant error. The local approximations to the dispersion tensors were identified as the source of the error in the concentration solution predictions. In particular $\overline{\lambda}_{22}$ is very sensitive to the strongly inhomogeneous nature of the turbulence in a boundary layer, and this finding is in agreement with [49]. In order to improve the continuum equation predictions for the concentration solutions it is necessary to develop non-local closure models for the dispersion tensors which take into account the inhomogeneous nature of the fluid turbulence and also the effect of the particle-wall collisions on the correlations of the flow field along the particle trajectories. Furthermore, it is necessary to develop new closure models for the dispersion tensors in order to circumvent the introduction of the passive scalar approximation, since this approximation removes a drift mechanism in the particle momentum equation which is surely a source of the error in the concentration solutions from the continuum equations.

In the following chapters new non-local closure models for the particle dispersion are developed in order to improve upon the standard local approximations which have been shown in this chapter to be a source of error in the momentum equation, leading to poor particle concentration predictions.

Chapter 6

Particle Dispersion Tensors in Boundary Layer Turbulence

In the previous chapter it was shown that for particle dispersion in a turbulent boundary layer, local approximations for the particle dispersion tensors can be in significant error. In this chapter a discussion is given concerning the nature of the particle dispersion tensors in boundary layer turbulence, in particular highlighting the deficiencies of local approximations, which will then serve as the basis upon which to consider the formulation of a new 'non-local' closure model for the dispersion tensors.

The definition of the velocity averaged particle dispersion tensors (with the Green tensor approximation for the response tensor), which are found in the continuum equations are (see chapter 4)

$$\overline{\lambda}_{ki}(\mathbf{x},t) = \int_0^t G_{kj}(t;t') \Big\langle R_{ji}(\boldsymbol{x}^{p\prime},t';\mathbf{x},t) \Big\rangle_{\mathbf{x}} dt' \tag{6.1}$$

$$\overline{\mu}_{ki}(\mathbf{x},t) = \int_0^t \dot{G}_{kj}(t;t') \Big\langle R_{ji}(\boldsymbol{x}^{p\prime},t';\mathbf{x},t) \Big\rangle_{\mathbf{x}} dt' \tag{6.2}$$

$$\overline{\kappa}_{i}(\mathbf{x},t) = \int_0^t G_{kj}(t;t') \left\langle \frac{\partial}{\partial \mathrm{x}_k} R_{ji}(\boldsymbol{x}^{p\prime},t';\mathbf{x},t) \right\rangle_{\mathbf{x}} dt' \tag{6.3}$$

The intrinsic non-locality of the dispersion tensors is bound up in the conditional averages they contain, that is, within

$$\Big\langle R_{ji}(\boldsymbol{x}^{p\prime},t';\mathbf{x},t) \Big\rangle_{\mathbf{x}}$$

and

$$\left\langle \frac{\partial}{\partial \mathrm{x}_k} R_{ji}(\boldsymbol{x}^{p\prime}, t'; \mathbf{x}, t) \right\rangle_{\mathbf{x}}$$

Consider figure 6.1

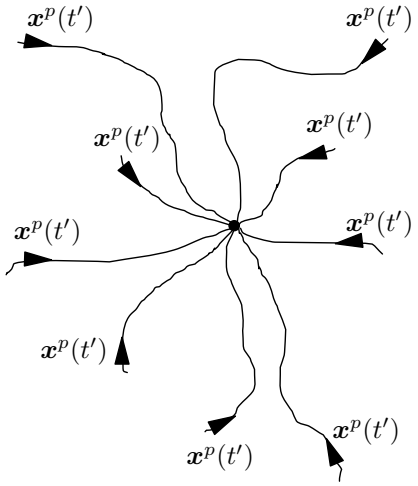

Figure 6.1: Diagram to illustrate the meaning of the conditional averages in the dispersion tensors. The lines with arrows represent different particle trajectories, $\boldsymbol{x}^p(t')$, which are coincident with $\mathbf{x}$ at time $t' = t$.

Figure 6.1 illustrates different particle trajectories arriving at position $\mathbf{x}$ at time t. Because the turbulent flow field is modelled as being stochastic, the particle trajectories are also stochastic, and therefore as the particles move through the flow field and approach $\mathbf{x}$ at time t they each sample differing values of $\boldsymbol{R}$ along their trajectories. The average of the values of $\boldsymbol{R}$ sampled along the particle trajectories is the meaning of the conditional average

$$\left\langle R_{ji}(\boldsymbol{x}^{p\prime}, t'; \mathbf{x}, t) \right\rangle_{\mathbf{x}}$$

and similarly for

$$\left\langle \frac{\partial}{\partial \mathrm{x}_k} R_{ji}(\boldsymbol{x}^{p\prime}, t'; \mathbf{x}, t) \right\rangle_{\mathbf{x}}$$

Clearly then, if the turbulence properties vary along the particle trajectory then this will affect the conditional averages, and this is the case for particle dispersion in a turbulent boundary layer where the turbulence is strongly inhomogeneous. In light of the results presented in the previous chapter it is clear that new 'non-local' models must be developed for the dispersion tensors which account for the inhomogeneity of the turbulence seen by the particles as they disperse through the boundary layer.

Furthermore, a new closure model for the dispersion tensors is required in order to

correctly close $\overline{\boldsymbol{\kappa}}$. In the particle momentum equation there is a flux

$$\rho\left(\overline{\kappa}_i - \frac{\partial}{\partial \mathrm{x}_k}\overline{\lambda}_{ki}\right)$$

which represents a flux due to the fluid turbulence inhomogeneities. Under the passive scalar approximation this flux is zero for all particle sizes. However, in reality this flux term is not zero for inertial particle dispersion in inhomogeneous turbulence, and therefore a new closure is also required in order to correctly close $\overline{\boldsymbol{\kappa}}$.

In equations (6.1),(6.2),(6.3) the terms requiring closure are given by

$$\left\langle R_{ji}(\boldsymbol{x}^{p\prime}, t'; \mathbf{x}, t)\right\rangle_{\mathbf{x}} = \int_{\mathbf{x}'} R_{ji}(\mathbf{x}', t'; \mathbf{x}, t)\rho\left(\mathbf{x}', t'|\mathbf{x}, t\right) d\mathbf{x}' \tag{6.4}$$

$$\left\langle \frac{\partial}{\partial \mathrm{x}_k} R_{ji}(\boldsymbol{x}^{p\prime}, t'; \mathbf{x}, t)\right\rangle_{\mathbf{x}} = \int_{\mathbf{x}'} \left[\frac{\partial}{\partial \mathrm{x}_k} R_{ji}(\mathbf{x}', t'; \mathbf{x}, t)\right] \rho\left(\mathbf{x}', t'|\mathbf{x}, t\right) d\mathbf{x}' \tag{6.5}$$

where $\rho\left(\mathbf{x}', t'|\mathbf{x}, t\right)$ is the PDF for particle positions at time t' for all particle trajectories which arrive at $\mathbf{x}$ at time t

$$\rho\left(\mathbf{x}', t'|\mathbf{x}, t\right) = \left\langle \delta(\boldsymbol{x}^p(t') - \mathbf{x}')\right\rangle_{\mathbf{x}} \tag{6.6}$$

Since it is statistically steady state systems that are of interest in the present work, equations (6.4) and (6.5) may be re-expressed as

$$\left\langle R_{ji}(\boldsymbol{x}^p(s), s; \mathbf{x}, 0)\right\rangle_{\mathbf{x}} = \int_{\mathbf{x}'} R_{ji}(\mathbf{x}', s; \mathbf{x}, 0)\rho\left(\mathbf{x}', s|\mathbf{x}\right) d\mathbf{x}' \tag{6.7}$$

$$\left\langle \frac{\partial}{\partial \mathrm{x}_k} R_{ji}(\boldsymbol{x}^p(s), s; \mathbf{x}, 0)\right\rangle_{\mathbf{x}} = \int_{\mathbf{x}'} \left[\frac{\partial}{\partial \mathrm{x}_k} R_{ji}(\mathbf{x}', s; \mathbf{x}, 0)\right] \rho\left(\mathbf{x}', s|\mathbf{x}\right) d\mathbf{x}' \tag{6.8}$$

where $s = t' - t$ and

$$\rho\left(\mathbf{x}', s|\mathbf{x}\right) = \left\langle \delta(\boldsymbol{x}^p(s) - \mathbf{x}')\right\rangle_{\mathbf{x}} \tag{6.9}$$

The intrinsic non-locality within the dispersion tensors therefore depends both upon the nature of $\boldsymbol{R}$ and $\rho\left(\mathbf{x}', s|\mathbf{x}\right)$, each of which shall now be discussed.

6.1 Characteristics of $\boldsymbol{R}$ in a turbulent boundary layer

In a turbulent channel flow, and in particular, in the turbulent boundary layer, the turbulence is very strongly inhomogeneous and anisotropic, and this is captured within $\boldsymbol{R}$. To simplify the present discussion only a Stokes drag force acting upon the particle will be considered here, for which

$$R_{ji}(\mathbf{x}', s; \mathbf{x}, 0) = \beta^2 \Big\langle u_j'(\mathbf{x}', s) u_i'(\mathbf{x}, 0) \Big\rangle \tag{6.10}$$

First, consider the Reynolds stress tensor

$$\Big\langle u_j'(\mathrm{x}_2, 0) u_i'(\mathrm{x}_2, 0) \Big\rangle = \langle u_j' u_i' \rangle$$

in a turbulent channel flow, as shown in figure (6.2)

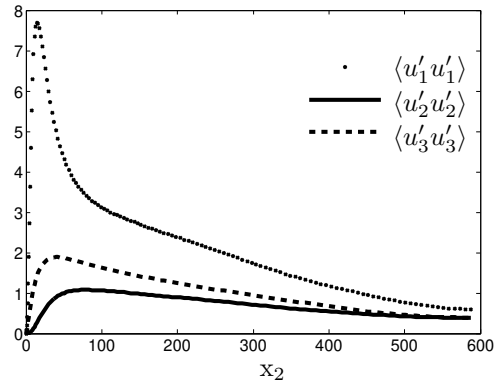

Figure 6.2: Plot showing the diagonal components of the fluid velocity Reynolds stress tensor, data taken from [4].

Figure 6.2 shows that the turbulence in a channel flow is very strongly inhomogeneous and anisotropic, and the effect that this has is that as particles disperse they move through regions in which the turbulence intensity may vary significantly along their trajectories. Clearly this will affect the dispersion tensors. Secondly, consider the two-point covariances of the field $\boldsymbol{u}'$ shown in figures 6.3 and 6.4

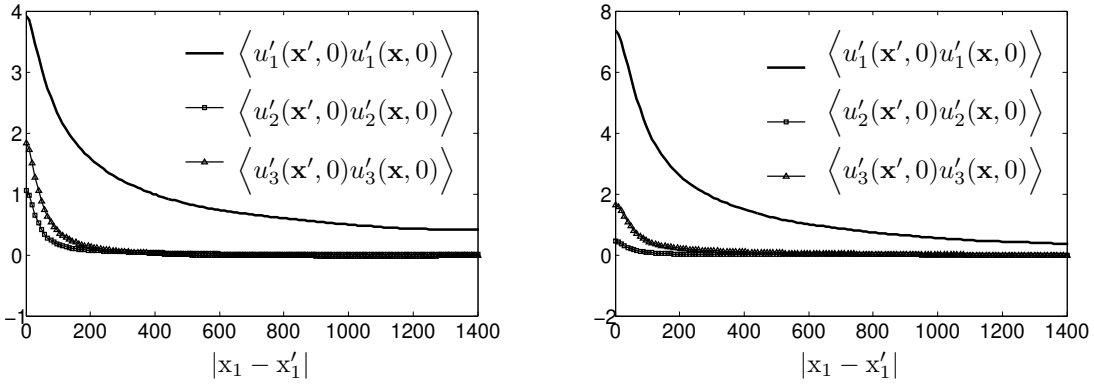

Figure 6.3: Plots of spatial covariances in a turbulent boundary layer at $\mathrm{x}_2 = 59.5$ (left plot) and $\mathrm{x}_2 = 5.34$ (right plot) wall units. Plots show spatial decorrelation in the homogeneous stream-wise direction. Data taken from [4].

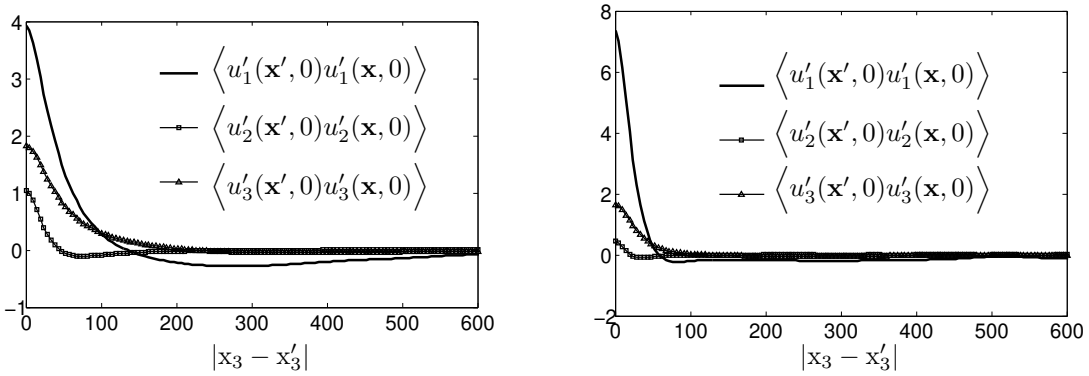

Figure 6.4: Plots of spatial covariances in a turbulent boundary layer at $\mathrm{x}_2 = 59.5$ (left plot) and $\mathrm{x}_2 = 5.34$ (right plot) wall units. Plots show spatial decorrelation in the homogeneous span-wise direction. Data taken from [4].

Figures 6.3 and 6.4 show that in addition to the Reynolds stresses being very strongly inhomogeneous and anisotropic, the two-point correlations of the turbulent velocity field are also strongly anisotropic and inhomogeneous. That is, the turbulent velocity field decorrelates in the stream-wise and span-wise directions differently and exhibits a wall-normal location (x_2) dependence. In addition, as shown in figure 6.5, the turbulent velocity field in a boundary layer may also feature negatively correlated regions

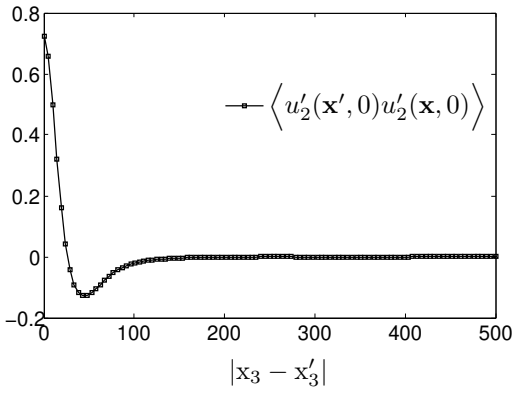

Figure 6.5: Plot of spatial covariance in a turbulent boundary layer at $\mathrm{x}_2 = 29.64$ wall units. Plot shows spatial decorrelation in the homogeneous span-wise direction. Data taken from [4]

The characteristics illustrated in figures 6.2 - 6.5 of the velocity field in a turbulent boundary layer (strong inhomogeneity, anisotropy and negatively correlated regions) all affect the particle dispersion tensors since they show that along particle trajectories the properties of the turbulence (e.g. the turbulence intensity) may vary significantly, and also that the decorrelation of the flow field experienced by the particles strongly depends upon the particular direction of the motion of the particle (since, for example, the spatial covariances of the flow field differ significantly for stream-wise and wall-normal spatial separations). Such properties of the turbulent velocity field in a boundary layer make the dispersion tensors (via their conditional averages) intrinsically non-local.

6.2 Non-local nature of $\rho\left(\mathbf{x}', s|\mathbf{x}\right)$

Not only do the characteristics of the turbulence described by $\boldsymbol{R}$ make the dispersion tensors intrinsically non-local, but so also do the characteristics of $\rho\left(\mathbf{x}', s|\mathbf{x}\right)$ since this describes the nature of the particle dispersion process in the turbulent flow field. To simplify the present discussion, dispersion in the wall-normal direction (1D) will be considered in order to consider the effect of turbulence inhomogeneity on $\rho\left(\mathbf{x}', s|\mathbf{x}\right)$. Then, 3D dispersion will be considered in order to highlight the effect of the turbulence anisotropy.

In the wall-normal direction of a channel flow the motion of a particle (subject only to Stokes drag and gravity, for simplicity) may be determined by solutions constructed using Green tensors as (the construction of this solution is discussed in detail in chapter 7)

$$x_2^p(s) = \mathrm{x}_2 + \frac{g_2}{\beta}\left[s + G_{22}(s)\right] - G_{22}(s)v_2^p(0) - \beta\int_s^0 G_{22}(s-s_1)u_2'(\boldsymbol{x}^p(s_1),s_1)ds_1 \tag{6.11}$$

where $s \leq 0$, x_2 is the wall-normal position of the particle at $s = 0$ and G_{22} is the wall-normal component of the Green tensor for the particle equation of motion

$$G_{22}(s) = \tau_p\left(1 - \exp[\beta s]\right) \tag{6.12}$$

Using equation (6.11) the statistical properties of $\rho\left(\mathrm{x}_2', s|\mathrm{x}_2\right)$ may be considered. The mean of $\rho\left(\mathrm{x}_2', s|\mathrm{x}_2\right)$ is given by

$$\left\langle x_2^p(s)\right\rangle_{\mathrm{x}_2} = \mathrm{x}_2 + \frac{g_2}{\beta}\left[s + G_{22}(s)\right] - G_{22}(s)\left\langle v_2^p(0)\right\rangle_{\mathrm{x}_2} - \beta\int_s^0 G_{22}(s-s_1)\left\langle u_2'(\boldsymbol{x}^p(s_1),s_1)\right\rangle_{\mathrm{x}_2} ds_1 \tag{6.13}$$

Note that in equation (6.13) $\left\langle v_2^p(0)\right\rangle_{\mathrm{x}_2} = \overline{\mathrm{v}}_2(\mathrm{x}_2)$ which is zero for statistically steady state particle dispersion with elastic particle-wall collisions. The term

$$\left\langle u_2'(\boldsymbol{x}^p(s_1),s_1)\right\rangle_{\mathrm{x}_2}$$

is strongly non-local and is the mean of the wall-normal fluctuating fluid velocities sampled at the particle positions at time s_1 for particle trajectories satisfying $x_2^p(0) = \mathrm{x}_2$. It is known that for particle dispersion in turbulent channel flows

$$\left\langle u_2'(\boldsymbol{x}^p(0),0)\right\rangle_{\mathrm{x}_2} \neq 0$$

in general, and the strongly inhomogeneous nature of the turbulent flow field in a channel flow is such that $\left\langle u_2'(\boldsymbol{x}^p(s_1),s_1)\right\rangle_{\mathrm{x}_2}$ is almost certainly also non-zero. Therefore, even without gravity, the mean of $\rho\left(\mathrm{x}_2', s|\mathrm{x}_2\right)$ as defined by equation (6.13) will be time dependent for particle dispersion in a turbulent channel flow.

The second central moment of $\rho\left(\mathrm{x}_2', s|\mathrm{x}_2\right)$ is given by

$$\begin{aligned}\left\langle \tilde{x}_2^p(s)\tilde{x}_2^p(s)\right\rangle_{\mathrm{x}_2} =& G_{22}(s)\left\langle v_2^{p\prime}(0)v_2^{p\prime}(0)\right\rangle_{\mathrm{x}_2} G_{22}(s) \\ &+ 2\beta G_{22}(s)\int_s^0 G_{22}(s-s_1)\left\langle v_2^{p\prime}(0)u_2'(\boldsymbol{x}^p(s_1),s_1)\right\rangle_{\mathrm{x}_2} ds_1 \\ &+ \beta^2\int_s^0\int_s^0 G_{22}(s-s_1)\left\langle u_2'(\boldsymbol{x}^p(s_1),s_1)u_2'(\boldsymbol{x}^p(s_2),s_2)\right\rangle_{\mathrm{x}_2} G_{22}(s-s_2)ds_1ds_2 \\ &- \beta^2\int_s^0\int_s^0 G_{22}(s-s_1)\left\langle u_2'(\boldsymbol{x}^p(s_1),s_1)\right\rangle_{\mathrm{x}_2}\left\langle u_2'(\boldsymbol{x}^p(s_2),s_2)\right\rangle_{\mathrm{x}_2} G_{22}(s-s_2)ds_1ds_2\end{aligned} \tag{6.14}$$

where

$$\tilde{x}_2^p(s) = x_2^p(s) - \left\langle x_2^p(s)\right\rangle_{\mathrm{x}_2} \tag{6.15}$$

$$\left\langle v_2^{p\prime}(0)v_2^{p\prime}(0)\right\rangle_{\mathrm{x}_2} = \overline{\mathrm{c}_2\mathrm{c}_2}(\mathrm{x}_2) \tag{6.16}$$

and the non-local nature of the second central moment is in the fluctuating particle-fluid velocity autocovariance

$$\left\langle v_2^{p\prime}(0)u_2'(\boldsymbol{x}^p(s_1),s_1)\right\rangle_{\mathrm{x}_2}$$

the fluid velocity autocovariance

$$\left\langle u_2'(\boldsymbol{x}^p(s_1),s_1)u_2'(\boldsymbol{x}^p(s_2),s_2)\right\rangle_{\mathrm{x}_2}$$

and again in

$$\left\langle u_2'(\boldsymbol{x}^p(s_1),s_1)\right\rangle_{\mathrm{x}_2}$$

Higher order moments of $\rho\,(\mathrm{x}_2', s|\mathrm{x}_2)$ can be constructed in the same manner and include higher order non-local correlations between the particle and fluid velocities. Of particular importance is that the first term in the third central moment of $\rho\,(\mathrm{x}_2', s|\mathrm{x}_2)$ is given by

$$G_{22}(s)G_{22}(s)G_{22}(s)\left\langle v_2^{p\prime}(0)v_2^{p\prime}(0)v_2^{p\prime}(0)\right\rangle_{\mathrm{x}_2} = G_{22}(s)G_{22}(s)G_{22}(s)\overline{\mathrm{c}_2\mathrm{c}_2\mathrm{c}_2}(\mathrm{x}_2)$$

For $s < 0$ this term is non-zero in general for particle dispersion in a turbulent boundary layer, and therefore $\rho\,(\mathrm{x}_2', s|\mathrm{x}_2)$ is a skewed PDF. Considering equations (6.4) and (6.5), if $\rho\,(\mathrm{x}_2', s|\mathrm{x}_2)$ is skewed, then the particles will sample the values of $R_{ji}(\mathrm{x}_2', s; \mathrm{x}_2)$ asymmetrically with respect to x_2 and hence this will also affect the particle dispersion tensors.

In addition to the effect of the fluid turbulence inhomogeneity in the wall-normal direction, the anisotropy of the turbulence also affects $\rho(\mathbf{x}', s|\mathbf{x})$ and hence also the way the particles sample the correlations of the turbulence. For example, suppose that the spatial correlations in $R_{ji}(\mathbf{x}', s; \mathbf{x}, 0)$ decay at equal rates in all directions, then it is clear that if the covariance of $\rho(\mathbf{x}', s|\mathbf{x})$ increases more rapidly in the x_1 direction than in the x_2 then the rate of decorrelation of the flow field seen by the particles will be more rapid in the x_1 direction than in the x_2.

6.3 Particle-wall collisions

Another factor which affects the dispersion tensors in a boundary layer is the effect of the particle-wall collisions.

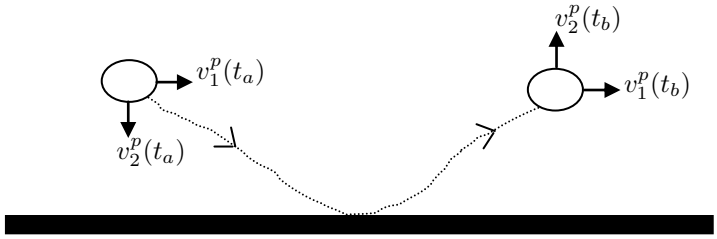

Figure 6.6: Trajectory of particle ($t_a < t_b$) which has collided with the wall of a pipe/channel.

Figure 6.6 shows the trajectory of a particle which collides with the wall. Consider the spatial correlations of the fluid velocity field that the particle will see as it moves from its wall-normal position at time t_a, $x_2^p(t_a) = \mathrm{x}_2$, towards the wall and then rebounds back. Figure 6.7 shows a function representing the assumed form of the two-point covariance of the wall-normal fluid velocities in a turbulent boundary layer (scaled to a maximum value of 1)

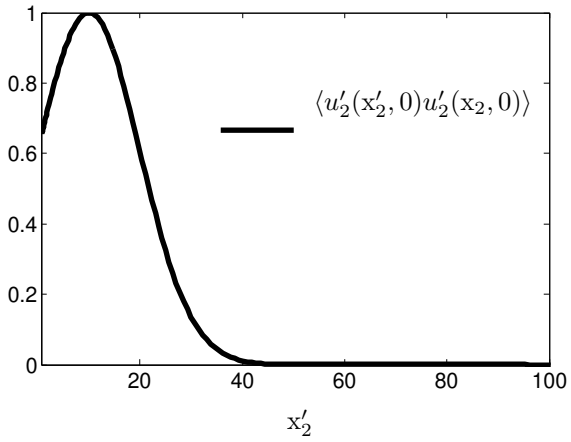

Figure 6.7: Plot of an assumed form for two-point covariance of the wall-normal fluid velocities in a boundary layer at $\mathrm{x}_2 = 10$ (minimum x_2' value is x_2^{min}, the point at which the particle makes contact with the wall).

Now if the particle in figure 6.6 is at $\mathrm{x}_2 = 10$ at time t_a and begins to move towards the wall, then according to figure 6.7 the particle will begin to see a spatial decorrelation of the fluid velocity field in the wall-normal direction. However upon rebounding back from the wall its wall-normal position will approach $\mathrm{x}_2 = 10$ once again, and hence the particle will see a velocity field which is 're-correlating' with itself (spatially). This 're-correlation' effect will affect the particle dispersion tensors.

The effect of the particle-wall collisions is described by the distribution of particle positions in the wall-normal direction $\rho\,(\mathrm{x}_2', s|\mathrm{x}_2)$. Due to the constraint imposed by the wall $x_2^p \geq \mathrm{x}_2^{min}$, where x_2^{min} is the location of the wall, then $\rho\,(\mathrm{x}_2', s|\mathrm{x}_2)$ becomes increasingly asymmetric for $\mathrm{x}_2 \to \mathrm{x}_2^{min}$.

6.4 Summary

The particle dispersion tensors $\overline{\boldsymbol{\lambda}}, \overline{\boldsymbol{\mu}}$ and $\overline{\boldsymbol{\kappa}}$ (under the Green tensor approximation) depend upon the non-local correlation tensors

$$\Big\langle R_{ji}(\boldsymbol{x}^p(s), s; \mathbf{x}, 0)\Big\rangle_{\mathbf{x}}$$

and

$$\Big\langle \frac{\partial}{\partial \mathrm{x}_k} R_{ji}(\boldsymbol{x}^p(s), s; \mathbf{x}, 0)\Big\rangle_{\mathbf{x}}$$

both of which require closure. In chapter 5 it was demonstrated that local approximations to such correlation tensors are insufficient for particles dispersing in turbulent boundary layers, except in the limit of very large particles. In this chapter the characteristics of inertial particle dispersion in turbulent boundary layers have been considered in order to highlight the features which make the dispersion tensors non-local in such a flow.

In summary, the non-local affects on the particle dispersion tensors can be identified and associated with

- The strongly inhomogeneous and anisotropic nature of the one-point and two-point statistics of the fluid turbulence described in $\boldsymbol{R}(\mathbf{x}', s; \mathbf{x}, 0)$
- The non-local effect of the turbulence on $\rho(\mathbf{x}', s|\mathbf{x})$ and the the skewness and anisotropic dispersion of the particles described by $\rho(\mathbf{x}', s|\mathbf{x})$
- The particle-wall collisions

In the next chapter a new non-local closure model for the particle dispersion tensors is developed which attempts to take into account these effects.

Chapter 7

Closure Model for Particle Dispersion Tensors

In this chapter a new non-local closure model is presented which attempts to take into account the effect of the inhomogeneity and anisotropy of the turbulence, as well as accounting for the effect of particle wall collisions for particles dispersing under a Stokes drag force (and in the next chapter the closure model is extended to account for added mass and gravitational forcing in addition to Stokes drag forcing acting on the particles).

The correlations that require closure in the dispersion tensors are given by

$$\Big\langle R_{ji}(\boldsymbol{x}^p(s),s;\mathbf{x},0)\Big\rangle_{\mathbf{x}} = \int_{\mathbf{x}'} R_{ji}(\mathbf{x}',s;\mathbf{x},0)\rho\left(\mathbf{x}',s|\mathbf{x}\right)d\mathbf{x}' \tag{7.1}$$

$$\Big\langle \frac{\partial}{\partial \mathrm{x}_k} R_{ji}(\boldsymbol{x}^p(s),s;\mathbf{x},0)\Big\rangle_{\mathbf{x}} = \int_{\mathbf{x}'} \left[\frac{\partial}{\partial \mathrm{x}_k} R_{ji}(\mathbf{x}',s;\mathbf{x},0)\right]\rho\left(\mathbf{x}',s|\mathbf{x}\right)d\mathbf{x}' \tag{7.2}$$

For Stokes drag forcing on the particles, the correlations of the fluctuating force field acting on the particles are given by

$$R_{ji}(\mathbf{x}',s;\mathbf{x},0) = \beta^2\Big\langle u_j'(\mathbf{x}',s)u_i'(\mathbf{x},0)\Big\rangle \tag{7.3}$$

$$\frac{\partial}{\partial \mathrm{x}_k}R_{ji}(\mathbf{x}',s;\mathbf{x},0) = \beta^2\frac{\partial}{\partial \mathrm{x}_k}\Big\langle u_j'(\mathbf{x}',s)u_i'(\mathbf{x},0)\Big\rangle \tag{7.4}$$

The tensor

$$\Big\langle u_j'(\mathbf{x}',s)u_i'(\mathbf{x},0)\Big\rangle$$

is the Eulerian 2-point, 2-time correlation tensor for the fluctuating fluid velocity field, some of the properties of which were discussed in the previous chapter. This fluid

statistic is assumed to be known and is an input to the closure model, and may be obtained either by a DNS, LES or experimental data[1]. Therefore the closure problem is related to developing a model for $\rho(\mathbf{x}', s|\mathbf{x})$.

There are then three issues to be considered in the formulation of a closure model for $\rho(\mathbf{x}', s|\mathbf{x})$; (i) how can the effect of the particle-wall collisions be accounted for, (ii) what type of PDF should be used to model $\rho(\mathbf{x}', s|\mathbf{x})$ and (iii) how can the moments of the PDF be modelled? These are now considered.

7.1 Accounting for the effect of the particle wall-collisions

As discussed in section 6.3, the particle-wall collisions will affect the values of $\boldsymbol{R}(\mathbf{x}', s; \mathbf{x}, 0)$ sampled by the particles in the near wall region and it is therefore important to take this effect into account. The most obvious way to account for the effect would be to account for individual particle-wall collisions in the construction of the moments for $\rho(\mathbf{x}', s|\mathbf{x})$. However, this is far from straightforward. Instead in this thesis where the focus is on elastic particle-wall collisions, a more elegant approach is possible. The particle-wall collisions only affect the particle motion in the wall-normal direction and it is therefore only necessary to consider the effect of the collisions upon $\rho(\mathrm{x}_2', s|\mathrm{x}_2)$.

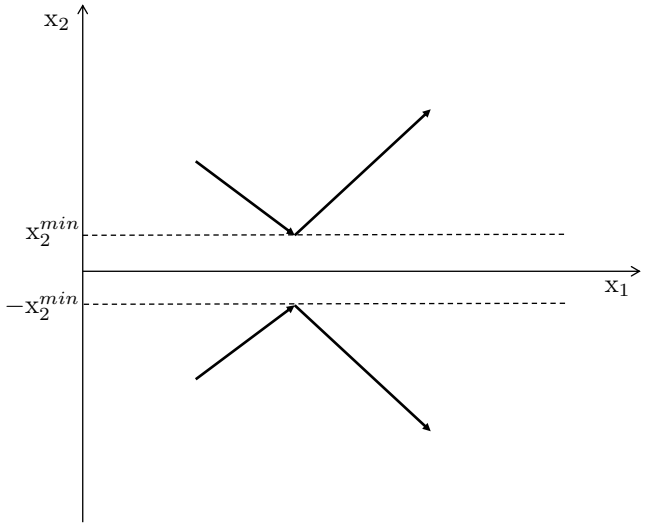

Figure 7.1: Plot to illustrate the line of symmetry approach. The thick black lines represent particle trajectories which collide with the wall.

[1]Note that this statistic can only strictly be considered as input data for a one-way coupled particle-turbulence system. For a two-way coupled system, these correlations would depend upon the particle dispersion itself.

Consider figure 7.1 which illustrates two particle trajectories, one dispersing in the region $\mathrm{x}_2 \geq \mathrm{x}_2^{min}$ and the other in the region $\mathrm{x}_2 \leq -\mathrm{x}_2^{min}$. The particle dynamics are symmetric with respect to the line $\mathrm{x}_2 = 0$ and the dynamics in both regions are described by the following system of particle equations of motion

$$\frac{d^2}{dt^2}x_i^p = \begin{cases} F_i(\boldsymbol{x}^p(t), \boldsymbol{v}^p(t), t) + f_i(\boldsymbol{x}^p(t), t) & \text{for } \mathrm{x}_2 \geq \mathrm{x}_2^{min} \\ J_{ij}F_j(\boldsymbol{J}\cdot\boldsymbol{x}^p(t), \boldsymbol{J}\cdot\boldsymbol{v}^p(t), t) + J_{ij}f_j(\boldsymbol{J}\cdot\boldsymbol{x}^p(t), t) & \text{for } \mathrm{x}_2 \leq -\mathrm{x}_2^{min} \end{cases} \tag{7.5}$$

where

$$J_{ij} = \begin{pmatrix} 1 & 0 & 0 \\ 0 & -1 & 0 \\ 0 & 0 & 1 \end{pmatrix} \tag{7.6}$$

Then for elastic particle-wall collisions, rather than constraining the particle motion to the domain $\mathrm{x}_2 \geq \mathrm{x}_2^{min}$ and reflecting the particle back into the domain upon collision with the wall, it is equivalent to define the particle motion over the whole domain $\mathrm{x}_2 \geq \mathrm{x}_2^{min}$ & $\mathrm{x}_2 \leq -\mathrm{x}_2^{min}$ but now with the particle equation of motion defined by equation (7.5). Trajectories in this symmetry-line model then generate the required trajectories of the original reflecting wall system through the mapping $(x_1^p, x_2^p, x_3^p) \rightarrow (x_1^p, |x_2^p|, x_3^p)$.

Given that the statistics of $\boldsymbol{f}$, defined by $\boldsymbol{R}(\mathbf{x}', s; \mathbf{x}, 0)$ will be symmetric with respect to the line $\mathrm{x}_2 = 0$, and that the particle motion is defined only for $\mathrm{x}_2 \geq \mathrm{x}_2^{min}$ & $\mathrm{x}_2 \leq -\mathrm{x}_2^{min}$, then for this symmetry-line model the integral over x_2' in equation (7.1) is replaced by

$$\begin{aligned} \Big\langle R_{ji}(x_2^p(s), s; \mathrm{x}_2, 0)\Big\rangle_{\mathrm{x}_2} = &\int_{+\mathrm{x}_2^{min}}^{+\mathrm{x}_2^{max}} R_{ji}(\mathrm{x}_2', s; \mathrm{x}_2, 0)\rho\left(\mathrm{x}_2', s|\mathrm{x}_2\right) d\mathrm{x}_2' \\ &+ \int_{-\mathrm{x}_2^{max}}^{-\mathrm{x}_2^{min}} R_{ji}(\mathrm{x}_2' + 2|\mathrm{x}_2'|, s; \mathrm{x}_2, 0)\rho\left(2\mathrm{x}_2^{min} + \mathrm{x}_2', s|\mathrm{x}_2\right) d\mathrm{x}_2' \end{aligned} \tag{7.7}$$

and similarly for equation (7.2). The advantage of this line of symmetry model is that it is no longer necessary to consider particle collisions at x_2^{min} since the effect of the elastically rebounded particle trajectories on $\Big\langle R_{ji}(x_2^p(s), s; \mathrm{x}_2, 0)\Big\rangle_{\mathrm{x}_2}$ is captured within the integral

$$\int_{-\mathrm{x}_2^{max}}^{-\mathrm{x}_2^{min}} R_{ji}(\mathrm{x}_2' + 2|\mathrm{x}_2'|, s; \mathrm{x}_2, 0)\rho\left(2\mathrm{x}_2^{min} + \mathrm{x}_2', s|\mathrm{x}_2\right) d\mathrm{x}_2'$$

7.2 Type of PDF for $\rho(\mathbf{x}', s|\mathbf{x})$

As discussed in section 6.2, as s increases the conditional PDF for particle dispersion in a turbulent boundary layer $\rho(\mathbf{x}', s|\mathbf{x})$ is undoubtedly skewed, due to the skewness of the particle velocity distributions and the inhomogeneous nature of the underlying fluid turbulence. Further, the intermittent nature of turbulence is such that one would also expect the distribution $\rho(\mathbf{x}', s|\mathbf{x})$ to have extended tails (at least for small to medium particles). A modelling limitation is that it is difficult to construct a closed form expression for the undoubtedly complex form that $\rho(\mathbf{x}', s|\mathbf{x})$ takes in a real turbulent boundary layer. However it is only the form of $\rho(\mathbf{x}', s|\mathbf{x})$ within the time for which the fluid is correlated that is important, and within these times it is possible that a simple Gaussian distribution may be an adequate approximation. Therefore as a first approximation, a Gaussian distribution will be used to model $\rho(\mathbf{x}', s|\mathbf{x})$, specifically

$$\rho(\mathbf{x}', s|\mathbf{x}) \approx \frac{1}{(2\pi)^{3/2}|\Sigma_{ij}|^{1/2}} \exp\left[-\frac{1}{2}(\mathrm{x}_i' - \mathrm{M}_i)\Sigma_{ij}^{-1}(\mathrm{x}_j' - \mathrm{M}_j)\right] \tag{7.8}$$

where Σ_{ij}^{-1} is the ij component of the inverted tensor $\mathbf{\Sigma}^{-1}$ and

$$\mathrm{M}_i = \left\langle x_i^p(s) \right\rangle_{\mathbf{x}} \tag{7.9}$$

$$\Sigma_{ij} = \left\langle \tilde{x}_i^p(s)\tilde{x}_j^p(s) \right\rangle_{\mathbf{x}} \tag{7.10}$$

It should be noted that it would also be possible to use more appropriate PDF's for $\rho(\mathbf{x}', s|\mathbf{x})$ should a Gaussian prove to be inadequate. For example, skew-normal distributions [124], epsilon-skew-normal distributions [125] along with skew-t and various other types of distributions [126] could be used to model $\rho(\mathbf{x}', s|\mathbf{x})$ as a skewed PDF which is perhaps more realistic than a Gaussian.

7.3 Modelling the moments of $\rho(\mathbf{x}', s|\mathbf{x})$

With a Gaussian PDF as an initial approximation to $\rho(\mathbf{x}', s|\mathbf{x})$ it is necessary to be able to model the mean of the distribution

$$\mathrm{M}_i = \left\langle x_i^p(s) \right\rangle_{\mathbf{x}}$$

and the second central moment

$$\Sigma_{ij} = \left\langle \tilde{x}_i^p(s)\tilde{x}_j^p(s) \right\rangle_{\mathbf{x}}$$

For particles dispersing only under the influence of a Stokes drag force the particle equation of motion is

$$\frac{d^2}{dt^2}x_i^p + \beta\frac{d}{dt}x_i^p = \beta\langle u_i\rangle^p + \beta u_i^{p\prime} \tag{7.11}$$

The particle trajectories described by $\rho\,(\mathbf{x}', s|\mathbf{x})$ are defined backwards in time, and the backwards in time motion is described by

$$\frac{d^2}{ds^2}x_i^p - \beta\frac{d}{ds}x_i^p = -\beta\langle u_i\rangle^p - \beta u_i^{p\prime} \tag{7.12}$$

where $s = t' - t \leq 0$. Since the trajectories in the moments are to be subject to the end condition $\boldsymbol{x}^p(0) = \mathbf{x}$, then if the mean shear of the fluid is assumed to be locally linear (i.e. linear about $\mathbf{x}$) then the mean force on the particle may be written as

$$\beta\langle u_i\rangle^p = \beta\langle u_i\rangle(x_2^p(s)) = \beta\delta_{i1}\left[\gamma(\mathrm{x}_2)\left(x_2^p(s) - \mathrm{x}_2\right) + \langle u_i(\mathrm{x}_2)\rangle\right] \tag{7.13}$$

where $\gamma(\mathrm{x}_2)$ is the mean shear at x_2

$$\gamma(\mathrm{x}_2) = \frac{\partial}{\partial \mathrm{x}_2}\langle u_1(\mathrm{x}_2)\rangle \tag{7.14}$$

The assumption that the mean shear of the fluid velocity field may be considered as locally linear in a turbulent boundary layer is of course a strong assumption, but it is neccesaary in order to construct fully analytic models for the moments of the distribution $\rho\,(\mathbf{x}', s|\mathbf{x})$, and it is a fully analytic closure model which is desired in the present work[2]. Strictly speaking, the locally linear assumption is only true in the viscous sublayer of the boundary layer ($\mathrm{x}_2 < 5$) in which the mean fluid velocity may be to a very high degree of accuracy considered linear in x_2. Away from the viscous sublayer, the mean fluid velocity varies nonlinearly with x_2, and as such the locally linear assumption is only strictly appropriate for infinitesimal displacements about x_2 (i.e. $|x_2^p(s) - \mathrm{x}_2| \ll 1$). However, away from the viscous sublayer, in the time for which the velocity field is correlated $|x_2^p(s) - \mathrm{x}_2|$ is expected to be sufficiently large so that the

[2]Note that the present closure modelling framework is not limited to this locally linear assumption; it is only a necessary assumption of one wishes to derive a fully analytical model for $\rho\,(\mathbf{x}', s|\mathbf{x})$. To account for a nonlinear dependence of $\langle u_1\rangle$ on x_2 it would be necessary to numerically compute the variation of $\langle u_1\rangle$ along particle paths (which are themselves unknown, but could be approximated), leading to a semi-analytical closure model.

particles see a nonlinear variation of the mean fluid velocity along their trajectories.

However two things should be noted. First of all, the locally linear assumption is valid within the viscous sublayer, and it is within the viscous sublayer that the large particle concentrations are found for particle dispersion in a turbulent boundary layer. Therefore, in this critical region, the locally linear assumption is valid and therefore does not compromise the model. Secondly, the locally linear assumption will only affect the particle dispersion in the x_1 direction, since in a fully developed turbulent boundary layer a mean velocity for the fluid only exists in this direction. Furthermore, since the fluid and particle statistics are homogeneous in the x_1 direction for a fully developed turbulent boundary layer, errors in the stream wise particle motion introduced by the locally linear assumption will not affect the statistics of the wall-normal particle motion. In accounting for the non-locality of the dispersion process it is the dispersion in the wall-normal direction which is the most important, since only in this direction are the flow statistics inhomogeneous, and only in this direction do the particle-wall collisions influence the system. Therefore, errors introduced by the locally linear assumption may be considered of secondary importance, since it does not affect the dominant contribution to the non-locality of the system.

Using equation (7.13) the particle equation of motion may be written as

$$\frac{d^2}{ds^2}x_i^p - \beta\frac{d}{ds}x_i^p + \beta\gamma(\mathrm{x}_2)\delta_{i1}x_2^p = \beta\delta_{i1}\left[\gamma(\mathrm{x}_2)\mathrm{x}_2 - \langle u_i(\mathrm{x}_2)\rangle\right] - \beta u_i^{p\prime} \tag{7.15}$$

Equation (7.15) may be solved by the use of a Green tensor defined by

$$\frac{d^2}{ds^2}G_{ij} - \beta\frac{d}{ds}G_{ij} + \beta\gamma(\mathrm{x}_2)\delta_{i1}G_{2j} = \delta_{ij}\delta(s - s_1) \tag{7.16}$$

and the solution to equation (7.15) with 'initial' condition $\boldsymbol{x}^p(0) = \mathbf{x}$ is then given by

$$x_i^p(s) = \mathrm{x}_i - G_{ij}(s)v_j^p(0) + \beta\int_s^0 G_{ij}(s - s_1)\left[\gamma(\mathrm{x}_2)\delta_{j1}\mathrm{x}_2 - \delta_{j1}\langle u_j(\mathrm{x}_2)\rangle - u_j'(\boldsymbol{x}^p(s_1), s_1)\right]ds_1 \tag{7.17}$$

The mean of $\rho\,(\mathbf{x}', s|\mathbf{x})$ can now be constructed from equation (7.17)

$$\left\langle x_i^p(s)\right\rangle_{\mathbf{x}} = \mathrm{x}_i - G_{ij}(s)\left\langle v_j^p(0)\right\rangle_{\mathbf{x}} + \beta\int_s^0 G_{ij}(s - s_1)\left[\gamma(\mathrm{x}_2)\delta_{j1}\mathrm{x}_2 - \delta_{j1}\langle u_j(\mathrm{x}_2)\rangle - \left\langle u_j'(\boldsymbol{x}^p(s_1), s_1)\right\rangle_{\mathbf{x}}\right]ds_1 \tag{7.18}$$

The mean particle velocity

$$\left\langle v_j^p(0)\right\rangle_{\mathbf{x}} = \overline{\mathrm{v}}_j(\mathbf{x})$$

is zero in the span-wise direction, and is zero in the wall-normal direction for elastic particle-wall collisions when the system is in a statistically steady state. However the mean stream-wise particle velocity is unknown. It is possible to construct an approximation for $\overline{\mathrm{v}}_1$ through local approximations to the particle stream-wise momentum equation. However this equation would need to be solved numerically and this additional complexity is undesirable. Therefore as an initial approximation take $\overline{\mathrm{v}}_1 \approx \langle u_1 \rangle$. This is of course simply an approximation, and whilst valid for small particles, it becomes less valid for particles of appreciable inertia, especially near the wall since inertial particle, unlike fluid particles, do not have zero stream-wise velocity at the wall (i.e. they are not subject to the 'no-slip' criteria). However, since the fluid and particle statistics are homogeneous in the x_1 direction for a fully developed turbulent boundary layer, errors in the stream wise particle motion introduced by the approximation $\overline{\mathrm{v}}_1 \approx \langle u_1 \rangle$ will not affect the statistics of the wall-normal particle motion. In accounting for the non-locality of the dispersion process it is the dispersion in the wall-normal direction which is the most important, since only in this direction are the flow statistics inhomogeneous, and only in this direction do the particle-wall collisions influence the system. Therefore, errors introduced by the approximation $\overline{\mathrm{v}}_1 \approx \langle u_1 \rangle$ may be considered of secondary importance, since it does not affect the dominant contribution to the non-locality of the system.

The second unknown term in equation (7.18) is

$$\left\langle u_j'(\boldsymbol{x}^p(s_1), s_1)\right\rangle_{\mathbf{x}}$$

which is the mean of the values of the fluctuating fluid velocity sampled at particle positions at time s_1 for particle trajectories which satisfy $\boldsymbol{x}^p(0) = \mathbf{x}$. This strongly non-local term is non zero even for fluid tracers in a turbulent boundary layer (except for $s_1 = s = 0$) due to the inhomogeneity of the flow. It is even more complex for inertial particle dispersion in a turbulent boundary layer since they preferentially sample the turbulent flow field. A possible approximation would be

$$\left\langle u_j'(\boldsymbol{x}^p(s_1), s_1)\right\rangle_{\mathbf{x}} \approx \left\langle u_j'(\boldsymbol{x}^p(0), 0)\right\rangle_{\mathbf{x}} \tag{7.19}$$

However the resulting term $\left\langle u_j'(\boldsymbol{x}^p(0), 0)\right\rangle_{\mathbf{x}}$ is also unknown (for Stokes drag it is of course essentially this term which the dispersion tensors model in the particle momentum equation). The following approximation is therefore made for this unknown term

$$\left\langle u_j'(\boldsymbol{x}^p(0),0)\right\rangle_{\mathbf{x}} \approx \left\langle u_j'(\mathbf{x},0)\right\rangle = 0 \tag{7.20}$$

though it is appreciated that it may be an important term to include. The components of the closure model for $\left\langle \boldsymbol{x}^p(s)\right\rangle_{\mathbf{x}}$ are then given by

$$\left\langle x_1^p(s)\right\rangle_{\mathbf{x}} = \mathrm{x}_1 - \left[\gamma(\mathrm{x}_2)\mathrm{x}_2 - \langle u_1(\mathrm{x}_2)\rangle\right] s - G_{11}(s)\Big(\overline{\mathrm{v}}_1(\mathrm{x}_2) + \gamma(\mathrm{x}_2)\mathrm{x}_2 - \langle u_1(\mathrm{x}_2)\rangle\Big) \tag{7.21}$$

$$\left\langle x_2^p(s)\right\rangle_{\mathbf{x}} = \mathrm{x}_2 \tag{7.22}$$

$$\left\langle x_3^p(s)\right\rangle_{\mathbf{x}} = \mathrm{x}_3 \tag{7.23}$$

From equation (7.17) the second central moment of $\rho\left(\mathbf{x}', s|\mathbf{x}\right)$ can be expressed as

$$\begin{aligned}\left\langle \tilde{x}_i^p(s)\tilde{x}_k^p(s)\right\rangle_{\mathbf{x}} =& G_{ij}(s)\left\langle v_j^{p\prime}(0)v_m^{p\prime}(0)\right\rangle_{\mathbf{x}} G_{km}(s) \\ &+ \beta G_{ij}(s)\int_s^0 G_{km}(s-s_1)\left\langle v_j^{p\prime}(0)u_m'(\boldsymbol{x}^p(s_1),s_1)\right\rangle_{\mathbf{x}} ds_1 \\ &+ \beta G_{km}(s)\int_s^0 G_{ij}(s-s_1)\left\langle u_j'(\boldsymbol{x}^p(s_1),s_1)v_m^{p\prime}(0)\right\rangle_{\mathbf{x}} ds_1 \\ &+ \beta^2\int_s^0\int_s^0 G_{ij}(s-s_1)\left\langle u_j'(\boldsymbol{x}^p(s_1),s_1)u_m'(\boldsymbol{x}^p(s_2),s_2)\right\rangle_{\mathbf{x}} G_{km}(s-s_2)ds_1ds_2\end{aligned} \tag{7.24}$$

where

$$\tilde{\boldsymbol{x}}^p(s) = \boldsymbol{x}^p(s) - \left\langle \boldsymbol{x}^p(s)\right\rangle_{\mathbf{x}}$$

with $\left\langle \boldsymbol{x}^p(s)\right\rangle_{\mathbf{x}}$ given by equations (7.21) to (7.23). The first unknown term in equation (7.24) is

$$\left\langle v_j^{p\prime}(0)v_m^{p\prime}(0)\right\rangle_{\mathbf{x}} = \overline{\mathrm{c}_j\mathrm{c}_m}(\mathbf{x})$$

which is the particle Reynolds stress tensor. This is approximated using a local approximation

$$\overline{\mathrm{c}_j\mathrm{c}_m}(\mathbf{x}) = \frac{1}{2\beta}\left(\overline{\mu}_{jm}(\mathbf{x}) + \overline{\mu}_{mj}(\mathbf{x})\right) \tag{7.25}$$

where for a simple linear shear flow with

$$\frac{\partial}{\partial \mathrm{x}_j}\langle u_i\rangle = \gamma\delta_{i1}\delta_{j2} \tag{7.26}$$

the local approximation to $\overline{\boldsymbol{\mu}}$ is given by [127]

$$\overline{\mu}_{jm}(\mathbf{x}) = \frac{\beta^2\tau^{Lp}}{1+\beta\tau^{Lp}}\left(\langle u_j'u_m'\rangle + \delta_{j1}\frac{\beta\gamma\tau^{Lp}}{1+\beta\tau^{Lp}}\langle u_2'u_m'\rangle\right) \tag{7.27}$$

where $\langle \boldsymbol{u}'\boldsymbol{u}'\rangle$ is the fluid velocity Reynolds stress tensor at $\mathbf{x}$ and $\tau^{Lp}(\mathbf{x},\tau_p)$ is the timescale of the fluid velocity correlations seen by inertial particles of response time τ_p which arrive at $\mathbf{x}$ (the specification of this timescale will be considered later).

A local approximation is invoked for the particle-fluid autocovariance in equation (7.24)

$$\left\langle v_j^{p\prime}(0)u_m'(\boldsymbol{x}^p(s_1),s_1)\right\rangle_{\mathbf{x}} \approx \left\langle v_j^{p\prime}(0)u_m'(\boldsymbol{x}^p(0),0)\right\rangle_{\mathbf{x}}\Psi(s_1,\tau^{Lp}) \tag{7.28}$$

where $\Psi(s_1,\tau^{Lp})$ is the particle-fluid velocity autocorrelation with timescale τ^{Lp} (strictly speaking, this timescale should differ from the the fluid velocity timescale seen by the particles; here they have been approximated as being equal). The form of the model chosen for Ψ is a matter of choice (i.e. simple exponential decay, bi-exponential etc) however it should be noted that the form of Ψ used to derive $\overline{\boldsymbol{\mu}}$ in equation (7.27) was

$$\Psi(s,\tau^{Lp}) = \exp\left[\frac{s}{\tau^{Lp}}\right], \qquad s\leq 0 \tag{7.29}$$

Should a different form of Ψ be chosen, then for consistency, the local solution for $\overline{\boldsymbol{\mu}}$ should be re-derived. The particle-fluid velocity correlation tensor in equation (7.28) may be approximated by [127]

$$\left\langle v_j^{p\prime}(0)u_m'(\boldsymbol{x}^p(0),0)\right\rangle_{\mathbf{x}} = \frac{\overline{\mu}_{jn}(\mathbf{x})}{\beta}\left(\delta_{nm} - \tau^{Lp}\frac{\partial\overline{\mathrm{v}}_n}{\partial \mathrm{x}_m}\right) \tag{7.30}$$

with $\overline{\boldsymbol{\mu}}$ given by equation (7.27). Finally in equation (7.24) the fluid velocity autocovariance along the particle trajectory is approximated by

$$\left\langle u_j'(\boldsymbol{x}^p(s_1),s_1)u_m'(\boldsymbol{x}^p(s_2),s_2)\right\rangle_{\mathbf{x}} \approx \left\langle u_j'(\boldsymbol{x}^p(0),0)u_m'(\boldsymbol{x}^p(0),0)\right\rangle_{\mathbf{x}} \Psi(s_1-s_2,\tau^{Lp}) \approx \langle u_j'u_m'\rangle \Psi(s_1-s_2,\tau^{Lp}) \tag{7.31}$$

In equations (7.27), (7.29) and (7.31) an approximation for $\tau^{Lp}(\mathbf{x},\tau_p)$ is required. This timescale is the same timescale that would be used to construct local approximations to the dispersion tensors and is unknown. One strategy would be

$$\tau^{Lp}(\mathbf{x},\tau_p) \approx 0 \tag{7.32}$$

which is equivalent to assuming that the fluctuating fluid velocity is constant along the particle trajectory. In [108] this approximation was used to develop a model for timescales of the turbulence seen by particles for particle dispersion in a homogeneous isotropic turbulent flow field, and comparisons with equivalent PT simulations showed that this level of approximation was adequate. However the fluid velocity along a particle trajectory in a turbulent flow field is far from constant and more appropriate approximations for τ^{Lp} than that given in equation (7.32) may be specified. Two further approximations are possible. The simplest would be

$$\tau^{Lp}(\mathbf{x},\tau_p) \approx \tau_L(\mathbf{x}) \tag{7.33}$$

that is, to approximate τ^{Lp} by the fluid velocity Lagrangian integral timescale τ_L. This is more appropriate than equation (7.32) since it captures the fact that the particles see a fluctuating flow field which decorrelates along its trajectory. However, it does not take into account the effect of the particle inertia which dictates that in the absence of any body forces acting on the particle τ^{Lp} varies between the fluid Lagrangian and Eulerian (one-point) integral timescales, being equal to the fluid Lagrangian integral timescale τ_L for $\tau_p \to 0$ and equal to the Eulerian integral timescale τ_E for $\tau_p \to \infty$. A more appropriate approximation for τ_L, and the one which is used in the closure model, is to use the function given by Wang & Stock [107]

$$\tau^{Lp} \approx \tau_E - \frac{\tau_E - \tau_L}{(1+St_E)^{0.4(1+0.01St)}} \tag{7.34}$$

where

$$St_E = \frac{\tau_p}{\tau_E} \tag{7.35}$$

Equation (7.34) was obtained by fitting a curve to data obtained for τ^{Lp} form particle dispersion in a homogeneous, isotropic KS flow field with

$$\frac{\tau_L}{\tau_E} = 1 - 0.644 \tag{7.36}$$

Using equation (7.34) to approximate τ^{Lp} is more appropriate than either equation (7.32) or (7.33) since it captures both the fact that the fluid velocity along the trajectory varies and the dependence on the particle Stokes number of the decorrellation of the fluid velocity along the particle trajectory. Using the function in equation (7.34) for τ^{Lp} is however still an approximation since τ^{Lp} is supposed to describe the timescale of the fluid velocity along the particle trajectory in an inhomogeneous, anisotropic flow field, whereas equation (7.34) is for homogeneous, isotropic turbulence. Nevertheless, even with τ^{Lp} approximated using equation (7.34) (or even (7.32) or (7.33)) which is only strictly appropriate for homogeneous, isotropic turbulence, this does *not* imply that the timescale that could be recovered from the closure model for

$$\Big\langle \boldsymbol{R}(\boldsymbol{x}^p(s), s; \mathbf{x}, 0) \Big\rangle_{\mathbf{x}}$$

is also homogeneous and isotropic. Regardless of the approximation for τ^{Lp} in the closure model, the effect of the turbulence inhomogeneity and anisotropy will still, to some degree, be captured by the closure model (the effect of the quality of the approximation for τ^{Lp} on the performance of the new closure model is assessed in section 7.4.5).

With all the unknown terms in equation (7.24) now specified, this equation can be evaluated analytically as shown in appendix A. Therefore an analytic closure model for $\rho(\mathbf{x}', s|\mathbf{x})$ has been constructed, and it may be used to construct new closures for the dispersion tensors, the performance of which shall now be tested.

7.4 Testing the Closure Model

Ideally, to test the closure model it is necessary to compute the particle dispersion tensors in a DNS PT simulation (or experiment) and compare this data against the closure model predictions. However, computing the dispersion tensors in a DNS of turbulent channel flow would be extremely computationally expensive, and in addition, the data for $\boldsymbol{R}$ required for the closure model would have to be obtained numerically

and curves fitted to the data. Therefore it is sensible to first test the closure model in a simpler test case in which the computation of the dispersion tensors via PT is simpler, and in which $\boldsymbol{R}$ can be specified analytically. This removes any source of error from curve fitting data for $\boldsymbol{R}$ (obtained experimentally or by DNS), meaning that the quality of the closure model predictions will depend solely upon the accuracy of the closure model for $\rho(\mathbf{x}', s|\mathbf{x})$.

Therefore a new flow field model was developed, based on KS, which produces an inhomogeneous, anisotropic flow field. The flow field provides a simplified system which resembles qualitatively a turbulent boundary layer (to an extent) in which the underlying inhomogeneity and anisotropy of the fluid flow field makes the particle dispersion process intrinsically non-local, and therefore serves as a meaningful initial test case for testing the new closure model for the dispersion tensors.

7.4.1 Inhomogeneous, anisotropic KS flow field

Kinematic Simulations (KS) (see chapter 2) provide a way to to construct turbulent-like flow fields through the linear superposition of many random Fourier modes and have been used extensively in the literature (e.g. [31, 32, 34–38]). Whilst possessing some shortcomings in representing real turbulent fields (e.g. KS does not account for the sweeping of the small scales by the large energy containing scales) KS is nevertheless able to represent sufficient features of a turbulent flow to make it a useful tool, especially for studying particle dispersion (e.g. [33]). However nearly all KS models available in the literature are constrained to homogeneous, isotropic flow fields and in the context of testing the closure model presented in this chapter a KS model for a turbulent boundary layer is required, which is both strongly inhomogeneous and anisotropic.

Recently in [38] a new KS model for turbulent channel flow was presented. However this model does not appear to yield simple analytic expressions for the two-point, two-time velocity correlation tensor, and this is required for the present test case. Therefore a new KS model was developed which produces a flow field which is both strongly inhomogeneous and anisotropic. The challenge was to construct a flow field which possessed the following features; (i) was inhomogeneous only in the wall-normal direction, (ii) was anisotropic, (iii) was statistically stationary and (iv) was incompressible. In order to produce such a flow field, begin by defining a 2D fluctuating flow field by

$$u_i'(\mathbf{x}, t) = \left(\frac{\partial \psi}{\partial \mathrm{x}_2}, -\frac{\partial \psi}{\partial \mathrm{x}_1} \right) \tag{7.37}$$

which produces a fluctuating fluid velocity field $\boldsymbol{u}'(\mathbf{x}, t)$ which is incompressible. The

flow field is then given by $\boldsymbol{u}(\mathbf{x},t) = \langle \boldsymbol{u}(\mathbf{x},t)\rangle + \boldsymbol{u}'(\mathbf{x},t)$. In order to produce a flow field which is inhomogeneous only in the x_2 direction and has a zero mean wall-normal velocity take

$$\langle u_i(\mathbf{x},t)\rangle = (\langle u_1(\mathrm{x}_2,t)\rangle, 0) \tag{7.38}$$

which again yields a field $\boldsymbol{u}(\mathbf{x},t)$ which is incompressible. The stream function ψ is taken in the form

$$\psi(\mathbf{x},t) = \frac{S_f}{\sqrt{N}} \sum_{n=-N}^{+N} \mathrm{z}_n(\mathrm{x}_2)(\mathrm{k}_{1n} + \mathrm{k}_{2n}) \exp[i(\mathbf{k}_n \cdot \mathbf{x} + \omega_n t)] \tag{7.39}$$

where S_f is a scaling factor (used to scale the values of the Reynolds stresses, specified later), and

$$\mathrm{z}_n(\mathrm{x}_2) = \frac{A(\mathrm{x}_2)}{2}(\zeta_n - i\xi_n) \tag{7.40}$$

where $A(\mathrm{x}_2)$ is a 'profiling function', ζ_n and ξ_n are stochastic variables, $\mathbf{k}_n$ are the wave numbers of the modes in the flow field and ω_n are the frequencies associated with the modes. ζ_n, ξ_n and ω_n are generated from zero mean Gaussian distributions. The way in which the wave numbers $\mathbf{k}_n$ are generated determines the resulting energy spectrum. The simplest way is to generate them from a zero mean Gaussian distribution, and this leads to a Kraichnan energy spectrum containing no inertial subrange [108]. More sophisticated methods are available, one of which captures the sweeping of the small scales by the large energy containing scales, and the other which allows an inertial subrange to be included in the KS flow field, usually with a Von Karman energy spectrum [31]. With a view to constructing relatively simple analytical expressions for the Eulerian two-point, two-time correlation tensor for the velocity field, the wave numbers were generated using a zero mean Gaussian distribution with isotropic covariance.

The 2D (fluctuating) flow field is therefore given by

$$u_1'(\mathbf{x},t) = \frac{S_f}{\sqrt{N}} \sum_{n=-N}^{+N} \left(\frac{d\mathrm{z}_n}{d\mathrm{x}_2}(\mathrm{k}_{1n} + \mathrm{k}_{2n}) + i\mathrm{z}_n(\mathrm{k}_{1n} + \mathrm{k}_{2n})\mathrm{k}_{2n} \right) \exp[i(\mathbf{k}_n \cdot \mathbf{x} + \omega_n t)] \tag{7.41}$$

$$u_2'(\mathbf{x},t) = -\frac{S_f}{\sqrt{N}} \sum_{n=-N}^{+N} i\mathrm{z}_n(\mathrm{k}_{1n} + \mathrm{k}_{2n})\mathrm{k}_{1n} \exp[i(\mathbf{k}_n \cdot \mathbf{x} + \omega_n t)] \tag{7.42}$$

Provided $A(0) = 0$ and $A'(0) = 0$, the fluid velocity field satisfies the no slip and im-

permeability conditions at the wall (where $\mathrm{x}_2 = 0$). To ensure ψ is real it is required that $\zeta_{-n} = -\zeta_n$, $\xi_{-n} = \xi_n$, $\mathbf{k}_{-n} = -\mathbf{k}_n$ and $\omega_{-n} = -\omega_n$ (in which case $\zeta_0 = 0$, $\mathbf{k}_0 = (0,0)$ and $\omega_0 = 0$). With these definitions

$$\begin{aligned}\langle \mathrm{z}_n \mathrm{z}_m \rangle &= \frac{A^2(\mathrm{x}_2)}{4}\left[\langle \zeta_n \zeta_m \rangle - \langle \xi_n \xi_m \rangle\right] \\ &= -\frac{A^2(\mathrm{x}_2)}{2}\sigma_z^2 \qquad (\text{for } m = -n;\ \langle \mathrm{z}_n \mathrm{z}_m \rangle = 0 \text{ if } m \neq -n)\end{aligned} \tag{7.43}$$

and

$$\langle \mathrm{k}_{in} \mathrm{k}_{jm} \rangle = \begin{cases} \sigma_k^2 & (\text{for } m = n,\ i = j) \\ -\sigma_k^2 & (\text{for } m = -n,\ i = j) \\ 0 & (\text{for } m \neq n, m \neq -n, \text{ or } i \neq j) \end{cases} \tag{7.44}$$

where σ_z^2 is the variance of ζ and ξ, and σ_k^2 is the variance of $\mathbf{k}$.

Mean velocity

With $\mathbf{k}_n$ and z_n mutually independent, since $\langle \zeta_n \rangle = \langle \xi_n \rangle = 0$, $\langle \mathrm{z}_n(\mathrm{x}, \mathrm{x}_2) \rangle = 0$ (and also $\langle \mathrm{z}'_n(\mathrm{x}, \mathrm{x}_2) \rangle = 0$) the mean fluid velocity vector is (in light of equation (7.38))

$$\langle u_i(\mathbf{x}, t) \rangle = \langle \langle u_i(\mathbf{x}, t) \rangle + u'_i(\mathbf{x}, t) \rangle = (\langle u_1(\mathrm{x}_2, t) \rangle, 0) \tag{7.45}$$

Reynolds Stress

The fluid Reynolds stresses are

$$\langle u'_1 u'_1 \rangle = 2S_f^2 \sigma_z^2 \sigma_k^2 \left[(A'(\mathrm{x}_2))^2 + 2(A(\mathrm{x}_2))^2 \sigma_k^2\right] \tag{7.46}$$

$$\langle u'_1 u'_2 \rangle = \langle u'_2 u'_1 \rangle = -2S_f^2 \sigma_z^2 \sigma_k^4 (A(\mathrm{x}_2))^2 \tag{7.47}$$

$$\langle u'_2 u'_2 \rangle = 4S_f^2 \sigma_z^2 \sigma_k^4 (A(\mathrm{x}_2))^2 \tag{7.48}$$

The scaling parameter S_f is then chosen so as to appropriately scale the values of the Reynolds stresses (i.e. so that the Reynolds stress values are comparable with that in a channel flow, for example).

Eulerian two-point, two-time velocity correlations

The two-point, two-time velocity correlation tensor for this KS field is given by

$$\Big\langle u_i'(\mathbf{x}',s)u_j'(\mathbf{x},0)\Big\rangle = \Big\langle u_i'(\mathrm{r}_1,\mathrm{x}_2',s)u_j'(0,\mathrm{x}_2,0)\Big\rangle = F_{ij}\exp\left[-\frac{1}{2}\sigma_k^2(\mathrm{r}_1^2+\mathrm{r}_2^2)\right]\exp\left[-\frac{1}{2}\sigma_w^2 s^2\right] \tag{7.49}$$

where $\mathbf{r} = \mathbf{x}' - \mathbf{x}$ and

$$\begin{aligned}
F_{11} =& S_f^2 A'(\mathrm{x}_2')A'(\mathrm{x}_2)\sigma_z^2\sigma_k^2\left[2(1-\mathrm{r}_1\mathrm{r}_2\sigma_k^2)-(\mathrm{r}_1^2+\mathrm{r}_2^2)\sigma_k^2)\right] \\
&- S_f^2 A'(\mathrm{x}_2')A(\mathrm{x}_2)\sigma_z^2\sigma_k^4\left[\mathrm{r}_2(1-\mathrm{r}_1^2\sigma_k^2)+2\mathrm{r}_1(1-\mathrm{r}_2^2\sigma_k^2)+\mathrm{r}_2(3-\mathrm{r}_2^2\sigma_k^2)\right] \\
&+ S_f^2 A(\mathrm{x}_2')A'(\mathrm{x}_2)\sigma_z^2\sigma_k^4\left[\mathrm{r}_2(1-\mathrm{r}_1^2\sigma_k^2)+2\mathrm{r}_1(1-\mathrm{r}_2^2\sigma_k^2)+\mathrm{r}_2(3-\mathrm{r}_2^2\sigma_k^2)\right] \\
&+ S_f^2 A(\mathrm{x}_2')A(\mathrm{x}_2)\sigma_z^2\sigma_k^4\left[3+(1-\mathrm{r}_1^2\sigma_k^2)(1-\mathrm{r}_2^2\sigma_k^2)-2\mathrm{r}_1\mathrm{r}_2\sigma_k^2(3-\mathrm{r}_2^2\sigma_k^2)-\mathrm{r}_2^2\sigma_k^2(6-\mathrm{r}_2^2\sigma_k^2)\right] \\
F_{12} =& S_f^2 A'(\mathrm{x}_2')A(\mathrm{x}_2)\sigma_z^2\sigma_k^4\left[\mathrm{r}_1(3-\mathrm{r}_1^2\sigma_k^2)+2\mathrm{r}_2(1-\mathrm{r}_1^2\sigma_k^2)+\mathrm{r}_1(1-\mathrm{r}_2^2\sigma_k^2)\right] \\
&+ S_f^2 A(\mathrm{x}_2')A(\mathrm{x}_2)\sigma_z^2\sigma_k^4\left[\mathrm{r}_1\mathrm{r}_2\sigma_k^2(6-(\mathrm{r}_1^2+\mathrm{r}_2^2)\sigma_k^2)-2(1-\mathrm{r}_1^2\sigma_k^2)(1-\mathrm{r}_2^2\sigma_k^2)\right] \\
F_{21} =& -S_f^2 A'(\mathrm{x}_2)A(\mathrm{x}_2')\sigma_z^2\sigma_k^4\left[\mathrm{r}_1(3-\mathrm{r}_1^2\sigma_k^2)+2\mathrm{r}_2(1-\mathrm{r}_1^2\sigma_k^2)+\mathrm{r}_1(1-\mathrm{r}_2^2\sigma_k^2)\right] \\
&+ S_f^2 A(\mathrm{x}_2')A(\mathrm{x}_2)\sigma_z^2\sigma_k^4\left[\mathrm{r}_1\mathrm{r}_2\sigma_k^2(6-(\mathrm{r}_1^2+\mathrm{r}_2^2)\sigma_k^2)-2(1-\mathrm{r}_1^2\sigma_k^2)(1-\mathrm{r}_2^2\sigma_k^2)\right] \\
F_{22} =& S_f^2 A(\mathrm{x}_2')A(\mathrm{x}_2)\sigma_z^2\sigma_k^4\left[3+(1-\mathrm{r}_1^2\sigma_k^2)(1-\mathrm{r}_2^2\sigma_k^2)-2\mathrm{r}_1\mathrm{r}_2\sigma_k^2(3-\mathrm{r}_1^2\sigma_k^2)-\mathrm{r}_1^2\sigma_k^2(6-\mathrm{r}_1^2\sigma_k^2)\right]
\end{aligned} \tag{7.50}$$

Input Parameters

The input parameters for the flow field are $A(\mathrm{x}_2)$, S_f , σ_z, σ_k and σ_w . In the present work the choice of these input parameters is not too critical since the objective is to test the performance of the new closure model for the particle dispersion tensors and compare the predictions to equivalent particle tracking data computed in this KS flow field. Nevertheless, it is desirable that the flow field should be to some extent qualitatively representative of a turbulent boundary layer. To this end the following were chosen

$$A(\mathrm{x}_2) = \left(1 - \exp\left(-\left(\mathrm{K}_1\mathrm{x}_2\right)^2\right)\right)\exp\left(-\mathrm{K}_2\mathrm{x}_2\right) \tag{7.51}$$

$$\mathrm{K}_1 = 0.04 \tag{7.52}$$

$$\mathrm{K}_2 = 0.003 \tag{7.53}$$

$$\sigma_z = 1 \tag{7.54}$$

$$\sigma_k = 0.1 \tag{7.55}$$

$$\sigma_w = 0.1 \tag{7.56}$$

$$S_f = \sqrt{\frac{1.5}{4\sigma_z^2\sigma_k^4}} \tag{7.57}$$

This choice of parameters produces fluid Reynolds stresses as shown in figure 7.2

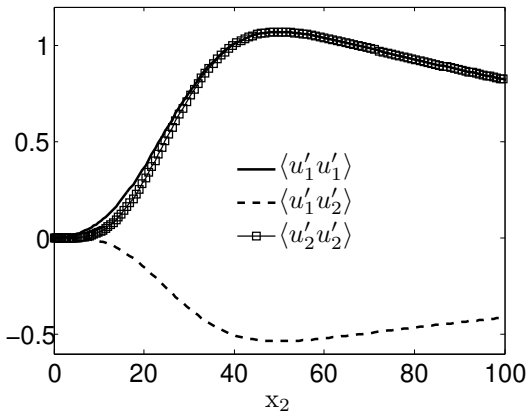

Figure 7.2: Reynolds stresses produced by the KS flow field with parameters specified by equations (7.51) to (7.57).

Figure 7.2 shows that this choice of the parameters produces a wall-normal Reynolds stress component $\langle u_2' u_2' \rangle$ which qualitatively and quantitatively resembles that found in a turbulent boundary layer (see figure (6.2)) as does the negatively valued shear stress $\langle u_1' u_2' \rangle$. With $\sigma_w = 0.1$ the Eulerian integral timescale is given by

$$\tau_E = \sqrt{\frac{\pi}{2}}\frac{1}{\sigma_w} \approx 12 \tag{7.58}$$

This value falls within the range of the stream-wise and wall-normal Eulerian integral timescales found in DNS of turbulent channel flow (see [43], in which it can also be seen that the Eulerian integral timescales in a turbulent boundary layer are only weakly inhomogeneous). In the closure model the fluid velocity Lagrangian integral timescale is

required as input data. A homogeneous value for the fluid velocity Lagrangian timescale was computed by tracking fluid particles in this KS flow field with the homogeneous setting $A(\mathrm{x}_2) = 1$, and its ratio to the Eulerian integral timescale was computed and found to be

$$\frac{\tau_L}{\tau_E} = 0.382 \tag{7.59}$$

which is close the the ratio in the Wang & Stock simulations (see equation (7.36)). Therefore equation (7.36) provides an appropriate timescale with which to construct LHA dispersion tensors which can be compared against both the PT data and the new closure model predictions to assess the performance of the new closure model compared to a LHA (but using the ratio $\tau_L/\tau_E = 0.382$ in equation (7.36) instead of the Wang & Stock value of $\tau_L/\tau_E = 0.356$ to be precise for this flow field).

Making the flow field seen by suspended particles periodic

For turbulent channel flows, the flow field in the homogeneous stream-wise direction is usually made periodic over a length L. It is not clear how the Eulerian flow field defined in equations (7.41) and (7.42) could be made strictly periodic in the homogeneous x_1 direction. However the following method can be used when using this KS flow field for PT simulations. Define a 'box' in which the particles are dispersing to have a 'stream-wise' domain $0 \leq \mathrm{x}_1 \leq L$. Then define a 'simulated particle stream-wise position' (SPSP) to be

$$\chi^p(t) = x_1^p(t) + N_L L \tag{7.60}$$

where $x_1^p(t)$ is the actual stream-wise particle position, and N_L is a number to record the number of times the particle has 'looped through' the domain. For example, if the particle position is in the region $L < x_1^p(t) < 2L$ then $N_L = -1$ etc. Then the particle statistics are recorded (i.e. the number density etc) based on $\chi^p(t)$, not $x_1^p(t)$. However, the fluid velocity at the particle position is evaluated using the *actual* particle position, *not* the SPSP, i.e. using $\boldsymbol{u}(x_1^p(t), x_2^p(t), t)$ *not* $\boldsymbol{u}(\chi^p(t), x_2^p(t), t)$. This makes the flow field seen by particles periodic over the length L and is equivalent to tracking particles through a box which is periodic over the length L in the x_1 direction in which particles would be periodically re-introduced into the box once they have reached the edges of the domain.

Note that the periodicity does not affect the correlations which will be computed in

the flow field against which the closure model will be tested, namely the computation of

$$\Big\langle R_{ji}(\boldsymbol{x}^p(s), s; \mathbf{x}, 0)\Big\rangle_{\mathbf{x}}$$

and

$$\Big\langle \frac{\partial}{\partial \mathrm{x}_k} R_{ji}(\boldsymbol{x}^p(s), s; \mathbf{x}, 0)\Big\rangle_{\mathbf{x}}$$

since these will be recorded along the actual particle trajectories not the periodic trajectories (i.e. using $x_1^p(t), x_2^p(t)$ *not* $\chi^p(t), x_2^p(t)$).

7.4.2 Particle Tracking

Particles subject to the equation of motion

$$\frac{d^2}{dt^2} x_i^p(t) = \frac{d}{dt} v_i^p(t) = \beta \left(u_i(\boldsymbol{x}^p(t), t) - v_i^p(t)\right) \tag{7.61}$$

were tracked through the flow field described in section 7.4.1 but with mean fluid velocity $\langle \boldsymbol{u} \rangle = \mathbf{0}$. 10^4 particles were tracked in the domain $0 \leq \mathrm{x}_2 \leq 200$, $0 \leq \mathrm{x}_1 \leq L = 100$ ($L = 100$ is sufficiently large for the periodic boundary condition effects to be considered negligible, $L = 100$ being several times larger than the integral length scale in the x_1 direction). The particles collided elastically with the wall when $x_2^p(t) = \mathrm{x}_2^{min}$ with

$$\mathrm{x}_2^{min} = \sqrt{\frac{9\tau_p \rho^f}{2\rho^p}} \tag{7.62}$$

with $\rho^f/\rho^p = 1/770$ [85]. The particle equation of motion was solved using a second-order Adams-Bashforth scheme with a time step $\delta t = 0.05$ (wall units). This time step ensured that $\tau_p/\delta t \geq 80$ for all particle sizes considered, which was considered sufficiently small to ensure numerical stability and accuracy (e.g. [9]). The particles were tracked until their statistics had reached a statistically steady state (determined in this context by monitoring the time evolution of $\rho(\mathbf{x}, t)$ and $\overline{\mathbf{v}}(\mathbf{x}, t)$ as recorded in the PT simulation) and then the necessary statistics were recorded. Since the KS flow field is only inhomogeneous in the x_2 direction the required statistics are ($r_1^p(s) = x_1^p(s) - \mathrm{x}_1$)

$$\Big\langle R_{ji}(r_1^p(s), x_2^p(s), s; 0, \mathrm{x}_2, 0)\Big\rangle_{\mathrm{x}_2}$$

and

$$\Big\langle \frac{\partial}{\partial \mathrm{x}_k} R_{ji}(r_1^p(s), x_2^p(s), s; 0, \mathrm{x}_2, 0)\Big\rangle_{\mathrm{x}_2}$$

where for Stokes drag

$$R_{ji}(\mathrm{r}_1, \mathrm{x}_2', s; 0, \mathrm{x}_2) = \beta^2 \Big\langle u_j'(\mathrm{r}_1, \mathrm{x}_2', s) u_i'(0, \mathrm{x}_2, 0) \Big\rangle \tag{7.63}$$

(the two-point, two-time velocity correlation tensor for this KS field is given by equation (7.49)) and these statistics were computed in the PT simulation from which the dispersion tensors could be evaluated using equations (6.1) to (6.3), with the appropriate Green tensor given by

$$G_{ij}(s) = \delta_{ij}\tau_p(1 - \exp[\beta s]), \qquad s \leq 0 \tag{7.64}$$

$$\dot{G}_{ij} = \delta_{ij} \exp[\beta s], \qquad s \leq 0 \tag{7.65}$$

The dispersion tensors computed from this particle tracking simulation will be denoted by the superscript 'PT' in the results section.

7.4.3 Closure Model Prediction

The closure model described in section 7 is used to construct a model for the statistics

$$\Big\langle R_{ji}(\boldsymbol{x}^p(s), s; \mathbf{x}, 0) \Big\rangle_{\mathbf{x}}$$

and

$$\Big\langle \frac{\partial}{\partial \mathrm{x}_k} R_{ji}(\boldsymbol{x}^p(s), s; \mathbf{x}, 0) \Big\rangle_{\mathbf{x}}$$

Recalling that the KS flow field is inhomogeneous in only the x_2 direction these statistics can be expressed as

$$\Big\langle R_{ji}(r_1^p(s), x_2^p(s), s; 0, \mathrm{x}_2, 0) \Big\rangle_{\mathrm{x}_2}$$

and

$$\Big\langle \frac{\partial}{\partial \mathrm{x}_k} R_{ji}(r_1^p(s), x_2^p(s), s; 0, \mathrm{x}_2, 0) \Big\rangle_{\mathrm{x}_2}$$

where $r_1^p(s) = x_1^p(s) - \mathrm{x}_1$. Therefore the required form of the spatial distribution is $(\mathrm{r}_1 = \mathrm{x}_1' - \mathrm{x}_1)$

$$\rho(\mathrm{r}_1, \mathrm{x}_2', s|\mathrm{x}_2)$$

Note that, since the flow field has zero mean velocity

$$\begin{aligned} r_1^p(s) &= x_1^p(s) - \mathrm{x}_1 \\ &= \tilde{x}_1^p(s) + \left\langle x_1^p(s) \right\rangle_{\mathrm{x}_2} - \mathrm{x}_1 \\ &= \tilde{x}_1^p(s) \end{aligned} \tag{7.66}$$

and therefore

$$\left\langle r_1^p(s) \right\rangle_{\mathrm{x}_2} = 0 \tag{7.67}$$

For the KS flow field outlined in section 7.4.1 the correct form of the autocorrelation is

$$\Psi(s, \sigma_{Lp}) = \exp\left[-\frac{1}{2}\sigma_{Lp}^2 s^2\right] \tag{7.68}$$

where

$$\sigma_{Lp} = \sqrt{\frac{\pi}{2}}\frac{1}{\tau^{Lp}} \tag{7.69}$$

with τ^{Lp} approximated using equation (7.34). For an autocorrelation of the form given in equation (7.68) (and with zero mean fluid velocity) the local form of $\overline{\boldsymbol{\mu}}$ required in the closure model for $\rho(\mathrm{r}_1, \mathrm{x}_2', s|\mathrm{x}_2)$ is given by

$$\overline{\mu}_{ij}^L(\mathrm{x}_2) = \beta^2 \left\langle u_i' u_j' \right\rangle \sqrt{\frac{\pi}{2\sigma_{Lp}^2}} \exp\left[\frac{\beta^2}{2\sigma_{Lp}^2}\right] \left(1 - \mathrm{erf}\left[\frac{\beta}{\sqrt{2}\sigma_{Lp}}\right]\right) \tag{7.70}$$

For later use, note that the corresponding local approximation for $\overline{\boldsymbol{\lambda}}$ is

$$\overline{\lambda}_{ij}^L(\mathrm{x}_2) = \beta \left\langle u_i' u_j' \right\rangle \sqrt{\frac{\pi}{2\sigma_{Lp}^2}} \left(1 - \exp\left[\frac{\beta^2}{2\sigma_{Lp}^2}\right] \left(1 - \mathrm{erf}\left[\frac{\beta}{\sqrt{2}\sigma_{Lp}}\right]\right)\right) \tag{7.71}$$

which have been derived using the appropriate Green tensor for this flow field (equation (7.65)). The closure model for $\rho(\mathrm{r}_1, \mathrm{x}_2', s|\mathrm{x}_2)$ can now be constructed for this KS flow field. The resulting form of the functions describing the closure model for $\rho(\mathrm{r}_1, \mathrm{x}_2', s|\mathrm{x}_2)$ are given in appendix A. The dispersion tensor predictions constructed using the new closure model will be denoted by the superscript 'CM' in the results section.

The only remaining issue is with regard to the integrals that must be evaluated (see

section 7.1), which in their 2D form are

$$\begin{aligned}\Big\langle R_{ji}(r_1^p, x_2^p(s), s; 0, \mathrm{x}_2, 0)\Big\rangle_{\mathrm{x}_2} &= \int_{+\mathrm{x}_2^{min}}^{+\mathrm{x}_2^{max}} \int_{\mathrm{r}_1^{min}}^{\mathrm{r}_1^{max}} R_{ji}(\mathrm{r}_1, \mathrm{x}_2', s; 0, \mathrm{x}_2, 0)\rho\left(\mathrm{r}_1, \mathrm{x}_2', s|\mathrm{x}_2\right) d\mathrm{r}_1 d\mathrm{x}_2' \\ &+ \int_{-\mathrm{x}_2^{max}}^{-\mathrm{x}_2^{min}} \int_{\mathrm{r}_1^{min}}^{\mathrm{r}_1^{max}} R_{ji}(\mathrm{r}_1, \mathrm{x}_2' + 2\mathrm{x}_2', s; 0, \mathrm{x}_2, 0)\rho\left(\mathrm{r}_1, 2\mathrm{x}_2^{min} + \mathrm{x}_2', s|\mathrm{x}_2\right) d\mathrm{r}_1 d\mathrm{x}_2'\end{aligned} \tag{7.72}$$

$$\begin{aligned}\Big\langle \frac{\partial}{\partial \mathrm{x}_k} R_{ji}(r_1^p, x_2^p(s), s; 0, \mathrm{x}_2, 0)\Big\rangle_{\mathrm{x}_2} &= \int_{+\mathrm{x}_2^{min}}^{+\mathrm{x}_2^{max}} \int_{\mathrm{r}_1^{min}}^{\mathrm{r}_1^{max}} \left[\frac{\partial}{\partial \mathrm{x}_k} R_{ji}(\mathrm{r}_1, \mathrm{x}_2', s; 0, \mathrm{x}_2, 0)\right] \rho\left(\mathrm{r}_1, \mathrm{x}_2', s|\mathrm{x}_2\right) d\mathrm{r}_1 d\mathrm{x}_2' \\ &+ \int_{-\mathrm{x}_2^{max}}^{-\mathrm{x}_2^{min}} \int_{\mathrm{r}_1^{min}}^{\mathrm{r}_1^{max}} \left[\frac{\partial}{\partial \mathrm{x}_k} R_{ji}(\mathrm{r}_1, \mathrm{x}_2' + 2\mathrm{x}_2', s; 0, \mathrm{x}_2, 0)\right] \rho\left(\mathrm{r}_1, 2\mathrm{x}_2^{min} + \mathrm{x}_2', s|\mathrm{x}_2\right) d\mathrm{r}_1 d\mathrm{x}_2'\end{aligned} \tag{7.73}$$

For this KS flow field the integrals in equation (7.72) and (7.73) may be evaluated analytically (albeit a rather lengthy process). However in general, especially if $\boldsymbol{R}$ was specified by non-trivial curve fits to DNS data, analytic integration would be unfeasible. Nevertheless, the integration may be performed easily using a simple numerical technique. In appendix B a brief note on the numerical computation of these integrals is given.

It is worth noting that the numerical evaluation of equations (7.72) and (7.73) is not, computationally, very demanding. Each of the results presented in the next section for the closure model predictions of the dispersion tensors took less than 50 seconds to produce for each particle size considered. Therefore it is clear that having to numerically integrate equations (7.72) and (7.73) in order to produce the closure models for the dispersion tensors does not make the new closure model cumbersome.

Of course it would be desirable to produce analytic expressions for the dispersion tensors using the new closure model. It is not the closure model for $\rho(\mathbf{x}', s|\mathbf{x})$ which makes this difficult, but the fact that the form of $\boldsymbol{R}$ in a real turbulent boundary layer would likely contain non-trivial functions.

7.4.4 Results

In this section the results for $\overline{\boldsymbol{\lambda}}$, $\overline{\boldsymbol{\mu}}$ and $\overline{\boldsymbol{\kappa}}$ as computed from the PT simulation and as predicted by both the new non-local closure model and the traditional local approximation are presented. The results obtained from the PT simulation are denoted by the superscript PT, the predictions from the new closure model are denoted by the superscript CM and the predictions from the local approximation are denoted by the superscript L.

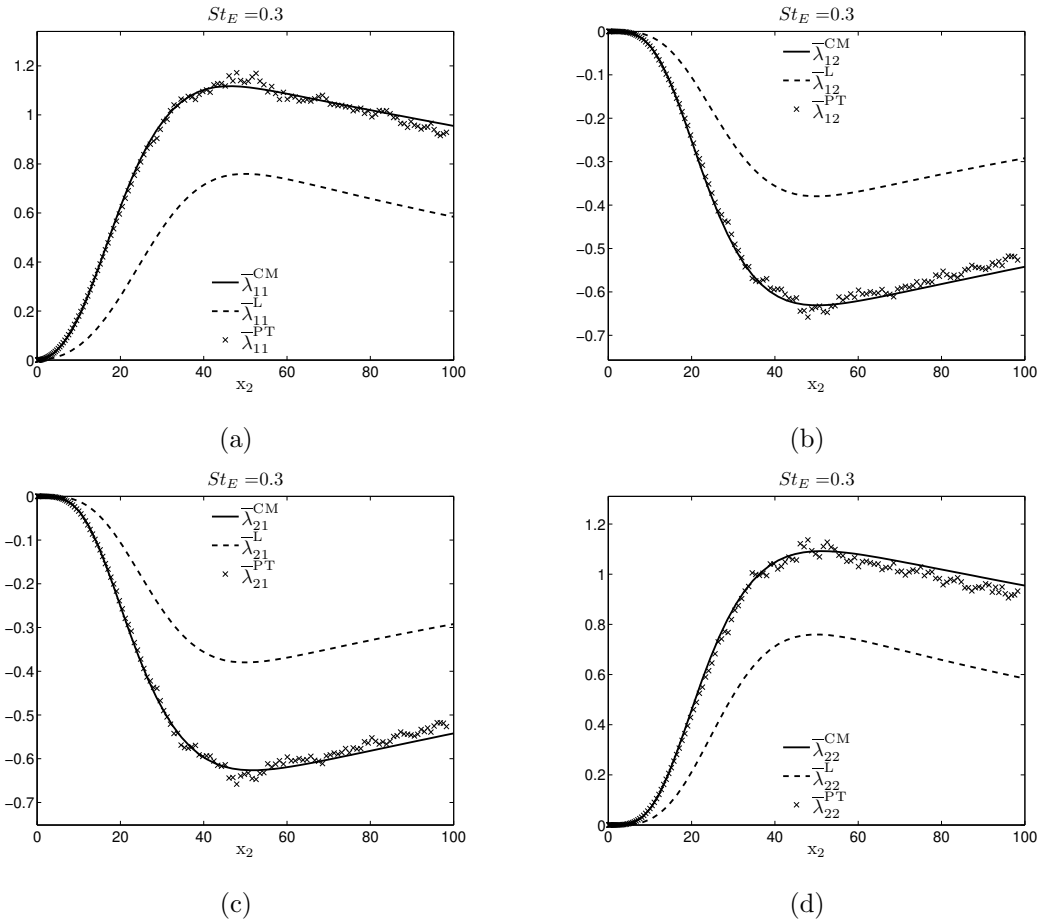

Figure 7.3: Comparison between particle tracking data (PT), closure model (CM) and the local approximation (L) for the components of $\overline{\boldsymbol{\lambda}}$ for $St_E = 0.3$.

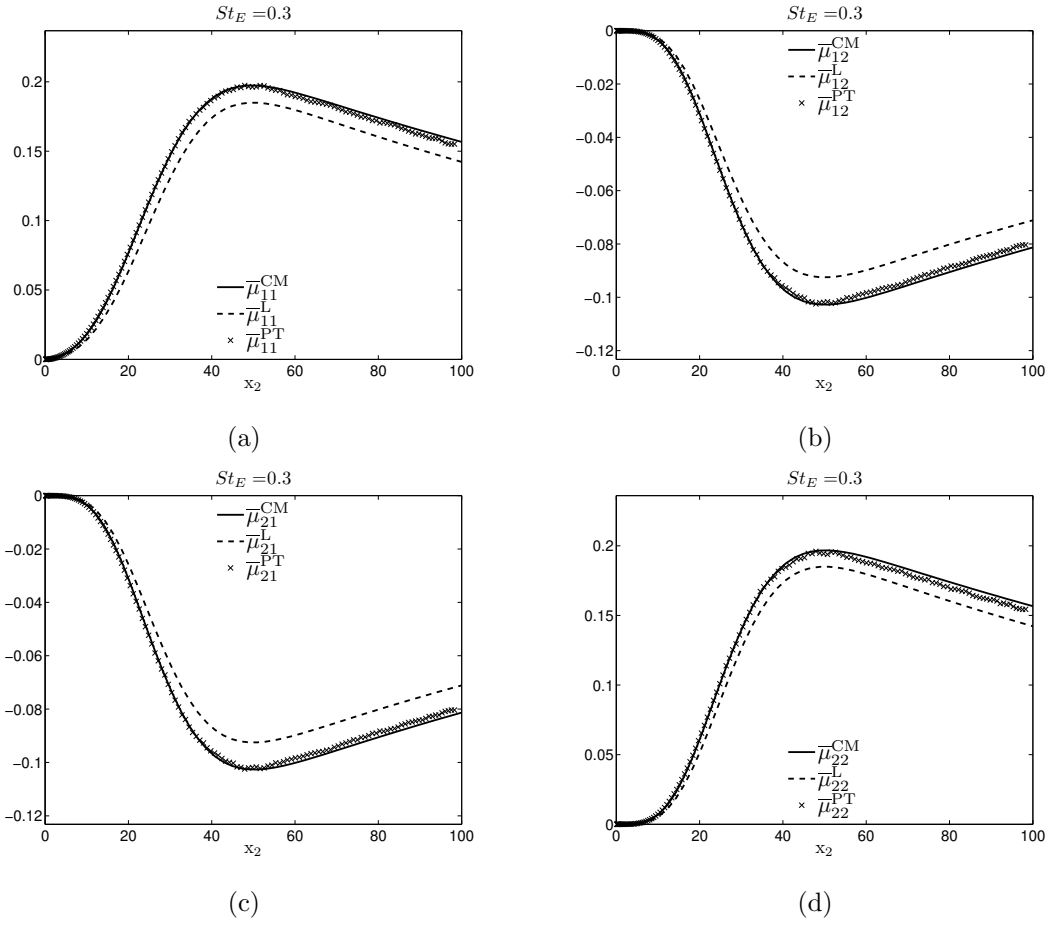

Figure 7.4: Comparison between particle tracking data (PT), closure model (CM) and the local approximation (L) for the components of $\overline{\boldsymbol{\mu}}$ for $St_E = 0.3$.

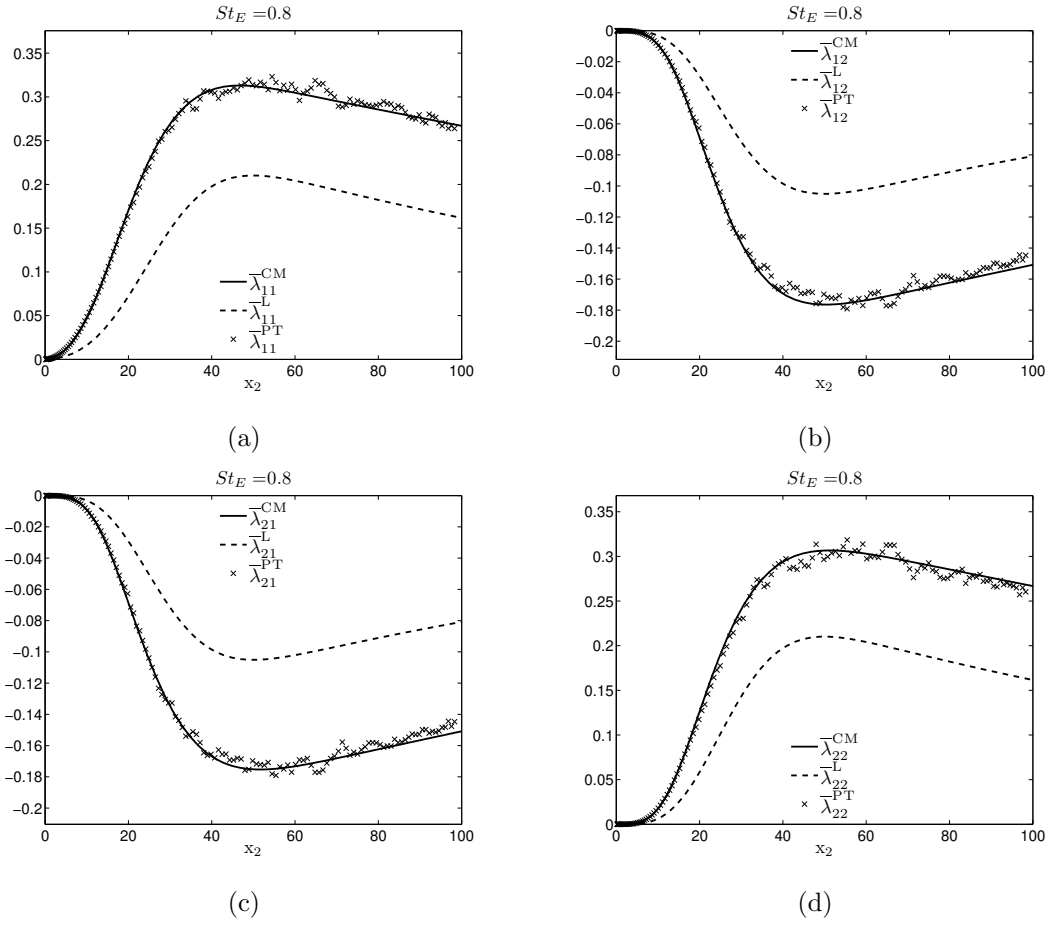

Figure 7.5: Comparison between particle tracking data (PT), closure model (CM) and the local approximation (L) for the components of $\overline{\boldsymbol{\lambda}}$ for $St_E = 0.8$.

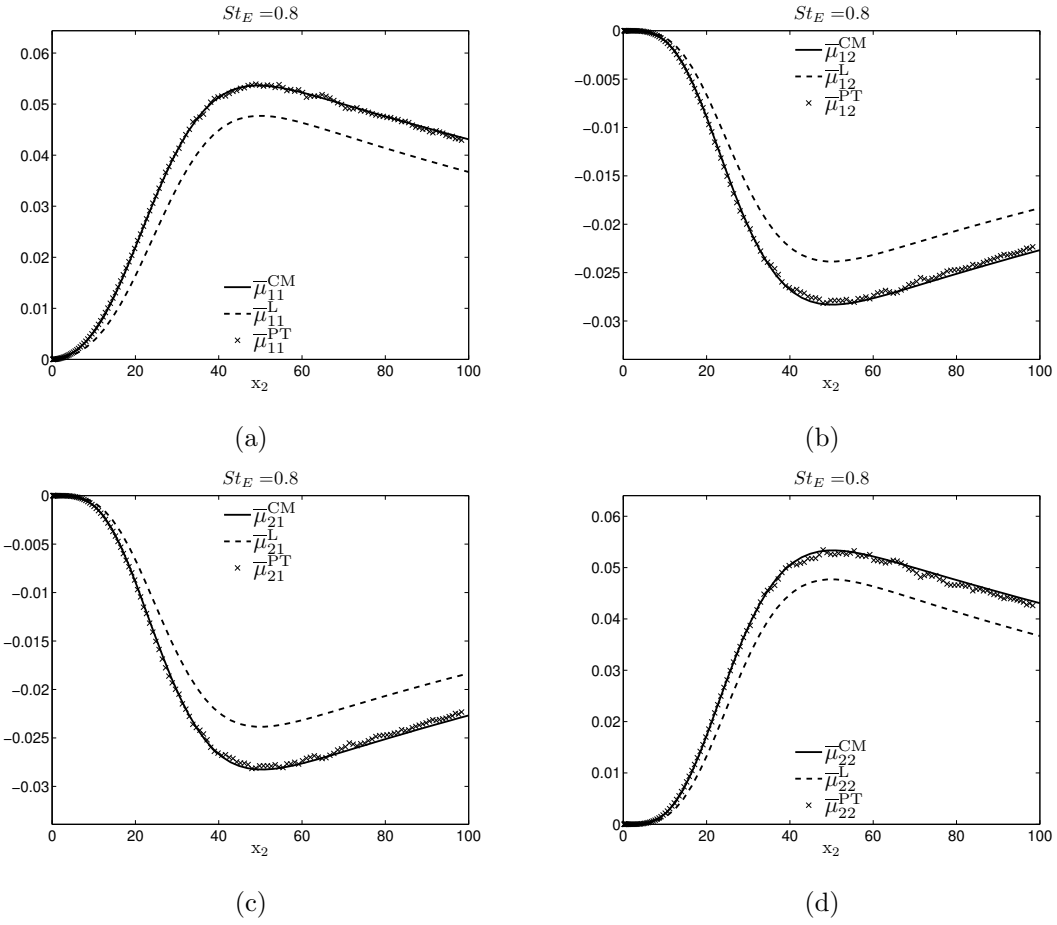

Figure 7.6: Comparison between particle tracking data (PT), closure model (CM) and the local approximation (L) for the components of $\overline{\boldsymbol{\mu}}$ for $St_E = 0.8$.

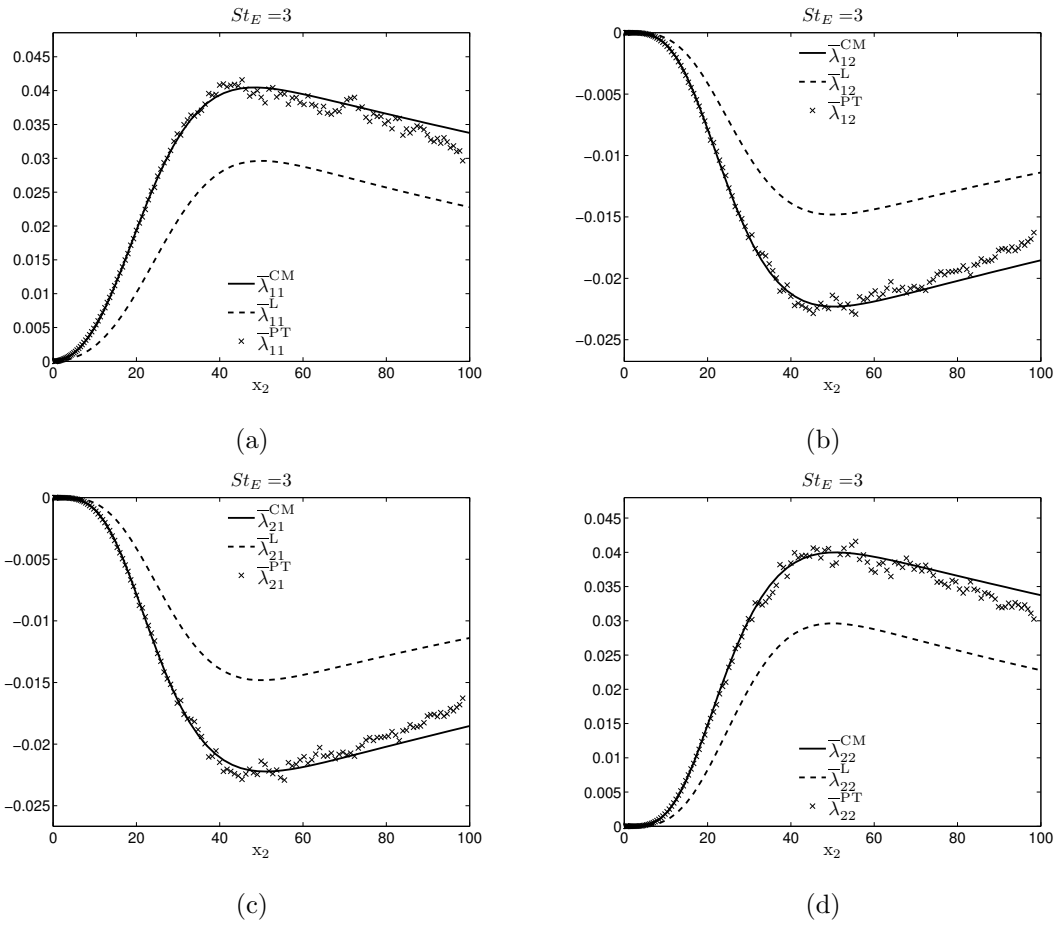

Figure 7.7: Comparison between particle tracking data (PT), closure model (CM) and the local approximation (L) for the components of $\overline{\boldsymbol{\lambda}}$ for $St_E = 3$.

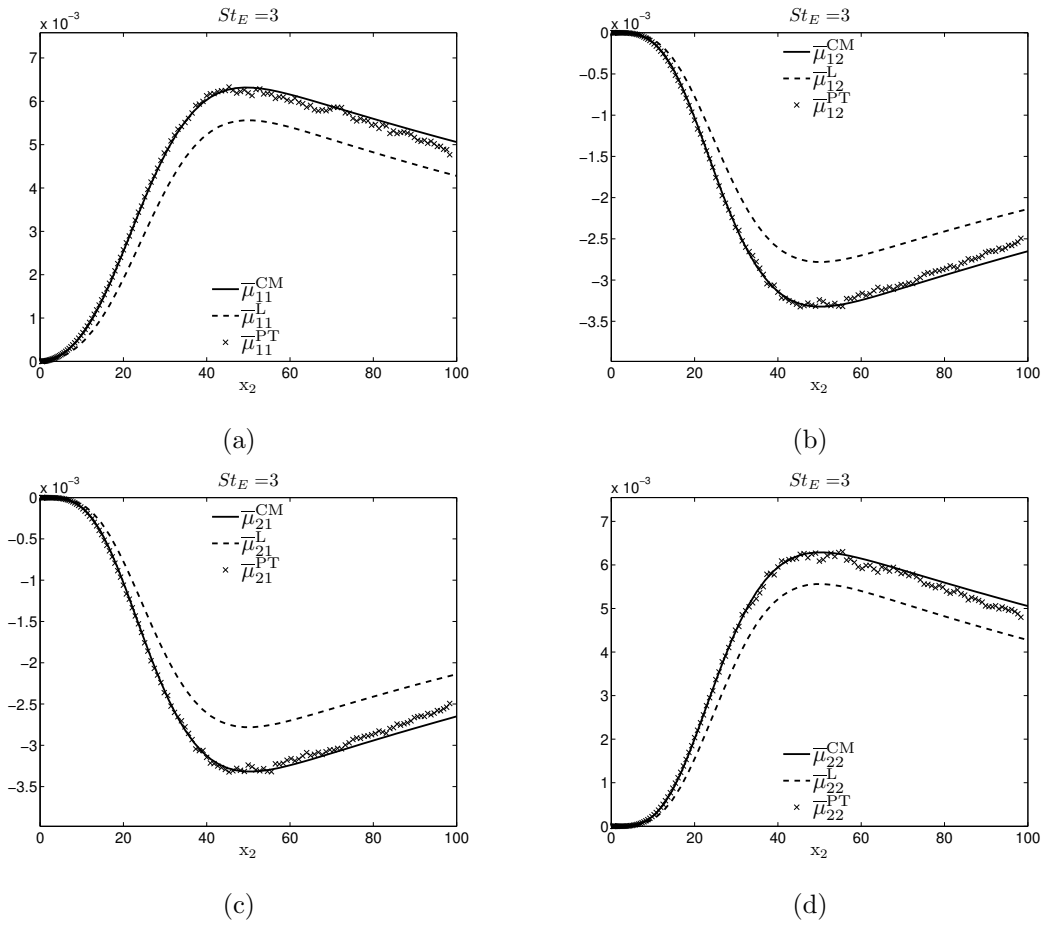

Figure 7.8: Comparison between particle tracking data (PT), closure model (CM) and the local approximation (L) for the components of $\overline{\boldsymbol{\mu}}$ for $St_E = 3$.

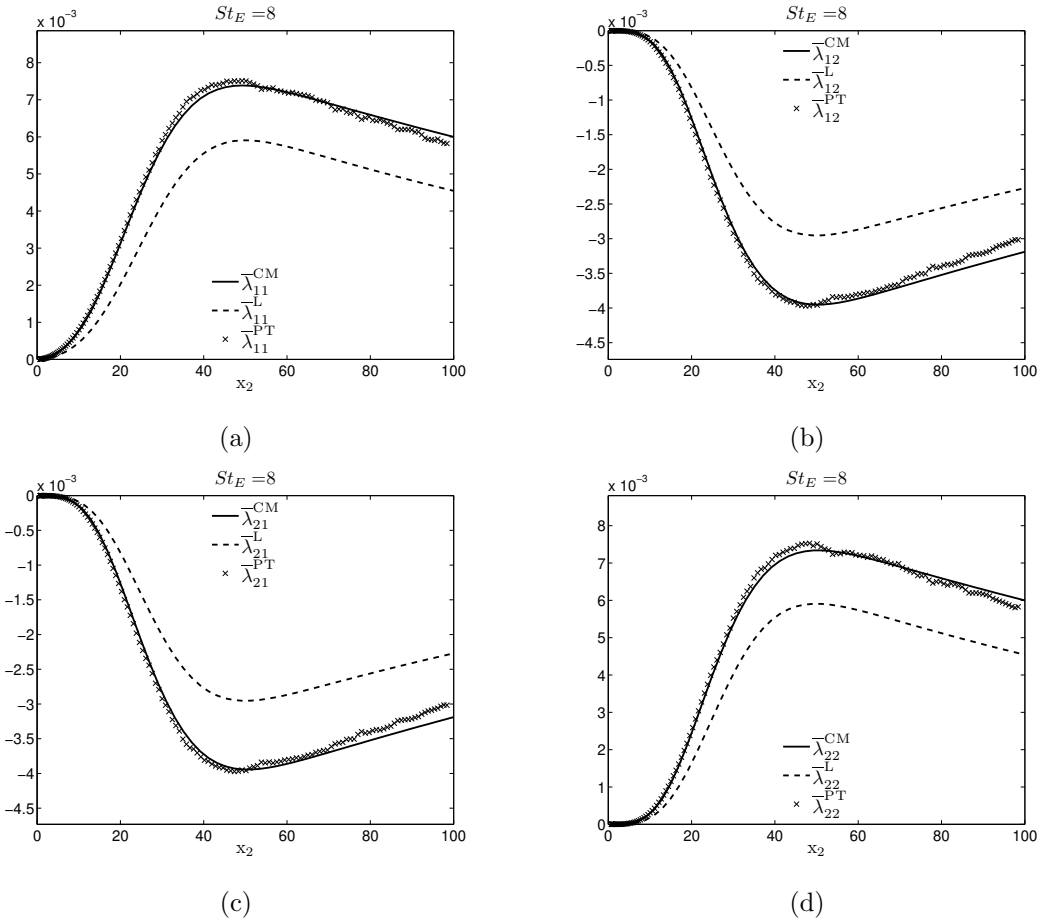

Figure 7.9: Comparison between particle tracking data (PT), closure model (CM) and the local approximation (L) for the components of $\overline{\boldsymbol{\lambda}}$ for $St_E = 8$.

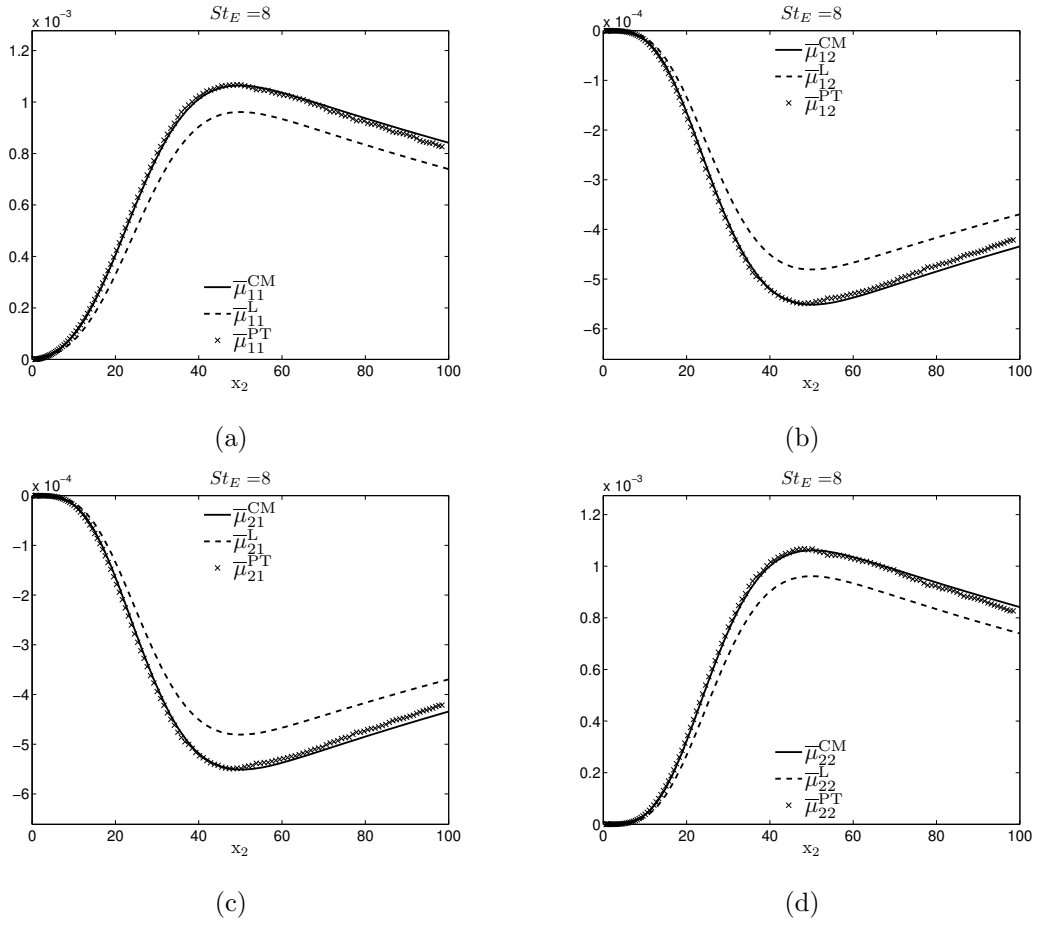

Figure 7.10: Comparison between particle tracking data (PT), closure model (CM) and the local approximation (L) for the components of $\overline{\boldsymbol{\mu}}$ for $St_E = 8$.

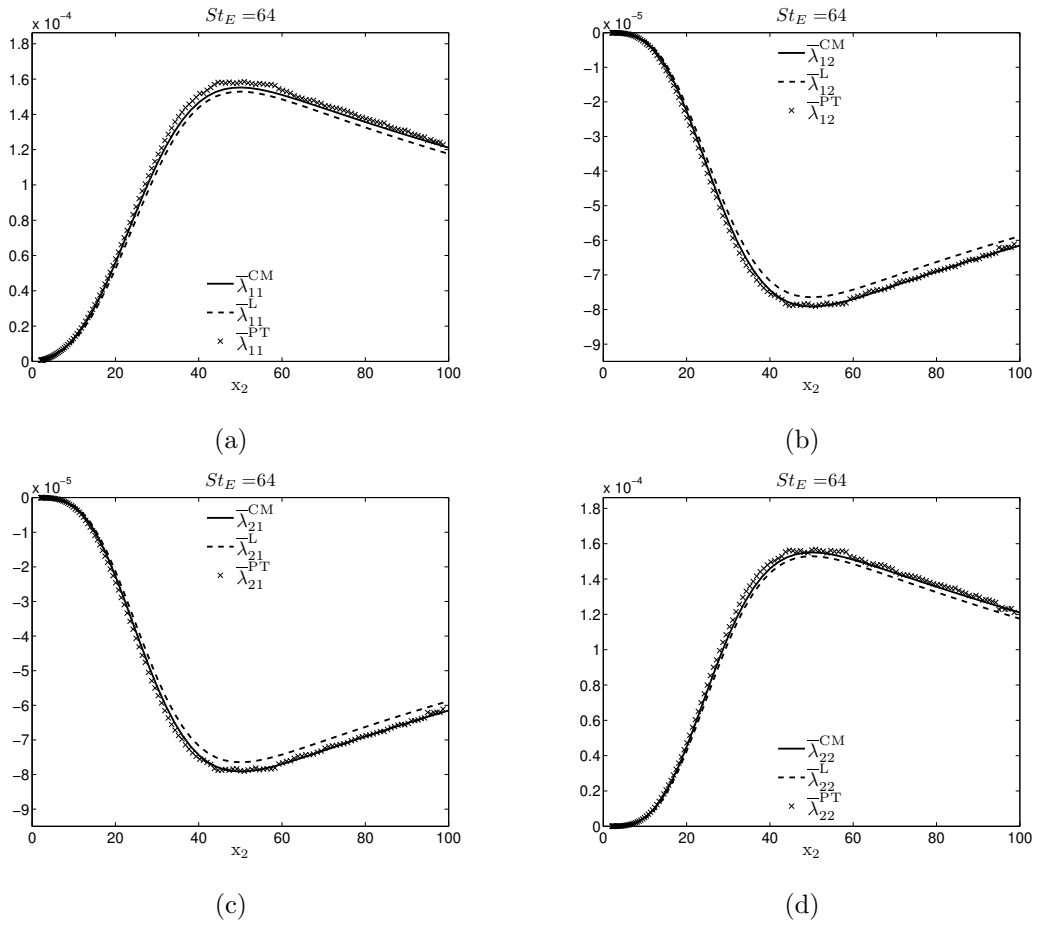

Figure 7.11: Comparison between particle tracking data (PT), closure model (CM) and the local approximation (L) for the components of $\overline{\boldsymbol{\lambda}}$ for $St_E = 64$.

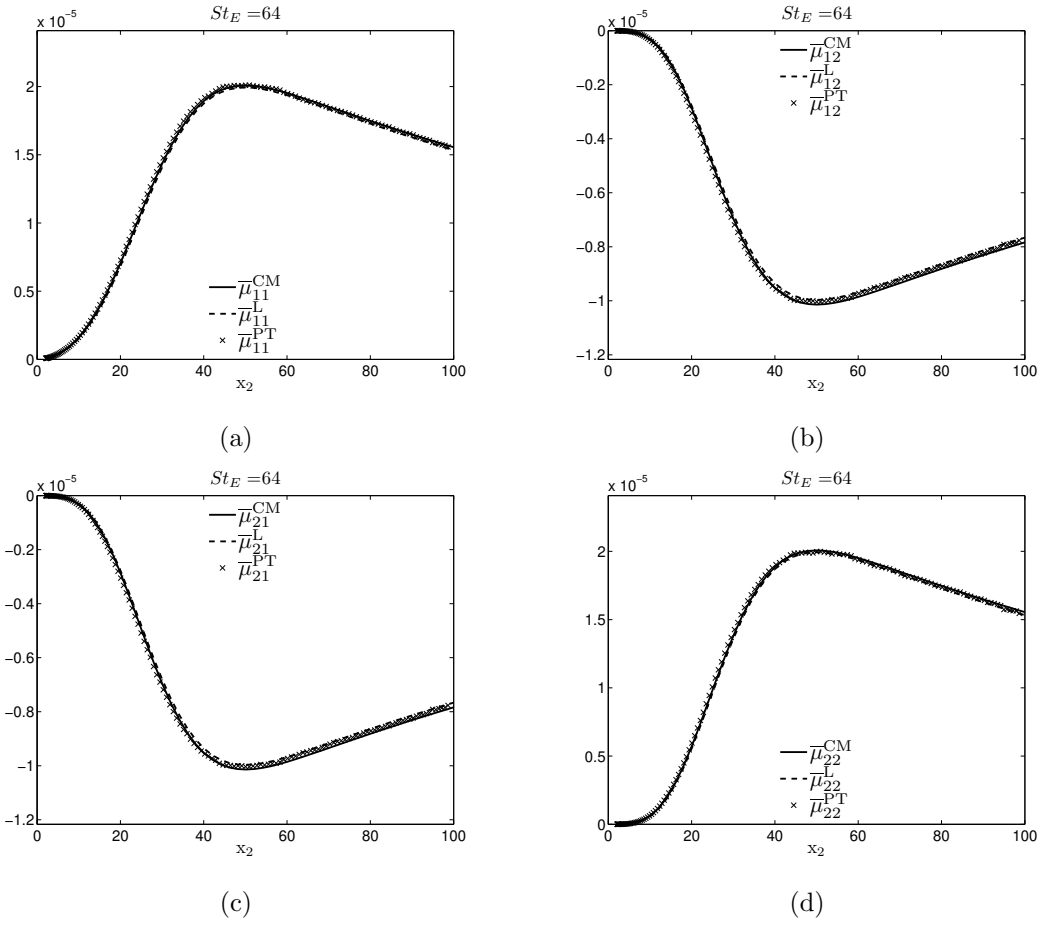

Figure 7.12: Comparison between particle tracking data (PT), closure model (CM) and the local approximation (L) for the components of $\overline{\boldsymbol{\mu}}$ for $St_E = 64$.

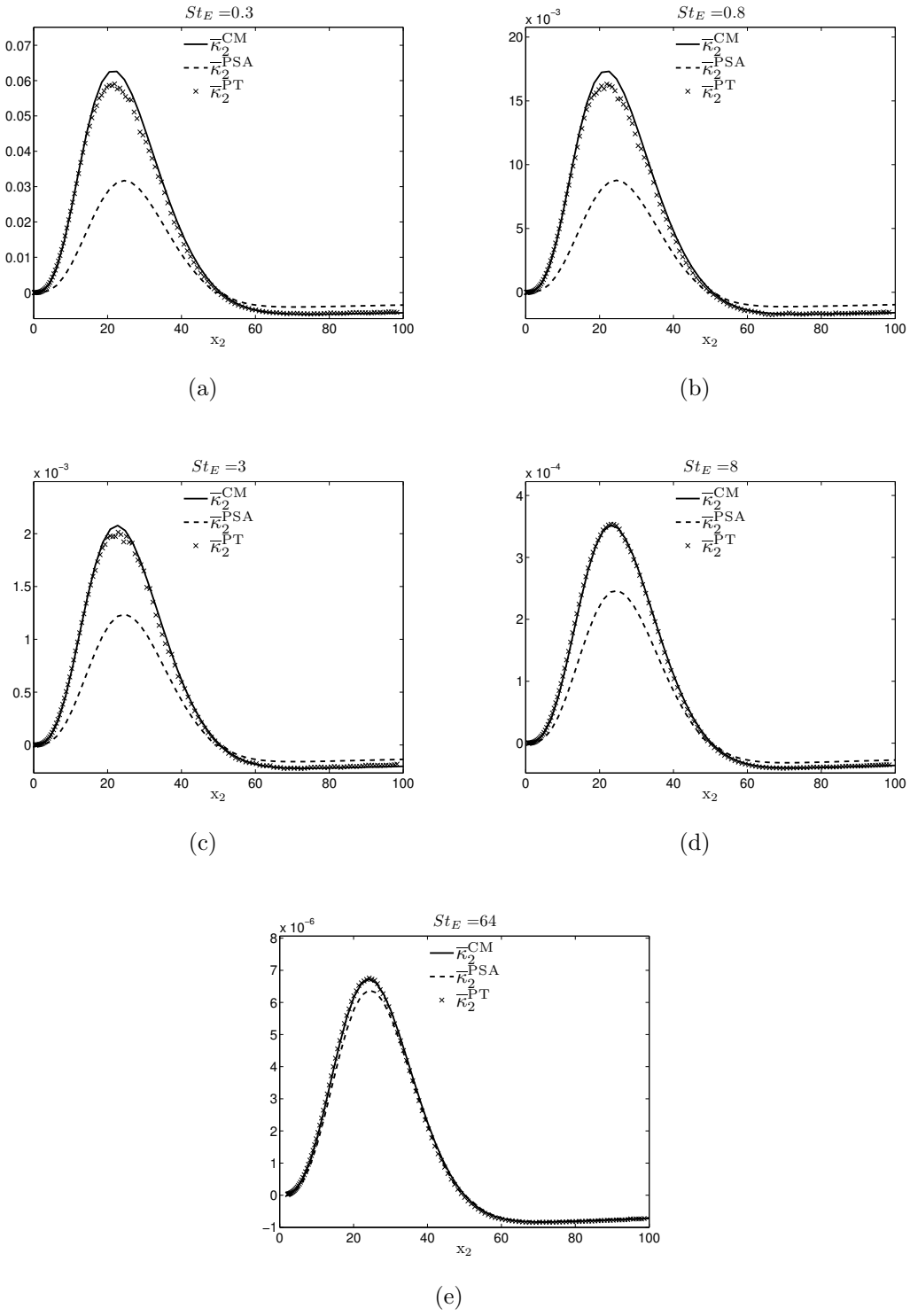

Figure 7.13: Comparison between particle tracking data (PT), closure model (CM) and the local approximation (L) for $\overline{\kappa}$.

7.4.5 Discussion

In section 7.4.4 results from particle tracking data (PT), the new closure model (CM) and the local approximation (L) for $\overline{\boldsymbol{\lambda}}$, $\overline{\boldsymbol{\mu}}$ and $\overline{\boldsymbol{\kappa}}$ are shown for a range of particle sizes.

In the system studied there are essentially three features which make the particle dispersion tensors non local; (i) the inhomogeneity and anisotropy of the fluid one-point statistics, (ii) the inhomogeneity and anisotropy of the fluid two-point statistics and (iii) the effect of the particle-wall collisions. In the region $\mathrm{x}_2 \leq 30$ the fluid Reynolds stresses are strongly non-uniform and nearer to the wall the particle-wall collisions influence the dispersion tensors. It can be seen from the results that across the range of particle sizes tested the new closure model predictions are in excellent agreement with the PT data in this region, and are a significant improvement on the local approximations. The closure model therefore captures very well the non-local influence of the turbulence inhomogeneity and the effect of the particle-wall collisions.

One of the approximations made in the construction of the closure model is that the distribution $\rho(\mathbf{x}', s|\mathbf{x})$ can be closely modelled using a Gaussian distribution. Even in this KS flow field, where the carrier phase velocities are Gaussian, $\rho(\mathbf{x}', s|\mathbf{x})$ is non-Gaussian since the particle velocity distributions are strongly skewed. However the results show that in the present test case the assumption of a Gaussian PDF for $\rho(\mathbf{x}', s|\mathbf{x})$ is sufficient. Of course in a real turbulent boundary layer the flow field is non-Gaussian, being both skewed and having extended non-Gaussian tails, owing to the intermittency of the fluid turbulence. Therefore it is still possible that a Guassian PDF approximation for $\rho(\mathbf{x}', s|\mathbf{x})$ may be insufficient for closing the dispersion tensors in a real turbulent boundary layer, and this is something which must be investigated in future work. Nevertheless, as discussed in section 7 it is possible to construct non-Gaussian closures for $\rho(\mathbf{x}', s|\mathbf{x})$ by using alternative closed PDF's such as skew-normal distributions [124], epsilon-skew-normal distributions [125] or skew-t distributions etc [126].

Figure 7.13 also shows that the new closure prediction for $\overline{\boldsymbol{\kappa}}$ is in very good agreement with the PT data, both of which are significantly different from the passive scalar approximation (except for very large particles). This is important since now the drift term

$$\overline{\kappa}_i - \frac{\partial}{\partial \mathrm{x}_j}\overline{\lambda}_{ji}$$

in the particle momentum equation can be modelled, whereas under the passive scalar approximation this drift term is incorrectly zero for inertial particles of all sizes. It should be noted that in figure 7.13 $\overline{\boldsymbol{\kappa}}^{PSA}$ is the passive scalar approximation derived from the local form of $\overline{\boldsymbol{\lambda}}^{L}$, that is

$$\overline{\kappa}_2^{PSA} = \frac{\partial}{\partial \mathrm{x}_2}\overline{\lambda}_{22}^{L} \tag{7.74}$$

The drift term and the closure model prediction of it will be discussed in greater detail in chapter 9.

Note that, in agreement with the results presented in chapter 5 and in [49], the results in section 7.4.4 show that $\overline{\boldsymbol{\lambda}}$ more sensitive to the non-local behavior of the system than $\overline{\boldsymbol{\mu}}$. In the limit of very large particles the new closure model predictions should tend to the local approximations and be equal as $\tau_p \to \infty$. The results in figures 7.11, 7.12 and 7.13 for $St_E = 64$ show that this is indeed the case; the new closure model predictions for the dispersion tensors tend to the local approximations in the limit of very large particles.

The results also show that the local approximation is still in error in the region $\mathrm{x}_2 \geq 40$ (except for $St_E = 64$) in which the non-uniformity of the fluid Reynolds stresses is not as strong in this region as in $0 \leq \mathrm{x}_2 \leq 30$ (see figure 7.2) and in which there is likely no influence of the particle wall collisions. It may therefore be expected that the dispersion tensors are not so sensitive to the non-locality of system in this region, in contrast to what the results show. This can be understood by the fact that in the region $\mathrm{x}_2 \geq 40$ the particles are moving with greater velocities than in the region $\mathrm{x}_2 \leq 30$. Having greater velocities, the characteristic distances the particles will move within the time for which the fluid is correlated are larger in the region $\mathrm{x}_2 \geq 40$ than in the region $\mathrm{x}_2 \leq 30$. Therefore, in the region $\mathrm{x}_2 \geq 40$ the particles still 'see' an appreciable variation in the fluid Reynolds stresses along their trajectories since they move relatively large distances within the time for which the fluid is correlated.

Furthermore, for small spatial separations the two-point statistics of this flow field are approximately isotropic, however for increasing spatial separations the two-point statistics begin to behave anisotropically (a feature of real boundary layers which affects the dispersion tensors, as noted in chapter 6). Consider figure 7.14

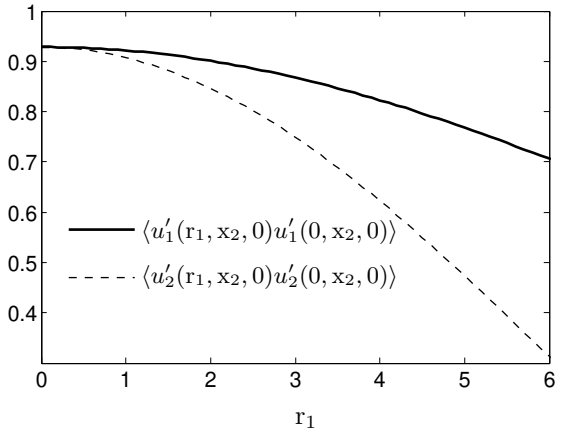

Figure 7.14: Plot of the two-point correlations in the KS flow field with separation r_1 for fixed $x_2 = 80$.

Figure 7.14 shows a plot of the two-point statistics in the KS flow field with separation r_1 for fixed $x_2 = 80$. The plot only shows their behavior in the region $0 \leq r_1 \leq 6$ in order to highlight their behavior at smaller separations. As figure 7.14 shows, for small separations the two-point statistics in the x_1 and x_2 directions are approximately equal, such that for $r_1^p(s) \approx 0$ the particles see an approximately isotropic flow. However with increasing r_1 the two-point statistics become increasingly anisotropic. Particles moving larger distances in the time for which the fluid is correlated will therefore see significant anisotropy in the two-point statistics of the flow field. The local approximation does not account for the anisotropy of the two-point statistics of the flow field, and this also explains why the local approximation is still in significant error in the region $x_2 \geq 40$ (even though the one-point statistics of the flow field in this region are only weakly non-uniform, relative to $x_2 \leq 30$ say), since in this region the particle velocities are relatively large and so the particles travel distances sufficiently large in the time for which the fluid is correlated such that they see significant anisotropy in the two-point statistics of the flow.

Finally, it is recalled that in the construction of the closure model (specifically in the construction of the moments of $\rho(\mathbf{x}', s|\mathbf{x})$, see section 7.3) that besides the single-phase fluid statistics (which are assumed to be fully known) the only other input required in the new closure model is an approximation to τ^{Lp}, which is the timescale of the fluid velocities seen by the inertial particles. In the closure model this timescale is approximated using the Wang & Stock function (see equation (7.34)) since this is the

simplest model which captures the inertial effects of the particles on the timescale. The only other simple alternative (besides setting $\tau^{Lp} = 0$) would be to approximate this timescale by τ_L, the fluid Lagrangian integral timescale (as discussed in section 7.3). In order to assess the sensitivity of the new closure model to the accuracy of the specification of τ^{Lp}, the closure model and local approximations to the dispersion tensors were once again tested against the particle tracking data, but this time making the approximation $\tau^{Lp} \approx \tau_L$ in both the new closure model and in the local approximations to the dispersion tensors. The results are shown for $St_E = 0.8, 3$

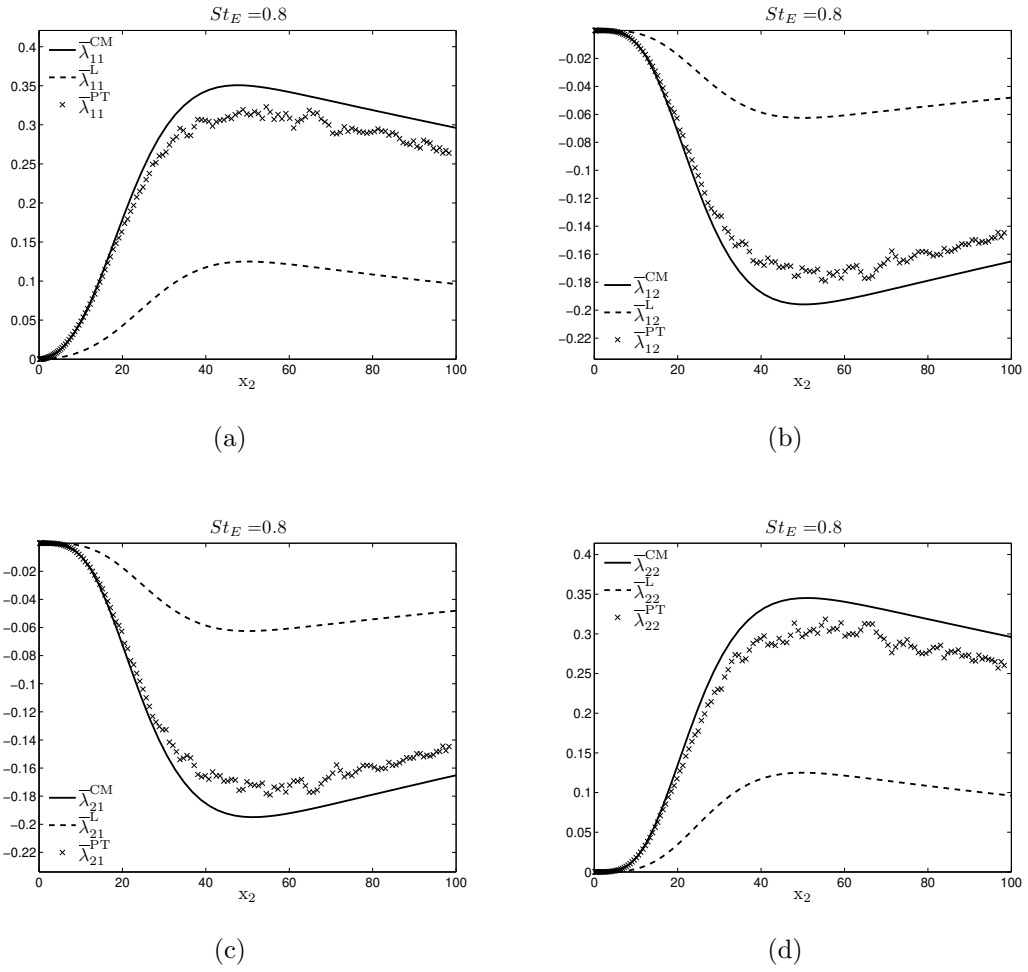

Figure 7.15: Comparison between particle tracking data (PT), closure model (CM) and the local approximation (L) for the components of $\overline{\boldsymbol{\lambda}}$ for $St_E = 0.8$, using the approximation $\tau^{Lp} \approx \tau_L$.

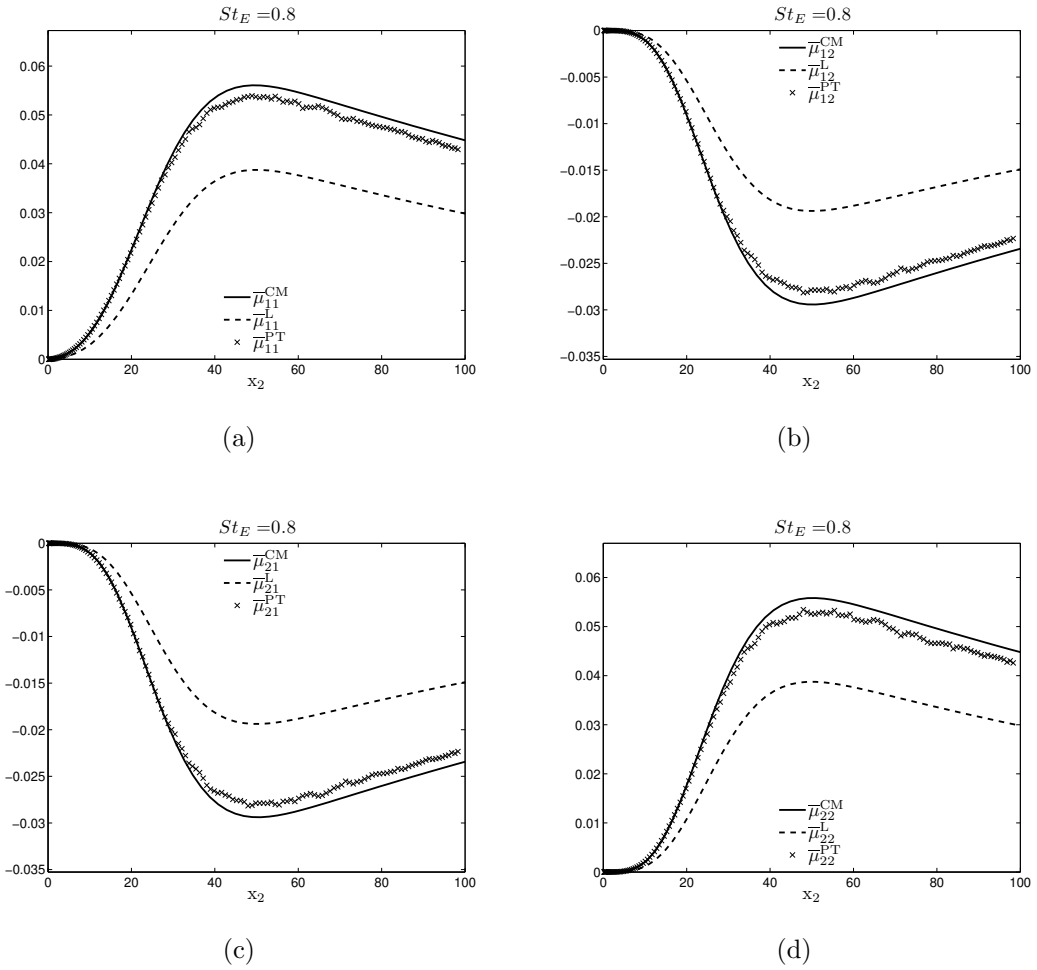

Figure 7.16: Comparison between particle tracking data (PT), closure model (CM) and the local approximation (L) for the components of $\overline{\boldsymbol{\mu}}$ for $St_E = 0.8$, using the approximation $\tau^{Lp} \approx \tau_L$.

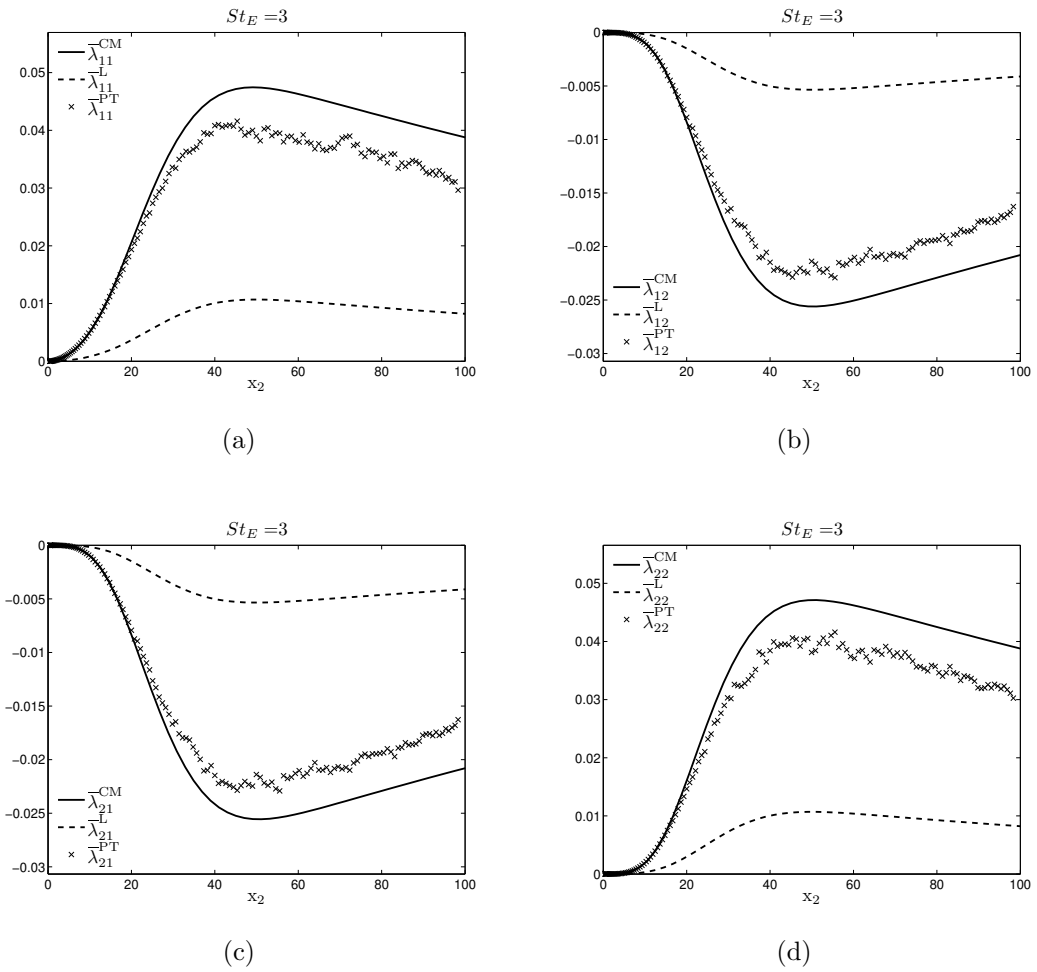

Figure 7.17: Comparison between particle tracking data (PT), closure model (CM) and the local approximation (L) for the components of $\overline{\boldsymbol{\lambda}}$ for $St_E = 3$, using the approximation $\tau^{Lp} \approx \tau_L$.

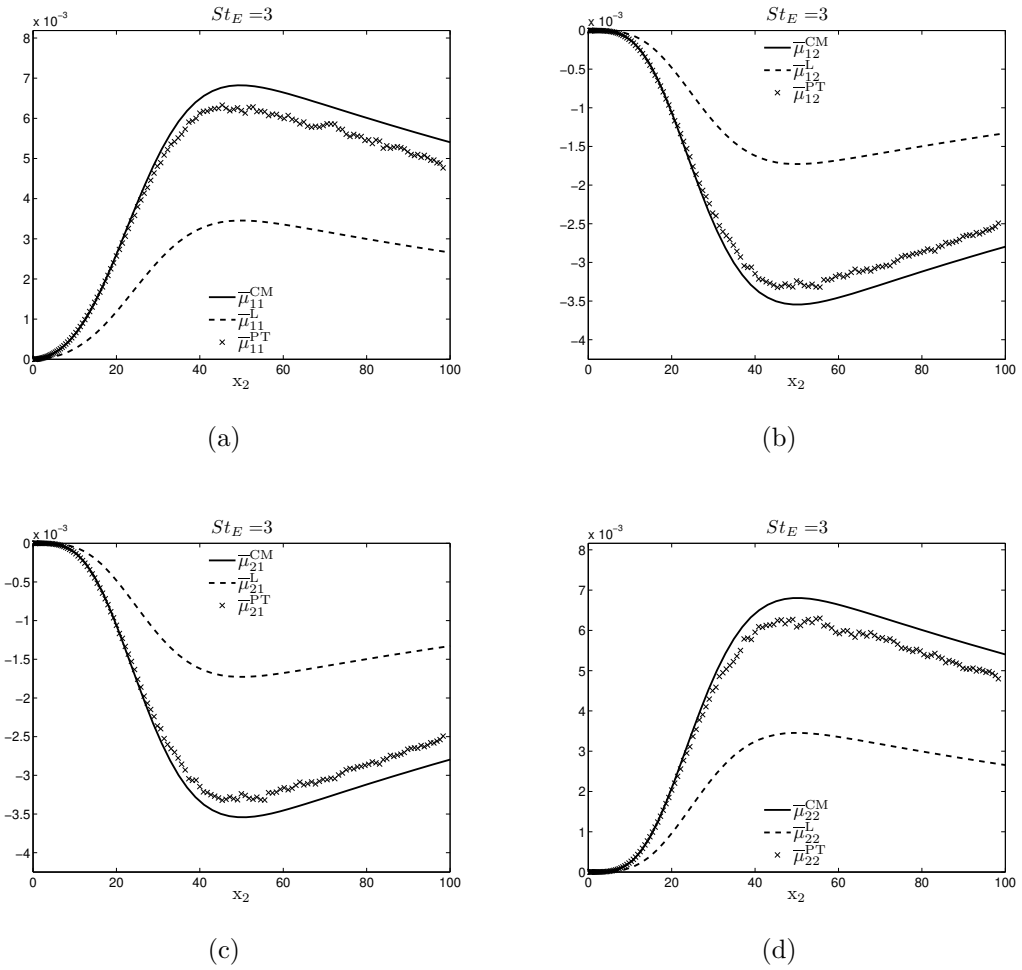

Figure 7.18: Comparison between particle tracking data (PT), closure model (CM) and the local approximation (L) for the components of $\overline{\boldsymbol{\mu}}$ for $St_E = 3$, using the approximation $\tau^{Lp} \approx \tau_L$.

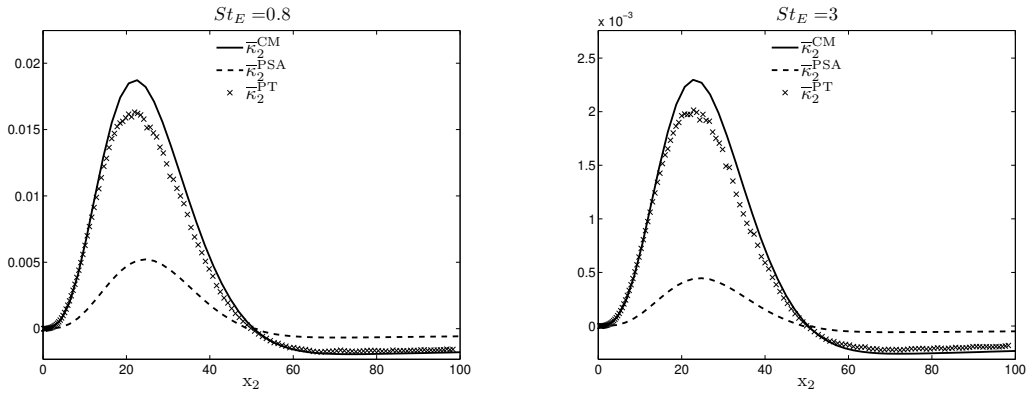

(a) (b)

Figure 7.19: Comparison between particle tracking data (PT), closure model (CM) and the local approximation (L) for $\overline{\kappa}$, using the approximation $\tau^{Lp} \approx \tau_L$.

The results in figures 7.15-7.19 demonstrate the effect of using the approximation $\tau^{Lp} \approx \tau_L$ in both the new closure model and local approximations for the dispersion tensors. Upon comparison with the results in section 7.4.4 (in which τ^{Lp} was approximated using equation (7.34)) it can be clearly seen that, as expected, both the new closure model and the local approximations perform worse with $\tau^{Lp} \approx \tau_L$ rather than with τ^{Lp} approximated using equation (7.34). However with $\tau^{Lp} \approx \tau_L$ the new closure model predictions are still in reasonable agreement with the PT data, whereas the local approximations with $\tau^{Lp} \approx \tau_L$ are in severe error. The finding being that the new non-local closure model for the dispersion tensors is much less sensitive to the approximation used for τ^{Lp} than the local approximations to the dispersion tensors are. The reason for this is that even with $\tau^{Lp} \approx \tau_L$ the non-local closure model still accounts for some of the inertial effects of the particle dispersion in $\rho(\mathbf{x}', s|\mathbf{x})$, since the closure model for $\rho(\mathbf{x}', s|\mathbf{x})$ described in section 7.3 depends upon the particle Reynolds stresses and the Green tensors for the particle equation of motion. By contrast, in a local approximation to the dispersion tensors τ^{Lp} is the only component of the closure which describes the effect of particle inertia on the correlations of the velocity field experienced by the particles, such that when $\tau^{Lp} \approx \tau_L$ the correlation timescales in the local approximations to the dispersion tensors no longer contain any dependence upon the particle inertia at all.

In the absence of body forces acting on the particles (so that the crossing trajectory effect induced by gravity, for example, is absent), the degree to which τ^{Lp} differs from τ_L is strongly dependent upon the ratio of the fluid Eulerian and Lagrangian integral timescales, i.e. τ_L/τ_E. Whenever this ratio is approximately equal to unity, the inertial effects of the particles (in the absence of body forces) on the correlations of the flow field they encounter will not be be significant, such that $\tau^{Lp} \approx \tau_L$. In the KS flow field

used in this test case, $\tau_L/\tau_E = 0.382$, such that the inertial effects of the particles on τ^{Lp} will be quite strong, and this explains why in figures 7.15-7.19 the approximation $\tau^{Lp} \approx \tau_L$ in the closure model was shown to lead to errors (especially for the local approximation). Nevertheless, this is not an artifact of the KS flow field used in the test case. In [128] the Lagrangian and Eulerian integral timescales were computed in a DNS of turbulent channel flow. Their results showed that the ratio τ_L/τ_E deviates very strongly from unity across the boundary layer, except for a small region close to the wall, and in fact the deviation of this ratio from unity is stronger in their DNS turbulent boundary layer than in the KS flow field used in this chapter. Consequently, in a real turbulent boundary layer, the inertial (and implicitly therefore, the non-local) effects on the turbulence statistics encountered along particle trajectories will be more significant in a real turbulent boundary layer than they have been shown to be in the present KS flow field test case. This further emphasises the need for a closure model which can both account for the inertial and non-local effects of the dispersion process on the dispersion tensors, such as has been developed in this chapter.

7.4.6 Conclusions

In this chapter a new non-local closure model for the particle dispersion tensors has been developed. It takes into account the effect of the turbulence inhomogeneity and anisotropy, as well as particle-wall collisions for particles dispersing under a Stokes drag force. Upon comparison with both equivalent PT data for the dispersion tensors and the local approximations it has been shown that whilst the local approximations can be in significant error, the new closure model predictions are in excellent agreement with the PT data. In addition, the new closure model provides a way to model $\overline{\boldsymbol{\kappa}}$ which avoids the use of the passive scalar approximation. The natural step forward would be to test the closure model against PT in DNS of a turbulent channel flow. However such a test case would be very time consuming, and time constraints put this beyond the scope of work presented in this thesis. Such a test case is left to future work.

It is also important to try and extend the closure model to include forces in addition to Stokes drag acting on the particles. In the next chapter the closure modelling is extended to attempt to account for added mass and gravitational forcing acting on the particles in addition to Stokes drag.

Chapter 8

The PDF Kinetic Framework Including Added Mass Forcing

Most of the work carried out on the PDF kinetic equation and its associated continuum equations has been restricted to Stokes drag forcing acting on the particles, with the possible addition of gravity. Whilst the formulation of the PDF and continuum equations in chapter 4 was for a general force $\boldsymbol{F} + \boldsymbol{f}$ acting on the particle, which could include drag, added mass, lift forces etc, additional consideration is required. For example, with added mass, Stokes drag and gravity the particle equation of motion is (see chapter 2)

$$\frac{d^2}{dt^2}x_i^p + \tilde{\beta}\frac{d}{dt}x_i^p = \tilde{\beta}\langle u_i\rangle^p + \tilde{\beta}u_i^{p\prime} + \alpha\left(\left\langle \frac{D}{Dt}u_i \right\rangle^p + \left(\frac{D}{Dt}u_i^p\right)'\right) + \theta g_i \tag{8.1}$$

where

$$\tilde{\beta} = \frac{1}{\tau_p\left(1 + \frac{1}{2}\frac{\rho^f}{\rho^p}\right)} \tag{8.2}$$

$$\alpha = \frac{3\rho^f}{2\rho^p + \rho^f} \tag{8.3}$$

$$\theta = \frac{2(\rho^p - \rho^f)}{2\rho^p + \rho^f} \tag{8.4}$$

In the PDF kinetic equation corresponding to equation (8.1) the phase-space diffusion current would be given by (see chapter 4)

$$p\Big\langle f_i(\boldsymbol{x}^p(t),t)\Big\rangle_{\mathbf{x},\mathbf{v}} = \beta p\Big\langle u_i'(\boldsymbol{x}^p(t),t)\Big\rangle_{\mathbf{x},\mathbf{v}} + \alpha p\Bigg\langle \left(\frac{D}{Dt}u_i(\boldsymbol{x}^p(t),t)\right)'\Bigg\rangle_{\mathbf{x},\mathbf{v}} \tag{8.5}$$

where

$$\begin{aligned}\left(\frac{D}{Dt}u_i(\boldsymbol{x}^p(t),t)\right)' &= \left(\frac{D}{Dt}u_i^p\right)' = \frac{D}{Dt}u_i(\boldsymbol{x}^p(t),t) - \left\langle \frac{D}{Dt}u_i(\boldsymbol{x}^p(t),t)\right\rangle \\ &= \frac{\partial}{\partial t}u_i^{p\prime} + \frac{\partial}{\partial \mathrm{x}_j}\left[\langle u_j\rangle^p u_i^{p\prime} + u_j^{p\prime}\langle u_i\rangle^p + u_j^{p\prime}u_i^{p\prime} - \langle u_j'u_i'\rangle^p\right]\end{aligned} \tag{8.6}$$

Now following the analysis in chapter 4 this phase-space diffusion current may be closed using FN by making the approximation that $\boldsymbol{f}$ is Gaussian. However in doing so there arises something of an inconsistency. If $\boldsymbol{u}'$ is Gaussian then it is apparent from equation (8.6) that

$$\left(\frac{D}{Dt}\boldsymbol{u}\right)'$$

is not Gaussian. Given the kinematic relationship between the acceleration and the velocity fields then it would be inconsistent to assume that both the fluid velocity and fluid acceleration fields are Gaussian. Nevertheless in [110] and [101] a PDF equation accounting for added mass was developed and in those works a Gaussian approximation was applied to both the fluid velocity and acceleration fields. In [110] the continuum equations derived from this PDF model were tested against experimental data for particle dispersion in the core of a turbulent channel flow (not the boundary layer) and the continuum equations were found to yield good predictions. In [101] the continuum equations derived from the new PDF model (i.e. containing added mass forcing) were tested against DNS data of a turbulent channel flow. The results showed reasonable agreement between the model predictions and the DNS data for the particle velocity statistics, however the continuum solutions for the particle concentration were in error.

With added mass forcing acting on the particles in addition to Stokes drag it is expected that the non-local nature of the particle dispersion tensors will become even more apparent since the additional added mass force will increase the dispersion rate. Also, for example in [110], it was shown that with added mass and Stokes drag forcing acting on the particles the particle Reynolds stresses could exceed those of the fluid. This will mean that the particles will travel characteristically greater distances within the time for which the fluid is correlated than they would have if added mass forcing was absent (in which case the particle Reynolds stresses are always less than that of the fluid, except very close to the wall). This again will make the dispersion tensors more sensitive to the non-local nature of the dispersion process.

Therefore, once again, non-local closures for the particle dispersion tensors are required, only now these closures must account for Stokes drag and added mass forcing, with gravity included also for generality. Once again, in the dispersion tensors the terms requiring closure are

$$\Big\langle R_{ji}(\boldsymbol{x}^p(s),s;\mathbf{x},0)\Big\rangle_{\mathbf{x}} = \int_{\mathbf{x}'} R_{ji}(\mathbf{x}',s;\mathbf{x},0)\rho\left(\mathbf{x}',s|\mathbf{x}\right)d\mathbf{x}' \tag{8.7}$$

$$\Big\langle \frac{\partial}{\partial \mathrm{x}_k} R_{ji}(\boldsymbol{x}^p(s),s;\mathbf{x},0)\Big\rangle_{\mathbf{x}} = \int_{\mathbf{x}'} \left[\frac{\partial}{\partial \mathrm{x}_k} R_{ji}(\mathbf{x}',s;\mathbf{x},0)\right]\rho\left(\mathbf{x}',s|\mathbf{x}\right)d\mathbf{x}' \tag{8.8}$$

however with Stokes drag and added mass forcing the two-point, two-time correlation tensor $\boldsymbol{R}$ is given by

$$\begin{aligned} R_{ji}(\mathbf{x},s;\mathbf{x},0) =& \tilde{\beta}^2\Big\langle u_j'(\mathbf{x}',s)u_i'(\mathbf{x},0)\Big\rangle \\ &+ \alpha\tilde{\beta}\Big\langle \left(\frac{D}{Dt}u_j(\mathbf{x}',s)\right)' u_i'(\mathbf{x},0)\Big\rangle \\ &+ \alpha\tilde{\beta}\Big\langle u_j'(\mathbf{x}',s)\left(\frac{D}{Dt}u_i(\mathbf{x},0)\right)'\Big\rangle \\ &+ \alpha^2\Big\langle \left(\frac{D}{Dt}u_j(\mathbf{x}',s)\right)'\left(\frac{D}{Dt}u_i(\mathbf{x},0)\right)'\Big\rangle \end{aligned} \tag{8.9}$$

Given the form of the fluctuating acceleration in equation (8.6) the corresponding correlations in equation (8.9) involving the acceleration will be quite involved, and certainly obtaining such correlations from DNS, for example, would be cumbersome. However, since the acceleration field fluctuates on a faster timescale than the velocity field, it is hypothesised that within the time for which the acceleration field is correlated (with itself and with the velocity field) the particles move sufficiently small distances such that the acceleration contribution to the dispersion tensors may be well approximated by a local closure. That is, if, for example, $\overline{\boldsymbol{\lambda}}$ is separated into four contributions (i.e. related to the four contributions to $\boldsymbol{R}$ in equation (8.9)) as

$$\overline{\boldsymbol{\lambda}} = \overline{\boldsymbol{\lambda}}^{dd} + \overline{\boldsymbol{\lambda}}^{ad} + \overline{\boldsymbol{\lambda}}^{da} + \overline{\boldsymbol{\lambda}}^{aa}$$

where the superscripts d and a denote contributions due to drag and added mass correlations, then the hypothesis made is that

$$\overline{\boldsymbol{\lambda}} = \underbrace{\overline{\boldsymbol{\lambda}}^{dd}}_{\text{Non-local}} + \underbrace{\overline{\boldsymbol{\lambda}}^{ad}}_{\approx \text{ local}} + \underbrace{\overline{\boldsymbol{\lambda}}^{da}}_{\approx \text{ local}} + \underbrace{\overline{\boldsymbol{\lambda}}^{aa}}_{\approx \text{ local}}$$

and similarly for $\overline{\boldsymbol{\mu}}$ and $\overline{\boldsymbol{\kappa}}$. Indeed, if the contributions $\overline{\boldsymbol{\lambda}}^{ad}$ and $\overline{\boldsymbol{\lambda}}^{da}$ are approximately locally homogeneous, then their wall-normal contributions (the important components since the wall-normal components of the dispersion tensors control the particle concentration) will cancel out [110] leaving

$$\overline{\lambda}_{22} \approx \underbrace{\overline{\lambda}_{22}^{dd}}_{\text{Non-local}} + \underbrace{\overline{\lambda}_{22}^{aa}}_{\approx \text{ local}}$$

Of course this hypothesis must be tested, but this is left to future work. For the present, the important issue is how well the non-local closure modelling can predict $\overline{\boldsymbol{\lambda}}^{dd}$, $\overline{\boldsymbol{\mu}}^{dd}$ and $\overline{\boldsymbol{\kappa}}^{dd}$ when the forcing on the particles includes Stokes drag, added mass and gravity, since these contributions to the dispersion tensors will be most sensitive to the non-locality of the dispersion process.

In order to close $\overline{\boldsymbol{\lambda}}^{dd}$, $\overline{\boldsymbol{\mu}}^{dd}$ and $\overline{\boldsymbol{\kappa}}^{dd}$ the following must be closed

$$\left\langle R_{ji}^{dd}(\boldsymbol{x}^p(s), s; \mathbf{x}, 0)\right\rangle_{\mathbf{x}} = \tilde{\beta}^2 \int_{\mathbf{x}'} \left\langle u_j'(\mathbf{x}', s) u_i'(\mathbf{x}, 0)\right\rangle \rho\left(\mathbf{x}', s|\mathbf{x}\right) d\mathbf{x}' \tag{8.10}$$

$$\left\langle \frac{\partial}{\partial \mathrm{x}_k} R_{ji}^{dd}(\boldsymbol{x}^p(s), s; \mathbf{x}, 0)\right\rangle_{\mathbf{x}} = \tilde{\beta}^2 \int_{\mathbf{x}'} \left[\frac{\partial}{\partial \mathrm{x}_k}\left\langle u_j'(\mathbf{x}', s) u_i'(\mathbf{x}, 0)\right\rangle\right] \rho\left(\mathbf{x}', s|\mathbf{x}\right) d\mathbf{x}' \tag{8.11}$$

where now $\rho\left(\mathbf{x}', s|\mathbf{x}\right)$ is for particles dispersing under Stokes drag, added mass and gravitational forcing. The particle-wall collisions in this closure model are handled in the same was as described in chapter 7. In the next section the closure model for $\rho\left(\mathbf{x}', s|\mathbf{x}\right)$ accounting for particles dispersing under such forcing is presented.

8.1 Closure Model for the Particle Dispersion Tensors

In chapter 7 a new non-local closure model was developed for the particle dispersion tensors, which attempts to take into account the effects of the turbulence inhomogeneity and anisotropy, and the effect of the particle-wall collisions on the dispersion tensors for particles dispersing under Stokes drag forcing. It was demonstrated that the new closure model predictions are in excellent agreement with equivalent PT data for the dispersion tensors. In this section the closure model will be further developed to account for particles dispersing under the influence of Stokes drag, added mass and gravitational forcing.

The particle equation of motion required is given in equation (8.1). The particle trajectories described by $\rho\left(\mathbf{x}', s|\mathbf{x}\right)$ are defined backwards in time, and the backwards in

time motion is described by

$$\frac{d^2}{ds^2}x_i^p - \tilde{\beta}\frac{d}{ds}x_i^p = -\tilde{\beta}\langle u_i\rangle^p - \tilde{\beta}u_i^{p\prime} - \alpha\left(\left\langle\frac{D}{Ds}u_i\right\rangle^p + \left(\frac{D}{Ds}u_i^p\right)'\right) - \theta g_i \tag{8.12}$$

where $s = t' - t \leq 0$. The mean component of the fluid acceleration is (for steady state turbulent channel flow)

$$\begin{aligned}\left\langle\frac{D}{Ds}u_i\right\rangle^p &= \left\langle\frac{\partial}{\partial s}u_i\right\rangle^p + \left\langle\frac{\partial}{\partial \mathrm{x}_j}u_j u_i\right\rangle^p \\ &= \frac{\partial}{\partial \mathrm{x}_2}\langle u_2' u_i'\rangle^p\end{aligned} \tag{8.13}$$

As in the initial closure model (see chapter 7), since the trajectories in $\rho(\mathbf{x}', s|\mathbf{x})$ are to be subject to the end condition $\boldsymbol{x}^p(0) = \mathbf{x}$, then if the mean shear of the fluid is approximated as locally linear (i.e. linear about $\mathbf{x}$), the mean fluid velocity may be written as

$$\langle u_i\rangle^p = \langle u_i\rangle(x_2^p(s)) = \gamma(\mathrm{x}_2)\delta_{i1}\left(x_2^p(s) - \mathrm{x}_2\right) + \langle u_i(\mathrm{x}_2)\rangle \tag{8.14}$$

where $\gamma(\mathrm{x}_2)$ is the mean fluid velocity gradient. The applicability of a locally linear mean shear approximation for dispersion in a turbulent boundary layer, and its implications for the closure model have been discussed in chapter 7. In addition, the gradient of the fluid Reynolds stresses will also be assumed to be locally linear, so that

$$\begin{aligned}\left\langle\frac{D}{Ds}u_i\right\rangle^p = \left\langle\frac{D}{Ds}u_i\right\rangle(x_2^p(s)) &= \Gamma_i(\mathrm{x}_2)\left(x_2^p(s) - \mathrm{x}_2\right) + \left\langle\frac{D}{Ds}u_i\right\rangle(\mathrm{x}_2) \\ &= \Gamma_i(\mathrm{x}_2)\left(x_2^p(s) - \mathrm{x}_2\right) + \frac{\partial}{\partial \mathrm{x}_2}\langle u_2' u_i'\rangle(\mathrm{x}_2)\end{aligned} \tag{8.15}$$

where

$$\Gamma_i(\mathrm{x}_2) = \frac{\partial^2}{\partial \mathrm{x}_2^2}\langle u_2' u_i'\rangle(\mathrm{x}_2) \tag{8.16}$$

Unlike the mean shear, the gradients of the fluid Reynolds stresses affect the particle dispersion in all directions, and therefore the implications or erroneous approximations for the gradients of the fluid Reynolds stresses have a greater effect on the validity of the model for $\rho(\mathbf{x}', s|\mathbf{x})$ than those made for the mean shear (see discussion in chap-

ter 7). Here a locally linear approximation has been made for the gradient of the fluid Reynolds stresses, and once again, this approximation is made in order that a fully analytic closure model for $\rho(\mathbf{x}', s|\mathbf{x})$ may be constructed[1]. In the closure model, as seen from equation (8.13) it is not the full tensor but only the wall-normal gradients of the components $\langle u_2' u_i' \rangle$ which require approximation. The wall-normal gradients of these componenets are, to leading order, proportional to x_2^2 for $i = 1, 3$ and x_2^3 for $i = 2$ (e.g. [21]). Consequently, the locally linear approximation for the gradient of the fluid Reynolds stress tensor expressed in equation (8.15) can only be strictly considered appropriate for $|x_2^p(s) - \mathrm{x}_2| \ll 1$. In the very near wall region (i.e. within the viscous sublayer) the particle displacements within the time for which the fluid is correlated are relatively small since the fluid and particle velocities in that region are small. Therefore, in the viscous sublayer it is possible that the locally linear approximation for the gradient of the fluid Reynolds stress is appropriate. However further away from the wall the particle displacements in the time for which the fluid is correlated will undoubtedly be large enough for the particles to see a nonlinear variation in the gradient of the fluid velocity Reynolds stresses along their trajectories. Nevertheless, motivated by the desire for a fully analytic closure model, as a first approximation, the locally linear approximation for the gradients of the fluid velocity Reynolds stress tensor will be adopted. If this proves to seriously compromise the closure model for $\rho(\mathbf{x}', s|\mathbf{x})$ (determined by comparison of the closure model with numerical simulations), a semi-analytic closure model could be constructed for $\rho(\mathbf{x}', s|\mathbf{x})$ which would take into account nonlinearities in gradients of the fluid velocity Reynolds stress tensor along the particle paths (as discussed in chapter 7 in the context of accounting for nonlinear variation in the mean fluid velocity along particle trajectories).

Using the locally linear approximation expressed in equation (8.15), equation (8.12) may then be written as

$$\begin{aligned} \frac{d^2}{ds^2}x_i^p - \tilde{\beta}\frac{d}{ds}x_i^p + \left[\tilde{\beta}\gamma(\mathrm{x}_2)\delta_{i1} + \alpha\Gamma_i(\mathrm{x}_2)\right] x_2^p = \tilde{\beta}\left[\gamma(\mathrm{x}_2)\delta_{i1}\mathrm{x}_2 - \langle u_i(\mathrm{x}_2)\rangle\right] \\ + \alpha\left[\Gamma_i(\mathrm{x}_2)\mathrm{x}_2 - \frac{\partial}{\partial \mathrm{x}_2}\langle u_2' u_i'\rangle(\mathrm{x}_2)\right] \\ - \tilde{\beta}u_i^{p\prime} - \alpha\left(\frac{D}{Ds}u_i^p\right)' - \theta g_i \end{aligned} \tag{8.17}$$

Equation (8.17) may be solved by the use of a Green tensor defined by

[1] Again this is not a limitation of the modelling framework here presented, but as discussed in chapter 7 it is possible to account for nonlinear variation in the fluid statistics along the particle paths, but this would lead to a semi-analytical closure model

$$\frac{d^2}{ds^2}G_{ij} - \tilde{\beta}\frac{d}{ds}G_{ij} + \left[\tilde{\beta}\gamma(\mathrm{x}_2)\delta_{i1} + \alpha\Gamma_i(\mathrm{x}_2)\right]G_{2j} = \delta_{ij}\delta(s - s_1) \tag{8.18}$$

and the solution to equation (8.17) with initial condition $\boldsymbol{x}^p(0) = \mathbf{x}$ is then given by

$$\begin{aligned} x_i^p(s) = \mathrm{x}_i - G_{ij}(s)v_j^p(0) &+ \tilde{\beta}\int_s^0 G_{ij}(s-s_1)\left[\gamma(\mathrm{x}_2)\delta_{j1}\delta_{m2}\mathrm{x}_m - \langle u_j(\mathrm{x}_2)\rangle - u_j'(\boldsymbol{x}^p(s_1),s_1)\right]ds_1 \\ &+ \alpha\int_s^0 G_{ij}(s-s_1)\left[\Gamma_j(\mathrm{x}_2)\delta_{m2}\mathrm{x}_m - \frac{\partial}{\partial \mathrm{x}_2}\langle u_2'u_j'\rangle(\mathrm{x}_2) - \left(\frac{D}{Ds_1}u_j^p\right)'\right]ds_1 \\ &- \int_s^0 G_{ij}(s-s_1)\theta g_j ds_1 \end{aligned} \tag{8.19}$$

The mean of $\rho\left(\mathbf{x}', s|\mathbf{x}\right)$ can now be constructed from equation (8.19)

$$\begin{aligned} \left\langle x_i^p(s)\right\rangle_{\mathbf{x}} =& \mathrm{x}_i - G_{ij}(s)\left\langle v_j^p(0)\right\rangle_{\mathbf{x}} \\ &+ \tilde{\beta}\int_s^0 G_{ij}(s-s_1)\left[\gamma(\mathrm{x}_2)\delta_{j1}\delta_{m2}\mathrm{x}_m - \langle u_j(\mathrm{x}_2)\rangle - \left\langle u_j'(\boldsymbol{x}^p(s_1),s_1)\right\rangle_{\mathbf{x}}\right]ds_1 \\ &+ \alpha\int_s^0 G_{ij}(s-s_1)\left[\Gamma_j(\mathrm{x}_2)\delta_{m2}\mathrm{x}_m - \frac{\partial}{\partial \mathrm{x}_2}\langle u_2'u_j'\rangle(\mathrm{x}_2) - \left\langle\left(\frac{D}{Ds_1}u_j(\boldsymbol{x}^p(s_1),s_1)\right)'\right\rangle_{\mathbf{x}}\right]ds_1 \\ &- \int_s^0 G_{ij}(s-s_1)\theta g_j ds_1 \end{aligned} \tag{8.20}$$

The treatment of the mean particle velocities and the closure of

$$\left\langle u_j'(\boldsymbol{x}^p(s_1),s_1)\right\rangle_{\mathbf{x}}$$

have been discussed in section 7.3 with the simplest approximation being

$$\left\langle u_j'(\boldsymbol{x}^p(s_1),s_1)\right\rangle_{\mathbf{x}} \approx \left\langle u_j'(\boldsymbol{x}^p(0),0)\right\rangle_{\mathbf{x}} \approx \left\langle u_j'(\mathbf{x},0)\right\rangle = 0 \tag{8.21}$$

The new drift term due to added mass requiring closure is

$$\left\langle \left(\frac{D}{Ds_1} u_j(\boldsymbol{x}^p(s_1), s_1) \right)' \right\rangle_{\mathbf{x}}$$

which is given by (for steady state channel flow)

$$\left\langle \left(\frac{D}{Ds_1} u_j(\boldsymbol{x}^p(s_1), s_1) \right)' \right\rangle_{\mathbf{x}} = \left\langle \frac{\partial}{\partial s_1} u_j^{p\prime} + \langle u_k \rangle^p \frac{\partial}{\partial \mathrm{x}_k} u_j^{p\prime} + u_k^{p\prime} \frac{\partial}{\partial \mathrm{x}_k} \langle u_j \rangle^p + \frac{\partial}{\partial \mathrm{x}_k} u_k^{p\prime} u_j^{p\prime} - \frac{\partial}{\partial \mathrm{x}_k} \langle u_k' u_j' \rangle^p \right\rangle_{\mathbf{x}} \tag{8.22}$$

This is the average value of the fluctuating fluid accelerations measured at time s_1 along particle paths which satisfy $\boldsymbol{x}^p(0) = \mathbf{x}$. In a turbulent boundary layer this strongly non-local drift is non-zero even for fluid tracers (except at $s_1 = s = 0$) owing to the inhomogeneity of the turbulence, and its complexity is enhanced for inertial particles since they preferentially sample the turbulent flow field in a boundary layer. It is zero only in the limit $\tau_p \to \infty$. However there is no simple way to approximate the terms in equation (8.22), and therefore as a first approximation this drift is set to zero

$$\left\langle \left(\frac{D}{Ds_1} u_j(\boldsymbol{x}^p(s_1), s_1) \right)' \right\rangle_{\mathbf{x}} \approx 0 \tag{8.23}$$

The implications of this approximation may be assessed when the closure model is tested against equivalent particle tracking data. The components of $\left\langle \boldsymbol{x}^p(s) \right\rangle_{\mathbf{x}}$ are then given by

$$\begin{aligned} \left\langle x_1^p(s) \right\rangle_{\mathbf{x}} =& \mathrm{x}_1 - G_{11}(s)\overline{\mathrm{v}}_1(\mathrm{x}_2) + C_{11}(s) \left[\tilde{\beta}\gamma(\mathrm{x}_2)\mathrm{x}_2 - \tilde{\beta}\langle u_1(\mathrm{x}_2) \rangle + \alpha\Gamma_1(\mathrm{x}_2)\mathrm{x}_2 - \alpha \frac{\partial}{\partial \mathrm{x}_2} \langle u_2' u_1' \rangle(\mathrm{x}_2) \right] \\ &+ C_{12}(s) \left[\alpha\Gamma_2(\mathrm{x}_2)\mathrm{x}_2 - \alpha \frac{\partial}{\partial \mathrm{x}_2} \langle u_2' u_2' \rangle(\mathrm{x}_2) - \theta g_2 \right] \end{aligned} \tag{8.24}$$

$$\left\langle x_2^p(s) \right\rangle_{\mathbf{x}} = \mathrm{x}_2 + C_{22}(s) \left[\alpha\Gamma_2(\mathrm{x}_2)\mathrm{x}_2 - \alpha \frac{\partial}{\partial \mathrm{x}_2} \langle u_2' u_2' \rangle(\mathrm{x}_2) - \theta g_2 \right] \tag{8.25}$$

$$\left\langle x_3^p(s) \right\rangle_{\mathbf{x}} = \mathrm{x}_3 + C_{33}(s) \left[\alpha\Gamma_3(\mathrm{x}_2)\mathrm{x}_2 - \alpha \frac{\partial}{\partial \mathrm{x}_2} \langle u_2' u_3' \rangle(\mathrm{x}_2) \right] \tag{8.26}$$

where

$$G_{11}(s) = G_{33}(s) = \frac{1}{\tilde{\beta}}\left(1 - \exp[\tilde{\beta}s]\right) \tag{8.27}$$

$$G_{12}(s) = \frac{b_1}{\tilde{\beta}b_2b_3}\left(\exp[-b_5 s] - \exp[-b_4 s] - b_3\left(1 - \exp[\tilde{\beta}s]\right)\right) \tag{8.28}$$

$$G_{22}(s) = \frac{1}{\tilde{\beta}b_3}\left(\exp[-b_5 s] - \exp[-b_4 s]\right) \tag{8.29}$$

and

$$C_{11}(s) = \int_s^0 G_{11}(s - s_1)ds_1 = -\frac{1}{\tilde{\beta}}[s + G_{11}(s)] \tag{8.30}$$

$$C_{12}(s) = \int_s^0 G_{12}(s - s_1)ds_1 = \frac{b_1}{\tilde{\beta}b_2b_3}\left[\frac{1}{b_5}\left(e^{-b_5 s} - 1\right) + \frac{1}{b_4}\left(1 - e^{-b_4 s}\right) + b_3\left(s + G_{11}(s)\right)\right] \tag{8.31}$$

$$C_{22}(s) = \int_s^0 G_{22}(s - s_1)ds_1 = \frac{1}{\tilde{\beta}b_3}\left[\frac{1}{b_4}\left(1 - e^{-b_4 s}\right) - \frac{1}{b_5}\left(1 - e^{-b_5 s}\right)\right] \tag{8.32}$$

$$C_{33}(s) = \int_s^0 G_{33}(s - s_1)ds_1 = C_{11}(s) \tag{8.33}$$

$$b_1 = \tilde{\beta}\gamma + \alpha\Gamma_1 \tag{8.34}$$

$$b_2 = \alpha\Gamma_2 \tag{8.35}$$

$$b_3 = \sqrt{1 + \left(\frac{4\alpha}{\tilde{\beta}}\right)^2 \Gamma_2} \tag{8.36}$$

$$b_4 = -\frac{\tilde{\beta}}{2}(1 + b_3) \tag{8.37}$$

$$b_5 = -\frac{\tilde{\beta}}{2}(1 - b_3) \tag{8.38}$$

Since $\mathbf{\Gamma}$ will be negative for certain regions in a turbulent boundary layer, it is therefore possible that b_3 can take on complex values. This result is unfortunately unavoidable, and to avoid its unphysical implications the approximation $b_3 \approx 1$ shall be henceforth adopted. With a Gaussian PDF for $\rho(\mathbf{x}', s|\mathbf{x})$ (see chapter 7) the only other moment required is the second central moment, which is constructed from equation (8.19)

$$
\begin{aligned}
\left\langle \tilde{x}_i^p(s)\tilde{x}_k^p(s)\right\rangle_{\mathbf{x}} =& G_{ij}(s)\left\langle v_j^{p\prime}(0)v_m^{p\prime}(0)\right\rangle_{\mathbf{x}} G_{km}(s) \\
&+ \tilde{\beta}G_{ij}(s)\int_s^0 G_{km}(s-s_1)\left\langle v_j^{p\prime}(0)u_m'(\boldsymbol{x}^p(s_1),s_1)\right\rangle_{\mathbf{x}} ds_1 \\
&+ \tilde{\beta}G_{km}(s)\int_s^0 G_{ij}(s-s_1)\left\langle u_j'(\boldsymbol{x}^p(s_1),s_1)v_m^{p\prime}(0)\right\rangle_{\mathbf{x}} ds_1 \\
&+ \alpha G_{ij}(s)\int_s^0 G_{km}(s-s_1)\left\langle v_j^{p\prime}(0)\left(\frac{D}{Ds_1}u_m(\boldsymbol{x}^p(s_1),s_1)\right)'\right\rangle_{\mathbf{x}} ds_1 \\
&+ \alpha G_{km}(s)\int_s^0 G_{ij}(s-s_1)\left\langle \left(\frac{D}{Ds_1}u_j(\boldsymbol{x}^p(s_1),s_1)\right)' v_m^{p\prime}(0)\right\rangle_{\mathbf{x}} ds_1 \\
&+ \alpha\tilde{\beta}\int_s^0\int_s^0 G_{ij}(s-s_1)\left\langle u_j'(\boldsymbol{x}^p(s_1),s_1)\left(\frac{D}{Ds_2}u_m(\boldsymbol{x}^p(s_2),s_2)\right)'\right\rangle_{\mathbf{x}} G_{km}(s-s_2)ds_1ds_2 \\
&+ \alpha\tilde{\beta}\int_s^0\int_s^0 G_{ij}(s-s_1)\left\langle \left(\frac{D}{Ds_1}u_j(\boldsymbol{x}^p(s_1),s_1)\right)' u_m'(\boldsymbol{x}^p(s_2),s_2)\right\rangle_{\mathbf{x}} G_{km}(s-s_2)ds_1ds_2 \\
&+ (\tilde{\beta})^2\int_s^0\int_s^0 G_{ij}(s-s_1)\left\langle u_j'(\boldsymbol{x}^p(s_1),s_1)u_m'(\boldsymbol{x}^p(s_2),s_2)\right\rangle_{\mathbf{x}} G_{km}(s-s_2)ds_1ds_2 \\
&+ \alpha^2\int_s^0\int_s^0 G_{ij}(s-s_1)\left\langle \left(\frac{D}{Ds_1}u_j(\boldsymbol{x}^p(s_1),s_1)\right)'\left(\frac{D}{Ds_2}u_m(\boldsymbol{x}^p(s_2),s_2)\right)'\right\rangle_{\mathbf{x}} G_{km}(s-s_2)ds_1ds_2
\end{aligned}
\tag{8.39}
$$

with

$$\tilde{\boldsymbol{x}}^p(s) = \boldsymbol{x}^p(s) - \left\langle \boldsymbol{x}^p(s)\right\rangle_{\mathbf{x}}$$

The treatment of the terms

$$\left\langle v_j^{p\prime}(0)v_m^{p\prime}(0)\right\rangle_{\mathbf{x}}$$

$$\left\langle v_j^{p\prime}(0)u_m'(\boldsymbol{x}^p(s_1),s_1)\right\rangle_{\mathbf{x}}$$

and

$$\left\langle u_j'(\boldsymbol{x}^p(s_1),s_1)u_m'(\boldsymbol{x}^p(s_2),s_2)\right\rangle_{\mathbf{x}}$$

has been discussed in chapter 7 and will not be repeated here, except to say that in the present closure model the approximations should account for the effects of added mass and gravity in addition to drag. That is, since these terms are closed using a local approximation to $\overline{\boldsymbol{\mu}}$ (see chapter 7), the local approximation to $\overline{\boldsymbol{\mu}}$ must now include the effects of added mass and gravity, and the required form is found in [110]. The

additional terms requiring closure are those involving the fluctuating fluid acceleration. Since the fluid velocity and fluid acceleration are kinematically related to one another it is possible to exploit this fact in order to relate the new unknown terms involving the fluctuating fluid acceleration to those involving the the fluctuating fluid velocity (e.g. [129]). Consider the autocovariance

$$\left\langle v_j^{p\prime}(0)u_m'(\boldsymbol{x}^p(s_1),s_1)\right\rangle_{\mathbf{x}}$$

Differentiating this with respect to s_1 gives (noting that the conditionality is not a function of either s or s_1)

$$\frac{d}{ds_1}\left\langle v_j^{p\prime}(0)u_m'(\boldsymbol{x}^p(s_1),s_1)\right\rangle_{\mathbf{x}} = \left\langle v_j^{p\prime}(0)\frac{d}{ds_1}u_m'(\boldsymbol{x}^p(s_1),s_1)\right\rangle_{\mathbf{x}} \tag{8.40}$$

Unfortunately

$$\left\langle v_j^{p\prime}(0)\frac{d}{ds_1}u_m'(\boldsymbol{x}^p(s_1),s_1)\right\rangle_{\mathbf{x}} \neq \left\langle v_j^{p\prime}(0)\left(\frac{D}{Ds_1}u_m(\boldsymbol{x}^p(s_1),s_1)\right)'\right\rangle_{\mathbf{x}} \tag{8.41}$$

Indeed

$$\left(\frac{D}{Ds_1}u_m\right)' = \frac{D}{Ds_1}u_m - \left\langle\frac{D}{Ds_1}u_m\right\rangle$$

so, for turbulent channel flow,

$$\left(\frac{D}{Ds_1}u_m(\boldsymbol{x}^p(s_1),s_1)\right)' = \frac{\partial}{\partial s_1}u_m^{p\prime} + u_2^{p\prime}\frac{\partial}{\partial \mathrm{x}_2}\langle u_m\rangle^p + u_n^{p\prime}\frac{\partial}{\partial \mathrm{x}_n}u_m^{p\prime} - \frac{\partial}{\partial \mathrm{x}_2}\langle u_2'u_m'\rangle^p \tag{8.42}$$

Whereas, in contrast,

$$\frac{d}{ds_1}u_m'(\boldsymbol{x}^p(s_1),s_1) = \frac{\partial}{\partial s_1}u_m^{p\prime} + v_n^p(s_1)\frac{\partial}{\partial \mathrm{x}_n}u_m^{p\prime} \tag{8.43}$$

Equations (8.42) and (8.43) are only equal in the limit $\tau_p \to 0$ in homogeneous turbulence with zero mean velocity. As a first step equations (8.42) and (8.43) will be assumed equal in the closure model so that the additional unknown autocovariances in equation (8.39) involving the fluctuating fluid acceleration can be approximately related to those involving the fluctuating fluid velocity as

$$\left\langle v_j^{p\prime}(0)\left(\frac{D}{Ds_1}u_m(\boldsymbol{x}^p(s_1),s_1)\right)'\right\rangle_{\mathbf{x}} \approx \frac{d}{ds_1}\left\langle v_j^{p\prime}(0)u_m'(\boldsymbol{x}^p(s_1),s_1)\right\rangle_{\mathbf{x}} \tag{8.44}$$

$$\left\langle \left(\frac{D}{Ds_1}u_j(\boldsymbol{x}^p(s_1),s_1)\right)' v_i^{p\prime}(0)\right\rangle_{\mathbf{x}} \approx \frac{d}{ds_1}\left\langle u_j'(\boldsymbol{x}^p(s_1),s_1)v_i^{p\prime}(0)\right\rangle_{\mathbf{x}} \tag{8.45}$$

$$\left\langle u_j'(\boldsymbol{x}^p(s_1),s_1)\left(\frac{D}{Ds_2}u_m(\boldsymbol{x}^p(s_2),s_2)\right)'\right\rangle_{\mathbf{x}} \approx \frac{d}{ds_2}\left\langle u_j'(\boldsymbol{x}^p(s_1),s_1)u_m'(\boldsymbol{x}^p(s_2),s_2)\right\rangle_{\mathbf{x}} \tag{8.46}$$

$$\left\langle \left(\frac{D}{Ds_1}u_j(\boldsymbol{x}^p(s_1),s_1)\right)' u_m'(\boldsymbol{x}^p(s_2),s_2)\right\rangle_{\mathbf{x}} \approx \frac{d}{ds_1}\left\langle u_j'(\boldsymbol{x}^p(s_1),s_1)u_m'(\boldsymbol{x}^p(s_2),s_2)\right\rangle_{\mathbf{x}} \tag{8.47}$$

$$\left\langle \left(\frac{D}{Ds_1}u_j(\boldsymbol{x}^p(s_1),s_1)\right)'\left(\frac{D}{Ds_2}u_m(\boldsymbol{x}^p(s_2),s_2)\right)'\right\rangle_{\mathbf{x}} \approx \frac{d}{ds_1}\frac{d}{ds_2}\left\langle u_j'(\boldsymbol{x}^p(s_1),s_1)u_m'(\boldsymbol{x}^p(s_2),s_2)\right\rangle_{\mathbf{x}} \tag{8.48}$$

For future work it is noted that it is possible to account for the difference between equations (8.42) and (8.43) so that the autocovariances involving the fluctuating fluid acceleration could be modelled using equation (8.40) with some additional terms. For example, consider the autocovariances

$$\begin{aligned}\left\langle v_j^{p\prime}(0)\left(\frac{D}{Ds_1}u_m(\boldsymbol{x}^p(s_1),s_1)\right)'\right\rangle_{\mathbf{x}} =& \left\langle v_j^{p\prime}(0)\frac{\partial}{\partial s_1}u_m'(\boldsymbol{x}^p(s_1),s_1)\right\rangle_{\mathbf{x}} \\ &+ \left\langle v_j^{p\prime}(0)u_2'(\boldsymbol{x}^p(s_1),s_1)\frac{\partial}{\partial \mathrm{x}_2}\langle u_m\rangle(\boldsymbol{x}^p(s_1),s_1)\right\rangle_{\mathbf{x}} \\ &+ \left\langle v_j^{p\prime}(0)u_n'(\boldsymbol{x}^p(s_1),s_1)\frac{\partial}{\partial \mathrm{x}_n}u_m'(\boldsymbol{x}^p(s_1),s_1)\right\rangle_{\mathbf{x}} \\ &- \left\langle v_j^{p\prime}(0)\frac{\partial}{\partial \mathrm{x}_2}\langle u_2'u_m'\rangle(\boldsymbol{x}^p(s_1),s_1)\right\rangle_{\mathbf{x}}\end{aligned} \tag{8.49}$$

$$\begin{aligned}\left\langle v_j^{p\prime}(0)\frac{d}{ds_1}u_m'(\boldsymbol{x}^p(s_1),s_1)\right\rangle_{\mathbf{x}} =& \left\langle v_j^{p\prime}(0)\frac{\partial}{\partial s_1}u_m'(\boldsymbol{x}^p(s_1),s_1)\right\rangle_{\mathbf{x}} \\ &+ \left\langle v_j^{p\prime}(0)v_n^p(s_1)\frac{\partial}{\partial \mathrm{x}_n}u_m'(\boldsymbol{x}^p(s_1),s_1)\right\rangle_{\mathbf{x}}\end{aligned} \tag{8.50}$$

Now consider the terms that differ between equations (8.49) and (8.50). Under the locally linear approximations used in the closure model for the mean fluid velocity and the gradient of the fluid Reynolds stresses (see equations (8.14) and (8.15))

$$\left\langle v_j^{p\prime}(0)u_2'(\boldsymbol{x}^p(s_1),s_1)\frac{\partial}{\partial \mathrm{x}_2}\langle u_m\rangle(\boldsymbol{x}^p(s_1),s_1)\right\rangle_{\mathbf{x}} = \left\langle v_j^{p\prime}(0)u_2'(\boldsymbol{x}^p(s_1),s_1)\right\rangle_{\mathbf{x}}\gamma(\mathrm{x}_2)\delta_{m1} \tag{8.51}$$

$$\left\langle v_j^{p\prime}(0)\frac{\partial}{\partial \mathrm{x}_2}\langle u_2'u_m'\rangle(\boldsymbol{x}^p(s_1),s_1)\right\rangle_{\mathbf{x}} = \left\langle v_j^{p\prime}(0)\right\rangle_{\mathbf{x}}\Gamma_m(\mathrm{x}_2) = 0 \tag{8.52}$$

The only remaining discrepancy between equations (8.49) and (8.50) to be dealt with is that

$$\left\langle v_j^{p\prime}(0)v_n^p(s_1)\frac{\partial}{\partial \mathrm{x}_n}u_m'(\boldsymbol{x}^p(s_1),s_1)\right\rangle_{\mathbf{x}} \neq \left\langle v_j^{p\prime}(0)u_n'(\boldsymbol{x}^p(s_1),s_1)\frac{\partial}{\partial \mathrm{x}_n}u_m'(\boldsymbol{x}^p(s_1),s_1)\right\rangle_{\mathbf{x}} \tag{8.53}$$

the source of the discrepancy being that $v_n^p(s_1) \neq u_n'(\boldsymbol{x}^p(s_1),s_1)$. Suppose that the approximation $v_n^{p\prime}(s_1) \approx u_n'(\boldsymbol{x}^p(s_1),s_1)$ can be made (of course this is only strictly valid for $\tau_p \to 0$) then the remaining source of discrepancy is

$$\left\langle v_j^{p\prime}(0)\overline{\mathrm{v}}_n(\boldsymbol{x}^p(s_1),s_1)\frac{\partial}{\partial \mathrm{x}_n}u_m'(\boldsymbol{x}^p(s_1),s_1)\right\rangle_{\mathbf{x}}$$

For statistically stationary turbulent channel flow, with elastic particle-wall collisions this reduces to

$$\left\langle v_j^{p\prime}(0)\overline{\mathrm{v}}_1(\boldsymbol{x}^p(s_1),s_1)\frac{\partial}{\partial \mathrm{x}_1}u_m'(\boldsymbol{x}^p(s_1),s_1)\right\rangle_{\mathbf{x}}$$

If the approximation is then made that $\overline{\mathrm{v}}_1(\boldsymbol{x}^p(s_1),s_1) \approx \overline{\mathrm{v}}_1(\boldsymbol{x}^p(0),0) = \overline{\mathrm{v}}_1(\mathrm{x}_2)$ then

$$\begin{aligned}\left\langle v_j^{p\prime}(0)\overline{\mathrm{v}}_1(\boldsymbol{x}^p(s_1),s_1)\frac{\partial}{\partial \mathrm{x}_1}u_m'(\boldsymbol{x}^p(s_1),s_1)\right\rangle_{\mathbf{x}} &\approx \left\langle v_j^{p\prime}(0)\overline{\mathrm{v}}_1(\mathrm{x}_2)\frac{\partial}{\partial \mathrm{x}_1}u_m'(\boldsymbol{x}^p(s_1),s_1)\right\rangle_{\mathbf{x}} \\ &= \overline{\mathrm{v}}_1(\mathrm{x}_2)\left\langle \frac{\partial}{\partial \mathrm{x}_1}v_j^{p\prime}(0)u_m'(\boldsymbol{x}^p(s_1),s_1)\right\rangle_{\mathbf{x}} \\ &\approx \overline{\mathrm{v}}_1(\mathrm{x}_2)\frac{\partial}{\partial \mathrm{x}_1}\left\langle v_j^{p\prime}(0)u_m'(\boldsymbol{x}^p(s_1),s_1)\right\rangle_{\mathbf{x}} \\ &= 0\end{aligned} \tag{8.54}$$

Therefore rather than using the approximation

$$\left\langle v_j^{p\prime}(0)\left(\frac{D}{Ds_1}u_m(\boldsymbol{x}^p(s_1),s_1)\right)'\right\rangle_{\mathbf{x}} \approx \frac{d}{ds_1}\left\langle v_j^{p\prime}(0)u_m'(\boldsymbol{x}^p(s_1),s_1)\right\rangle_{\mathbf{x}}$$

a better approximation is

$$\left\langle v_j^{p\prime}(0)\left(\frac{D}{Ds_1}u_m(\boldsymbol{x}^p(s_1),s_1)\right)'\right\rangle_{\mathbf{x}} \approx \frac{d}{ds_1}\left\langle v_j^{p\prime}(0)u_m'(\boldsymbol{x}^p(s_1),s_1)\right\rangle_{\mathbf{x}} + \left\langle v_j^{p\prime}(0)u_2'(\boldsymbol{x}^p(s_1),s_1)\right\rangle_{\mathbf{x}}\gamma(\mathrm{x}_2)\delta_{m1} \tag{8.55}$$

where the closure of $\left\langle \boldsymbol{v}^{p\prime}(0)\boldsymbol{u}'(\boldsymbol{x}^p(s_1),s_1)\right\rangle_{\mathbf{x}}$ has been discussed in chapter 7. Similar ideas can be used to close terms in equation (8.39) involving a single acceleration term, such as

$$\left\langle u_j'(\boldsymbol{x}^p(s_1),s_1)\left(\frac{D}{Ds_2}u_m(\boldsymbol{x}^p(s_2),s_2)\right)'\right\rangle_{\mathbf{x}}$$

however similar approximation methodologies for the fluctuating acceleration autocovariance

$$\left\langle \left(\frac{D}{Ds_1}u_j(\boldsymbol{x}^p(s_1),s_1)\right)'\left(\frac{D}{Ds_2}u_m(\boldsymbol{x}^p(s_2),s_2)\right)'\right\rangle_{\mathbf{x}}$$

are more complex. Therefore, more comprehensive approximations such as in equation (8.55) are left to future work. Testing the closure model against simulation data will reveal whether more comprehensive approximations such as in equation (8.55) are required (although for testing against the KS flow field described in chapter 7 there would be no difference if $\langle \boldsymbol{u}\rangle = \mathbf{0}$).

It is also noted that under the local approximation for $\left\langle u_j'(\boldsymbol{x}^p(s_1),s_1)u_m'(\boldsymbol{x}^p(s_2),s_2)\right\rangle_{\mathbf{x}}$ used in the closure model (see chapter 7)

$$\frac{d}{ds_2}\left\langle u_j'(\boldsymbol{x}^p(s_1),s_1)u_m'(\boldsymbol{x}^p(s_2),s_2)\right\rangle_{\mathbf{x}} + \frac{d}{ds_1}\left\langle u_j'(\boldsymbol{x}^p(s_1),s_1)u_m'(\boldsymbol{x}^p(s_2),s_2)\right\rangle_{\mathbf{x}} = 0 \tag{8.56}$$

With these approximations equation (8.39) simplifies to

$$\begin{aligned}\left\langle \tilde{x}_i^p(s)\tilde{x}_k^p(s)\right\rangle_{\mathbf{x}} =& G_{ij}(s)\left\langle v_j^{p\prime}(0)v_m^{p\prime}(0)\right\rangle_{\mathbf{x}}G_{mk}(s)\\ &+ G_{ij}(s)\int_s^0 G_{mk}(s-s_1)\left[\tilde{\beta}+\alpha\frac{d}{ds_1}\right]\left\langle v_j^{p\prime}(0)u_m'(\boldsymbol{x}^p(s_1),s_1)\right\rangle_{\mathbf{x}}ds_1\\ &+ G_{km}(s)\int_s^0 G_{mj}(s-s_1)\left[\tilde{\beta}+\alpha\frac{d}{ds_1}\right]\left\langle u_j'(\boldsymbol{x}^p(s_1),s_1)v_i^{p\prime}(0)\right\rangle_{\mathbf{x}}ds_1\\ &+ \int_s^0\int_s^0 G_{ij}(s-s_1)\left[(\tilde{\beta})^2+\alpha^2\frac{d}{ds_1}\frac{d}{ds_2}\right]\left\langle u_j'(\boldsymbol{x}^p(s_1),s_1)u_m'(\boldsymbol{x}^p(s_2),s_2)\right\rangle_{\mathbf{x}}G_{mk}(s-s_2)ds_1ds_2\end{aligned} \tag{8.57}$$

where

$$\left[\tilde{\beta}+\alpha\frac{d}{ds_1}\right]\Big\langle v_j^{p\prime}(0)u_m'(\boldsymbol{x}^p(s_1),s_1)\Big\rangle_{\mathbf{x}}=\tilde{\beta}\Big\langle v_j^{p\prime}(0)u_m'(\boldsymbol{x}^p(s_1),s_1)\Big\rangle_{\mathbf{x}}+\alpha\frac{d}{ds_1}\Big\langle v_j^{p\prime}(0)u_m'(\boldsymbol{x}^p(s_1),s_1)\Big\rangle_{\mathbf{x}}$$

etc. As discussed in chapter 7 the approximations to

$$\Big\langle v_j^{p\prime}(0)u_m'(\boldsymbol{x}^p(s_1),s_1)\Big\rangle_{\mathbf{x}}$$

and

$$\Big\langle u_j'(\boldsymbol{x}^p(s_1),s_1)u_m'(\boldsymbol{x}^p(s_2),s_2)\Big\rangle_{\mathbf{x}}$$

involve an unknown timescale τ^{Lp}, which is the timescale of the fluid velocities seen by the inertial particles. In the present closure model the approximation used for this timescale should depend not only on drag but also the added mass and gravitational forces acting on the particles. However in the absence of any simple alternative, τ^{Lp} will still be approximated by the Wang & Stock curve fit function (see equation (7.34)) which only accounts for drag forcing, and does not take into account added mass or gravitational forcing on the particles. Nevertheless, as is clear from equations (8.20) and (8.39), the closure model accounts for drag, added mass and gravitational forcing, such that the correlation times in

$$\Big\langle R_{ji}(\boldsymbol{x}^p(s),s;\mathbf{x},0)\Big\rangle_{\mathbf{x}}$$

as predicted by the closure model *will* depend not only upon drag but also added mass and gravity, regardless of the approximation used for τ^{Lp} (although of course the approximation used for τ^{Lp} will quantitatively affect the predictions from the closure model).

The form chosen for the autocorrelations in the local approximations to

$$\Big\langle v_j^{p\prime}(0)u_m'(\boldsymbol{x}^p(s_1),s_1)\Big\rangle_{\mathbf{x}}$$

and

$$\Big\langle u_j'(\boldsymbol{x}^p(s_1),s_1)u_m'(\boldsymbol{x}^p(s_2),s_2)\Big\rangle_{\mathbf{x}}$$

(see chapter 7) will depend upon the nature of the flow field (this is discussed in appendix A). Then with the form of the autocorrelations chosen, equation (8.57) may be solved analytically as discussed in appendix A, and therefore an analytical model for $\rho\left(\mathbf{x}',s|\mathbf{x}\right)$ accounting for Stokes drag, added mass and gravity has been produced. In the absence of gravity and in the limit $\rho^p\gg\rho^f$ the closure model presented in this chapter reduces to that presented in chapter 7, which describes the closure for heavy particles

dispersing under a Stokes drag force.

Time constrainsts place the testing of the closure model presented in this chapter against equivalent PT data beyond the scope of the present work; but this test must be done in future work. However, it is nevertheless interesting to see how the closures presented in this chapter compare to the alternative local closures, and also to compare the results with those in chapter 7 to see what effect the additional added mass force has.

8.2 Model Results

The closure model presented in the previous section will now be compared to the alternative local approximations, and comparison will also be made to the results in chapter 7 in order to consider the effect of the additional added mass forcing on the dispersion tensors.

The closure model is once again tested for particles dispersing in the KS flow field presented in chapter 7 (the details of this test case is the same as that presented in section 7.4.3 (except that now the models account for added mass) and will therefore not be repeated here). In order to see the effect of the added mass force and for comparison with the results in chapter 7 gravity is absent in these initial results. Furthermore, the results in this section are for a fixed value of $St_E = 3$ and varying values of the ratio ρ^p/ρ^f in order to asses the effect of the added mass force contribution over a range of particle to fluid material density ratios. The final expressions for the closure model for $\rho(\mathbf{x}', s|\mathbf{x})$ and the local approximations to the dispersion tensors are given in appendix A.

The results in this section are for $\overline{\boldsymbol{\lambda}}^{dd}$, $\overline{\boldsymbol{\mu}}^{dd}$ and $\overline{\boldsymbol{\kappa}}^{dd}$ (see beginning of chapter 8). However, *for notational convenience, the superscripts 'dd' shall be dropped henceforth in this chapter.* The superscript 'CM' shall be used to denote the predictions given by the non-local closure model presented in section 8.1, whilst the superscript 'L' shall be used to denote the local approximation predictions.

Note that, as usual, the particles collide with the wall when their wall-normal position is one particle radius from the wall, where the particle radius is

$$\mathrm{x}_2^{min} = \sqrt{\frac{9\tau_p\rho^f}{2\rho^p}} \tag{8.58}$$

Therefore since the ratio ρ^p/ρ^f is varied in the results that follow, x_2^{min} also varies (quite significantly).

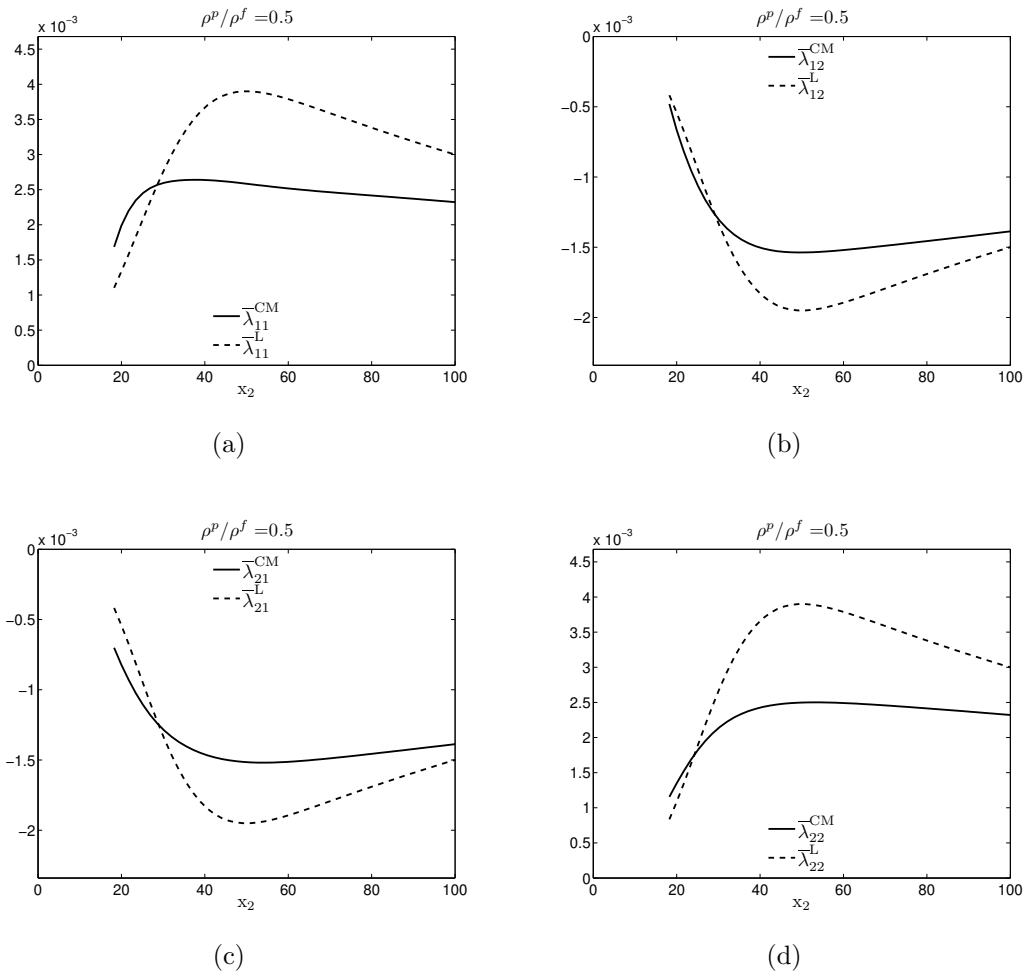

Figure 8.1: Comparison between closure model (CM) and the local approximation (L) for the components of $\overline{\boldsymbol{\lambda}}$ for $St_E = 3$, $\rho^p/\rho^f = 0.5$.

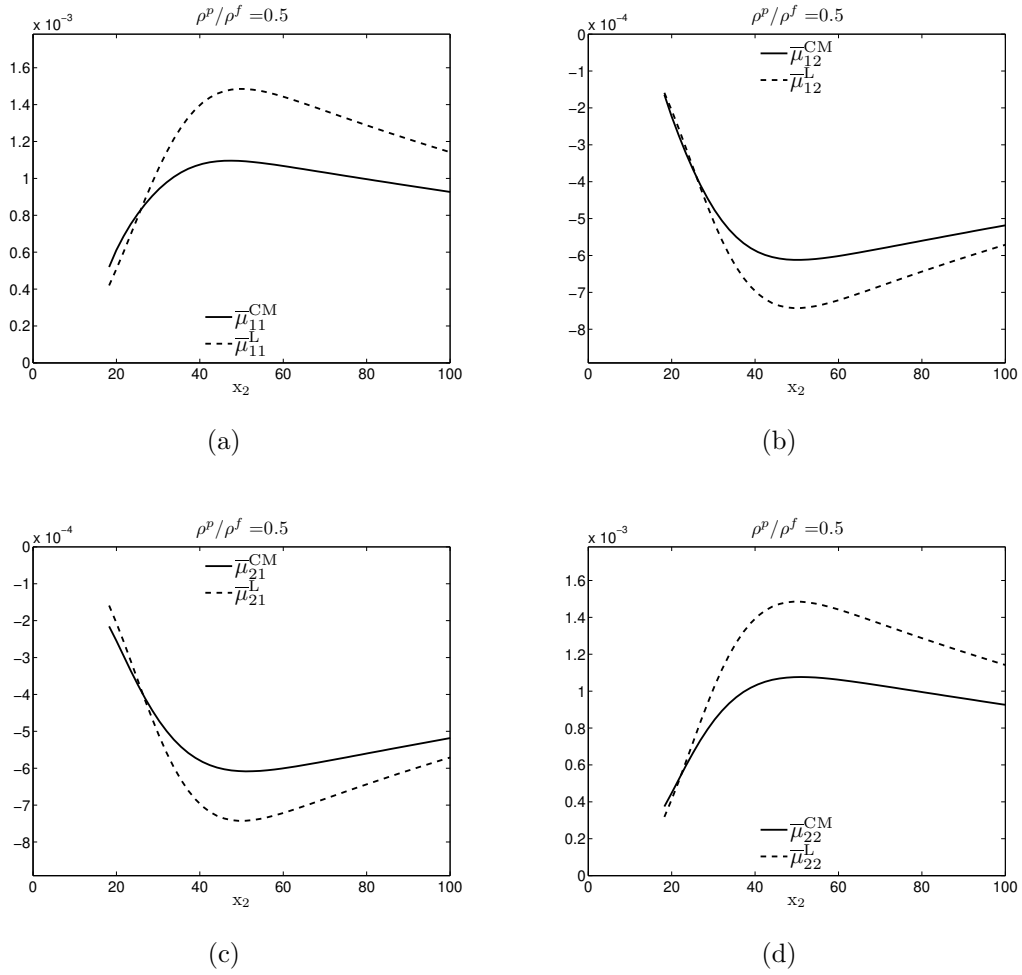

Figure 8.2: Comparison between closure model (CM) and the local approximation (L) for the components of $\overline{\boldsymbol{\mu}}$ for $St_E = 3$, $\rho^p/\rho^f = 0.5$.

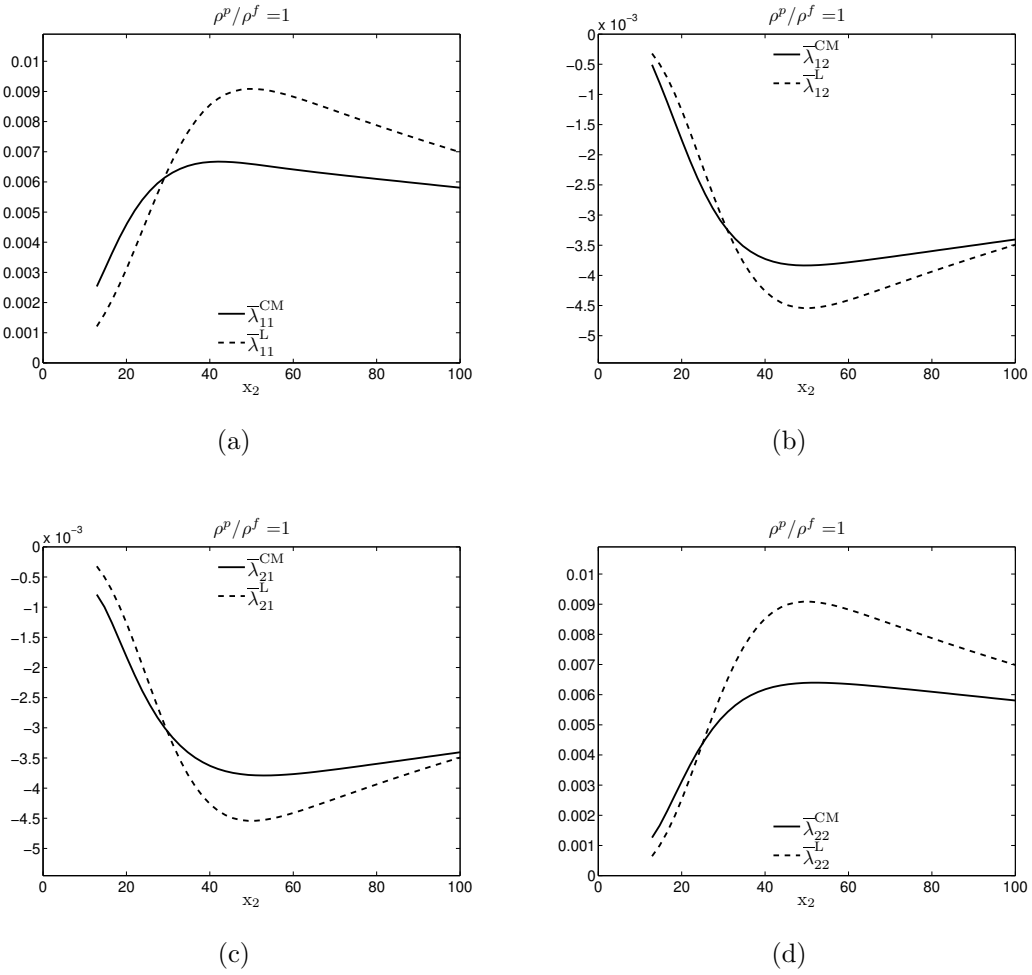

Figure 8.3: Comparison between closure model (CM) and the local approximation (L) for the components of $\overline{\boldsymbol{\lambda}}$ for $St_E = 3$, $\rho^p/\rho^f = 1$.

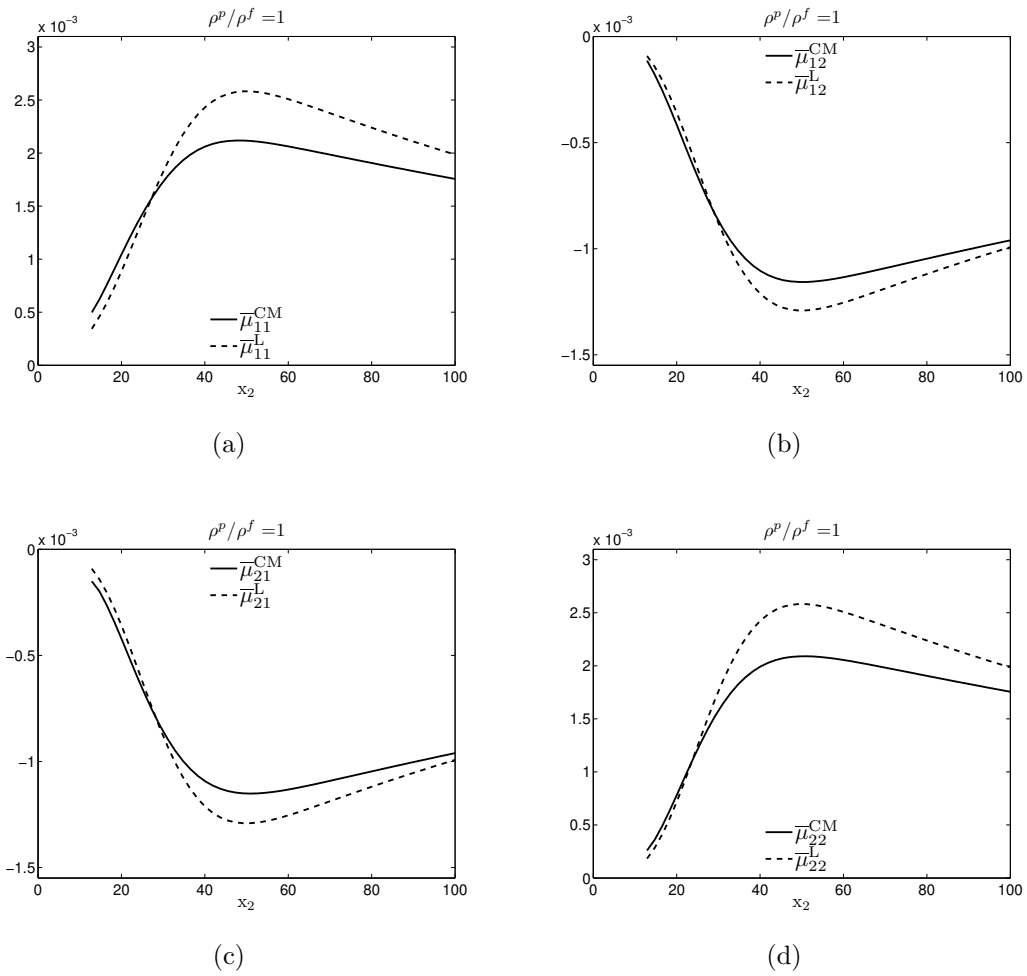

Figure 8.4: Comparison between closure model (CM) and the local approximation (L) for the components of $\overline{\boldsymbol{\mu}}$ for $St_E = 3$, $\rho^p/\rho^f = 1$.

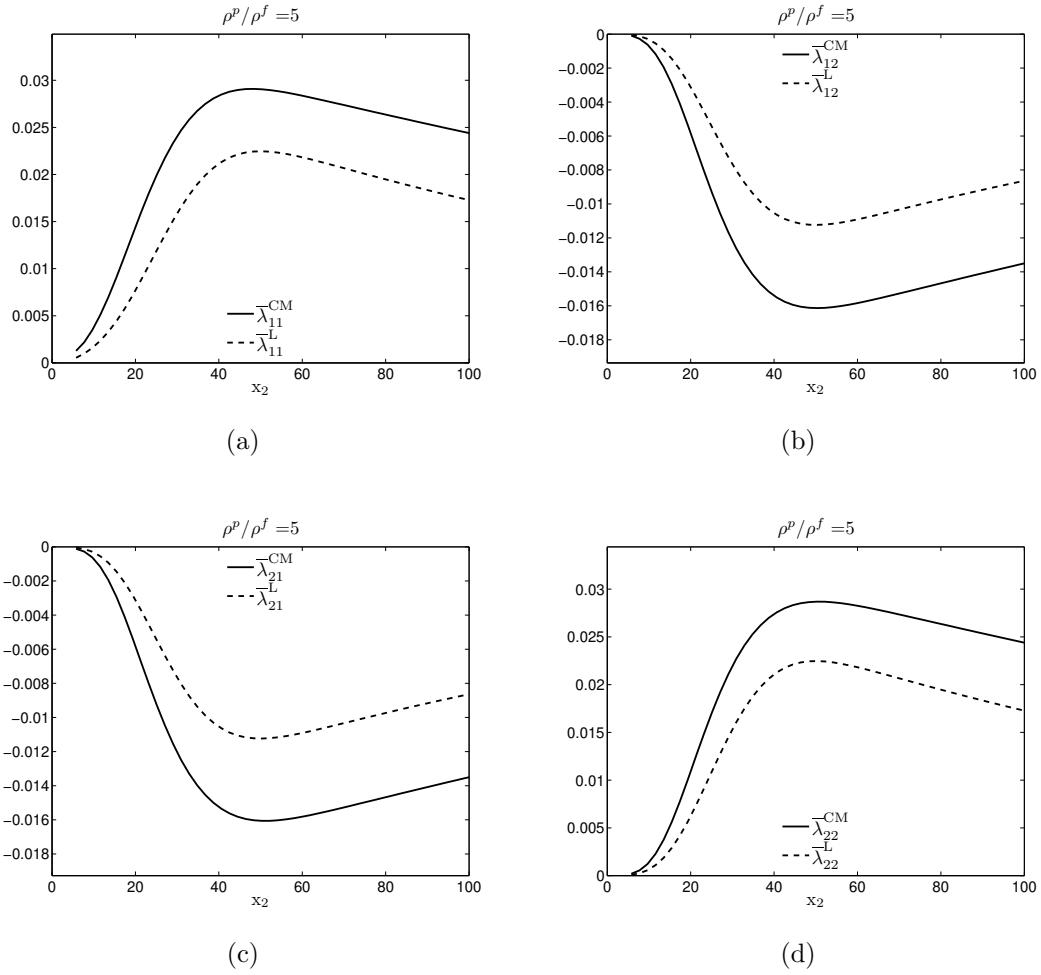

Figure 8.5: Comparison between closure model (CM) and the local approximation (L) for the components of $\overline{\boldsymbol{\lambda}}$ for $St_E = 3$, $\rho^p/\rho^f = 5$.

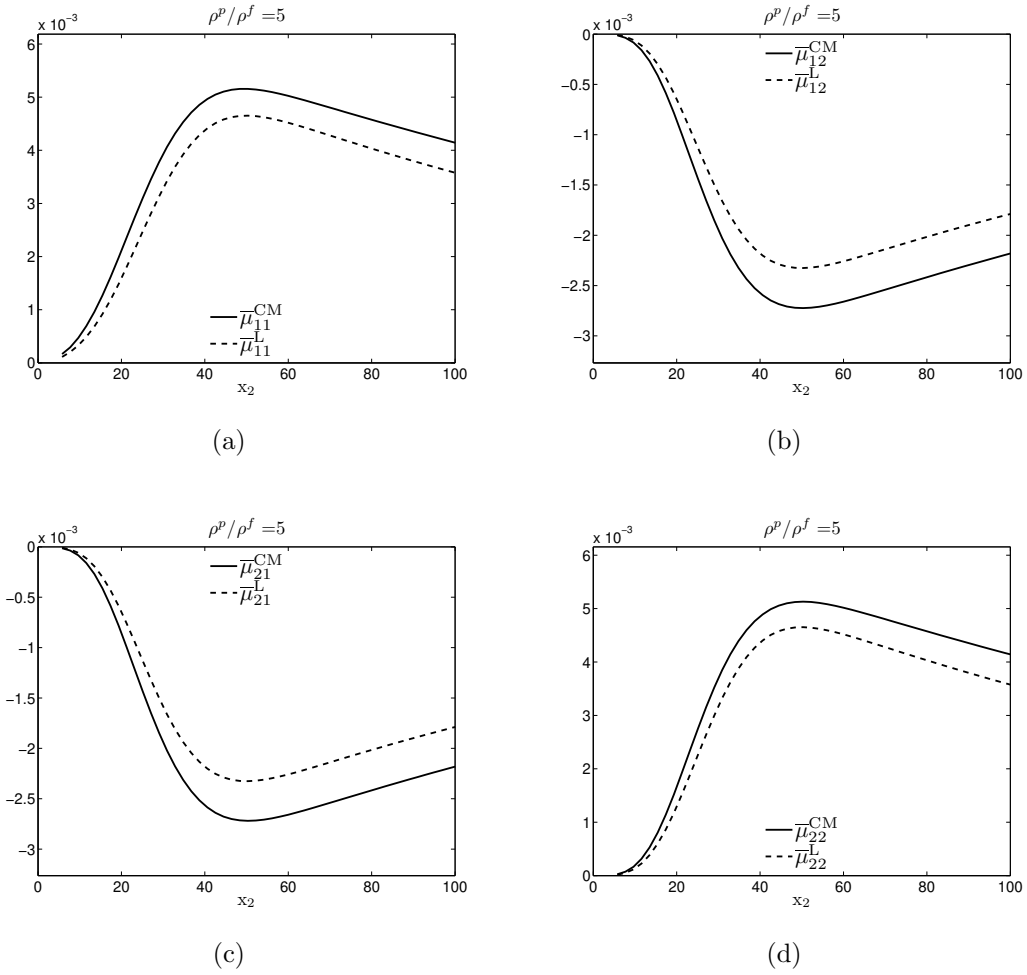

Figure 8.6: Comparison between closure model (CM) and the local approximation (L) for the components of $\overline{\boldsymbol{\mu}}$ for $St_E = 3$, $\rho^p/\rho^f = 5$.

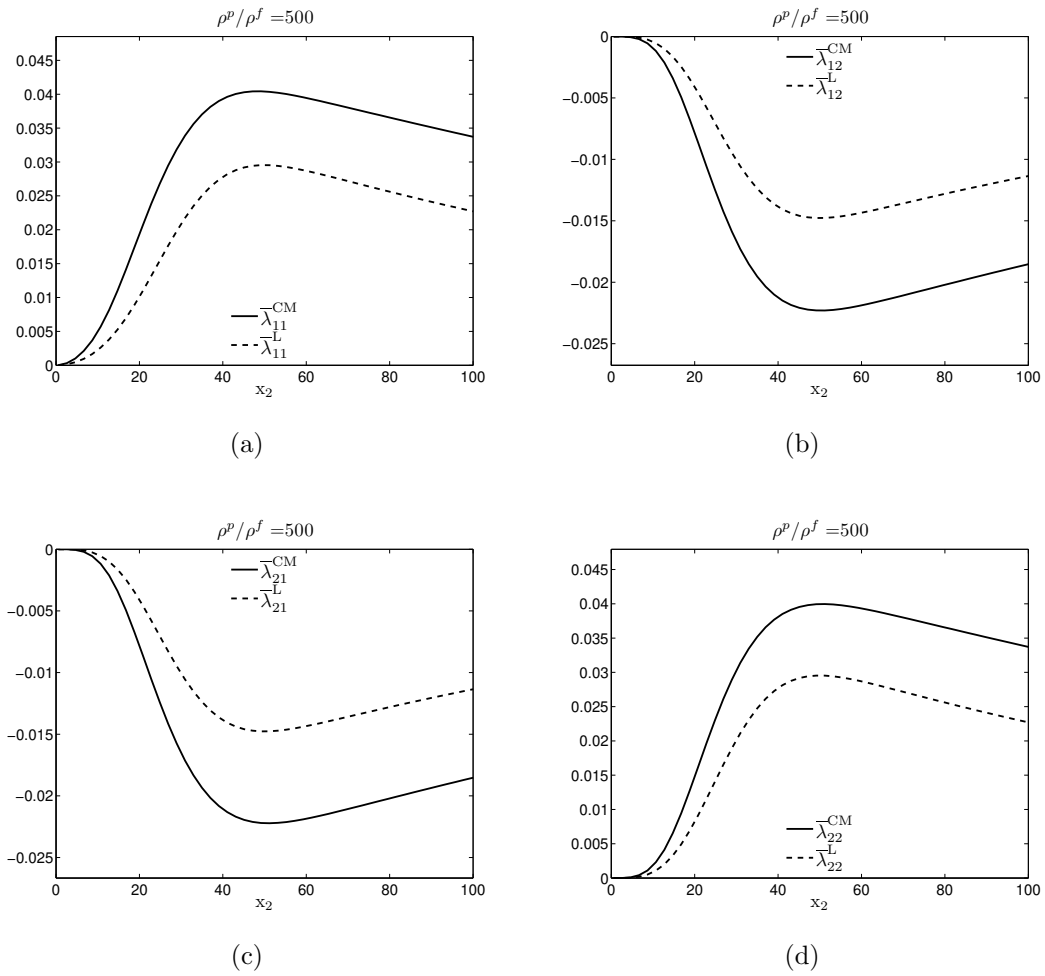

Figure 8.7: Comparison between closure model (CM) and the local approximation (L) for the components of $\overline{\boldsymbol{\lambda}}$ for $St_E = 3$, $\rho^p/\rho^f = 500$.

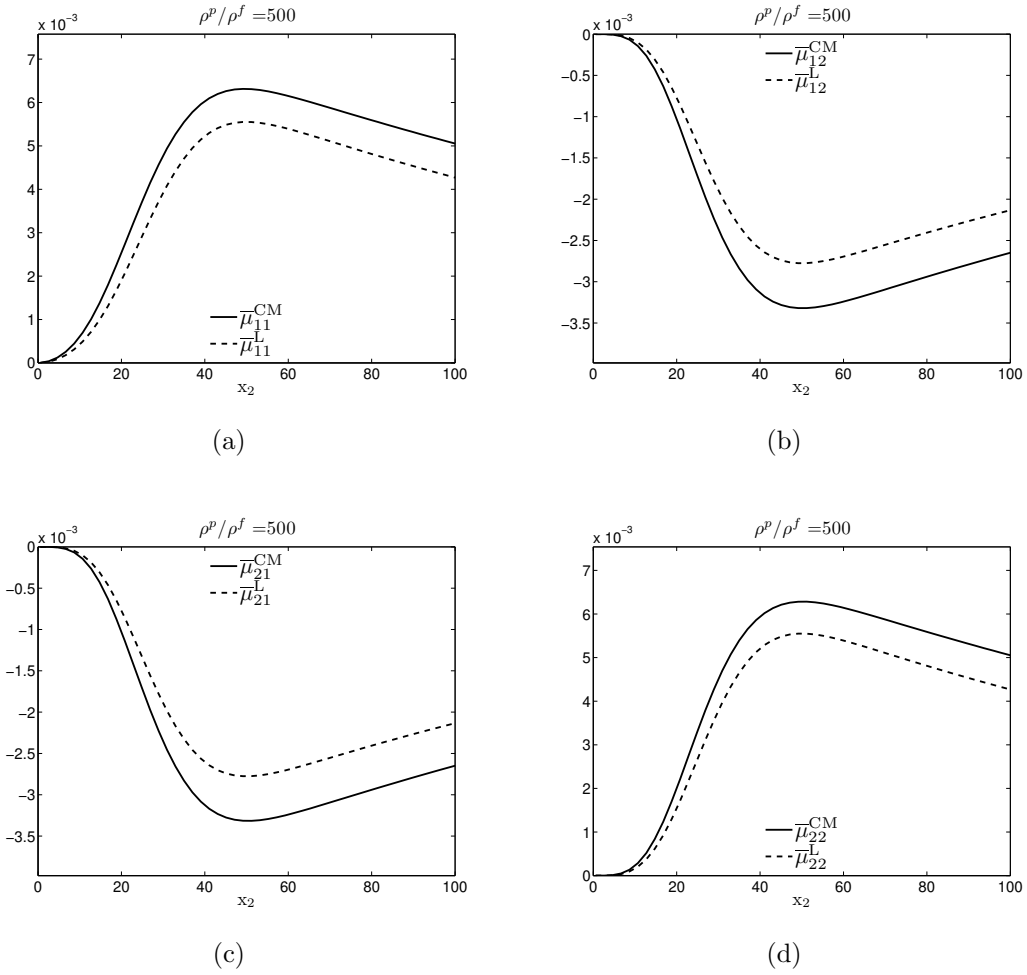

Figure 8.8: Comparison between closure model (CM) and the local approximation (L) for the components of $\overline{\boldsymbol{\mu}}$ for $St_E = 3$, $\rho^p/\rho^f = 500$.

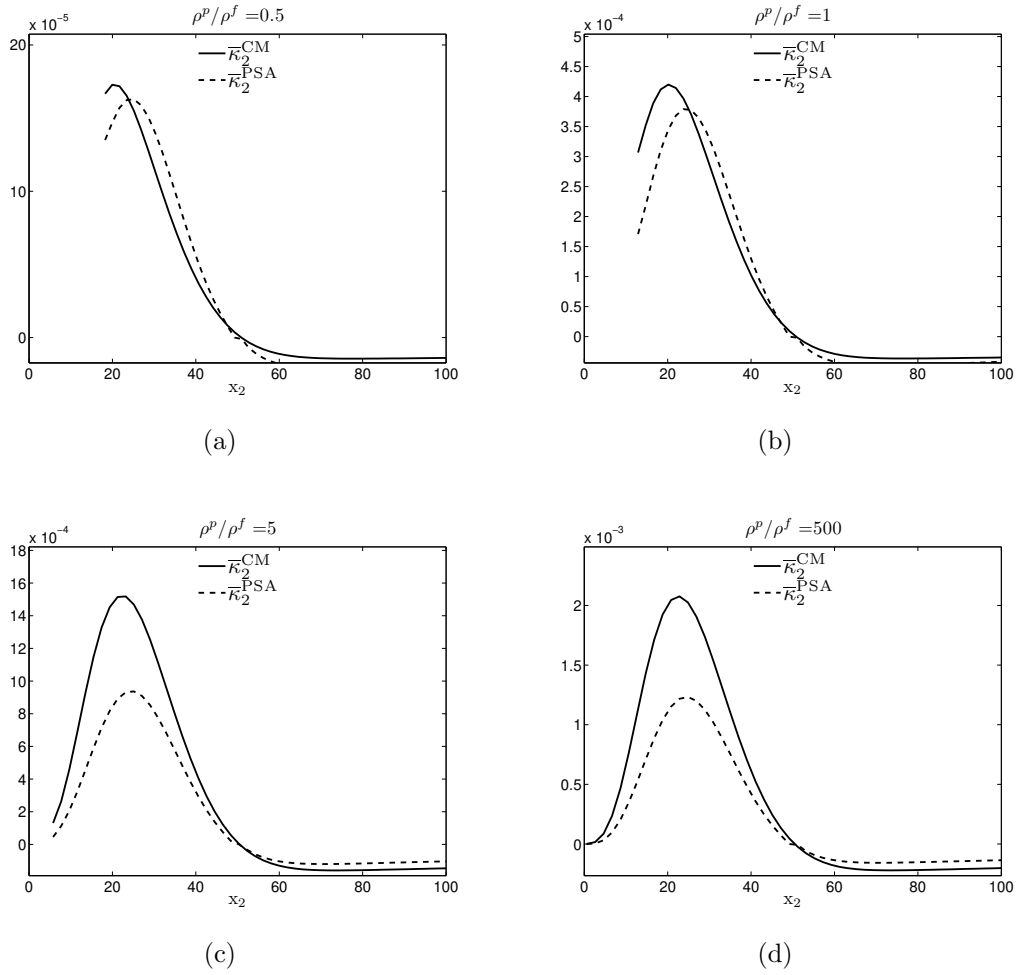

Figure 8.9: Comparison between closure model (CM) and the passive scalar approximation (PSA) for $\overline{\boldsymbol{\kappa}}$ for $St_E = 3$ and differing values of ρ^p/ρ^f.

8.3 Discussion

In section 8.2 results are shown comparing the predictions of the non-local closure model presented in section 8.1 and the local approximations to the dispersion tensors, for particles dispersing under Stokes drag and added mass forcing. In the absence of particle tracking data, it is not possible to determine how well the new non-local closure model performs when compared with the 'real answer' (i.e. the equivalent PT data). However, comments can be made regarding differences between the non-local model and local predictions, and their dependence upon ρ^p/ρ^f.

First of all, it can be seen from figures 8.7-8.9 that for $\rho^p/\rho^f = 500$ the results are identical to those in section 7.4.4 for $St_E = 3$, showing that the closure model in section 8.1 correctly reduces to that in chapter 7 in the limit $\rho^p/\rho^f \to \infty$ (i.e. when the added mass forcing contribution vanishes). The same figures also show that in the absence of added mass (or at least when it is very small) the errors in the local approximations, compared to the non-local model, are mainly quantitative in nature (the same is seen for the other results in section 7.4.4 corresponding to different St_E). In contrast, when the added mass force becomes important, such as for $\rho^p/\rho^f = 0.5, 1$ in figures 8.1-8.4, there is an appreciable qualitative difference between the non-local and local predictions, such that the wall-normal gradients of the predicted dispersion tensors differ considerably. This is important, since, for example, the wall normal gradients of $\overline{\lambda}_{22}$ contribute to the particle diffusion coefficient in the particle momentum equation (see chapter 4). The qualitative difference is most likely due to the fact that for $\rho^p/\rho^f = 0.5, 1$ the added mass force is very significant and therefore the rate of the dispersion of the particles, relative to their rate of dispersion under only Stokes drag forcing, is enhanced. The increase in the rate of dispersion will make the dispersion tensors more non-local, such that the effect of the highly non-uniform spatial variation in the fluid turbulence properties along the particle paths will become more important. It can also be seen in those same figures that, for the same reasons, the differences between the non-local and local predictions of $\overline{\boldsymbol{\mu}}$ for $\rho^p/\rho^f = 0.5, 1$ are also now increased, whereas in chapter 7 when only drag force was acting on the particles the differences between the non-local and local predictions of $\overline{\boldsymbol{\mu}}$ were not too great across the range of St_E considered.

The results also show that for $\rho^p/\rho^f = 0.5, 1$ the local predictions are greater in magnitude than the non-local predictions, whilst for $\rho^p/\rho^f = 5, 500$ the local predictions are smaller in magnitude than the non-local predictions. An interesting question is why this transition occurs? One reason is as follows. In the local approximations, the rate of decorrelation of the turbulence along the particle trajectory is given entirely by the timescale τ^{Lp}, and as discussed in section 8.1 the model used for this does not account for the dispersion due to added mass (only that due to the drag force). In contrast, in

the closure model presented in section 8.1 the decorrelation of the turbulence along the particle trajectory is governed by the model for $\rho(\mathbf{x}', s|\mathbf{x})$, which *does* account for the dispersion due to the added mass force. With the addition of an added mass force the particles will disperse at a greater rate than they would have if they were only dispersing under a drag force, and in the KS flow field this would lead to a faster decorrelation of the turbulence along the particle trajectory. Therefore, when the added mass force begins to dominate the particle dispersion (i.e. for smaller values of ρ^p/ρ^f) the increased rate of decorrelation of the turbulence along the particle trajectory is captured by the non-local closure model, but not by the local approximation. This leads to the local approximations to the dispersion tensors being greater in magnitude than the non-local predictions.

8.4 Conclusions

In this chapter a non-local closure model for the particle dispersion tensors has been developed for particles dispersing under Stokes drag, added mass and gravitational forcing.

Due to time constraints, it was not possible to test the closure model against PT data, however the non-local model predictions were compared against the local predictions. The comparison showed that for small ρ^p/ρ^f when the added mass force becomes important, the difference between the local and non-local predictions can be both qualitatively and quantitatively significant, and that the added mass force can enhance the non-locality of the system due to the enhanced rate of particle dispersion in produces. In future work the new non-local closure model must be tested against PT data to see how accurate its predictions are.

Chapter 9

The Implications of a Green Tensor Approximation For The Response Tensor

In this chapter the implications of approximating the response tensor in the dispersion tensors by a Green tensor will be discussed, and the implications for the closure models presented in chapters 7 and 8 will be considered.

9.1 Green Tensor Approximation

The response tensor (RT) in the dispersion tensors (see chapter 4) is governed by an evolution equation which is constructed by taking the functional derivative of the particle equation of motion

$$\frac{d^2}{dt^2}\frac{\delta x_k^p(t)}{\delta f_j(\boldsymbol{x}^{p\prime},t')dt'} = \frac{\delta}{\delta f_j(\boldsymbol{x}^{p\prime},t')dt'}[F_k(\boldsymbol{x}^p(t),\boldsymbol{v}^p(t),t) + f_k(\boldsymbol{x}^p(t),t)] \tag{9.1}$$

where

$$\mathcal{G}_{kj} = \frac{\delta x_k^p(t)}{\delta f_j(\boldsymbol{x}^{p\prime},t')dt'}$$

is the RT describing the effect of a perturbation of the field $\boldsymbol{f}$ at the particle position at time t' upon the the particle position at a later time t.
Then

$$\frac{d^2}{dt^2}\mathcal{G}_{kj} = \frac{\partial F_k}{\partial \mathrm{v}_i}\frac{d}{dt}\mathcal{G}_{ij} + \frac{\partial F_k}{\partial \mathrm{x}_i}\mathcal{G}_{ij} + \frac{\delta f_k(\boldsymbol{x}^p,t)}{\delta f_j(\boldsymbol{x}^{p\prime},t')dt'} \tag{9.2}$$

The tensor

$$\frac{\delta f_k(\boldsymbol{x}^p, t)}{\delta f_j(\boldsymbol{x}^{p\prime}, t')dt'}$$

describes the effect of a perturbation in the field $\boldsymbol{f}$ at the particle position at time t' upon the force $\boldsymbol{f}$ that the particle will experience at a later time t. Two approximations are then made in order to reduce equation (9.2) into an equation whose solution is a Green tensor (GT) for the particle equation of motion. The first is that $\boldsymbol{F}$ is assumed to be linear in $\mathbf{x}$ and $\mathbf{v}$. The second is the approximation

$$\frac{\delta f_k(\boldsymbol{x}^p, t)}{\delta f_j(\boldsymbol{x}^{p\prime}, t')dt'} \approx \delta_{kj}\delta(t' - t) \tag{9.3}$$

This approximation is exact if $\boldsymbol{f}$ is only a function of t, or equivalently if $\boldsymbol{x}^{p\prime} = \boldsymbol{x}^p$ (as would be the case for $\tau_p \to \infty$). These two approximations lead to significant simplification, since the RT then becomes deterministic, moreover, and becomes a GT for the particle equation of motion (i.e. $\boldsymbol{\mathcal{G}} \to \boldsymbol{G}$). However it is important to consider what effect this approximation has on the dispersion tensors and consequently on the continuum equations.

In the particle momentum equation the term associated with the preferential sampling of the flow field $\boldsymbol{f}$ is given by

$$\rho\Big\langle f_i(\boldsymbol{x}^p(t), t)\Big\rangle_{\mathbf{x}} = -\overline{\lambda}_{ki}\frac{\partial}{\partial \mathrm{x}_k}\rho + \rho\left[\overline{\kappa}_i - \frac{\partial}{\partial \mathrm{x}_k}\overline{\lambda}_{ki}\right] \tag{9.4}$$

For a system of initially uniformly distributed fluid particles in an incompressible turbulent channel flow, the LHS of equation (9.4) should be zero (i.e. when $\boldsymbol{x}^p(t)$ are trajectories of fluid particles) since such fluid particles must remain uniformly distributed for all times and since and therefore not preferentially sample the flow field. Clearly the first term on the RHS of equation (9.4) is zero in this limiting case since the concentration ρ is spatially uniform. It is therefore necessary that the second term on the RHS of equation (9.4) should also be zero for this system. In appendix C it is shown that, with the full RT in the dispersion tensors, the RHS. of equation (9.4) is identically zero for fully mixed fluid particles, and hence that the underlying PDF equation does not exhibit any features of spurious drift[1]. However, with a Green tensor approximation (GTA) for the RT this is not the case. With this approximation the expressions for the

[1]Fluid particles which are initially uniformly distributed in an incompressible, inhomogeneous turbulent flow field should remain uniformly distributed for all times. Any model which fails to satisfy this criteria is said to possess 'spurious drift'. In the continuum equations, spurious drift arises when the model for $\Big\langle \boldsymbol{f}(\boldsymbol{x}^p(t), t)\Big\rangle_{\mathbf{x}}$, given by the dispersion tensors, does not approach zero in the limit $\tau_p \to 0$.

tensors $\overline{\boldsymbol{\lambda}}$ and $\overline{\boldsymbol{\kappa}}$ are

$$\overline{\lambda}_{ki}(\mathbf{x},t) = \int_0^t G_{kj}(t;t') \Big\langle R_{ji}(\boldsymbol{x}^{p\prime},t';\mathbf{x},t) \Big\rangle_{\mathbf{x}} dt' \tag{9.5}$$

$$\overline{\kappa}_{i}(\mathbf{x},t) = \int_0^t G_{kj}(t;t') \left\langle \frac{\partial}{\partial \mathrm{x}_k} R_{ji}(\boldsymbol{x}^{p\prime},t';\mathbf{x},t) \right\rangle_{\mathbf{x}} dt' \tag{9.6}$$

It is these forms in the wall-normal direction which is important, since these components contribute to the concentration profiles via the momentum (in a turbulent boundary layer), and therefore determine whether or not the continuum equations are free from spurious drift. In the limit of fluid particles the wall-normal components of $\overline{\boldsymbol{\lambda}}$ and $\overline{\boldsymbol{\kappa}}$ reduce to the forms (with the GTA)

$$\overline{\lambda}^f_{22}(\mathbf{x},t) = \int_0^t \Big\langle R^f_{22}(\boldsymbol{x}^{f\prime},t';\mathbf{x},t) \Big\rangle_{\mathbf{x}} dt' \tag{9.7}$$

$$\overline{\kappa}^f_{2}(\mathbf{x},t) = \int_0^t \left\langle \frac{\partial}{\partial \mathrm{x}_2} R^f_{22}(\boldsymbol{x}^{f\prime},t';\mathbf{x},t) \right\rangle_{\mathbf{x}} dt' \tag{9.8}$$

where

$$R^f_{ji}(\mathbf{x}',t';\mathbf{x},t) = \Big\langle u'_j(\mathbf{x}',t') u'_i(\mathbf{x},t) \Big\rangle \tag{9.9}$$

and the trajectories in equations (9.7) and (9.8) are governed by

$$\frac{d}{dt} x^f_i(t) = u_i(\boldsymbol{x}^f(t),t) \tag{9.10}$$

Therefore, under the GTA, and in the limit of fluid particles the wall-normal drift term is given by

$$\begin{aligned} \overline{\kappa}^f_2(\mathbf{x},t) - \frac{\partial}{\partial \mathrm{x}_2}\overline{\lambda}^f_{22}(\mathbf{x},t) &= \int_0^t \left[\left\langle \frac{\partial}{\partial \mathrm{x}_2} R^f_{22}(\boldsymbol{x}^{p\prime},t';\mathbf{x},t) \right\rangle_{\mathbf{x}} - \frac{\partial}{\partial \mathrm{x}_k} \Big\langle R^f_{22}(\boldsymbol{x}^{p\prime},t';\mathbf{x},t) \Big\rangle_{\mathbf{x}} \right] dt' \\ &= -\int_0^t \int_{\mathbf{x}'} R^f_{22}(\mathbf{x}',t';\mathbf{x},t) \frac{\partial}{\partial \mathrm{x}_2} \rho^f(\mathbf{x}',t'|\mathbf{x},t) d\mathbf{x}' dt' \end{aligned} \tag{9.11}$$

where

$$\rho^f(\mathbf{x}', t'|\mathbf{x}, t) = \Big\langle \delta(\boldsymbol{x}^f(t') - \mathbf{x}') \Big\rangle_{\mathbf{x}} \tag{9.12}$$

For the case of fluid particle dispersion in turbulent boundary layers, the RHS of equation (9.11) will not be zero in general, and therefore it is evident that the GTA introduces a spurious drift into the momentum equation. This spurious drift arises because of the fact that the GTA does not account for the fact that in the PDF model particle dispersion is governed by a differentiable, inhomogeneous stochastic field. Since the closure models for the dispersion tensors presented in chapters 7 and 8 have invoked the use of the GTA, this means that the new closure models for the dispersion tensors can give rise to spurious drift effects in the corresponding continuum equations involving these.

The analysis in appendix C which shows that equation (9.4) is zero for fluid particles (when the true RT is used) relies upon the observation that the RT is precisely the inverse of the Jacobian. That is, with the Jacobian defined by

$$\mathrm{J}_{ij}(t'|\mathbf{x}, t) = \frac{\partial}{\partial \mathrm{x}_j} x_i^f(t'|\mathbf{x}, t) \tag{9.13}$$

where $\boldsymbol{x}^f(t'|\mathbf{x}, t)$ is the position of a fluid particle at time t' which is at $\mathbf{x}$ at time t, and with a RT $\mathcal{G}^f(t', t, \mathbf{x})$ which is the RT for a fluid particle at time t' which is at $\mathbf{x}$ at time t then

$$\mathcal{G}_{ij}^f(t', t, \mathbf{x}) = \Big[\mathrm{J}_{ij}(t'|\mathbf{x}, t)\Big]^{-1}$$

Any model for $\mathcal{G}^f(t', t, \mathbf{x})$ which is not *precisely* equal to the inverse of the Jacobian will necessarily result in the introduction of a spurious drift into the continuum equations. Therefore since it is not possible to model the RT exactly (some level of closure approximation would always have to be invoked in modelling the RT; this is unavoidable) it is not strictly possible to avoid the introduction of a spurious drift into the continuum equations (except by artificially invoking the passive scalar approximation for $\overline{\boldsymbol{\kappa}}$) .

However, the models presented in this thesis are aimed towards modelling the dispersion of inertial particles, not fluid particles, therefore it is important to consider whether or not this 'spurious drift' affects the quality of the closure models for inertial particles. It may be that the GTA has little effect on the dispersion tensors for the particle sizes that are of interest. Therefore, in the next section the dispersion tensors are computed in PT simulations with both the true RT included and also with the GT included, and the results are compared over the range of particle sizes for which the closure model was tested in chapter 7.

9.2 PT simulation test case

Even though as discussed in section 9.1 the introduction of a GTA for the RT introduces a spurious drift into the continuum equations via the dispersion tensors, the purpose of the continuum equations in the context of this thesis is for modelling inertial particle dispersion, not dispersion of fluid particles. Therefore, the important question to answer is whether or not the GTA significantly affects the dispersion tensors in the case of inertial particles. That is, whilst the true drift

$$\overline{\kappa}_i(\mathbf{x},t) - \frac{\partial}{\partial \mathrm{x}_k}\overline{\lambda}_{ki}(\mathbf{x},t)$$

is not equal to zero for inertial particles (except in the limit $\tau_p \to \infty$); how much of the drift predicted when using a GTA is 'real' and how much of it is an artificial drift? The simplest way to assess this is to compute the dispersion tensors in a PT simulation in two ways; first with the RT and second with the GT. Comparing the results will show how much, if at all, the GTA affects the dispersion tensors in the case of inertial particle dispersion.

In this study attention is confined to the case of particles dispersing under only a Stokes drag force. Furthermore, PT is performed using the KS flow field described in chapter 7 (since, besides other benefits such as computational efficiency, that flow field yields analytic solutions for the Eulerian two-point, two-time correlation tensor required in the dispersion tensors). The approximation free dispersion tensors, that is those with the RT, will be denoted by the superscript '$\mathcal{G}$', and are given by

$$\overline{\lambda}^{\mathcal{G}}_{ki}(\mathbf{x},t) = \int_0^t \Big\langle \mathcal{G}_{kj}(t;t')R_{ji}(\boldsymbol{x}^{p\prime},t';\mathbf{x},t)\Big\rangle_{\mathbf{x}} dt' \tag{9.14}$$

$$\overline{\mu}^{\mathcal{G}}_{ki}(\mathbf{x},t) = \int_0^t \Big\langle \dot{\mathcal{G}}_{kj}(t;t')R_{ji}(\boldsymbol{x}^{p\prime},t';\mathbf{x},t)\Big\rangle_{\mathbf{x}} dt' \tag{9.15}$$

$$\overline{\kappa}^{\mathcal{G}}_{i}(\mathbf{x},t) = \int_0^t \left\langle \mathcal{G}_{kj}(t;t')\frac{\partial}{\partial \mathrm{x}_k}R_{ji}(\boldsymbol{x}^{p\prime},t';\mathbf{x},t)\right\rangle_{\mathbf{x}} dt' \tag{9.16}$$

The Eulerian two-point, two-time correlation tensor for $\boldsymbol{f}$ required is

$$R_{ji}(\mathbf{x}',t';\mathbf{x},t) = \beta^2\Big\langle u'_j(\mathbf{x}',t')u'_i(\mathbf{x},t)\Big\rangle \tag{9.17}$$

For Stokes drag forcing acting on the particles the evolution equation for the RT in the KS flow field is

$$\frac{d^2}{dt^2}\mathcal{G}_{kj} = -\beta\frac{d}{dt}\mathcal{G}_{kj} + \beta\frac{\partial u'_k}{\partial \mathrm{x}_i}\mathcal{G}_{ij} \tag{9.18}$$

with end conditions $\boldsymbol{\mathcal{G}}(t;t) = \mathbf{0}$ and $\dot{\boldsymbol{\mathcal{G}}}(t;t) = \mathbf{I}$. Solving equation (9.18) amounts to a backward in time problem (since in the integrand of the dispersion tensors it is the variation of $\mathcal{G}$ with t' that is required given its state at time t, and $t' \leq t$). In order to solve equation (9.18) as an initial value problem the substitution $s = t' - t \leq 0$ is made and then equation (9.18) is replaced with

$$\frac{d^2}{ds^2}\mathcal{G}_{kj} = \beta\frac{d}{ds}\mathcal{G}_{kj} - \beta\frac{\partial u'_k}{\partial \mathrm{x}_i}\mathcal{G}_{ij} \tag{9.19}$$

which describes the evolution of $\boldsymbol{\mathcal{G}}$ going 'backward in time'. This equation, with the 'initial' conditions $\boldsymbol{\mathcal{G}}(s=0) = \mathbf{0}$ and $\dot{\boldsymbol{\mathcal{G}}}(s=0) = \mathbf{I}$ was solved using a third-order Runge-Kutta scheme which was found to be sufficiently accurate.

In addition, since the 2D KS flow field is statistically stationary and inhomogeneous only in the wall-normal direction, the forms of the dispersion tensors required are

$$\overline{\lambda}^{\mathcal{G}}_{ki}(\mathrm{x}_2) = \beta^2 \int_{-\infty}^{0} \Big\langle \mathcal{G}_{kj}(s) R_{ji}(x_1^p(s) - \mathrm{x}_1, x_2^p(s), s; 0, \mathrm{x}_2, 0) \Big\rangle_{\mathrm{x}_2} ds \tag{9.20}$$

$$\overline{\mu}^{\mathcal{G}}_{ki}(\mathrm{x}_2) = \beta^2 \int_{-\infty}^{0} \Big\langle \dot{\mathcal{G}}_{kj}(s) R_{ji}(x_1^p(s) - \mathrm{x}_1, x_2^p(s), s; 0, \mathrm{x}_2, 0) \Big\rangle_{\mathrm{x}_2} ds \tag{9.21}$$

$$\overline{\kappa}^{\mathcal{G}}_{i}(\mathrm{x}_2) = \beta^2 \int_{-\infty}^{0} \Big\langle \mathcal{G}_{2j}(s) \frac{\partial}{\partial \mathrm{x}_2} R_{ji}(x_1^p(s) - \mathrm{x}_1, x_2^p(s), s; 0, \mathrm{x}_2, 0) \Big\rangle_{\mathrm{x}_2} ds \tag{9.22}$$

where $s \leq 0$ and $\boldsymbol{x}^p(0) = \mathbf{x}$.

The dispersion tensors computed using the GTA are denoted by the superscript 'G' and are given by

$$\overline{\lambda}^{G}_{ki}(\mathrm{x}_2) = \beta^2 \int_{-\infty}^{0} G_{kj}(s) \Big\langle R_{ji}(x_1^p(s) - \mathrm{x}_1, x_2^p(s), s; 0, \mathrm{x}_2, 0) \Big\rangle_{\mathrm{x}_2} ds \tag{9.23}$$

$$\overline{\mu}^{G}_{ki}(\mathrm{x}_2) = \beta^2 \int_{-\infty}^{0} \dot{G}_{kj}(s) \Big\langle R_{ji}(x_1^p(s) - \mathrm{x}_1, x_2^p(s), s; 0, \mathrm{x}_2, 0) \Big\rangle_{\mathrm{x}_2} ds \tag{9.24}$$

$$\overline{\kappa}^{G}_{i}(\mathrm{x}_2) = \beta^2 \int_{-\infty}^{0} G_{2j}(s) \Big\langle \frac{\partial}{\partial \mathrm{x}_2} R_{ji}(x_1^p(s) - \mathrm{x}_1, x_2^p(s), s; 0, \mathrm{x}_2, 0) \Big\rangle_{\mathrm{x}_2} ds \tag{9.25}$$

where for the flow field in question (with $\langle \boldsymbol{u} \rangle = \mathbf{0}$) and for Stokes drag

$$G_{kj}(s) = \delta_{kj}\tau_p \left(1 - \exp[\beta s]\right), \qquad s \leq 0 \tag{9.26}$$

$$\dot{G}_{kj}(s) = \delta_{kj} \exp[\beta s], \qquad s \leq 0 \tag{9.27}$$

The details of the particle tracking simulation are the same as those in chapter 7. The dispersion tensors are computed for the lower range of particle Stokes numbers that the closure model was tested for in chapter 7 (i.e. $0.3 \leq St_E \leq 3$) since $\mathcal{G} \to \boldsymbol{G}$ for increasing St_E.

9.3 Results

In this section the results of the test case described in section 9.2 are presented. The dispersion tensors containing the RT are denoted by the superscript $\mathcal{G}$ (solid black lines in the plots), whilst those containing the GT are denoted by the superscript G ($\times$ symbol in the plots). Note that the data obtained involving $\boldsymbol{G}$ can be seen to be less noisy than that involving $\boldsymbol{\mathcal{G}}$; this is simply due to the fact that $\boldsymbol{\mathcal{G}}$ is stochastic whilst $\boldsymbol{G}$ is deterministic and hence the data involving $\boldsymbol{\mathcal{G}}$ contains an additional source of 'noise'.

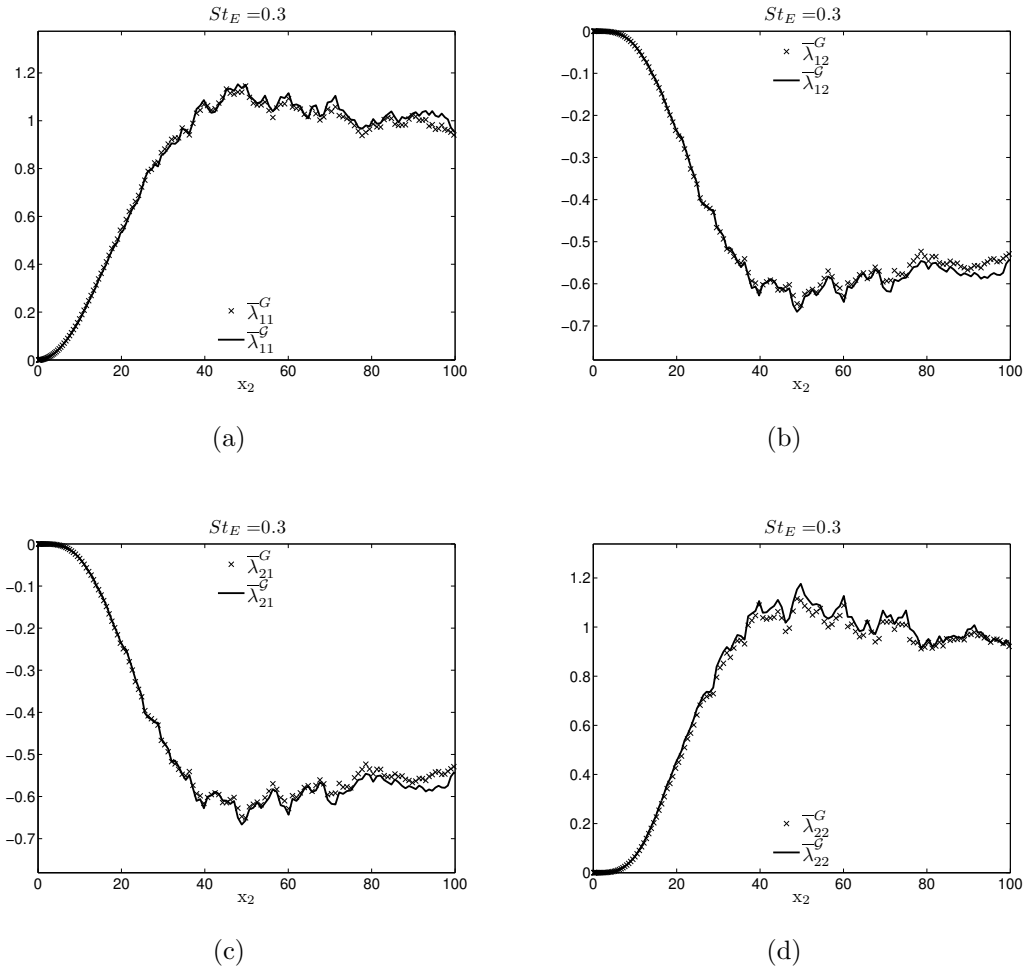

(a) (b)

(c) (d)

Figure 9.1: Comparison between $\overline{\boldsymbol{\lambda}}^{\mathcal{G}}$ and $\overline{\boldsymbol{\lambda}}^{G}$ for $St_E = 0.3$.

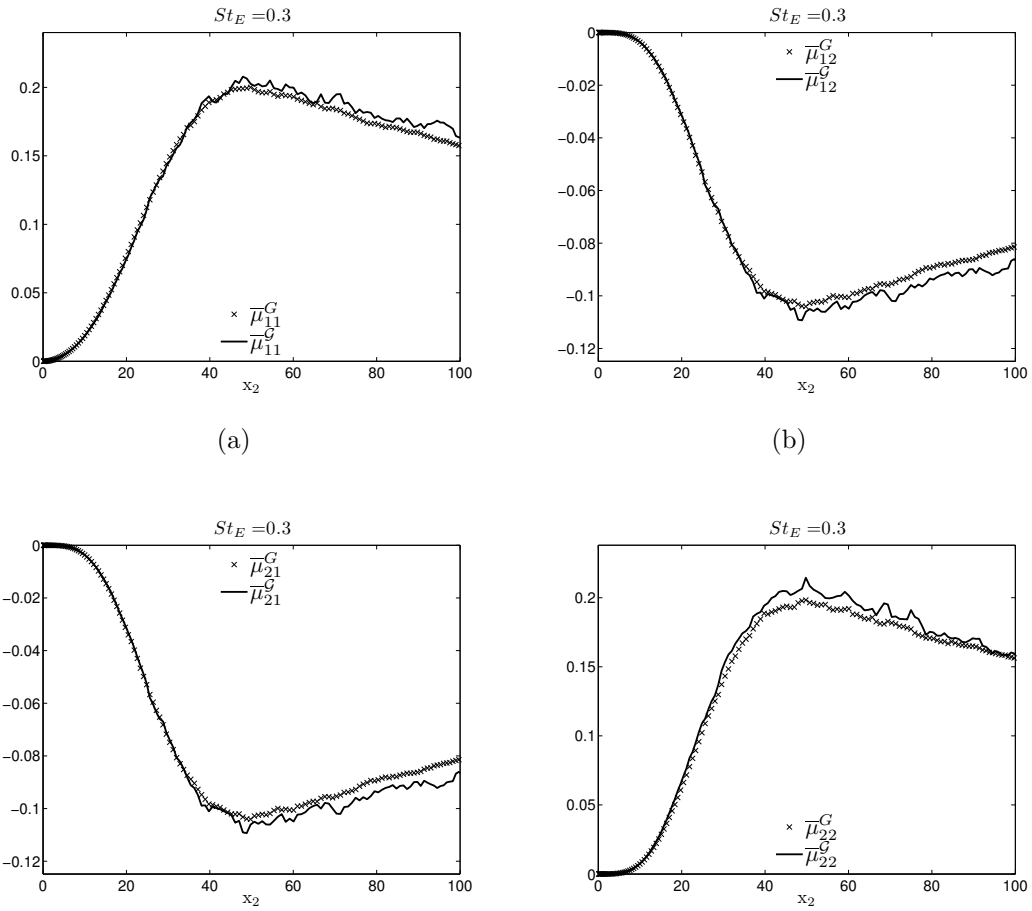

Figure 9.2: Comparison between $\overline{\boldsymbol{\mu}}^{\mathcal{G}}$ and $\overline{\boldsymbol{\mu}}^{G}$ for $St_E = 0.3$.

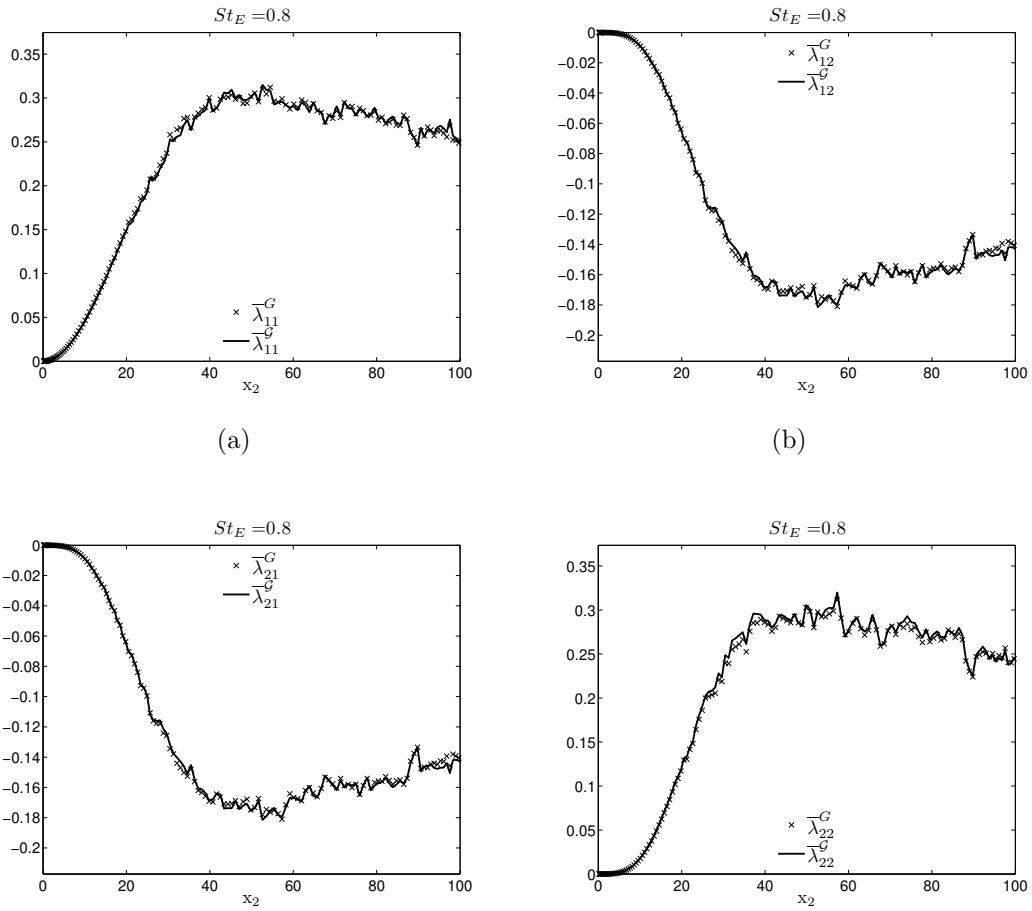

Figure 9.3: Comparison between $\overline{\boldsymbol{\lambda}}^{\mathcal{G}}$ and $\overline{\boldsymbol{\lambda}}^{G}$ for $St_E = 0.8$.

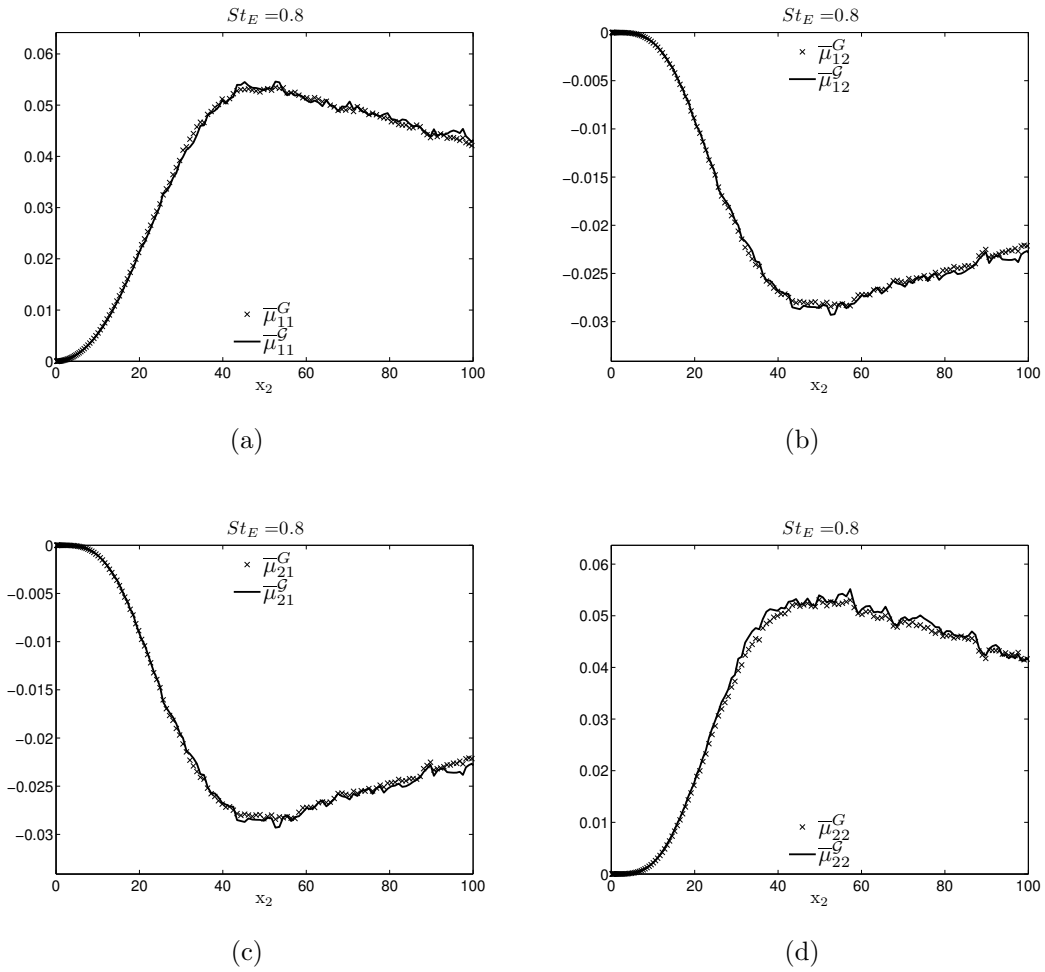

Figure 9.4: Comparison between $\overline{\boldsymbol{\mu}}^{\mathcal{G}}$ and $\overline{\boldsymbol{\mu}}^{G}$ for $St_E = 0.8$.

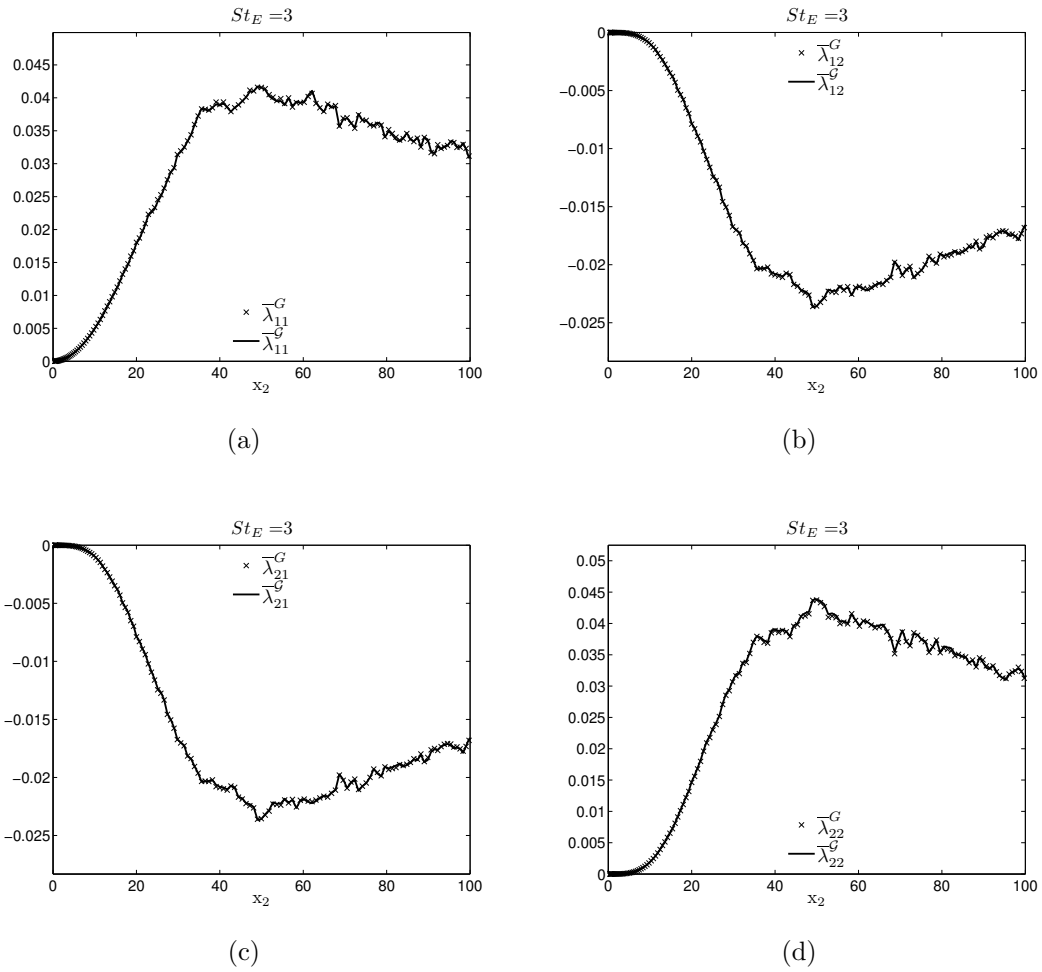

Figure 9.5: Comparison between $\overline{\boldsymbol{\lambda}}^{\mathcal{G}}$ and $\overline{\boldsymbol{\lambda}}^{G}$ for $St_E = 3$.

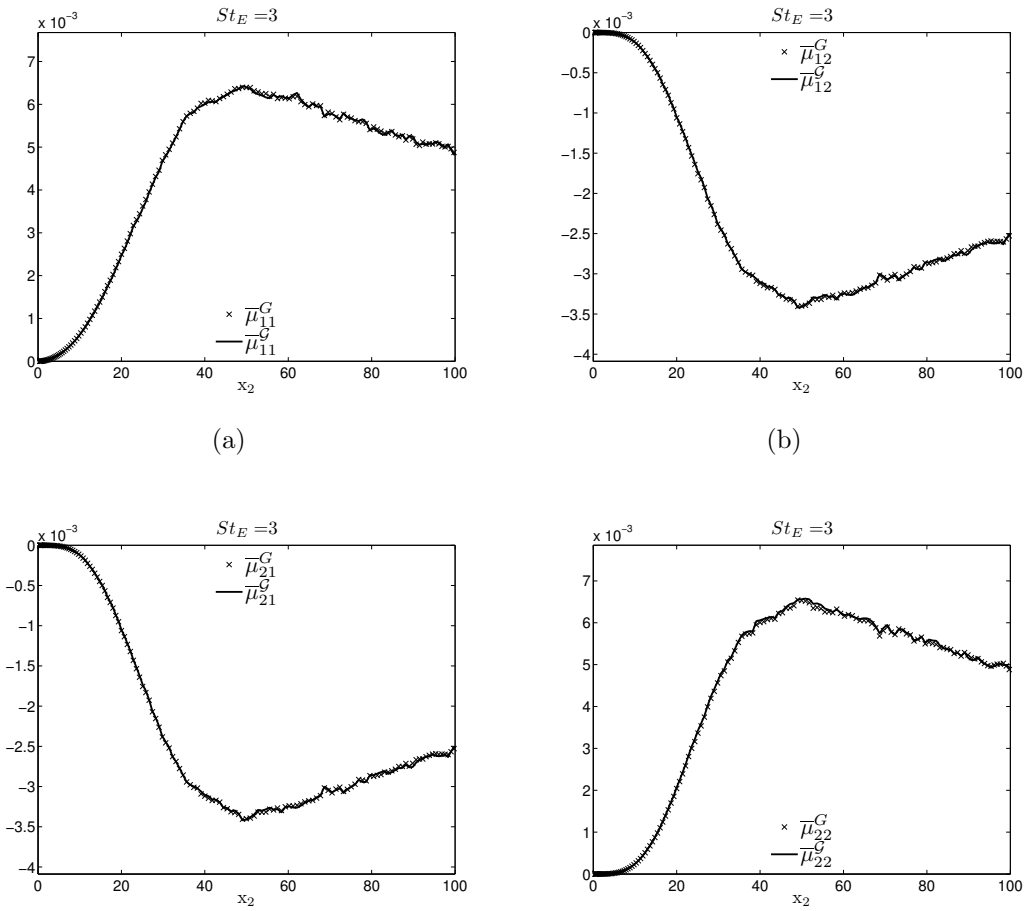

Figure 9.6: Comparison between $\overline{\boldsymbol{\mu}}^{\mathcal{G}}$ and $\overline{\boldsymbol{\mu}}^{G}$ for $St_E = 3$.

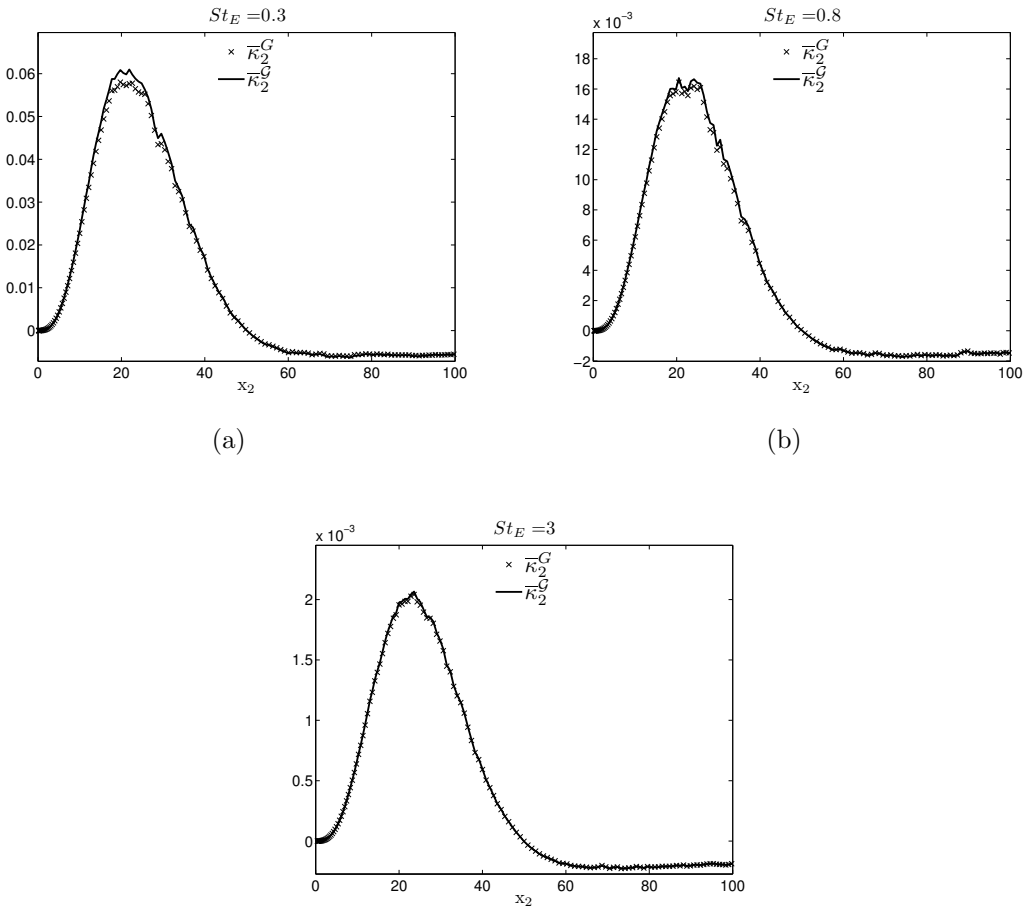

(a) (b)

(c)

Figure 9.7: Comparison between $\overline{\boldsymbol{\kappa}}^{\mathcal{G}}$ and $\overline{\boldsymbol{\kappa}}^{G}$.

9.4 Discussion

For inertial particles the drift term

$$\overline{\kappa}_2 - \frac{\partial}{\partial \mathrm{x}_2}\overline{\lambda}_{22}$$

is not zero, but in the limit of fluid particles this drift term should vanish, otherwise the continuum equations contain a spurious drift. In appendix C it is demonstrated that the dispersion tensors, containing the full RT, do not contain any spurious drift. However, in section 9.1 it was demonstrated that the GTA for the RT introduces a spurious drift into the continuum equations. Therefore, it is important to examine whether or not this spurious drift has any effect on modelling inertial particle dispersion. That is to say, if a GT is used in the dispersion tensors for describing inertial particle dispersion, how much of the drift

$$\overline{\kappa}_2 - \frac{\partial}{\partial \mathrm{x}_2}\overline{\lambda}_{22}$$

predicted is artificial (i.e. produced by errors in the use of the GTA), and how much of it is real. Comparing the dispersion tensors containing the GT and those containing the true RT will demonstrate if the GTA introduces an appreciable artificial drift in the case of inertial particle dispersion.

The results showing the comparisons between the dispersion tensors containing the GT and RT are shown in section 9.3. The results indicate that over the range of St_E examined (which covers small to medium sized particles), the error introduced by the GTA is negligible. In fact only the results for $St_E = 0.3$ show any noticeable difference. This is as expected since the approximation $\mathcal{G} \approx \boldsymbol{G}$ becomes increasingly invalid as the particle size decreases. Figure 9.7 shows that for $St_E = 0.3$ there is a slight difference between the peak values of $\overline{\kappa}_2^{\mathcal{G}}$ and $\overline{\kappa}_2^{G}$, a difference which can only be attributed to the effect of the GTA. However, again, the difference is negligible.

Also for $St_E = 0.3$, figure 9.2 shows a small but noticeable difference between $\overline{\boldsymbol{\mu}}^{\mathcal{G}}$ and $\overline{\boldsymbol{\mu}}^{G}$, the difference for each component almost always being $|\overline{\boldsymbol{\mu}}^{\mathcal{G}}| \geq |\overline{\boldsymbol{\mu}}^{G}|$. Recalling that $\overline{\boldsymbol{\mu}}$ is a stress source for the particles, the reason for $|\overline{\boldsymbol{\mu}}^{\mathcal{G}}| \geq |\overline{\boldsymbol{\mu}}^{G}|$ can be understood by the fact that $\overline{\boldsymbol{\mu}}^{\mathcal{G}}$ accounts for the stochasticity of the underlying field $\boldsymbol{f}$ in $\mathcal{G}$, whereas $\overline{\boldsymbol{\mu}}^{G}$ does not, since $\boldsymbol{G}$ is deterministic and does not account for $\boldsymbol{f}$. Therefore the inclusion of the stochasticity of the underlying field $\boldsymbol{f}$ in $\mathcal{G}$ leads to an additional stress which is captured in $\overline{\boldsymbol{\mu}}^{\mathcal{G}}$ and not in $\overline{\boldsymbol{\mu}}^{G}$, leading to $|\overline{\boldsymbol{\mu}}^{\mathcal{G}}| \geq |\overline{\boldsymbol{\mu}}^{G}|$. However the effect of the GTA on $\overline{\boldsymbol{\mu}}$ has no bearing on the issue of spurious drift (although this result is noted for future work since it suggests that the GTA would lead to small errors in the particle Reynolds stress equation via errors in $\overline{\boldsymbol{\mu}}^{G}$).

It would be interesting to perform the test case presented in the previous sections

for successively smaller St_E in order to find out to what limit the GTA can be applied without having any appreciable effect on the dispersion tensors. This is left to future work. Nevertheless, given that the results in section 9.3 demonstrate that the GTA has negligible effect on the dispersion tensors over the range of St_E tested, the closure models developed in this thesis, which assume the GTA, will therefore provide accurate models for the true dispersion tensors (i.e. those containing the RT) over the range $0.3 \leq St_E \leq \infty$.

Finally, a comment about possible future work concerning the modelling of the RT. It is somewhat unfortunate that closure approximations applied to the RT may result in the introduction of a spurious drift into the continuum equations, via the dispersion tensors. Nevertheless, even though it may not be possible to eradicate spurious drift entirely, it may certainly be reduced by developing approximations for $\mathcal{G}$ which are more appropriate than the GTA. For example, consider the unclosed form of $\overline{\boldsymbol{\lambda}}$

$$\overline{\lambda}_{ki}(\mathbf{x},t) = \int_0^t \int_{\mathbf{x}'} \left\langle \mathcal{G}_{kj}\delta\left(\boldsymbol{x}^{p\prime} - \mathbf{x}'\right)\right\rangle_{\mathbf{x}} R_{ji}(\mathbf{x}',t';\mathbf{x},t)\ d\mathbf{x}'dt' \tag{9.28}$$

The modelling procedure for the joint distribution

$$\left\langle \mathcal{G}_{kj}\delta\left(\boldsymbol{x}^{p\prime} - \mathbf{x}'\right)\right\rangle_{\mathbf{x}}$$

is not straightforward by any means, however it may be re-written in terms of conditional probabilities so that

$$\overline{\lambda}_{ki}(\mathbf{x},t) = \int_0^t \int_{\mathbf{x}'} \left\langle \mathcal{G}_{kj}\right\rangle_{\mathbf{x}',\mathbf{x}} \left\langle \delta\left(\boldsymbol{x}^{p\prime} - \mathbf{x}'\right)\right\rangle_{\mathbf{x}} R_{ji}(\mathbf{x}',t';\mathbf{x},t)\ d\mathbf{x}'dt' \tag{9.29}$$

The closure models presented in chapters 7 and 8 could then be used once again to close $\left\langle \delta\left(\boldsymbol{x}^{p\prime} - \mathbf{x}'\right)\right\rangle_{\mathbf{x}}$. The difficulty in closing $\left\langle \mathcal{G}_{kj}\right\rangle_{\mathbf{x}',\mathbf{x}}$ would be in constructing a model for

$$\frac{\delta f_k(\boldsymbol{x}^p(t),t)}{\delta f_j(\boldsymbol{x}^p(t'),t')dt'} = \left(\frac{\partial}{\partial \mathrm{x}_m} f_k(\boldsymbol{x}^p(t),t)\right)\mathcal{G}_{mj} \tag{9.30}$$

or more specifically, the difficult lies in modelling

$$\frac{\partial}{\partial \mathrm{x}_m} f_k(\boldsymbol{x}^p(t),t)$$

The difficult is two-fold; first, a stochastic description for the gradients of $\boldsymbol{f}$ is required, and secondly, models for the stochastic trajectories $\boldsymbol{x}^p(t)$ along which the gradients of $\boldsymbol{f}$ are evaluated, are also required. The statistics of the model for the gradients of $\boldsymbol{f}$ must account for its inhomogeneous nature since local approximations to it would essentially result in the same deficiencies as the GTA.

A further difficulty is that in closing

$$\left\langle \mathcal{G}_{kj} \right\rangle_{\mathbf{x}',\mathbf{x}}$$

the particle trajectories contained in $\boldsymbol{\mathcal{G}}$ which would need to be modelled would have to be subject to the dual conditionality $\boldsymbol{x}^p(t') = \mathbf{x}'$ & $\boldsymbol{x}^p(t) = \mathbf{x}$. It may be possible to develop models that satisfy this based on the idea of Brownian bridges.

Clearly then, developing closure models which account for the effect of the stochastic field $\boldsymbol{f}$ on $\mathcal{G}$ is a significant challenge, and would be necessary if one wished to use the PDF derived continuum equations for modelling the dispersion of very small particles ($St_E \to 0$). However, the results in this chapter show that for modelling the dispersion of inertial particles, even relatively small particles, the effect of the GTA is negligible, making the GT a sufficient level of approximation to the RT in this case.

9.5 Conclusions

In this chapter the effects of approximating the RT by a GT in the dispersion tensors has been examined. It has been demonstrated that whilst the GTA is invalid in the limit of fluid particles, it presents a good approximation for inertial particle dispersion, at least over the range of St_E examined in this chapter.

The closure models for the dispersion tensors presented in chapters 7 and 8 rely on the GTA, and therefore the test case in this chapter provides important confirmation that such an approximation is sufficient for modelling inertial particle dispersion.

Chapter 10

Conclusions and Future Work

As described in chapters 1 and 2, the aim of the research conducted and presented in this thesis was to develop mathematical models to describe the dispersion of inertial particles in turbulent pipe flows, such as encountered in various flow assurance problems in the oil industry. Specifically, the aim was to improve the modelling capabilities for inertial particle dispersion in turbulent boundary layers, where the particle dispersion process is complex and far from understood.

In chapter 4 a PDF kinetic equation was introduced which describes the temporal evolution of the PDF for particle position and velocity in phase-space, from which continuum equations are constructed whose solutions are the moments of the PDF itself (particle concentration, mean particle velocity, particle Reynolds stresses etc). The PDF equation provides a theoretically robust way to construct continuum equations which can be used to reliably model the dispersion of inertial particles in turbulent boundary layers since the PDF equation is derived directly from the underlying particle equation of motion. In the same chapter, various terms requiring closure in the continuum equations were discussed and presented, which included the closure of the Reynolds stress flux tensor $\overline{\mathbf{ccc}}$ and the closure of the particle dispersion tensors $\overline{\boldsymbol{\lambda}}$, $\overline{\boldsymbol{\mu}}$ and $\overline{\boldsymbol{\kappa}}$. The Reynolds stress flux tensor is closed using a Chapman-Enskog type closure, whilst the particle dispersion tensors are closed using a local homogeneous approximation.

In addition it was highlighted that the continuum equations include the correct physical features for describing particle dispersion in turbulent boundary layers, especially a general, exact (when the turbulence is assumed to be Gaussian) closure for the flux associated with the preferential sampling of the turbulent force field; a term difficult to model and yet of critical importance for accurately predicting particle concentration solutions in turbulent boundary layers.

In chapter 5 the continuum equations were tested against particle tracking data in

a simplified system intended to represent particle dispersion in a turbulent boundary layer. It was found that whilst the continuum solutions for the particle kinetic stresses were in general in very good agreement with the particle tracking data, the continuum solutions for the particle concentration were in significant error. The local approximations to the particle dispersion tensors in the continuum equations were identified as the source of error in the continuum solutions for the particle concentration. By comparing the local forms of the dispersion tensors to the dispersion tensors as computed from the particle tracking simulation, it was seen that the local approximations, especially that for $\overline{\boldsymbol{\lambda}}$, could be in significant error for small to medium sized particles (whereas the local approximation becomes valid in the limit of very large particles). It was therefore highlighted that new non-local closure models for the particle dispersion tensors must be developed in order to improve the prediction capabilities of the continuum equations.

In chapter 6 the features of particle dispersion in turbulent boundary layers which make the dispersion tensors intrinsically non-local were identified and discussed. Based upon these observations, in chapter 7 a new non-local closure model for the particle dispersion tensors was derived which is appropriate for particles dispersing under Stokes drag forcing. The new closure model was then tested against equivalent particle tracking data. The results showed that the new non-local closure model predictions were in excellent agreement with the particle tracking data, whereas by contrast, the traditional local approximations were shown again to be in significant error, in agreement with the results found in chapter 5.

With a view to applying the continuum equations to systems where the particle to fluid material density is comparable, the closure model presented in chapter 7 was then extended in chapter 8 to account for added mass forcing and gravity acting on the particles, in addition to Stokes drag. The modelling procedure was presented and various terms requiring approximation in the closure model were considered. Due to time constraints, testing the closure model against simulation data was beyond the scope of the present work, and such testing is left to future work. However the closure model predictions were compared against the alternative local approximations for a fixed value of St_E and varying values of ρ^p/ρ^f. It was shown that in the limit $\rho^p/\rho^f \to \infty$ the model correctly reduces to that presented in chapter 7 where only Stokes drag forcing was acting on the particles. However, for small values of ρ^p/ρ^f, the local approximation was both qualitatively and quantitatively different to the non-local closure model prediction, whereas under drag force only the difference is mainly quantitative. The reason is that with the added mass force, in addition to the drag force, the rate of particle dispersion is increased and therefore the non-locality of the system is more pronounced.

The increase in accuracy obtained by the new closure modelling for the dispersion tensors comes at a cost, and that of additional complexity. Rather than the dispersion

tensors being defined by simple analytic functions as they are under a local approximation, the new closure modelling requires the dispersion tensors to be computed (at least partially) numerically. Of course analytic solutions obtained using the non-local closure would be desirable, but this is not feasible. Furthermore, given the complexity of the non-local nature of the particle dispersion process in a turbulent boundary layer it is unreasonable to expect that accurate closure solutions to such a problem should be simple. However it was highlighted that the numerical procedure for computing the dispersion tensors using the new closure model is very simple and fast and is therefore not cumbersome.

It is at this point that it is worth considering whether or not the kinetic form of the PDF equation is the most appropriate for particle dispersion in turbulent boundary layers. As discussed in chapter 4, when developing PDF equations, one has to make the choice as to which variables to retain in the phase-space vector. In the current context, the two approaches most commonly used are the kinetic approach, where only the particle position and velocity are retained in the phase-space vector (e.g. [93]), and the higher dimensional approach where, in addition to particle position and velocity, the fluid velocity at the particle position is retained in the phase-space vector (e.g. [42], sometimes referred to as a 'GLM' (Generalised Langevin Model) approach). The predefined scope of the research undertaken in this thesis was to consider developments to the kinetic approach, and so only this form has been considered in this thesis.

The choice of a kinetic approach leads to a need for closure of the density weighted average of the flucutating fluid velocity (more generally the stochastic force $\boldsymbol{f}$, but here only Stokes drag is discussed for simplicity) at the particle phase-space position. As demonstrated in this thesis, this term is highly non-local and is therefore difficult to close completely for inertial particle dispersion in turbulent boundary layers. Furthermore, for reasons discussed in chapter 4, it is necessary to assume that the fluctuating fluid velocity field is Gaussian in order to develop closure for the PDF kinetic equation (using FN), and boundary layer turbulence, even at the large scales of the flow, is non-Gaussian. On the other hand, as discussed in [42], some of these difficulties could have been avoided somewhat by the choice of a GLM PDF equation. In the GLM PDF equation, closure is no longer required for the fluid velocity but rather for the fluid acceleration at the particle phase-space position. This can be closed through the use of Langevin equations, and in inhomogeneous turbulence these models lead to non-Gaussian fluid velocities at the particle position. Closure of the fluid accelerations at the particle position are much easier than those of the fluid velocity since, as they fluctuate on a faster timescale, they are much less sensitive to the non-local nature of the particle dispersion process in a turbulent boundary layer. It should be noted that the GLM

model does require a timescale[1]for the fluid velocities seen by the inertial particles. Strictly speaking, in boundary layer dispersion, this timescale should capture inertial, crossing trajectory and non-local effects. However recent work (e.g. [123]) has shown that with an appropriate Langevin equation, the GLM model predictions are in very good agreement with DNS data of inertial particle dispersion in a turbulent channel flow, even when a local timescale is used in the GLM model. It may therefore be considered that the GLM PDF equation is more applicable to boundary layer dispersion than the kinetic appproach simply because the terms requiring closure in the GLM model are easier to close than those in the kinetic approach in a reliable and robust way (see [42] for an extended discussion on the GLM and kinetic approaches and their respective advantages/disadvantages).

Finally in chapter 9 the implications of approximating the response tensor (which features in the particle dispersion tensors) by a Green tensor was examined. It was demonstrated that the Green tensor approximation introduces a spurious drift into the continuum equations via the particle dispersion tensors. Based upon observations of the proof presented in appendix C, it was concluded that avoiding the introduction of a spurious drift into the continuum equations is very difficult since producing an accurate model for the response tensor for particle dispersion in a turbulent boundary layer is complicated (an accurate model for the response tensor would be required in order for the continuum equations to be free of spurious drift). However, given that the models in this thesis are intended to model the dispersion of inertial particles, not fluid particles, an investigation was carried out to see how the Green tensor approximation affects the dispersion tensors for inertial particles. The dispersion tensors were computed for small to medium sized particles in a particle tracking simulation in two ways; (i) using the true response tensor and (ii) using the Green tensor approximation, and the results were then compared. The results showed that over the range of particle sizes considered the errors introduced by the Green tensor approximation are completely negligible.

In conclusion, the work presented in this thesis has achieved the objectives outlined in chapters 1 and 2 in that it provides developments to the applicability of a closed set of continuum equations, derived from the PDF kinetic equation, for modelling the dispersion of inertial particle dispersion in turbulent pipe flows, specifically in the boundary layer. However, whilst the work in this thesis provides developments towards this ultimate modelling goal, there is still some work to be done before the PDF derived

[1]For dispersion in homogeneous turbulence, the timescale in the Langevin equation can be shown to be the Lagrangian integral timescale for the fluid. In inhomogeneous turbulence, such a direct relation cannot be made. However in the GLM model the Langevin equation timescale is invariably set equal to the Lagrangian integral timescale of the fluid (either for fluid particles or that of the fluid velocities seen by inertial particles).

continuum equations can be reliably used to predict the dispersion of inertial particles in turbulent boundary layers. Such future work shall now be considered; first considering future work related to the modelling developed in this thesis (i.e. closure modelling for the dispersion tensors), and secondly, more general future work related to the PDF/continuum equations. Within each subgroup, the items are placed in the perceived order of importance.

10.1 Future work concerning closure models for particle dispersion tensors

10.1.1 Testing the Dispersion Tensor Closure Models against DNS data

Whilst the closure models in chapter 7 performed very well when compared to the PT data, the PT data against which they were compared was computed in a Gaussian, inhomogeneous, anisotropic flow field. Given that the flow field was Gaussian, then the Gaussian approximation made in the closure model for $\rho(\mathbf{x}', s|\mathbf{x})$ may have been quite reasonable (although still approximate since the skewed particle velocity distributions obtained from the PT data imply that $\rho(\mathbf{x}', s|\mathbf{x})$ was in reality non-Gaussian, even in the KS flow field). However real boundary layer turbulence is non-Gaussian, and therefore the Gaussian approximation to $\rho(\mathbf{x}', s|\mathbf{x})$ in the closure model may result in the new closure models for the dispersion tensors not performing so well when compared to PT data obtained using DNS of particle dispersion in a turbulent channel flow (or experiment). Therefore future would should involve testing the new closure models against data obtained from DNS.

10.1.2 Particle-Wall Collisions in the Dispersion Tensor Closure Models

The non-local closure models presented in chapters 7 and 8 assume that the particle-wall collisions are perfectly elastic. In real particle laden flows, this may not be a suitable assumption since particles may either collide inelastically or else deposit on the wall. In order to account for inelastic particle-wall collisions (of which deposition is a special case) two modifications would be required in the closure model. First of all the symmetry-line model (see section 7.1) would need to be modified to account for the fact that there would be an energy loss for the particles upon collision with the wall. However the more complicated issue would be the specification of the approximations

for $\overline{\mathrm{v}}_2(\mathrm{x}_2)$ and $\overline{\mathbf{cc}}$ in the moments of the closure model for $\rho(\mathbf{x}', s|\mathbf{x})$. It may still be possible to approximate $\overline{\mathbf{cc}}$ by a local approximation, as was done in chapter 7. However, for inelastic particle-wall collisions $\overline{\mathrm{v}}_2(\mathrm{x}_2)$ is no longer zero and would therefore require a model. It could in principle be approximated through local approximations to the wall-normal particle momentum and continuity equations, however the difficulty would then be that a boundary condition for $\overline{\mathrm{v}}_2(\mathrm{x}_2)$ would be required, and this in itself is far from trivial. An initial approximation would be to set $\overline{\mathrm{v}}_2(\mathrm{x}_2) = 0$ and account for the inelastic collisions only through the modified symmetry-line model, modified for inelastic collisions.

10.2 Future work concerning the PDF/continuum equations

10.2.1 The Limitations of the Gaussian approximation for $\boldsymbol{f}$ in the PDF Kinetic Equation

The only real concern with the PDF kinetic framework is that it assumes that the stochastic force field $\boldsymbol{f}(\mathbf{x}, t)$ may be approximated as being Gaussian. For dispersion in homogeneous, isotropic turbulence a Gaussian approximation for $\boldsymbol{f}$ is reasonable, especially for drag forcing since the velocity field at the large scales is near Gaussian in such turbulence. However in a boundary layer, the turbulence is non-Gaussian even at the large scales of the turbulence. It would be important therefore in future work to assess the limitations of the Gaussian approximation for $\boldsymbol{f}$ in the PDF kinetic equation.

Regardless of how good the closure modelling made in the continuum equations is, ultimately the continuum equations derived from the PDF kinetic equation will never give solutions which are in perfect agreement with data obtained from particle tracking in either DNS or experiment of a turbulent boundary layer. The reason being that real boundary layer turbulence is non-Gaussian and this has an effect on the transport of the particles, an effect which is not captured in the current PDF model. An interesting and insightful way to assess the limitations of the Gaussian assumption in the PDF equation would be as follows

- The unknown/unclosed terms in the continuum equations (up to the particle Reynolds stress equation) are the phase-space dispersion tensors $\boldsymbol{\lambda}(\mathbf{x}, \mathbf{v}, t)$, $\boldsymbol{\mu}(\mathbf{x}, \mathbf{v}, t)$ and $\boldsymbol{\kappa}(\mathbf{x}, \mathbf{v}, t)$ (and their velocity averaged forms which can be found from these), the Reynolds stress flux tensor $\overline{\mathbf{ccc}}$ and the boundary conditions for the particle Reynolds stress tensor $\overline{\mathbf{cc}}$. Each of these unknown terms could be computed from particle tracking in a DNS of particle laden turbulent channel flow.

- Then the DNS data for these unknown terms can be fed into the continuum equations which could then be solved, obtaining solutions for the particle concentration ρ, the particle mean velocity $\overline{\mathbf{v}}$ and the particle Reynolds stress tensor $\overline{\mathbf{cc}}$ which can then be compared to the equivalent DNS particle tracking data.

- Any discrepancy between the continuum solutions and the DNS data can then be only due to the Gaussian assumption for $\boldsymbol{f}$ in the underlying PDF equation[1].

This test case would certainly be very computational demanding, however it would be important to do since it would highlight how much of a limitation the Gaussian assumption for $\boldsymbol{f}$ in the PDF equation is to accurately modelling particle dispersion in turbulent boundary layers.

10.2.2 Boundary Conditions and Chapman-Enskog closure in the Continuum Equations

Future work should also address the specification of boundary conditions for the continuum equations and improvements to the Chapman-Enskog closure approximation for $\overline{\mathbf{ccc}}$ required to close the particle Reynolds stress equation. As discussed in chapter 4, there are existing models available to specify boundary conditions for the continuum equations, however the most fruitful approach would be to specify them through solutions to the PDF kinetic equation itself. By doing so one does not need to assume a Gaussian distribution for the particle velocities at the wall (a Gaussian PDF is assumed at the wall in most boundary condition models) and therefore likely improving the accuracy and generality of the boundary conditions derived. In addition future work should involve the development of more appropriate closures for $\overline{\mathbf{ccc}}$ than the Chapman-Enskog approximation. It is recalled that the Chapman-Enskog closure assumes that the fourth order moment $\overline{\mathbf{cccc}}$ is Gaussian and can therefore be directly related to the second order moment $\overline{\mathbf{cc}}$. This is the shortcoming of the approximation, since particle velocity distributions in turbulent boundary layers are in general strongly non-Gaussian. The challenge then would be to invoke a closure which does not make assumptions of Gaussianity for $\overline{\mathbf{cccc}}$, however this would be challenging.

[1]Actually there would be one minor inconsistency; with the dispersion tensors computed from the DNS data, then the force field $\boldsymbol{f}$ in the dispersion tensors themselves would be non-Gaussian, and would depend upon the distributions of $\boldsymbol{f}$ in the actual DNS turbulent field. However this is something of a secondary effect; the main implication of the Gaussian assumption in the PDF equation is that it leads to a simple gradient diffusion term in the particle momentum equation (see chapter 4). This simple gradient diffusion term would still be present in the continuum equations in this test case and hence the main effect of the Gaussian assumption could still be assessed.

Bibliography

[1] CT Crowe. *Multiphase Flow Handbook*. CRC Press, 2005.

[2] B Arcen, A Tanière, and B Oesterlé. On the influence of near-wall forces in particle-laden channel flows. *Int. J. Multiphase Flow*, 32:1326–1339, 2006.

[3] GA Kallio and MW Reeks. A numerical simulation of particle deposition in turbulent boundary layers. *Int. J. Multiphase Flow*, 15:433–446, 1989.

[4] RD Moser, J Kim, and NN Mansour. Direct numerical simulation of turbulent channel flow up to $\mathrm{Re}_\tau = 590$. *Phys. Fluids*, 11:943–945, 1999.

[5] TA Johnson and VC Patel. Flow past a sphere up to a reynolds number of 300. *J. Fluid Mech.*, 378:19–70, 1999.

[6] S Sundaram and LR Collins. A numerical study of the modulation of isotropic turbulence by suspended particles. *J. Fluid Mech.*, 379:105–143, 1999.

[7] LG Gibilaro, K Galluci, R Di Felice, and P Pagliai. On the apparent viscosity of a fluidized bed. *Chem. Eng.Sci.*, 62:294–300, 2007.

[8] LM Portela, P Cota, and RVA Oliemans. Numerical study of the near-wall behaviour of particles in turbulent pipe flows . *Powder Technology*, 125:149–157, 2002.

[9] C Marchioli, A Soldati, JGM Kuerten, B Arcen, A Tanière, G Goldensoph, KD Squires, MF Cargnelutti, and LM Portela. Statistics of particle dispersion in direct numerical simulations of wall-bounded turbulence: Results of an international collaborative benchmark test. *Int. J. Multiphase Flow*, 34:879–893, 2008.

[10] SA Orszag and GS Patterson. Numerical simulation of three-dimensional homogeneous isotropic turbulence. *Phys. Rev. Lett.*, 28:76–79, 1972.

[11] J Kim, P Moin, and R Moser. Turbulence statistics in fully developed channel flow at low Reynolds number. *J. Fluid Mech.*, 177:133–166, 1987.

[12] YG Guezennec, U Piomelli, and J Kim. On the shape and dynamics of wall structures in turbulent channel flow. *Phys. Fluids A*, 4:764–766, 1989.

[13] JW Brooke and TJ Hanratty. Origin of turbulence-producing eddies in a channel flow. *Phys. Fluids A*, 4:1011–1022, 1993.

[14] W Schoppa and F Hussain. *New aspects of vortex dynamics relevant to coherent structures in turbulent flows. In Eddy structure Identification, CISM Courses and Lectures, vol.353*. Springer, 1996.

[15] W Schoppa and F Hussain. Genesis and dynamics of coherent structures in near-wall turbulence. in self sustaining mechanisms of wall turbulence, advances in fluid mechanics, vol.15. *Computational Mechanics Publications*, pages 61–143, 1997.

[16] W Schoppa and F Hussain. Coherent structure dynamics in near-wall turbulence. *Fluid Dynamics Research*, 26:119–139, 2000.

[17] J Jeong and F Hussain. On the identification of a vortex. *J. Fluid Mech.*, 285:69–94, 1995.

[18] J Jiménez and A Pinelli. The autonomous cycle of near-wall turbulence. *J. Fluid Mech.*, 389:335–359, 1999.

[19] J Zhou, RJ Adrian, S Balachandar, and TM Kendall. Mechanisms for generating coherent packets of hairpin vortices in channel flow. *J. Fluid Mech.*, 387:353–396, 1999.

[20] X Wu and P Moin. Direct numerical simulation of turbulence in a nominally zero-pressure gradient flat-plate boundary layer. *J. Fluid Mech.*, 630:5–41, 2009.

[21] SB Pope. *Turbulent Flows*. Cambridge University Press, 2000.

[22] JS Smagorinsky. General circulation experiments with the primitive equations. *Monthly Weather Rev.*, 91:99–164, 1963.

[23] M Germano, U Piomelli, P Moin, and WH Cabot. A dynamic subgrid-scale eddy viscosity model. *Phys. Fluids*, 3:1760–1765, 1991.

[24] J Frohlich and W Rodi. Introduction to large eddy simulations of turbulent flows. *Closure strategies for Turbulent and Transitional Flows.*, pages 267–298, 2002.

[25] SB Pope. Ten questions concerning the large-eddy simulation of turbulent flows. *New Journal of Physics*, 2004.

[26] C Marchioli, MV Salvetti, and A Soldati. Some issues concerning large-eddy simulation of inertial particle dispersion in turbulent bounded flows. *Phys. Fluids*, 20, 2008.

[27] B Ray and LR Collins. Preferential concentration and relative velocity statistics of inertial particles in navierstokes turbulence with and without filtering. *J. Fluid Mech.*, 680:488–510, 2011.

[28] FH Harlow and PI Nakayama. Transport of turbulence energy decay rate. *Los Alamos Sci.Lab..*, 1968.

[29] BE Launder, GJ Reece, and W Rodi. Progress in the development of a Reynolds-stress turbulent closure. *J. Fluid Mech.*, 68:537–566, 1975.

[30] RH Kraichnan. Diffusion by a random velocity field. *Phys. Fluids*, 13:22–31, 1970.

[31] JCH Fung, JCR Hunt, and NA Malik. Kinematic simulation of homogeneous turbulence by unsteady random fourier modes. *J. Fluid Mech.*, 236:281–318, 1992.

[32] DJ Thomson and BJ Devenish. Particle pair separation in kinematic simulations. *J. Fluid Mech.*, 526:277–302, 2005.

[33] JCH Fung and JC Vassilicos. Two-particle dispersion in turbulent-like flows. *Phys. Rev. E*, 57:1677–1690, 1998.

[34] NA Malik and JC Vassilicos. A lagrangian model for turbulent dispersion with turbulent-like flow structure: comparison with direct numerical simulation for two-particle statistics. *Phys. Fluids*, 11:1572–1580, 1999.

[35] FW Elliott and AJ Majda. Pair dispersion over an inertial range spanning many decades. *Phys. Fluids*, 8:1052–1060, 1996.

[36] P Flohr and JC Vassilicos. Scalar subgrid model with flow structure for large-eddy simulations of scalar variances. *J. Fluid Mech.*, 407:315–349, 2000.

[37] F Nicolleau and A ElMaihy. Study of the development of a 3-d material surface and an iso-concentration field using ks. *J. Fluid Mech.*, 517:229–249, 2004.

[38] Nl Clark and JC Vassilicos. Kinematic simulation of fully developed turbulent channel flow. *Flow, Turbulence and Combustion*, pages 1–31, 2010.

[39] DJ Thomson. Random walk modeling of dispersion in inhomogeneous turbulence. *Quart.J.Roy.Meteorol.Soc.*, 110:1107–1120, 1984.

[40] DJ Thomson. Criteria for the selection of stochastic models of particle trajectories in turbulent flows. *J. Fluid Mech.*, 180:529–559, 1987.

[41] I Iliopoulos and TJ Hanratty. Turbulent dispersion in a non-homogeneous field. *J. Fluid Mech.*, 392:45–71, 1999.

[42] JP Minier and E Peirano. The pdf approach to turbulent polydispersed two-phase flows. *Physics Reports*, 352:1–214, 2001.

[43] Y Mito and TJ Hanratty. Use of a modified langevin equation to describe turbulent dispersion of fluid particles in a channel flow. *Flow, Turbulence and Combustion*, 68:1–26, 2002.

[44] I Iliopoulos, Y Mito, and TJ Hanratty. A stochastic model for solid particle dispersion in a nonhomogeneous turbulent field. *Int. J. Multiphase Flow*, 29:375–394, 2003.

[45] Y Mito and TJ Hanratty. A stochastic description of wall sources in a turbulent field: part 2. calculation for a simplified model of horizontal annular flows. *Int. J. Multiphase Flow*, 30:803–825, 2005.

[46] A Dehbi. A stochastic langevin model of turbulent particle dispersion in the presence of thermophoresis. *Int. J. Multiphase Flow*, 35:219–226, 2008.

[47] A Dehbi. Turbulent particle dispersion in arbitrary wall-bounded geometries: A coupled cfd-langevin-equation based approach. *Int. J. Multiphase Flow*, 34:819–828, 2008.

[48] TL Bocksell and E Loth. Stochastic modeling of particle diffusion in a turbulent boundary layer. *Int. J. Multiphase Flow*, 32:1234–1253, 2006.

[49] R Skartlien. Kinetic modeling of particles in stratified flow – Evaluation of dispersion tensors in inhomogeneous turbulence. *Int. J. Multiphase Flow*, 33:1006–1022, 2007.

[50] N Patankar, P Singh, D Joseph, R Glowinski, and T Pan. A new formulation of the distributed lagrange multiplier/fictitious domain method for particulate flows. *Int. J. Multiphase Flow*, 26:1509, 2000.

[51] R Glowinski, TW Pan, TI Hesla, DD Joseph, and J Periaux. A fictitious domain approach to the direct numerical simulation of incompressible viscous flow past moving rigid bodies. application to particulate flow. *J. Comp. Phys.*, 169:363–426, 2001.

[52] AJC Ladd and R Verberg. Lattice-boltzmann simulations of particle-fluid suspensions. *J. Statist. Phys.*, 104:1191–1251, 2001.

[53] Z Zhang and A Prosperetti. A second-order method for three-dimensional particle flow simulations. *J. Comp. Phys.*, 210:292–324, 2005.

[54] ZG Feng and EE Michaelides. Proteus: a direct forcing method for three-dimensional particle flow simulations. *J. Comp. Phys.*, 202:20–51, 2005.

[55] K Taira and T Colonius. The immersed boundary method: A projection approach. *J. Comp. Phys.*, 225:2118–2137, 2007.

[56] A Ten Cate, JJ Derksen, LM Portela, and HEA Van den Akker. Fully resolved simulations of colliding monodisperse spheres in forced isotropic turbulence. *J. Fluid Mech.*, 519:233–271, 2004.

[57] VA Sourabh and Patankar N. A formulation for fully resolved simulations (frs) of particle-turbulence interactions in two-phase flows. *Int. J. Numer. Analysis and Modeling*, 5:1–16, 2008.

[58] TM Burton and JK Eaton. Fully resolved simulations of particle-turbulence interaction. *J. Fluid Mech.*, 545:67–111, 2005.

[59] RA Gore and CT Crowe. Effect of particle-size on modulating turbulent intensity. *Int. J. Multiphase Flow*, 15:279–285, 1989.

[60] S Geiß, A Sadiki, A Maltsev, A Dreizler, and J Janicka. Investigations of turbulence modulation in turbulent particle laden flows. *J. App. Math. and Mech.*, 81:527–528, 2001.

[61] C Crowe, M Sommerfeld, and Y Tsuji. *Multiphase Flows with Droplets and Particles*. CRC Press, 1997.

[62] MR Maxey and JJ Riley. Equation of motion for a small rigid sphere in a nonuniform flow. *Phys. Fluids*, 26:883–889, 1983.

[63] TR Auton, JCR Hunt, and M Prud'homme. The force exerted on a body in inviscid unsteady non-uniform rotational flow. *J. Fluid Mech.*, 197:241–257, 1988.

[64] E Loth and AJ Dorgan. An equation of motion for particles of finite reynolds number and size. *Environ. Fluid Mech.*, 9:187–206, 2009.

[65] MR Maxey. Equation of motion for a small rigid sphere in a nonuniform or unsteady flow. *ASME/FED*, 166:57–62, 1993.

[66] L Schiller and A Neumann. Uber die grundlegenden berechungen bei der schwerkraftaufereitung. *Z.Ver.Dtsch.*, 77, 1993.

[67] L Zeng, F Najjar, S Balachandar, and P Fischer. Forces on a finite-sized particle located close to a wall in a linear shear flow. *Phys. Fluids*, 21, 2009.

[68] S Elghobashi and GC Truesdell. Direct simulation of particle dispersion in a decaying isotropic turbulence. *J. Fluid Mech.*, 242:655–700, 1992.

[69] BPB Hoomans, JAM Kuipers, WJ Briels, and WPM van Swaaij. Discrete particle simulation of bubble and slug formation in a two-dimensional gas-fluidised bed: a hard sphere approach. *Chem. Eng. Sci*, 51:99–108, 1996.

[70] P Kosinski and AC Hoffmann. Extension of the hard-sphere particle-wall collision model to account for particle deposition. *Phys. Rev. E*, 79, 2009. 061302.

[71] Y Tsuji, T Kawaguchi, and T Tanaka. Discrete particle simulation of agglomerate impact coalescence. *Powder Technol.*, 77:79–87, 1993.

[72] GG Joseph and ML Hunt. Oblique particle-wall collisions in a liquid. *J. Fluid Mech.*, 510:71–93, 2004.

[73] RH Davis, JM Serayssol, and EJ Hinch. The elastohydrodynamic collision of two spheres. *J. Fluid Mech.*, 163:479–497, 1986.

[74] RH Davis. Elastohydrodynamic collisions of particles. *PhysioCehm.Hydrodyn.*, 9:41–52, 1987.

[75] D Legendre, R Zenit, C Daniel, and P Guiraud. A note on the modelling of the bouncing of spherical drops or solid spheres on a wall in viscous fluid. *Chem.Eng. Sci.*, 61:3543–3549, 2006.

[76] G Barnocky and Rh Davis. The influence of pressure-dependent density and viscosity on the elastohydrodynamic collision and rebound of two spheres. *J. Fluid Mech.*, 209:501–519, 1989.

[77] M Benson, T Tanaka, and JK Eaton. Effects of wall roughness on particle velocities in a turbulent channel flow. *J. Fluids Eng.*, 127:250–256, 2005.

[78] M Sommerfeld. Modelling of particle-wall collisions in confined gas-particle flows. *Int. J. Multiphase Flow*, 18:905–926, 1992.

[79] NA Konan, O Kannengieser, and O Simonin. Stochastic modeling of the multiple rebound effects for particle-rough wall collisions. *Int. J. Multiphase Flow*, 35:933–945, 2009.

[80] MW Reeks. Simulation of particle diffusion, segregation, and intermittency in turbulent flows. *Fluid Mechanics and Its Applications.*, 81:21–30, 2006.

[81] M Picciotto, C Marchioli, MW Reeks, and A Soldati. Statistics of velocity and preferential accumulation of micro-particles in boundary layer turbulence. *Nuclear Engineering and Design*, 235:1239–1249, 2005.

[82] MW Reeks. The transport of discrete particles in inhomogeneous turbulence. *J. Aerosol Sci.*, 14:729–739, 1983.

[83] MW Reeks. On a kinetic equation for the transport of particles in turbulent flows. *Phys. Fluids*, 3:446–456, 1991.

[84] C Marchioli, M Picciotto, and A Soldati. Particle dispersion and wall-dependent turbulent flow scales: implications for local equilibrium models. *Journal of Turbulence*, 7:1–13, 2006.

[85] C Marchioli and A Soldati. Mechanisms for particle transfer and segregation in a turbulent boundary layer. *J. Fluid Mech.*, 468:283–315, 2002.

[86] C Narayanan, D Lakehal, L Botto, and A Soldati. Mechanisms of particle deposition in a fully developed turbulent open channel flow. *Phys. Fluids*, 15:763–775, 2003.

[87] Q Wang and KD Squires. Large eddy simulation of particle deposition in a vertical turbulent channel flow. *In. J. Heat and Fluid flow*, 22:667–683, 1996.

[88] AJ Dorgan, E Loth, TL Bocksell, and PK Yeung. Boundary layer dispersion of near wall injected particles of various inertias. *AIAA*, 43:1537–1548, 2005.

[89] S Pedinotti, G Mariotti, and S Banerjee. Direct numerical simulation of particle behavior in the wall region of turbulent flow in horizontal channels. *Int. J. Multiphase Flow*, 18:927–941, 1992.

[90] JK Eaton and JR Fessler. Preferential concentration of particles by turbulence. *Int. J. Multiphase Flow*, 20:169–209, 1994.

[91] Y Niño and MH Garcia. Experiments on particle-turbulence interactions in the near-wall region of an open channel flow: implications for sediment transport. *J. Fluid Mech.*, 326:285–319, 1996.

[92] Y Pan and S Banerjee. Numerical simulation of particle interactions with wall turbulence. *Phys. Fluids*, 8:2733–2755, 1996.

[93] D Swailes and K Darbyshire. A generalized Fokker-Planck equation for particle transport in random media. *Physica A*, 242:38–48, 1997.

[94] KE Hyland, S M^{c}Kee, and MW Reeks. Derivation of a pdf kinetic equation for the transport of particles in turbulent flows. *J. Phys. A: Math. Gen.*, 32:6169–6190, 1999.

[95] LI Zaichik. A statistical model of particle transport and heat transfer in turbulent shear flows. *Phys. Fluids*, 11:1521–1534, 1999.

[96] J Pozorski and JP Minier. Probability density function modeling of dispersed two-phase turbulent flows. *Physical Review E*, 59:855–863, 1998.

[97] O Simonin, E Deutsch, and JP Minier. Eulerian prediction of the fluid/particle correlated motion in turbulent two-phase flows. *Applied Scientific Research*, 51:275–283, 1993.

[98] F Mashayek and RVR Pandya. Analytical description of particle/droplet-laden turbulent flows. *Progress in Energy and Combustion Science*, 29:329–378, 2003.

[99] U Frisch and AN Kolmogorov. *Turbulence: The Legacy of A.N. Kolmogorov*. Cambridge University Press, 1995.

[100] VM Alipchenkov and LI Zaichik. Modeling of the turbulent motion of particles in a vertical channel. *Fluid Dynamics*, 41:531–544, 2006.

[101] LI Zaichik and VM Alipchenkov. Modelling of transport and dispersion of arbitrary-density particles in turbulent flows. *In. J. Heat and Fluid flow*, 31:850–861, 2010.

[102] NG Van Kampen. Stochastic differential equations. *Physics Reports (Section C of Physics Letters).*, 20:171–228, 1976.

[103] NG Van Kampen. Stochastic processes in physics and chemistry. *2nd ed. (North-Holland, Amsterdam, 1992).*

[104] DC Swailes, YA Sergeev, and A Parker. Chapman-Enskog closure approximation in the kinetic theory of dilute turbulent gas-particulate suspensions. *Physica A*, 254:517–547, 1998.

[105] Q Wang, KD Squires, and O Simonin. Large eddy simulation of turbulent gas-solid flows in a vertical channel and evaluation of second-order models. *In. J. Heat and Fluid flow*, 19:505–511, 1998.

[106] D Swailes and K Darbyshire. Probabilistic models for particle and scalar transport in fluctuating flows: An evaluation of simple closure approximations. *Physica A*, 262:307–327, 1999.

[107] LP Wang and DE Stock. Dispersion of heavy particles by turbulent motion. *J. Atmospheric Sciences.*, 50:1897–1913, 1993.

[108] B Oesterlé and LI Zaichik. Time scales for predicting dispersion of arbitrary-density particles in isotropic turbulence. *Int. J. Multiphase Flow*, 32:838–849, 2006.

[109] MW Reeks. On the constitutive relations for dispersed particles in nonuniform flows. 1: Dispersion in a simple shear flow. *Phys. Fluids*, 5:750–761, 1993.

[110] R Skartlien, D Drazen, DC Swailes, and A Jensen. Suspensions in turbulent liquid pipe flow: Kinetic modelling and added mass effects. *Int. J. Multiphase Flow*, 35:1017–1035, 2009.

[111] VM Alipchenkov, LI Zaichik, and O Simonin. A comparison of two approaches to derivation of boundary conditions for continuous equations of particle motion in turbulent flow. *High Temperature.*, 39:104–110, 2001.

[112] LI Zaichik, VM Alipchenkov, and AR Avetissian. Transport and deposition of colliding particles in turbulent channel flows. *In. J. Heat and Fluid flow*, 30:443–451, 2009.

[113] M Sakiz and O Simonin. Development and validation of continuum particle wall boundary conditions using lagrangian simulation of a vertical gassolid channel flow. *Proc. 3rd ASME/JSME Joint Fluids Eng. Conf.San-Francisco, CA. Paper No. 7898.*, 1999.

[114] J He and O Simonin. Non-equilibrium predictions of the particle phase stress tensor in vertical pneumatic conveying. *Stock, D. (Ed.), Proc. 5th Int. Symp. on GasSolid Flows, ASME Fluids Engineering Division Summer Meeting, Washington, DC, vol. 166. pp. 253263.*, 1993.

[115] B. Oesterlé A. Tanière, M. Khalij. Focus on the dispersed phase boundary conditions at the wall for irregular particle bouncing. *Int. J. Multiphase Flow*, 30:327–345, 2004.

[116] PJ van Dijk and DC Swailes. Hermite-dg method for pdf-equations modelling dispersions in turbulent boundary layers including streamwise velocity. *Proc. ASME 2010 3rd Joint US-European Fluids Engineering Summer Meeting collocated with 8th International Conference on Nanochannels, Microchannels, and Minichannels (FEDSM2010) August 15, 2010 , Montreal, Quebec, Canada .*, pages 99–106, 2010.

[117] PJ van Dijk and DC Swailes. Spectral-dg methods for pdf equations modelling particle transport and deposition in turbulent boundary layers. *Proc. THE 6TH INTERNATIONAL SYMPOSIUM ON MULTIPHASE FLOW, HEAT MASS TRANSFER AND ENERGY CONVERSION.*, pages 693–701, 2010.

[118] MW Reeks. On model equations for particle dispersion in inhomogeneous turbulence. *Int. J. Multiphase Flow*, 31:93–114, 2005.

[119] J Young and A Leeming. Particle deposition in turbulent pipe flow. *J. Fluid Mech.*, 340:129–159, 1997.

[120] MW Reeks. On the continuum equations for dispersed particles in nonuniform flows. *Phys. Fluids*, 4:1290–1303, 1992.

[121] D Swailes and M Reeks. Particle deposition from a turbulent flow. i: A steady-state model for high-inertia particles. *Phys. Fluids*, 6:3392–3403, 1994.

[122] KE Hyland, S M^{c}Kee, and MW Reeks. Exact analytic solutions to turbulent particle flow equations. *Phys. Fluids*, 11:1249–1261, 1999.

[123] B Arcen and A Tanière. Simulation of a particle-laden turbulent channel flow using an improved stochastic lagrangian model. *Phys. Fluids*, 21.

[124] A Azzalini and AD Valle. The multivariate skew-normal distribution. *Biometrika.*, 83:715–726, 1996.

[125] RB Arellano-Valle, MA Cortés, and HW Gómez. An extension of the epsilon-skew-normal distribution. *Communications in StatisticsTheory and Methods.*, 39:912–922, 2010.

[126] S Nadarajah and S Kotz. Skewed distributions generated by the cauchy kernel. *Brazilian Journal of Probability and Statistics*, 19:39–51, 2005.

[127] MW Reeks. On the probability density function equation for particle dispersion in a uniform shear flow. *J. Fluid Mech.*, 522:263–302, 2005.

[128] J Luo, T Ushijima, O Kitoh, Z Lu, and Y Liu. Lagrangian dispersion in turbulent channel flow and its relationship to eulerian statistics. *In. J. Heat and Fluid flow*, 28:871–881, 2007.

[129] SB Pope. A stochastic lagrangian model for acceleration in turbulent flows. *Phys. Fluids*, 14:2360–2375, 2002.

Appendix A

Closure Model Integrals

In this appendix the procedure for the analytic solution to the integrals defining the second central moment in the closure model for $\rho(\mathbf{x}', s|\mathbf{x})$ is outlined. Firstly, the expression needed for the closure model in chapter 8 is derived since this is the most difficult. Then, using the same procedure the expression required for the closure model in chapter 7 is derived.

A.1 Closure Integral for Stokes drag, added mass and gravity closure model

The integral equation for the covariance in the closure model is given by (see equation (8.57))

$$\begin{aligned}\left\langle \tilde{x}_i^p(s)\tilde{x}_k^p(s)\right\rangle_{\mathbf{x}} =& G_{ij}(s)\left\langle v_j^{p\prime}(0)v_m^{p\prime}(0)\right\rangle_{\mathbf{x}} G_{km}(s) \\ &+ G_{ij}(s)\int_s^0 G_{km}(s-s_1)\left[\tilde{\beta}+\alpha\frac{d}{ds_1}\right]\left\langle v_j^{p\prime}(0)u_m'(\boldsymbol{x}^p(s_1),s_1)\right\rangle_{\mathbf{x}} ds_1 \\ &+ G_{km}(s)\int_s^0 G_{ij}(s-s_1)\left[\tilde{\beta}+\alpha\frac{d}{ds_1}\right]\left\langle u_j'(\boldsymbol{x}^p(s_1),s_1)v_m^{p\prime}(0)\right\rangle_{\mathbf{x}} ds_1 \\ &+ \int_s^0\int_s^0 G_{ij}(s-s_1)\left[(\tilde{\beta})^2+\alpha^2\frac{d}{ds_1}\frac{d}{ds_2}\right]\left\langle u_j'(\boldsymbol{x}^p(s_1),s_1)u_m'(\boldsymbol{x}^p(s_2),s_2)\right\rangle_{\mathbf{x}} G_{km}(s-s_2)ds_1ds_2\end{aligned} \tag{A.1}$$

Under the closure approximations for the autocovariances discussed in chapters 7 and 8, equation (A.1) becomes

$$\begin{aligned}\left\langle \tilde{x}_i^p(s)\tilde{x}_k^p(s)\right\rangle_{\mathbf{x}} =& G_{ij}(s)\frac{1}{2\tilde{\beta}}\left(\overline{\mu}_{jm}+\overline{\mu}_{mj}\right)G_{km}(s) \\ &+ G_{ij}(s)\int_s^0 G_{km}(s-s_1)\left[\tilde{\beta}+\alpha\frac{d}{ds_1}\right]\Psi(s_1)ds_1\frac{\overline{\mu}_{jn}}{\tilde{\beta}}\left(\delta_{nm}-\tau^{Lp}\frac{\partial\overline{\mathrm{v}}_n}{\partial \mathrm{x}_m}\right) \\ &+ G_{km}(s)\int_s^0 G_{ij}(s-s_1)\left[\tilde{\beta}+\alpha\frac{d}{ds_1}\right]\Psi(s_1)ds_1\frac{\overline{\mu}_{mn}}{\tilde{\beta}}\left(\delta_{nj}-\tau^{Lp}\frac{\partial\overline{\mathrm{v}}_n}{\partial \mathrm{x}_j}\right) \\ &+ \int_s^0\int_s^0 G_{ij}(s-s_1)\left[(\tilde{\beta})^2+\alpha^2\frac{d}{ds_1}\frac{d}{ds_2}\right]\langle u_j'u_m'\rangle\Psi(s_1-s_2)G_{km}(s-s_2)ds_1ds_2\end{aligned} \tag{A.2}$$

The only remaining issue is the choice of the form for $\Psi(s_1)$. The usual choice for this autocorrelation would be

$$\Psi(s_1)=\exp\left[\frac{s_1}{\tau^{Lp}}\right], \qquad \Psi(s_1-s_2)=\exp\left[\frac{s_1-s_2}{\tau^{Lp}}\right], \quad s\le 0 \tag{A.3}$$

In the absence of added mass ($\alpha\to 0$) this simple exponential function is in general an appropriate choice for the autocorrelation. Then since $\boldsymbol{G}$ is a simple combination of exponential functions, equation (A.2) is relatively straightforward to solve. However, with added mass it can be seen from equation (A.2) that the derivatives of Ψ become important. In this case the autocorrelation given in equation (A.3) is not appropriate, and this may be demonstrated as follows. As discussed in chapter 8 the fluid acceleration autocovariance may be approximated from the fluid velocity autocovariance as

$$\left\langle\left(\frac{D}{Ds_1}u_j^p(\boldsymbol{x}^p(s_1),s_1)\right)'\left(\frac{D}{Ds_2}u_m^p(\boldsymbol{x}^p(s_2),s_2)\right)'\right\rangle_{\mathbf{x}}=\frac{d}{ds_1}\frac{d}{ds_2}\langle u_j'u_m'\rangle\Psi(s_1-s_2) \tag{A.4}$$

Using the autocorrelation given in equation (A.3) this gives

$$\left\langle\left(\frac{D}{Ds_1}u_j^p(\boldsymbol{x}^p(s_1),s_1)\right)'\left(\frac{D}{Ds_2}u_m^p(\boldsymbol{x}^p(s_2),s_2)\right)'\right\rangle_{\mathbf{x}}=-\left(\frac{1}{\tau^{Lp}}\right)^2\langle u_j'u_m'\rangle\Psi(s_1-s_2) \tag{A.5}$$

The autocovariance for the acceleration given in equation (A.5) cannot be correct since firstly it predicts a negative trace for the acceleration covariance tensor, and secondly because it suggests that the timescale of the fluid acceleration fluctuations is the same as the timescale for the fluid velocity fluctuations. One of reasons for this unphysical

prediction is that the autocorrelation given in equation (A.3) does not satisfy the necessary physical criteria, namely a zero gradient at the origin when $s_1 = s_2 = 0$. One way around this problem is to define a bi-exponential autocorrelation similar to that in [129] where in the present context the two timescales could be given by both τ^{Lp} and perhaps the fluid velocity Taylor micro-scale in order to satisfy the condition of a zero gradient at the origin in the autocorrelation when $s_1 = s_2 = 0$.

Since the closure model in chapters 7 and 8 was tested against data in the KS field described in section 7.4.1 then the appropriate choice is

$$\Psi(s_1) = \exp\left[-\frac{1}{2}\sigma_L^2 s_1^2\right], \qquad \Psi(s_1 - s_2) = \exp\left[-\frac{1}{2}\sigma_L^2 \left(s_1 - s_2\right)^2\right] \tag{A.6}$$

where

$$\sigma_L = \sqrt{\frac{\pi}{2}}\frac{1}{\tau^{Lp}} \tag{A.7}$$

which satisfy the condition of having a zero gradient at the origin when $s_1 = s_2 = 0$. Such a choice of Ψ makes the integration in equation (A.2) much more difficult and lengthy. However Ψ was chosen to be that given in equation (A.6) for comparison with data from the KS flow field so as not to introduce any unnecessary sources of error in the closure model predictions. In general simple exponentials (perhaps bi-exponential) could be used for Ψ since it is known that against DNS data simple exponentials form a good approximation to the autocorrelations (except as small times).

It is emphasised therefore that the evaluation of the integrals in equation (A.2) with Ψ given by simple exponentials are relatively straightforward, and the solutions are far simpler than the results shown in this appendix which are lengthy because Ψ was given by the Gaussian form in equation (A.6).

However the integrals in equation (A.2) only need to be evaluated once and then the analytic closure model for $\rho(\mathbf{x}', s|\mathbf{x})$ is complete. The solutions are given in terms of simple functions which may then be written in a computer code so that the analytic expression for $\rho(\mathbf{x}', s|\mathbf{x})$ can be evaluated at each value of s required when performing the integrals in equations (7.72) and (7.73).

Single Integrals

For the KS flow field the mean fluid (and therefore particle) velocities are zero, and with Ψ given in equation (A.6) the single integrals in equation (A.2) become

$$G_{ij}(s)\int_s^0 G_{mk}(s-s_1)\left[\tilde{\beta}-\alpha\sigma_L^2 s_1\right]\exp\left[-\frac{1}{2}\sigma_L^2 s_1^2\right]ds_1\frac{\overline{\mu}_{jm}}{\tilde{\beta}} \tag{A.8}$$

$$G_{km}(s)\int_s^0 G_{mj}(s-s_1)\left[\tilde{\beta}-\alpha\sigma_L^2 s_1\right]\exp\left[-\frac{1}{2}\sigma_L^2 s_1^2\right]ds_1\frac{\overline{\mu}_{ji}}{\tilde{\beta}} \tag{A.9}$$

Because the components of the Green tensor $\boldsymbol{G}$ are essentially combinations of exponential functions, it is efficient to solve the integrals in equations (A.8) and (A.9) in a more generic form

$$I^1(a,b,s)=\int_s^0\left[\tilde{\beta}-\alpha\sigma_L^2 s_1\right]\exp[as-bs_1]\exp\left[-\frac{1}{2}\sigma_L^2 s_1^2\right]ds_1 \tag{A.10}$$

The particular integral corresponding to the component of the Green tensor in question may then be found using equation (A.10). For example, suppose for the integral in equation (A.8) the components required are $m=k=1$. Then with

$$G_{11}(s-s_1)=\frac{1}{\tilde{\beta}}\left(1-\exp\left[\tilde{\beta}(s-s_1)\right]\right)$$

the solution required is

$$\int_s^0 G_{11}(s-s_1)\left[\tilde{\beta}-\alpha\sigma_L^2 s_1\right]\exp\left[-\frac{1}{2}\sigma_L^2 s_1^2\right]ds_1=\frac{1}{\tilde{\beta}}\left(I^1(0,0,s)-I^1(\tilde{\beta},\tilde{\beta},s)\right) \tag{A.11}$$

To solve equation (A.10) the exponentials are first combined giving

$$\begin{aligned}I^1(a,b,s)=&\exp\left[as+\frac{b^2}{2\sigma_L^2}\right]\int_s^0\left[\tilde{\beta}-\alpha\sigma_L^2 s_1\right]\exp\left[-\frac{1}{2}\left(\sigma_L s_1+\frac{b}{\sigma_L}\right)^2\right]ds_1\\ =&\exp\left[as+\frac{b^2}{2\sigma_L^2}\right]\int_s^0 P(s_1)\exp\left[-(Q(s_1))^2\right]ds_1\end{aligned} \tag{A.12}$$

where

$$P(s_1)=\tilde{\beta}-\alpha\sigma_L^2 s_1 \tag{A.13}$$

$$Q(s_1)=\frac{1}{\sqrt{2}}\left(\sigma_L s_1+\frac{b}{\sigma_L}\right) \tag{A.14}$$

The integral in equation (A.12) may be solved using integration by parts, giving

$$
\begin{aligned}
&I^1(a,b,s) \\
&= \exp\left[as + \frac{b^2}{2\sigma_L^2}\right] \int_s^0 P(s_1) \exp\left[-(Q(s_1))^2\right] ds_1 \\
&= \exp\left[as + \frac{b^2}{2\sigma_L^2}\right] \left[P(s_1) \int \exp\left[-(Q(s_1))^2\right] ds_1\right]_s^0 - \exp\left[as + \frac{b^2}{2\sigma_L^2}\right] \frac{dP}{ds_1} \int_s^0 \int \exp\left[-(Q(s_1))^2\right] ds_1 ds_1 \\
&= \exp\left[as + \frac{b^2}{2\sigma_L^2}\right] \frac{\sqrt{\pi}}{2} \left[P(s_1) \left(\frac{dQ}{ds_1}\right)^{-1} \mathrm{erf}[Q(s_1)] - \frac{dP}{ds_1} \left(\frac{dQ}{ds_1}\right)^{-2} \left[Q(s_1)\mathrm{erf}[Q(s_1)] + \frac{1}{\sqrt{\pi}} \exp\left[-(Q(s_1))^2\right]\right]\right]_s^0
\end{aligned}
\tag{A.15}
$$

Double Integrals

For the KS flow field with Ψ given in equation (A.6) the double integral in equation (A.2) becomes

$$
\int_s^0 \int_s^0 G_{ij}(s-s_1) \left[\tilde{\beta}^2 + \alpha^2 \sigma_L^2 (1 - \sigma_L^2 (s_1 - s_2)^2)\right] \langle u_j' u_m' \rangle \exp\left[-\frac{1}{2}\sigma_L^2 (s_1 - s_2)^2\right] G_{mk}(s - s_2) ds_1 ds_2 \tag{A.16}
$$

Once again, because the components of the Green tensor $\boldsymbol{G}$ are essentially combinations of exponential functions, it is efficient to solve the integral in equation (A.16) in a more generic form

$$
I^2(a,b,c,s) = \int_s^0 \int_s^0 \left[\tilde{\beta}^2 + \alpha^2 \sigma_L^2 (1 - \sigma_L^2 (s_1 - s_2)^2)\right] \exp[as - bs_1 - cs_2] \exp\left[-\frac{1}{2}\sigma_L^2 (s_1 - s_2)^2\right] ds_1 ds_2 \tag{A.17}
$$

The particular integral corresponding to the components of the Green tensor required may then be found using equation (A.17). For example, suppose for the integral in equation (A.16) the components required are $i = j = m = k = 1$. Then with

$$
G_{11}(s - s_1) = \frac{1}{\tilde{\beta}} \left(1 - \exp\left[\tilde{\beta}(s - s_1)\right]\right)
$$

and

$$
G_{11}(s - s_2) = \frac{1}{\tilde{\beta}} \left(1 - \exp\left[\tilde{\beta}(s - s_2)\right]\right)
$$

the solution required is

$$\begin{aligned}&\int_s^0 \int_s^0 G_{11}(s-s_1)\left[\tilde{\beta}^2+\alpha^2\sigma_L^2(1-\sigma_L^2(s_1-s_2)^2)\right]\langle u_1'u_1'\rangle \exp\left[-\frac{1}{2}\sigma_L^2(s_1-s_2)^2\right] G_{11}(s-s_2)ds_1ds_2\\&=\frac{\langle u_1'u_1'\rangle}{\tilde{\beta}^2}\left(I^2(0,0,0,s)-I^2(\tilde{\beta},0,\tilde{\beta},s)-I^2(\tilde{\beta},\tilde{\beta},0,s)+I^2(2\tilde{\beta},\tilde{\beta},\tilde{\beta},s)\right)\end{aligned} \tag{A.18}$$

To solve equation (A.17) the exponentials in it are combined and then separated again into an exponential which is only a function of s_2 and another which is a function of s_1 and s_2

$$I^2(a,b,c,s)=\exp[as]\int_s^0 \exp[M(s_2)]\int_s^0 L(s_1,s_2)\exp\left[-N(s_1,s_2)^2\right]ds_1ds_2 \tag{A.19}$$

with

$$M(s_2)=\frac{1}{2\sigma_L^2}\left(b^2-2(b+c)\sigma_L^2 s_2\right) \tag{A.20}$$

$$L(s_1,s_2)=\tilde{\beta}^2+\alpha^2\sigma_L^2(1-\sigma_L^2(s_1-s_2)^2) \tag{A.21}$$

$$N(s_1,s_2)=\frac{1}{\sqrt{2}}\left(\sigma_L s_1-\frac{1}{\sigma_L}(\sigma_L^2 s_2-b)\right) \tag{A.22}$$

Since $L(s_1,s_2)$ is a 2^{nd} order polynomial in s_1, to solve the integral over s_1 in equation (A.19) integration by parts must be performed twice. The integral over s_1 is given by

$$\begin{aligned}\int_s^0 L(s_1,s_2)\exp\left[-N(s_1,s_2)^2\right]ds_1=&\left[L\int\exp[-N^2]ds_1\right]_s^0-\left[\frac{\partial L}{\partial s_1}\int\int\exp[-N^2]ds_1ds_1\right]_s^0\\&+\left[\frac{\partial^2 L}{\partial s_1^2}\int\int\int\exp[-N^2]ds_1ds_1ds_1\right]_s^0\end{aligned} \tag{A.23}$$

with

$$\int \exp[-N^2] ds_1 = \left(\frac{\partial N}{\partial s_1}\right)^{-1} \frac{\sqrt{\pi}}{2} \mathrm{erf}[N] \tag{A.24}$$

$$\int\int \exp[-N^2] ds_1 ds_1 = \left(\frac{\partial N}{\partial s_1}\right)^{-2} \frac{\sqrt{\pi}}{2} \left[N\mathrm{erf}[N] + \frac{1}{\sqrt{\pi}} \exp[-N^2] \right] \tag{A.25}$$

$$\int\int\int \exp[-N^2] ds_1 ds_1 ds_1 = \left(\frac{\partial N}{\partial s_1}\right)^{-3} \frac{\sqrt{\pi}}{2} \left[\left(\frac{2N^2+1}{4} \right) \mathrm{erf}[N] + \frac{N}{2\sqrt{\pi}} \exp[-N^2] \right] \tag{A.26}$$

The solution to equation (A.23) is therefore given by

$$\int_s^0 L(s_1, s_2) \exp\left[-N(s_1, s_2)^2\right] ds_1 = \Big[E(s_1, s_2)\mathrm{erf}[N] + F(s_1, s_2) \exp[-N^2] \Big]_s^0 \tag{A.27}$$

where

$$E(s_1, s_2) = \frac{\sqrt{\pi}}{2} \left[L \left(\frac{\partial N}{\partial s_1}\right)^{-1} - N \frac{\partial L}{\partial s_1} \left(\frac{\partial N}{\partial s_1}\right)^{-2} + \left(\frac{2N^2+1}{4} \right) \frac{\partial^2 L}{\partial s_1^2} \left(\frac{\partial N}{\partial s_1}\right)^{-3} \right] \tag{A.28}$$

$$F(s_1, s_2) = -\frac{1}{2} \left[\frac{\partial L}{\partial s_1} \left(\frac{\partial N}{\partial s_1}\right)^{-2} - \frac{N}{2} \frac{\partial^2 L}{\partial s_1^2} \left(\frac{\partial N}{\partial s_1}\right)^{-3} \right] \tag{A.29}$$

The solution to equation (A.19) is therefore given by

$$\begin{aligned} I^2(a, b, c, s) = &\exp[as] \int_s^0 \exp\left[M(s_2)\right] \Big[E(0, s_2)\mathrm{erf}[N(0, s_2)] + F(0, s_2) \exp\left[-(N(0, s_2))^2\right] \Big] ds_2 \\ &- \exp[as] \int_s^0 \exp\left[M(s_2)\right] \Big[E(s, s_2)\mathrm{erf}[N(s, s_2)] + F(s, s_2) \exp\left[-(N(s, s_2))^2\right] \Big] ds_2 \end{aligned} \tag{A.30}$$

To solve equation (A.30), first, the exponentials must be combined and then separated again into an exponential which is only a function of s_1 and another which is a function of s_1 and s_2

$$M(s_2) - \Big[N(s_1, s_2) \Big]^2 = C(s_1) - \Big[D(s_1, s_2) \Big]^2 \tag{A.31}$$

with

$$C(s_1) = \frac{c^2}{2\sigma_L^2} - (b+c)s_1 \tag{A.32}$$

$$D(s_1, s_2) = -\frac{1}{\sqrt{2}}\left(\sigma_L s_2 - \frac{1}{\sigma_L}(\sigma_L^2 s_1 - c)\right) \tag{A.33}$$

Since $F(s_1, s_2)$ is linear in s_2, the following integral (which features in equation (A.30)) is easily solved (using equation (A.31))

$$\begin{aligned} A^1(s_1, s_2) = \exp[as] \int F \exp\left[M - N^2\right] ds_2 = \frac{\sqrt{\pi}}{2} \exp[as + C] F \left(\frac{\partial D}{\partial s_2}\right)^{-1} \operatorname{erf}[D] \\ - \frac{\sqrt{\pi}}{2} \exp[as + C] \frac{\partial F}{\partial s_2} \left(\frac{\partial D}{\partial s_2}\right)^{-2} \left(D \operatorname{erf}[D] + \frac{1}{\sqrt{\pi}} \exp[-D^2]\right) \end{aligned} \tag{A.34}$$

Now the following integral must be evaluated (which features in equation (A.30))

$$\exp[as] \int E \exp[M] \operatorname{erf}[N] ds_2 \tag{A.35}$$

Once again, since E is a 2^{nd} order polynomial in s_2, equation (A.35) must be solved using integration by parts twice

$$\begin{aligned} A^2(s_1, s_2) = \exp[as] \int E \exp[M] \operatorname{erf}[N] ds_2 = \exp[as] E \int \exp[M] \operatorname{erf}[N] ds_2 \\ - \exp[as] \frac{\partial E}{\partial s_2} \int \int \exp[M] \operatorname{erf}[N] ds_2 ds_2 \\ + \exp[as] \frac{\partial^2 E}{\partial s_2^2} \int \int \int \exp[M] \operatorname{erf}[N] ds_2 ds_2 ds_2 \end{aligned} \tag{A.36}$$

and so the following antiderivatives are required

$$\int \exp[M] \operatorname{erf}[N] ds_2 = \left(\frac{dM}{ds_2}\right)^{-1} \left[\operatorname{erf}[N] \exp[M] - \frac{\partial N}{\partial s_2} \left(\frac{\partial D}{\partial s_2}\right)^{-1} \exp[C] \operatorname{erf}[D]\right] \tag{A.37}$$

$$\begin{aligned} \int \int \exp[M] \operatorname{erf}[N] ds_2 ds_2 = \left(\frac{dM}{ds_2}\right)^{-2} \left[\operatorname{erf}[N] \exp[M] - \exp[C] \operatorname{erf}[D]\right] \\ - \left(\frac{dM}{ds_2}\right)^{-1} \left(\frac{\partial N}{\partial s_2}\right)^{-1} \exp[C] \left[D \operatorname{erf}[D] + \frac{1}{\sqrt{\pi}} \exp[-D^2]\right] \end{aligned} \tag{A.38}$$

$$\int\int\int \exp[M]\mathrm{erf}[N]ds_2ds_2ds_2 = \left(\frac{dM}{ds_2}\right)^{-3}\Big[\mathrm{erf}[N]\exp[M] - \exp[C]\mathrm{erf}[D]\Big]$$
$$-\left(\frac{dM}{ds_2}\right)^{-2}\left(\frac{\partial D}{\partial s_2}\right)^{-1}\exp[C]\left[D\mathrm{erf}[D] + \frac{1}{\sqrt{\pi}}\exp[-D^2]\right] \tag{A.39}$$
$$-\frac{1}{2}\left(\frac{dM}{ds_2}\right)^{-1}\left(\frac{\partial N}{\partial s_2}\right)^{-1}\left(\frac{\partial D}{\partial s_2}\right)^{-1}\exp[C]\left[\left(\frac{2D^2+1}{2}\right)\mathrm{erf}[D] + \frac{D}{\sqrt{\pi}}\exp[-D^2]\right]$$

For the special case when $M = 0$ the antiderivatives required in equation (A.36) are

$$\int \mathrm{erf}[N]ds_2 = \left(\frac{\partial N}{\partial s_2}\right)^{-1}\left[N\mathrm{erf}[N] + \frac{1}{\sqrt{\pi}}\exp\left[-N^2\right]\right] \tag{A.40}$$

$$\int\int \mathrm{erf}[N]ds_2ds_2 = \left(\frac{\partial N}{\partial s_2}\right)^{-2}\left[\left(\frac{2N^2+1}{4}\right)\mathrm{erf}[N] + \frac{N}{2\sqrt{\pi}}\exp\left[-N^2\right]\right] \tag{A.41}$$

$$\int\int\int \mathrm{erf}[N]ds_2ds_2ds_2 = \left(\frac{\partial N}{\partial s_2}\right)^{-3}\left[\left(\frac{2N^3+3N}{12}\right)\mathrm{erf}[N] + \left(\frac{N^2+1}{6\sqrt{\pi}}\right)\exp\left[-N^2\right]\right] \tag{A.42}$$

The solution to equation (A.17) may now be constructed using the solutions in equation (A.34) and (A.36) as

$$I^2(a,b,c,s) = A^1(s_1,s_2) + A^2(s_1,s_2)\Big|_{s_1=s}^{s_1=0}\Big|_{s_2=s}^{s_2=0} \tag{A.43}$$

Local form for the dispersion tensors

For the purposes of testing the closure models against particle tracking data obtained in the KS flow field described in chapter 7, an analytic expression for the local approximation to $\overline{\boldsymbol{\mu}}$ is required in the closure model, which takes into account Stokes drag and added mass forcing. The $\overline{\boldsymbol{\mu}}$ dispersion tensor is defined as (for steady state)

$$\overline{\mu}_{ij}(\mathbf{x},s) = \int_s^0 \dot{G}_{ik}(s_1)\Big\langle R_{kj}(\boldsymbol{x}^p(s_1),s_1;\mathbf{x},0)\Big\rangle_{\mathbf{x}} ds_1 \tag{A.44}$$

For the KS flow field where $\langle \boldsymbol{u}\rangle = 0$, then under a local approximation the assymptotic form of $\overline{\boldsymbol{\mu}}$ accounting for Stokes drag and added mass becomes (for the KS flow field, where a Gaussian form for the autocorrelation is required)

$$\overline{\mu}_{ij}(\mathbf{x}) = \int_{-\infty}^{0} \dot{G}_{ik}(s_1)\left[\tilde{\beta}^2 + \alpha^2\sigma_{Lp}^2(1-\sigma_{Lp}^2 s_1^2)\right]\langle u_k' u_j'\rangle \exp\left[-\frac{\sigma_{Lp}^2 s_1^2}{2}\right] ds_1 \tag{A.45}$$

Since $\dot{\boldsymbol{G}}$ are essentially linear combinations of exponential functions (see chapter 8, and also note that since the dispersion being modelled is backwards in time, with $s \leq 0$, $\dot{G}(s) = -\frac{d}{ds}G(s)$), it is efficient to solve equation (A.45) in the generic form

$$M1(a) = \int_{-\infty}^{0} \exp\left[as_1\right]\left[\tilde{\beta}^2 + \alpha^2\sigma_{Lp}^2(1-\sigma_{Lp}^2 s_1^2)\right]\exp\left[-\frac{\sigma_{Lp}^2 s_1^2}{2}\right] ds_1 \tag{A.46}$$

The solution to equation (A.46) is

$$M1(a) = \sqrt{\frac{\pi}{2\sigma_{Lp}^2}}\left[\left(\tilde{\beta}^2 - a^2\alpha^2\right)\exp\left[\frac{a^2}{2\sigma_{Lp}^2}\right]\left(1-\operatorname{erf}\left[\frac{a}{\sqrt{2}\sigma_{Lp}}\right]\right) + \sqrt{\frac{2}{\pi}}a\alpha^2\sigma_{Lp}\right] \tag{A.47}$$

Using equation (A.47) the local form of $\overline{\boldsymbol{\mu}}$ may be constructed, and its components in 2D are

$$\begin{aligned}
\overline{\mu}_{11} = &\left(\langle u_1'u_1'\rangle - \frac{b_1}{b_2}\langle u_2'u_1'\rangle\right)\sqrt{\frac{\pi}{2\sigma_{Lp}^2}}\left[\tilde{\beta}^2\left(1-\alpha^2\right)\exp\left[\frac{\tilde{\beta}^2}{2\sigma_{Lp}^2}\right]\left(1-\operatorname{erf}\left[\frac{\tilde{\beta}}{\sqrt{2}\sigma_{Lp}}\right]\right) + \sqrt{\frac{2}{\pi}}\tilde{\beta}\alpha^2\sigma_{Lp}\right] \\
&+ \frac{b_1 b_5}{\tilde{\beta}b_2 b_3}\langle u_2'u_1'\rangle\sqrt{\frac{\pi}{2\sigma_{Lp}^2}}\left[\left(\tilde{\beta}^2 - b_5^2\alpha^2\right)\exp\left[\frac{b_5^2}{2\sigma_{Lp}^2}\right]\left(1+\operatorname{erf}\left[\frac{b_5}{\sqrt{2}\sigma_{Lp}}\right]\right) - \sqrt{\frac{2}{\pi}}b_5\alpha^2\sigma_{Lp}\right] \\
&- \frac{b_1 b_4}{\tilde{\beta}b_2 b_3}\langle u_2'u_1'\rangle\sqrt{\frac{\pi}{2\sigma_{Lp}^2}}\left[\left(\tilde{\beta}^2 - b_4^2\alpha^2\right)\exp\left[\frac{b_4^2}{2\sigma_{Lp}^2}\right]\left(1+\operatorname{erf}\left[\frac{b_4}{\sqrt{2}\sigma_{Lp}}\right]\right) - \sqrt{\frac{2}{\pi}}b_4\alpha^2\sigma_{Lp}\right]
\end{aligned} \tag{A.48}$$

$$\begin{aligned}
\overline{\mu}_{12} = &\left(\langle u_1'u_2'\rangle - \frac{b_1}{b_2}\langle u_2'u_2'\rangle\right)\sqrt{\frac{\pi}{2\sigma_{Lp}^2}}\left[\tilde{\beta}^2\left(1-\alpha^2\right)\exp\left[\frac{\tilde{\beta}^2}{2\sigma_{Lp}^2}\right]\left(1-\operatorname{erf}\left[\frac{\tilde{\beta}}{\sqrt{2}\sigma_{Lp}}\right]\right) + \sqrt{\frac{2}{\pi}}\tilde{\beta}\alpha^2\sigma_{Lp}\right] \\
&+ \frac{b_1 b_5}{\tilde{\beta}b_2 b_3}\langle u_2'u_2'\rangle\sqrt{\frac{\pi}{2\sigma_{Lp}^2}}\left[\left(\tilde{\beta}^2 - b_5^2\alpha^2\right)\exp\left[\frac{b_5^2}{2\sigma_{Lp}^2}\right]\left(1+\operatorname{erf}\left[\frac{b_5}{\sqrt{2}\sigma_{Lp}}\right]\right) - \sqrt{\frac{2}{\pi}}b_5\alpha^2\sigma_{Lp}\right] \\
&- \frac{b_1 b_4}{\tilde{\beta}b_2 b_3}\langle u_2'u_2'\rangle\sqrt{\frac{\pi}{2\sigma_{Lp}^2}}\left[\left(\tilde{\beta}^2 - b_4^2\alpha^2\right)\exp\left[\frac{b_4^2}{2\sigma_{Lp}^2}\right]\left(1+\operatorname{erf}\left[\frac{b_4}{\sqrt{2}\sigma_{Lp}}\right]\right) - \sqrt{\frac{2}{\pi}}b_4\alpha^2\sigma_{Lp}\right]
\end{aligned} \tag{A.49}$$

$$\begin{aligned}\overline{\mu}_{21} =& \frac{b_5}{\tilde{\beta} b_3}\langle u_2' u_1'\rangle \sqrt{\frac{\pi}{2\sigma_{Lp}^2}}\left[\left(\tilde{\beta}^2 - b_5^2\alpha^2\right)\exp\left[\frac{b_5^2}{2\sigma_{Lp}^2}\right]\left(1+\text{erf}\left[\frac{b_5}{\sqrt{2}\sigma_{Lp}}\right]\right) - \sqrt{\frac{2}{\pi}} b_5 \alpha^2 \sigma_{Lp}\right] \\ & - \frac{b_4}{\tilde{\beta} b_3}\langle u_2' u_1'\rangle \sqrt{\frac{\pi}{2\sigma_{Lp}^2}}\left[\left(\tilde{\beta}^2 - b_4^2\alpha^2\right)\exp\left[\frac{b_4^2}{2\sigma_{Lp}^2}\right]\left(1+\text{erf}\left[\frac{b_4}{\sqrt{2}\sigma_{Lp}}\right]\right) - \sqrt{\frac{2}{\pi}} b_4 \alpha^2 \sigma_{Lp}\right]\end{aligned} \tag{A.50}$$

$$\begin{aligned}\overline{\mu}_{22} =& \frac{b_5}{\tilde{\beta} b_3}\langle u_2' u_2'\rangle \sqrt{\frac{\pi}{2\sigma_{Lp}^2}}\left[\left(\tilde{\beta}^2 - b_5^2\alpha^2\right)\exp\left[\frac{b_5^2}{2\sigma_{Lp}^2}\right]\left(1+\text{erf}\left[\frac{b_5}{\sqrt{2}\sigma_{Lp}}\right]\right) - \sqrt{\frac{2}{\pi}} b_5 \alpha^2 \sigma_{Lp}\right] \\ & - \frac{b_4}{\tilde{\beta} b_3}\langle u_2' u_2'\rangle \sqrt{\frac{\pi}{2\sigma_{Lp}^2}}\left[\left(\tilde{\beta}^2 - b_4^2\alpha^2\right)\exp\left[\frac{b_4^2}{2\sigma_{Lp}^2}\right]\left(1+\text{erf}\left[\frac{b_4}{\sqrt{2}\sigma_{Lp}}\right]\right) - \sqrt{\frac{2}{\pi}} b_4 \alpha^2 \sigma_{Lp}\right]\end{aligned} \tag{A.51}$$

where b_1,b_2,b_3,b_4 and b_5 are defined in chapter 8.

In section 8.2 local forms for the drag components of the dispersion tensors $\overline{\boldsymbol{\lambda}}^{dd}$, $\overline{\boldsymbol{\mu}}^{dd}$, $\overline{\boldsymbol{\kappa}}^{dd}$ are required. The local approximations to these are given by (where the superscript 'dd' is dropped and is now replaced by 'L', as explained in section 8.2)

$$\overline{\lambda}_{ij}^{L}(\mathrm{x}_2) = \int_{-\infty}^{0} G_{ik}(s_1)\tilde{\beta}^2 \left\langle u_k' u_j' \right\rangle \exp\left[-\frac{1}{2}\sigma_L^2 s_1^2\right] ds_1 \tag{A.52}$$

$$\overline{\mu}_{ij}^{L}(\mathrm{x}_2) = \int_{-\infty}^{0} \dot{G}_{ik}(s_1)\tilde{\beta}^2 \left\langle u_k' u_j' \right\rangle \exp\left[-\frac{1}{2}\sigma_L^2 s_1^2\right] ds_1 \tag{A.53}$$

$$\overline{\kappa}_i^{PSA}(\mathrm{x}_2) = \frac{\partial}{\partial \mathrm{x}_j}\overline{\lambda}_{ij}^{L} \tag{A.54}$$

where the components of $\boldsymbol{G}$ are given in equations (8.27)-(8.29). For convenience, the integrals in equations (A.52)-(A.54) were solved numerically in order to obtain the solutions for the local dispersion tensors.

A.2 Closure Integral for Stokes drag closure model

In the case of the closure model presented in chapter 7, where only Stokes drag forcing is acting on the particles, the expression for the second central moment for the closure model for $\rho(\mathbf{x}', s|\mathbf{x})$ is significantly simpler than that containing added mass effects. Following the solution procedure outlined in the previous section, the solution for the second central moment of the closure model for Stokes drag, required in the test case presented in chapter 7 (where $\langle \boldsymbol{u} \rangle = \mathbf{0}$), is

$$\left\langle \tilde{x}_i^p(s)\tilde{x}_k^p(s)\right\rangle_{\mathrm{x}_2} =$$
$$G^2(s)\frac{\overline{\mu}_{ik}}{\beta}$$
$$+ 2\frac{\overline{\mu}_{ik}}{\beta}G\sqrt{\frac{\pi}{2\sigma_L^2}}\left[\Delta^1 - \Delta^3(\Delta^4 - \Delta^5)\right]$$
$$+ \frac{\langle u_i' u_k'\rangle}{\beta}\sqrt{\frac{\pi}{2\sigma_L^2}}\left[2\beta\Delta^1 s + \frac{2\sqrt{2}\beta}{\sqrt{\pi}\sigma_L}(\Delta^2 - 1) - 2\Delta^1(1-\dot{G}) + \Delta^5(2\Delta^6 + \Delta^3) - 2\Delta^6\Delta^8 - \Delta^3\Delta^4 - \Delta^7(\Delta^5 - \Delta^8)\right] \tag{A.55}$$

where

$$\Delta^1 = \mathrm{erf}\left[-\frac{\sigma_L^2 s}{\sqrt{2}}\right] \tag{A.56}$$
$$\Delta^2 = \exp\left[-\frac{\sigma_L^2 s^2}{2}\right] \tag{A.57}$$
$$\Delta^3 = \exp\left[\frac{\beta^2}{2\sigma_L^2}\right] \tag{A.58}$$
$$\Delta^4 = \mathrm{erf}\left[\frac{\beta - \sigma_L^2 s}{\sqrt{2}\sigma_L}\right] \tag{A.59}$$
$$\Delta^5 = \mathrm{erf}\left[\frac{\beta}{\sqrt{2}\sigma_L}\right] \tag{A.60}$$
$$\Delta^6 = \exp\left[\beta\left(s + \frac{\beta}{2\sigma_L^2}\right)\right] \tag{A.61}$$
$$\Delta^7 = \exp\left[\beta\left(2s + \frac{\beta}{2\sigma_L^2}\right)\right] \tag{A.62}$$
$$\Delta^8 = \mathrm{erf}\left[\frac{\beta + \sigma_L^2 s}{\sqrt{2}\sigma_L}\right] \tag{A.63}$$
$$G = \tau_p\left(1 - \exp[\beta s]\right) \tag{A.64}$$
$$\dot{G} = \exp[\beta s] \tag{A.65}$$

Appendix B

Method for Computing the Dispersion Tensors

Unlike the simple local approximations for $\overline{\boldsymbol{\lambda}}$, $\overline{\boldsymbol{\mu}}$ and $\overline{\boldsymbol{\kappa}}$ which may be specified analytically, approximations to the dispersion tensors obtained using the new non-local closure model, as presented in chapters 7 and 8, must be obtained numerically (in general). In this appendix the method to obtain the approximations to $\overline{\boldsymbol{\lambda}}$, $\overline{\boldsymbol{\mu}}$ and $\overline{\boldsymbol{\kappa}}$ using the non-local closure model is outlined.

Inputs

The input data required for the closure model is

- Data for $\boldsymbol{R}(\mathbf{x}', s; \mathbf{x}, 0)$
- Data for the mean fluid velocity $\langle \boldsymbol{u} \rangle$
- Data/model for τ^{Lp}, the timescale of the fluid velocity correlations seen by the inertial particles

Data for $\boldsymbol{R}(\mathbf{x}', s; \mathbf{x}, 0)$ and $\langle \boldsymbol{u} \rangle$ are obtained for the flow field in which the particles are dispersing (in general via either DNS or experimental data). As discussed in chapter 7, τ^{Lp} is approximated using equation (7.34).

Numerical integration

With the input data specified, $\overline{\boldsymbol{\lambda}}$, $\overline{\boldsymbol{\mu}}$ and $\overline{\boldsymbol{\kappa}}$ may be approximated using the non-local closure model as follows. First, $\rho(\mathbf{x}', s|\mathbf{x})$ is specified using a Gaussian distribution, and as such the models for the mean and second central moments must be supplied. The analytic solutions to these moments is given in appendix A. With the closure model for

this distribution specified then the following integrals must be evaluated numerically (given here in their 2D form)

$$\begin{aligned}\Big\langle R_{ji}(r_1^p, x_2^p(s), s; 0, \mathrm{x}_2, 0)\Big\rangle_{\mathrm{x}_2} &= \int_{+\mathrm{x}_2^{min}}^{+\mathrm{x}_2^{max}} \int_{\mathrm{r}_1^{min}}^{\mathrm{r}_1^{max}} R_{ji}(\mathrm{r}_1, \mathrm{x}_2', s; 0, \mathrm{x}_2, 0)\rho\left(\mathrm{r}_1, \mathrm{x}_2', s|\mathrm{x}_2\right) d\mathrm{r}_1 d\mathrm{x}_2' \\ &+ \int_{-\mathrm{x}_2^{max}}^{-\mathrm{x}_2^{min}} \int_{\mathrm{r}_1^{min}}^{\mathrm{r}_1^{max}} R_{ji}(\mathrm{r}_1, \mathrm{x}_2' + 2\mathrm{x}_2', s; 0, \mathrm{x}_2, 0)\rho\left(\mathrm{r}_1, 2\mathrm{x}_2^{min} + \mathrm{x}_2', s|\mathrm{x}_2\right) d\mathrm{r}_1 d\mathrm{x}_2'\end{aligned} \tag{B.1}$$

$$\begin{aligned}\Big\langle \frac{\partial}{\partial \mathrm{x}_k} R_{ji}(r_1^p, x_2^p(s), s; 0, \mathrm{x}_2, 0)\Big\rangle_{\mathrm{x}_2} &= \int_{+\mathrm{x}_2^{min}}^{+\mathrm{x}_2^{max}} \int_{\mathrm{r}_1^{min}}^{\mathrm{r}_1^{max}} \left[\frac{\partial}{\partial \mathrm{x}_k} R_{ji}(\mathrm{r}_1, \mathrm{x}_2', s; 0, \mathrm{x}_2, 0)\right] \rho\left(\mathrm{r}_1, \mathrm{x}_2', s|\mathrm{x}_2\right) d\mathrm{r}_1 d\mathrm{x}_2' \\ &+ \int_{-\mathrm{x}_2^{max}}^{-\mathrm{x}_2^{min}} \int_{\mathrm{r}_1^{min}}^{\mathrm{r}_1^{max}} \left[\frac{\partial}{\partial \mathrm{x}_k} R_{ji}(\mathrm{r}_1, \mathrm{x}_2' + 2\mathrm{x}_2', s; 0, \mathrm{x}_2, 0)\right] \rho\left(\mathrm{r}_1, 2\mathrm{x}_2^{min} + \mathrm{x}_2', s|\mathrm{x}_2\right) d\mathrm{r}_1 d\mathrm{x}_2'\end{aligned} \tag{B.2}$$

The x_2' domain in these integrals is determined by the location of the wall (actually one particle radius), x_2^{min}, and the upper bound of the domain, such as the location of the upper pipe wall. The r_1 domain is determined by the integral length scales of the flow and should be at least as large as the range over which $\boldsymbol{R}$ is spatially correlated in the r_1 direction. The integrals in equations (B.1) and (B.2) are easily solved numerically, and are solved for each value of s, where the range of s must cover at least the time span over which $\boldsymbol{R}$ remains temporally correlated.

However the integration of equations (B.1) and (B.2) may be simplified considerably (in terms of computational expense). For increasing r_1 and increasing $|\mathrm{x}_2 - \mathrm{x}_2'|$ the spatial distributions in equations (B.1) and (B.2), e.g. $\rho\left(\mathrm{r}_1, \mathrm{x}_2', s|\mathrm{x}_2\right)$, decay to zero and therefore also do the integrands in equations (B.1) and (B.2). Therefore when computing equations (B.1) and (B.2) numerically, the domain of the integrals may be reduced to a domain over which the integrands are non-negligible. It was found that the domain ranges of the integrals in equations (B.1) and (B.2) may be reduced as

$$\int_{+\mathrm{x}_2^{min}}^{+\mathrm{x}_2^{max}} \int_{\mathrm{r}_1^{min}}^{\mathrm{r}_1^{max}} \approx \int_{\mathrm{x}_2 - 4\sqrt{\Sigma_{22}(\mathrm{x}_2, s)}}^{\mathrm{x}_2 + 4\sqrt{\Sigma_{22}(\mathrm{x}_2, s)}} \int_{\mathrm{r}_1 - 4\sqrt{\Sigma_{11}(\mathrm{x}_2, s)}}^{\mathrm{r}_1 + 4\sqrt{\Sigma_{11}(\mathrm{x}_2, s)}}$$

(where $\boldsymbol{\Sigma}$ is the covariance tensor for $\rho\left(\mathrm{r}_1, \mathrm{x}_2', s|\mathrm{x}_2\right)$) with negligible affects to the results. Then with the integrals in equations (B.1) and (B.2), the solutions are then used to compute the dispersion tensors via

$$\overline{\lambda}_{ki}^{CM}(\mathbf{x}) = \int_s^0 G_{kj}(s)\Big\langle R_{ji}(r_1^p, x_2^p(s), s; 0, \mathrm{x}_2, 0)\Big\rangle_{\mathrm{x}_2} ds \tag{B.3}$$

$$\overline{\mu}_{ki}^{CM}(\mathbf{x}) = \int_s^0 \dot{G}_{kj}(s)\Big\langle R_{ji}(r_1^p, x_2^p(s), s; 0, \mathrm{x}_2, 0)\Big\rangle_{\mathrm{x}_2} ds \tag{B.4}$$

$$\overline{\kappa}_{i}^{CM}(\mathbf{x}) = \int_s^0 G_{kj}(s)\Big\langle \frac{\partial}{\partial \mathrm{x}_k} R_{ji}(r_1^p, x_2^p(s), s; 0, \mathrm{x}_2, 0)\Big\rangle_{\mathrm{x}_2} ds \tag{B.5}$$

Equations (B.3)-(B.5) are easily solved numerically, from which the non-local closure approximations to the dispersion tensors are obtained.

Appendix C

Spurious Drift in PDF Kinetic Equations

In this appendix a formal proof is presented which demonstrates that the PDF equation, and hence its associated continuum equations, are free from any spurious drift.

C.1 Statement of Problem

Consider fluid particle trajectories $\boldsymbol{x}^f(t)$ determined by the equation of motion

$$\frac{d}{dt}x_i^f = u_i(\boldsymbol{x}^f(t), t) \tag{C.1}$$

with initial condition $\boldsymbol{x}^f(0) = \mathbf{x}^0$, where $\mathbf{x}^0$ is a random variable with PDF $\varphi^0(\mathbf{x})$. Now define the following PDF's

$$\varrho(\mathbf{x}, t) = \delta\left(\boldsymbol{x}^f(t) - \mathbf{x}\right) \tag{C.2}$$

$$\varphi(\mathbf{x}, t) = \Big\langle \varrho(\mathbf{x}, t) \Big\rangle_{\boldsymbol{u}}^{\mathbf{x}^0} \tag{C.3}$$

$$\rho(\mathbf{x}, t) = \Big\langle \varrho(\mathbf{x}, t) \Big\rangle = \Big\langle \varphi(\mathbf{x}, t) \Big\rangle^{\boldsymbol{u}} \tag{C.4}$$

Here $\langle\,\cdot\,\rangle_{\boldsymbol{u}}^{\mathbf{x}^0}$ denotes an ensemble average over all realisations of $\mathbf{x}^0$ for a given, single realisation of the flow field $\boldsymbol{u}$, and $\langle\,\cdot\,\rangle^{\boldsymbol{u}}$ denotes an ensemble average over all $\boldsymbol{u}$. The decomposition

$$\langle\,\cdot\,\rangle = \Big\langle \langle\,\cdot\,\rangle_{\boldsymbol{u}}^{\mathbf{x}^0} \Big\rangle^{\boldsymbol{u}}$$

is used later in the analysis.

From equation (C.2) an evolution equation is obtained

$$\frac{\partial}{\partial t}\varrho(\mathbf{x},t) = -\frac{\partial}{\partial \mathrm{x}_i}\left[\frac{d}{dt}x_i^f\,\varrho(\mathbf{x},t)\right] = -\frac{\partial}{\partial \mathrm{x}_i}\left[u_i(\boldsymbol{x}^f(t),t)\varrho(\mathbf{x},t)\right] \tag{C.5}$$

Averaging equation (C.5) over all realisations of $\mathbf{x}^0$ (for a single realisation of $\boldsymbol{u}$) gives

$$\frac{\partial}{\partial t}\varphi(\mathbf{x},t) = -\frac{\partial}{\partial \mathrm{x}_i}\left[u_i(\mathbf{x},t)\varphi(\mathbf{x},t)\right] \tag{C.6}$$

The solution to equation (C.6) with initial condition $\varphi(\mathbf{x},0) = \varphi^0(\mathbf{x})$ can be expressed as

$$\varphi(\mathbf{x},t) = \varphi^0\Big(\boldsymbol{x}^f(0|\mathbf{x},t)\Big)\exp\left[-\int_0^t \frac{\partial}{\partial \mathrm{x}_i}u_i\Big(\boldsymbol{x}^f(t'|\mathbf{x},t),t'\Big)dt'\right] \tag{C.7}$$

where $\Big(\boldsymbol{x}^f(t'|\mathbf{x},t)\Big)$ denotes the fluid particle trajectory $\boldsymbol{x}^f(t')$ which satisfies $\boldsymbol{x}^f(t) = \mathbf{x}$. Now suppose that the fluid particles are uniformly distributed at $t = 0$. Suppose, further, that the fluid velocity field is incompressible. Then from equation (C.7)

$$\varphi(\mathbf{x},t) = \varphi^0 \quad \text{for all } \mathbf{x},t \tag{C.8}$$

and hence also

$$\rho(\mathbf{x},t) = \rho^0 = \varphi^0 \quad \text{for all } \mathbf{x},t \tag{C.9}$$

that is, the fluid particles remain uniformly distributed (they remain 'fully mixed'). Note further then that

$$\Big\langle \varrho u_i' \Big\rangle = \Big\langle \Big\langle \varrho u_i' \Big\rangle_{\boldsymbol{u}}^{\mathbf{x}^0} \Big\rangle^{\boldsymbol{u}} = \Big\langle \varphi u_i' \Big\rangle^{\boldsymbol{u}} = \rho^0 \Big\langle u_i' \Big\rangle^{\boldsymbol{u}} = 0 \tag{C.10}$$

Now consider the PDF equation for $\rho(\mathbf{x},t)$: from equation (C.5)

$$\frac{\partial}{\partial t}\rho(\mathbf{x},t) = -\frac{\partial}{\partial \mathrm{x}_i}\rho\langle u_i\rangle - \frac{\partial}{\partial \mathrm{x}_i}\rho\Big\langle u_i'(\boldsymbol{x}^f(t),t)\Big\rangle_{\mathbf{x}} \tag{C.11}$$

With $\boldsymbol{u}'$ a Gaussian field, then using FN (Furutsu-Novikov, see chapter 4) the closure for $\rho\Big\langle u_i'(\boldsymbol{x}^f(t),t)\Big\rangle_{\mathbf{x}}$ is given by the exact result

$$\rho\Big\langle u_i'(\boldsymbol{x}^f(t),t)\Big\rangle_{\mathbf{x}} = \rho\kappa_i - \frac{\partial}{\partial \mathrm{x}_i}\rho\lambda_{ji} \tag{C.12}$$

so that equation (C.11) becomes

$$\frac{\partial}{\partial t}\rho(\mathbf{x},t) = -\frac{\partial}{\partial \mathrm{x}_i}\rho\left(\langle u_i\rangle + \kappa_i - \frac{\partial}{\partial \mathrm{x}_j}\lambda_{ji}\right) + \frac{\partial}{\partial \mathrm{x}_i}\left(\lambda_{ji}\frac{\partial}{\partial \mathrm{x}_j}\rho\right) \tag{C.13}$$

In order to prove that the PDF kinetic equation does not contain any spurious drift it must be demonstrated that with $\rho(\mathbf{x},0) = \rho^0$ (constant) and $\partial_i u_i = 0$, equation (C.13) has the solution $\rho(\mathbf{x},t) = \rho^0$ for all $\mathbf{x}, t$. From a physical perspective, since fluid particles, by definition, do not preferentially sample turbulent flow fields, it must be demonstrated that the forms of $\boldsymbol{\kappa}$ and $\boldsymbol{\lambda}$ given by FN imply that equation (C.12) is identically zero for an initially uniform distribution of fluid particles in an inhomogeneous incompressible turbulent flow field. Such a proof reduces to demonstrating that

$$\kappa_i - \frac{\partial}{\partial \mathrm{x}_j}\lambda_{ji} = 0 \tag{C.14}$$

since then equation (C.13) would reduce to

$$\frac{\partial}{\partial t}\rho(\mathbf{x},t) = -\frac{\partial}{\partial \mathrm{x}_i}\rho\langle u_i\rangle + \frac{\partial}{\partial \mathrm{x}_i}\left(\lambda_{ji}\frac{\partial}{\partial \mathrm{x}_j}\rho\right) \tag{C.15}$$

which satisfies the required solution $\rho(\mathbf{x},t) = \rho^0$ for all $\mathbf{x}, t$ when $\rho(\mathbf{x},0) = \rho^0$ (constant) and $\partial_i u_i = 0$.

C.2 Proof that $\kappa_i - \frac{\partial}{\partial \mathrm{x}_j}\lambda_{ji} = 0$ for fluid particles

For a given realisation of the field $\boldsymbol{u}$ let $\boldsymbol{x}^f(s|\mathbf{y},t)$ denote a fluid particle trajecotry $\boldsymbol{x}^f(s)$ satisfying $\boldsymbol{x}^f(t) = \mathbf{y}$. For an incompressible flow field this trajectory will be unique.

Now define the Jacobian tensor $J_{mn}(\mathbf{y},t,s)$ by

$$J_{mn}(\mathbf{y},t,s) = \frac{\partial}{\partial \mathrm{y}_n}x_m^f(s|\mathbf{y},t) \tag{C.16}$$

The evolution of $\boldsymbol{J}$ with respect to s is given by

$$\frac{\partial}{\partial s}J_{mn}(\mathbf{y},t,s)=\frac{\partial}{\partial \mathrm{x}_k}u_m\Big(\boldsymbol{x}^f(s|\mathbf{y},t),s\Big)J_{kn}(\mathbf{y},t,s) \tag{C.17}$$

Noting that $\boldsymbol{J}(\mathbf{y},t,t)=\mathbf{I}$ (all $\mathbf{y},t$), the solution to equation (C.17) is

$$J_{mn}(\mathbf{y},t,s)=\left(\exp\left[\int_t^s\frac{\partial}{\partial\mathbf{x}}\boldsymbol{u}^\top\Big(\boldsymbol{x}^f(s'|\mathbf{y},t),s'\Big)ds'\right]\right)_{mn} \tag{C.18}$$

Therefore the components of $\boldsymbol{J}^{-1}(\mathbf{y},t,s)$ are given by

$$J^{-1}_{mn}(\mathbf{y},t,s)=\left(\exp\left[\int_s^t\frac{\partial}{\partial\mathbf{x}}\boldsymbol{u}^\top\Big(\boldsymbol{x}^f(s'|\mathbf{y},t),s'\Big)ds'\right]\right)_{mn} \tag{C.19}$$

Now consider the response tensor $\boldsymbol{\mathcal{G}}(t;t')$ appearing the the (FN defined) PDF equation dispersion tensors: for a given realisation of $\boldsymbol{u}$ and a corresponding trajectory $\boldsymbol{x}^f$ then (for $t'\le t$)

$$\mathcal{G}_{mn}(t;t')=\frac{\delta x^f_m(t)}{\delta u_n(\boldsymbol{x}^f(t'),t')} \tag{C.20}$$

Therefore

$$\frac{\partial}{\partial t}\mathcal{G}_{mn}(t;t')=\frac{\partial}{\partial \mathrm{x}_k}u_m(\boldsymbol{x}^f(t),t)\mathcal{G}_{kn}(t;t') \tag{C.21}$$

With the condition $\boldsymbol{\mathcal{G}}(t;t)=\mathbf{I}$ the solution to equation (C.21) is

$$\mathcal{G}_{mn}(t;t')=\left(\exp\left[\int_{t'}^t\frac{\partial}{\partial\mathbf{x}}\boldsymbol{u}^\top(\boldsymbol{x}^f(t''),t'')dt''\right]\right)_{mn} \tag{C.22}$$

If the trajectory $\boldsymbol{x}^f$ is given by $\boldsymbol{x}^f(t'')=\boldsymbol{x}^f(t''|\mathbf{y},t)$, then $\boldsymbol{\mathcal{G}}(t;t')$ becomes dependant on $\mathbf{y},t$

$$\mathcal{G}_{mn}(t;t')=\left(\exp\left[\int_{t'}^t\frac{\partial}{\partial\mathbf{x}}\boldsymbol{u}^\top\Big(\boldsymbol{x}^f(t''|\mathbf{y},t),t''\Big)dt''\right]\right)_{mn}=H_{mn}(\mathbf{y},t,t') \tag{C.23}$$

Comparing equations (C.23) and (C.19) indicates that

$$H_{mn}(\mathbf{y},t,t') = J^{-1}_{mn}(\mathbf{y},t,t') \tag{C.24}$$

Now consider the FN expressions for $\boldsymbol{\kappa}$ and $\boldsymbol{\lambda}$ which are

$$\kappa_i(\mathbf{x},t) = \int_0^t \left\langle \mathcal{G}_{jn}(t;t') \frac{\partial}{\partial \mathrm{x}_j} R_{ni}(\boldsymbol{x}^f(t'),t';\mathbf{x},t) \right\rangle_{\boldsymbol{x}^f=\mathbf{x}} dt' \tag{C.25}$$

$$\lambda_{ji}(\mathbf{x},t) = \int_0^t \left\langle \mathcal{G}_{jn}(t;t') R_{ni}(\boldsymbol{x}^f(t'),t';\mathbf{x},t) \right\rangle_{\boldsymbol{x}^f=\mathbf{x}} dt' \tag{C.26}$$

where $\boldsymbol{R}$ is the two-point, two-time correlation tensor for $\boldsymbol{u}$, that is

$$R_{ni}(\mathbf{x}',t';\mathbf{x},t) = \left\langle u'_n(\mathbf{x}',t') u'_i(\mathbf{x},t) \right\rangle \tag{C.27}$$

Note that if $\partial_i u_i = 0$ then

$$\frac{\partial}{\partial \mathrm{x}'_n} R_{ni}(\mathbf{x}',t';\mathbf{x},t) = 0 \tag{C.28}$$

Then

$$\kappa_i - \frac{\partial}{\partial \mathrm{x}_j}\lambda_{ji} = \int_0^t \left\langle \mathcal{G}_{jn}(t;t') \frac{\partial}{\partial \mathrm{x}_j} R_{ni}(\boldsymbol{x}^f(t'),t';\mathbf{x},t) \right\rangle_{\boldsymbol{x}^f=\mathbf{x}} - \frac{\partial}{\partial \mathrm{x}_j} \left\langle \mathcal{G}_{jn}(t;t') R_{ni}(\boldsymbol{x}^f(t'),t';\mathbf{x},t) \right\rangle_{\boldsymbol{x}^f=\mathbf{x}} dt' \tag{C.29}$$

In the first term of the integrand in equation (C.29) the differentiation $\frac{\partial}{\partial \mathrm{x}_j}$ acts only on the second spatial input of $\boldsymbol{R}$. In the second term in the integrand the differentiation is with respect to both this dependence in $\boldsymbol{R}$ and also the conditionality $\boldsymbol{x}^f(t) = \mathbf{x}$. Consequently equation (C.29) can be written

$$\kappa_i - \frac{\partial}{\partial \mathrm{x}_j}\lambda_{ji} = -\int_0^t \frac{\partial}{\partial \mathrm{y}_j} \left\langle \mathcal{G}_{jn}(t;t') R_{ni}(\boldsymbol{x}^f(t'),t';\mathbf{x},t) \right\rangle_{\boldsymbol{x}^f=\mathbf{y}} dt' \Bigg|_{\mathbf{y}=\mathbf{x}} \tag{C.30}$$

where $\frac{\partial}{\partial \mathrm{y}_j}$ is now used instead of $\frac{\partial}{\partial \mathrm{x}_j}$ to emphasise that this differentiation is now with respect to the condition $\boldsymbol{x}^f = \mathbf{y}$ and not the $\mathbf{x}$ dependence in $\boldsymbol{R}$.

It follows that a sufficient condition to ensure

$$\kappa_i - \frac{\partial}{\partial \mathrm{x}_j}\lambda_{ji} = 0$$

is that

$$\frac{\partial}{\partial \mathrm{y}_j}\left\langle \mathcal{G}_{jn}(t;t')R_{ni}(\boldsymbol{x}^f(t'),t';\mathbf{x},t)\right\rangle_{\boldsymbol{x}^f=\mathbf{y}} = 0 \tag{C.31}$$

Decompose the ensemble in equation (C.31) into an average over $\mathbf{x}^0$ (for a single realisation of $\boldsymbol{u}$) averaged over all realisations of $\boldsymbol{u}$. So that

$$\begin{aligned}\frac{\partial}{\partial \mathrm{y}_j}\left\langle \mathcal{G}_{jn}(t;t')R_{ni}(\boldsymbol{x}^f(t'),t';\mathbf{x},t)\right\rangle_{\boldsymbol{x}^f=\mathbf{y}} &= \frac{\partial}{\partial \mathrm{y}_j}\left[\frac{1}{\rho(\mathbf{y},t)}\left\langle \delta(\boldsymbol{x}^f(t)-\mathbf{y})\mathcal{G}_{jn}(t;t')R_{ni}(\boldsymbol{x}^f(t'),t';\mathbf{x},t)\right\rangle\right] \\ &= \frac{1}{\rho(\mathbf{y},t)}\left\langle \frac{\partial}{\partial \mathrm{y}_j}\left\langle \delta(\boldsymbol{x}^f(t)-\mathbf{y})\mathcal{G}_{jn}(t;t')R_{ni}(\boldsymbol{x}^f(t'),t';\mathbf{x},t)\right\rangle^{\mathbf{x}^0}_{\boldsymbol{x}^f=\mathbf{y},\boldsymbol{u}}\right\rangle^{\boldsymbol{u}}\end{aligned} \tag{C.32}$$

For a given realisation of $\boldsymbol{u}$ (and with $\partial_i u_i = 0$) there is a unique trajectory satisfying $\boldsymbol{x}^f(t) = \mathbf{y}$, namely $\boldsymbol{x}^f(t'|\mathbf{y},t)$. The contribution of this trajectory to the inner ensemble in equation (C.32) is weighted by $\varphi^0\Big(\boldsymbol{x}^f(0|\mathbf{y},t)\Big)$. Also with this trajectory $\boldsymbol{\mathcal{G}}(t;t') = \boldsymbol{H}(\mathbf{y},t,t')$, so that equation (C.32) may be written as

$$\frac{\partial}{\partial \mathrm{y}_j}\left\langle \mathcal{G}_{jn}(t;t')R_{ni}(\boldsymbol{x}^f(t'),t';\mathbf{x},t)\right\rangle_{\boldsymbol{x}^f=\mathbf{y}} = \frac{1}{\rho(\mathbf{y},t)}\left\langle \frac{\partial}{\partial \mathrm{y}_j}\left[\varphi^0\Big(\boldsymbol{x}^f(0|\mathbf{y},t)\Big)H_{jn}(\mathbf{y},t,t')R_{ni}(\boldsymbol{x}^f(t'|\mathbf{y},t),t';\mathbf{x},t)\right]\right\rangle^{\boldsymbol{u}} \tag{C.33}$$

Therefore with $\varphi^0 = \rho^0$ constant, it follows that a sufficient condition to ensure

$$\kappa_i - \frac{\partial}{\partial \mathrm{x}_j}\lambda_{ji} = 0$$

is

$$\frac{\partial}{\partial \mathrm{y}_j}\Big[H_{jn}(\mathbf{y},t,t')R_{ni}(\boldsymbol{x}^f(t'|\mathbf{y},t),t';\mathbf{x},t)\Big] = 0 \quad \text{(for all } i\text{)} \tag{C.34}$$

The left hand side of equation (C.34) can be written

$$\underbrace{\left[\frac{\partial}{\partial \mathrm{y}_j} H_{jn}(\mathbf{y},t,t')\right] R_{ni}(\boldsymbol{x}^f(t'|\mathbf{y},t),t';\mathbf{x},t)}_{\mathbf{1}} \quad + \quad \underbrace{H_{jn}(\mathbf{y},t,t')\left[\frac{\partial}{\partial \mathrm{y}_j} R_{ni}(\boldsymbol{x}^f(t'|\mathbf{y},t),t';\mathbf{x},t)\right]}_{\mathbf{2}} \tag{C.35}$$

It is therefore sufficient to show that in equation (C.35), **1** and **2** are identically zero.

Consider term **2** in equation (C.35):

$$\begin{aligned}
&H_{jn}(\mathbf{y},t,t')\left[\frac{\partial}{\partial \mathrm{y}_j} R_{ni}(\boldsymbol{x}^f(t'|\mathbf{y},t),t';\mathbf{x},t)\right] \\
&= H_{jn}(\mathbf{y},t,t')\frac{\partial}{\partial \mathrm{y}_j} x_k^f(t'|\mathbf{y},t)\frac{\partial}{\partial \mathrm{x}'_k} R_{ni}(\boldsymbol{x}^f(t'|\mathbf{y},t),t';\mathbf{x},t) \\
&= H_{jn}(\mathbf{y},t,t')J_{kj}(\mathbf{y},t,t')\frac{\partial}{\partial \mathrm{x}'_k} R_{ni}(\boldsymbol{x}^f(t'|\mathbf{y},t),t';\mathbf{x},t) \\
&= \delta_{nk}\frac{\partial}{\partial \mathrm{x}'_k} R_{ni}(\boldsymbol{x}^f(t'|\mathbf{y},t),t';\mathbf{x},t) \quad \text{(using equation (C.24))} \\
&= \frac{\partial}{\partial \mathrm{x}'_n} R_{ni}(\boldsymbol{x}^f(t'|\mathbf{y},t),t';\mathbf{x},t) = 0 \quad \text{(using equation (C.28))}
\end{aligned} \tag{C.36}$$

It remains, therefore, to show that term **1** in equation (C.35) is identically zero. That is

$$\frac{\partial}{\partial \mathrm{y}_j} H_{jn}(\mathbf{y},t,t') = 0 \tag{C.37}$$

This can be demonstrated using equation (C.24). In 3-dimensions the inverse of $\boldsymbol{J}$ is given by

$$\boldsymbol{J}^{-1} = \begin{pmatrix} +(J_{22}J_{33} - J_{23}J_{32}) - (J_{12}J_{33} - J_{13}J_{32}) + (J_{12}J_{23} - J_{13}J_{22}) \\ -(J_{21}J_{33} - J_{23}J_{31}) + (J_{11}J_{33} - J_{13}J_{31}) - (J_{11}J_{23} - J_{13}J_{21}) \\ +(J_{21}J_{32} - J_{22}J_{31}) - (J_{11}J_{32} - J_{12}J_{31}) + (J_{11}J_{22} - J_{12}J_{21}) \end{pmatrix} \tag{C.38}$$

So

$$\frac{\partial}{\partial \mathrm{y}_j} H_{j1}(\mathbf{y},t,t') = +\frac{\partial}{\partial \mathrm{y}_1}(J_{22}J_{33} - J_{23}J_{32}) - \frac{\partial}{\partial \mathrm{y}_2}(J_{21}J_{33} - J_{23}J_{31}) + \frac{\partial}{\partial \mathrm{y}_3}(J_{21}J_{32} - J_{22}J_{31}) \tag{C.39}$$

$$\frac{\partial}{\partial \mathrm{y}_j} H_{j2}(\mathbf{y},t,t') = -\frac{\partial}{\partial \mathrm{y}_1}(J_{12}J_{33} - J_{13}J_{32}) + \frac{\partial}{\partial \mathrm{y}_2}(J_{11}J_{33} - J_{13}J_{31}) - \frac{\partial}{\partial \mathrm{y}_3}(J_{11}J_{32} - J_{12}J_{31}) \tag{C.40}$$

$$\frac{\partial}{\partial \mathrm{y}_j} H_{j3}(\mathbf{y},t,t') = +\frac{\partial}{\partial \mathrm{y}_1}(J_{12}J_{23} - J_{13}J_{22}) - \frac{\partial}{\partial \mathrm{y}_2}(J_{11}J_{23} - J_{13}J_{21}) + \frac{\partial}{\partial \mathrm{y}_3}(J_{11}J_{22} - J_{12}J_{21}) \tag{C.41}$$

It is easy to verify that each of these components $\frac{\partial}{\partial y_j} H_{jn}$ is identically zero using the fact that $\frac{\partial}{\partial y_i} J_{kj} = \frac{\partial}{\partial y_j} J_{ki}$.

This, therefore, presents proof that the PDF equation does not contain spurious drift.